Trade-Offs Between Emissions, Cost and Resilience in Emerging Technologies Supporting Deep Decarbonization of the Electric Grid

A

Dissertation

Presented to

the faculty of the School of Engineering and Applied Science

University of Virginia

in partial fulfillment

of the requirements for the degree

Doctor of Philosophy

by

Jeffrey A. Bennett

May 2021

APPROVAL SHEET

This

Dissertation

is submitted in partial fulfillment of the requirements
for the degree of

Doctor of Philosophy

Author: Jeffrey A. Bennett

This Dissertation has been read and approved by the examing committee:

Advisor: Andres Clarens

Advisor:

Committee Member: Lisa Colosi-Peterson

Committee Member: Roger Fittro

Committee Member: Eric Loth

Committee Member: Julianne Quinn

Committee Member:

Committee Member:

Accepted for the School of Engineering and Applied Science:

Craig H. Benson, School of Engineering and Applied Science

May 2021

Abstract

Decarbonization of the electric grid is necessary to limit the impact of climate change, however important questions remain about the architecture and operation of a grid heavily dependent on intermittent renewable generation. Four emerging technologies are evaluated here to understand their ability to support the decarbonization of electricity generation: distributed electric grids, supercritical carbon dioxide power cycles (sCO_2), offshore compressed air energy storage (OCAES), and bioenergy with carbon capture and storage (BECCS). Distributed electric grids are expected to be more resilient to severe weather and may be well-suited to wind turbines and solar photovoltaics which are inherently distributed as they require large areas of land. sCO_2 cycles offer high efficiencies and have compact machinery making them of interest for fast response. OCAES is a novel type of energy storage that combines isothermal thermodynamic cycles with aquifer air storage. BECCS power plants offer the ability to produce electricity while reducing atmospheric CO_2 levels. These technologies could be deployed independently or in tandem. It is understood that energy technologies are not selected for technical feasibility alone, thus a systems perspective is used to interpret results, considering environmental impact, cost, and grid resilience.

This work makes the following contributions to the academic literature: (1) quantified the impact of grid topology (distributed vs. centralized) and fuel mix (natural gas vs. natural gas, wind and solar) on costs, emissions and grid resilience; (2) modeled the feasibility and cost of sCO_2 power cycles for delivering load-balancing when integrated into a grid involving high deployment of solar photovoltaics; (3) evaluated the performance, cost and value of OCAES to the electric grid; and (4) identified locations off the United States Mid-Atlantic coast suitable for OCAES; (5) performed a life cycle assessment of power plant and carbon capture technologies for BECCS; and (6) projected the impact of emerging energy technologies on the cost of decarbonized electricity generation. These outcomes further the understanding of each technology and consider their ability to support the transition to a decarbonized electric grid. This understanding contributes to the discussion of what energy technologies should be deployed to meet the climate goals set by the United

Nations. Additionally, the research used and developed open source models and datasets that enable verification of results by third parties and future collaboration.

Dedicated to Lisa and Banga

Acknowledgements

First, I wish to thank my advisor, Dr. Andres Clarens, for challenging me to think big, aim to make a large impact, and seek out interdisciplinary collaboration. I am also grateful to have had the opportunity to co-teach Introduction to Green Engineering with you.

To my committee: to Dr. Lisa Colosi-Peterson for guidance throughout my time at UVA, and challenging me to ask questions, to Dr. Roger Fittro for supporting me cross the boundaries of mechanical and environmental engineering, to Dr. Julie Quinn for helping me think more broadly about the importance of uncertainty results, and to Dr. Eric Loth for helping Juliet and I develop the offshore compressed air energy storage concept, and for giving us the opportunity to present to researchers from the National Renewable Energy Laboratory and National Energy Technology Laboratory.

Next, I would like to acknowledge two other researchers who had a very large impact on my work. To Dr. Joe DeCarolis for teaching me how to use Temoa, and be a better energy system modeler. To Dr. Jeff Fitts for helping me think about the challenges of developing underground energy storage resources.

This work would not have been possible without the help and collaboration of other students. First to Dr. Jay Fuhrman for being a great officemate and for encouraging me to keep running. Thanks to Claire Trevisan for the impetus to research Puerto Rico’s electric grid, to Juliet Simpson for helping analyze and write about OCAES, to Joe Sansalone for his help with Chapter 7, to Dr. Roger Zhu for his help creating the model of Virginia, to Immanuel Ndumbe for helping with plots in Chapter 6, and to Tyler Brown and Haley Neuhoff for their help with Chapter 3.

Thanks to the many other researchers who helped me refine research questions, and write for a broad audience: Dr. Mohammad Abotalib, Nathan Andrews, Dr. Anthony Artuso, Dr. Bevin Etienne, Dr. Gary Koenig, Dr. Cecilio Ortiz-García, Dr. Marla Pérez-Lugo, Dr. Chao Qin, Dr. William Shobe, and Dr. Fu Zhao.

Thank you for the financial support from the University of Virginia including the School of Engineering and Applied Science, Rotating Machinery and Controls (ROMAC) Laboratory, Environmental Resilience Institute, David and Joy Peyton Fellowship and Office of Sustainability. Also, for support from the ASME International Gas Turbine Institute, ASME Turbo Expo Student Advisory Committee and CIRP Life Cycle Engineering Conference.

I could not have done this without the support of my family and friends: to my Mom for helping me stay balanced, to my Dad for teaching me that life is better with pie and chocolate, to Mutti for knowing I could do it, to Vati for encouraging me to pursue research I was passionate about, to Scott for reminding me of the importance of music, to Sea Jeff for always being there to talk shop, and to Colin and Kim for being both the best teammates and adversaries.

To Banga, for providing me company as I wrote the majority of this dissertation, and for reminding me to always take a moment to enjoy the sunny days.

Finally, I would like to thank Lisa for always encouraging me to do my best, and to keep going throughout this endeavor.

Table of Contents

List of Figures

List of Tables

1 Introduction

1.1 Background and Motivation

In 2015, the United Nations agreed to take climate action with the target of limiting global warming to 1.5°C [1]. The Intergovernmental Panel on Climate Change has shown that limiting global warming to 1.5°C will require net zero CO_2 emissions by 2050 [2]. Transforming the electric grid is especially important because 89% of CO_2 emissions are from the consumption of fossil fuel [3], and in the United States, 28% of fossil fuels are used to generate electricity [4]. Eliminating CO_2 emissions from the production of electricity, or decarbonization, is challenging and needs to be done while also considering the other Sustainable Development Goals outlined by the United Nations [2]. The goals of "Affordable and Clean Energy," "Clean Water and Sanitation," and "Industry, Innovation and Infrastructure" are especially pertinent, as decarbonization of the electric grid with today's technology would be expensive, could have large impacts on water consumption, and as demonstrated by severe weather events, needs to be resilient. During the writing of this dissertation, severe weather events in the United States have raised questions about the design of the modern electric grid including the 2017 devastation of Puerto Rico's electric grid due to Hurricane Maria [5], 2019 power outages due to wildfires in California [6], and the 2021 failure of the Texas electric grid due to severe cold [7]. Technological advancements are needed in order to provide affordable, carbon-free and resilient electricity.

Decarbonization of the electric grid is expected to rely largely on renewable energies [2], including wind and solar. Wind turbines and solar photovoltaics (PV) are the least expensive energy generation technologies today [8], and are expected to provide 70% of new generation in 2021 [9]. However, electricity supply must always match demand, therefore the inherently variable generation of wind and solar means that the grid cannot rely on these technologies alone (Figure 1-1). At low deployment levels, diurnal and weather-related fluctuations in solar and wind power generation are balanced by conventional fossil-based generation. At 80% wind and solar deployment levels, Denholm and Hand have projected that enabling technologies such as energy storage and/or demand response are required, and that the remaining 20% of generation would come from dispatchable technologies with fast start times and quick ramp rates [10]. Full decarbonization, as projected with the Integrated Assessment Models used by the Intergovernmental Panel on Climate Change, also rely on fossil fuels with carbon capture and storage, and bioenergy with capture and storage (BECCS) [11].

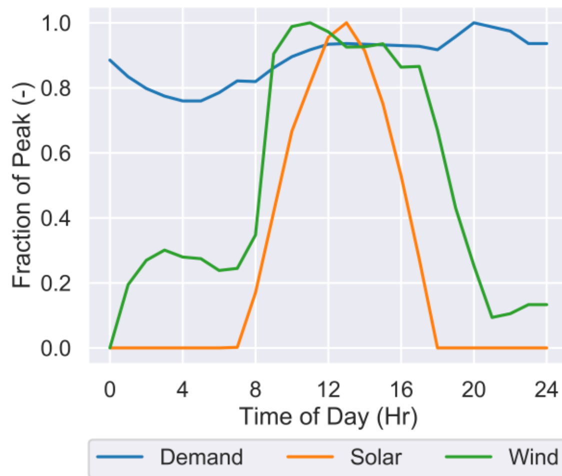

Figure 1-1. Solar and wind generation do not reliably align with electricity demand.

In many regions of the world, the generation landscape is dominated by power plants that are not particularly well suited to balance wind and solar. In the United States, 19% of installed generation capacity came from large coal turbines and 20% came from nuclear plants in 2020 [12], both use steam cycles that are slow to adjust power output. This makes the transition to high deployment of solar and wind power challenging. Gonzalez-Salazar et al. provide a comparison of power plant flexibilities which show that responsive dispatchable generation is limited to open cycle gas turbines and combined cycle gas turbine power plants [13]. It is not understood whether these technologies will be capable of balancing high deployment of intermittent renewables or if advanced power plant technologies are needed as countries transition to decarbonization.

Energy storage enables temporal decoupling of electricity production and consumption [14], which is ideal for the variability of wind and solar power. Long duration energy storage, capable of storing energy for more than 10 hours, has been shown by Dowling et al. to reduce the cost of decarbonization [15]. The most widely investigated forms of energy storage include pumped hydro, flywheels and batteries. Pumped hydro is the most deployed, however the remaining technically and economically feasible sites are limited [16]. Flywheels have seen limited success due to cost and safety concerns [17]. Although the cost of battery energy storage has decreased; they are not well-suited to long duration storage and concerns remain over the toxicity of the construction materials [18]. Energy storage continues to be limited at the grid scale because it is not cost-effective [14], thus alternative are needed.

Power plants with carbon capture and storage are of high interest for deep decarbonization. Carbon capture and storage (CCS) is the process of reducing power plant CO_2 emission and storing the CO_2 in the subsurface. When applied to power plants that use fossil fuels such as coal and natural gas, the result is a power plant with low emissions across the lifecycle of the plant. When applied to bioenergy power plants, the resulting emissions can be negative, meaning that it actively reduces atmospheric levels of CO_2 [19]. With limited deployment to date of power plants with CCS, more research is needed before they can be relied on for deep decarbonization.

Conventional electric grids utilize a centralized architecture, where a major power plant generates electricity that is carried by transmission lines to substations where a distribution system then delivers the electricity to consumers. A single critical failure in a centralized electric grid can lead to widespread power loss [20]. Solar PV and wind turbines are inherently distributed generators; thus, they may be better suited to an alternative electric grid architecture. Therefore, grid architectures also need to be considered in addition to exploring advanced power plants, and energy storage.

1.2 Problem Statement

This dissertation seeks to answer several fundamental research questions related to the feasibility of emerging technologies to enable deep decarbonization of the electric grid while considering impacts on cost, emissions and grid resilience. The motivation behind this work is to identify engineering solutions to climate change that complement low-cost wind turbine and solar PV technologies. Four emerging technologies are considered here; distributed electric grids, supercritical carbon dioxide power cycles (sCO_2), offshore compressed air energy storage (OCAES) and bioenergy with carbon capture and storage (BECCS). These technologies could be implemented separately or in tandem.

1.3 Emerging Energy Technologies

This section provides a review of knowledge gaps with respect to the four emerging energy technologies considered.

1.3.1 Grid Architecture: Distributed Electric Grids

Distributed grid architectures employ widespread generation intermixed with consumers, which provide several advantages over conventional centralized architectures (Figure 1-2). One benefit shown by Jufri et al. is that a distributed grid architecture is less affected by a single point of failure [21]. Other benefits include reduced transmission losses [22], the potential to combine power generation with heating and cooling [23] and reduced construction time through modular designs [24]. Distributed generation also enables the operation of microgrids, which operate independently from the larger grid, and could continue operating even if the larger grid were to shut down [25,26]. Although the modern electric grid is centralized, there are some

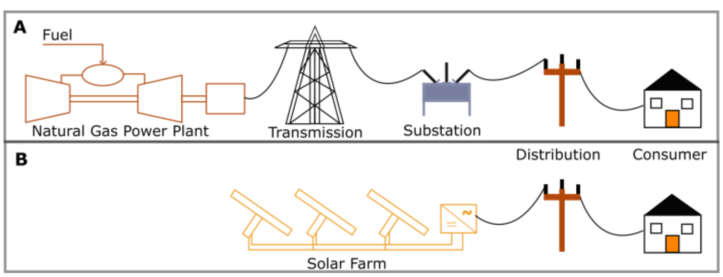

Figure 1-2. Comparison of A) centralized and B) distributed electric grid architectures.

localized applications of distributed grids. Distributed thermal plants face several challenges as compared with centralized plants including generally lower thermal efficiency, inability to share auxiliary systems, and coordinating fuel delivery [27]. Solar and wind energy are naturally distributed power plants; thus, they may be well-suited for a distributed architecture, however they need to be accompanied by a load-balancing technology, and their impact on grid resilience is unexplored.

1.3.2 Load-Balancing: Supercritical Carbon Dioxide Power Cycles

Supercritical carbon dioxide (sCO_2) power cycles offer an alternative to the widespread steam cycles used in coal, nuclear and biomass power plants [28]. sCO_2 cycles use CO_2 in a supercritical state as the working fluid (>74 bar and >31°C) [29]. At these conditions CO_2 is very dense, has a high heat capacity, and very low viscosity, thus it offers the potential for compact machinery, expected to be ten times smaller than conventional steam turbines (Figure 1-3) [30]. Smaller machines could result in machinery that is able to respond more quickly to transient events. Additionally, sCO_2 cycles are projected to be more efficient than steam at firing temperatures greater than 450°C [31]. A variety of sCO_2 cycles have been proposed including the recompression cycle which could be used with any fuel source, and the Allam cycle which is designed to combust natural gas and output pipeline ready CO_2, ready for CCS [32]. Crespi et al. have reviewed sCO_2 cycle configurations for a variety of applications and found that many designs achieve cycle efficiencies greater than 50% [33]. The sCO_2 cycle has been demonstrated at several scales including a 100 kW cycle [34], 250 kW cycle [35], 1 MW turbine tests [36], a 10 MW plant is under construction, expected to start-up in 2021 [37] , and a 300 MW with CCS expected in 2022 [38]. These experiments have so far focused

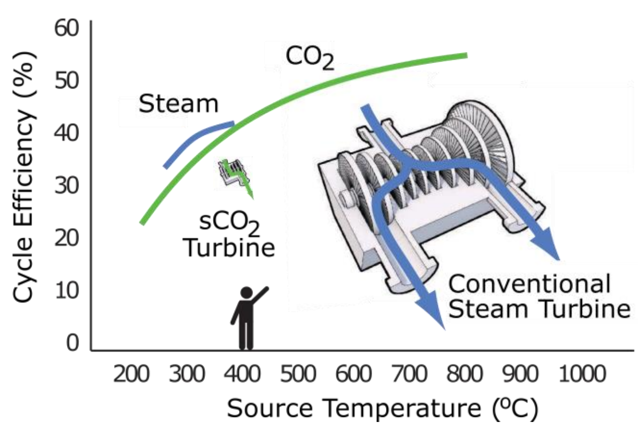

Figure 1-3. sCO_2 cycles are an emerging power plant technology that offers higher efficiency and smaller footprints than conventional steam power plants.

on steady state operation, thus transient abilities remain unproven. sCO_2 power cycles present a variety of challenges for modeling including rapidly changing fluid properties near the critical point and the nature of a closed thermodynamic cycle [39]. Modeling studies have provided predictions of transient behavior [40,41], however they have yet to explore their ability to perform in a dynamically varying electric grid with renewable generation. It is also not understood what role sCO_2 when combined with CCS could play in deep decarbonization.

1.3.3 Energy Storage: Offshore Compressed Air Energy Storage (OCAES)

Compressed air energy storage (CAES) systems operate by storing energy in the form of compressed air and later expand the air through a turbine to produce electricity when generation is required. There are two utility scale CAES plants; a 321 MW plant located in Huntorf, Germany and a 110 MW plant in McIntosh, Alabama [42]. The Huntorf and McIntosh CAES plants operate with a diabatic thermodynamic cycle which requires the use of natural gas for the turbine and store air in an underground solution mined salt cavern [42]. Alternative thermodynamic cycles and storage options have been proposed for CAES that may be more suitable for deep decarbonization, including Offshore Compressed Air Energy Storage (OCAES). OCAES was first proposed by Seymour and was envisioned for storing air in an open-ended container at the bottom of the ocean [43]. Li and DeCarolis showed the techno-economic potential of OCAES using isothermal cycles but did not examine the air storage in detail [44]. Isothermal cycles do not require the use of fossil fuels, and are expected to have much higher efficiencies than diabatic cycles [42]. The limited

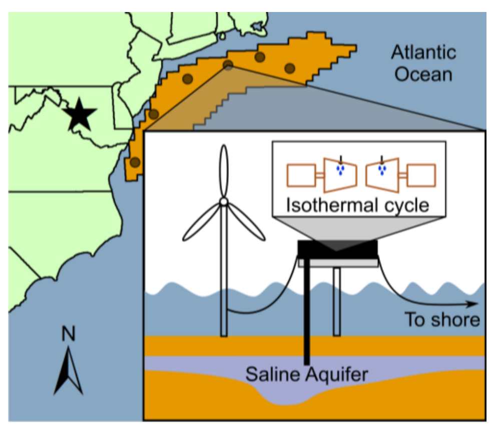

Figure 1-4. Offshore Compressed Air Energy Storage using saline aquifers for air storage and isothermal thermodynamic cycles provide high round-trip efficiencies, use abundant geologic formations and can be co-located with wind farms.

availability of salt caverns [45] has led to investigations into other air storage structures such as abandoned mines, saline aquifers and other porous media in the subsurface [42]. Mouli-Castillo et al. evaluated the potential for OCAES using saline aquifers, but used a diabatic thermodynamic cycle [46]. OCAES systems combining isothermal thermodynamics cycles with saline aquifers for storage have not been investigated (Figure 1-4).

1.3.4 Negative Emissions: Bioenergy with Carbon Capture and Storage (BECCS)

BECCS power plants use a bioenergy crop (for example poplar) for fuel, capture the CO_2 and then store the CO_2 in the subsurface [47]. BECCS power plants have the potential to reduce atmospheric CO_2 levels by temporarily storing atmospheric CO_2 in the bioenergy crop and then storing the captured CO_2 in the subsurface (Figure 1-5). However, if the harvesting and transportation of the bioenergy crop produces excessive emissions then the power plant may not provide negative emissions. Therefore, Stavrakas et al., and others have highlighted the importance of life cycle assessment to determine whether a BECCS power plant is indeed a negative emission technology [48]. Today, there are two BECCS power plants in operation, a demonstration plant in the United Kingdom and a 50 MW plant in Japan [49,50]. Both are retrofitted coal plants. With limited BECCS power plants in operation, it is unknown what the optimal BECCS power plant configuration is, and what the deployment of BECCS will be like as countries decarbonize their electric grid.

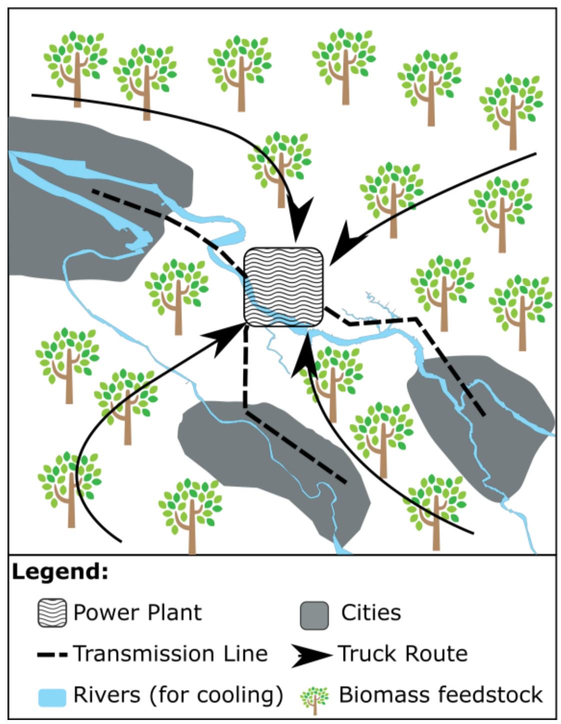

Figure 1-5. Bioenergy with carbon capture and storage (BECCS) power plants store use bioenergy crops as a medium for moving CO_2 from the atmosphere into the subsurface while co-producing electricity.

1.4 Research Objectives and Overview of Dissertation

The emerging technologies considered in this dissertation are at various stages of development, therefore research questions were selected to advance their respective state-of-the-art (Table 1-1). It is understood that energy system planning is not based on technical feasibility alone, thus many of the questions utilize a systems perspective to also consider cost, environmental impact and grid resilience. A secondary goal of this work was to develop open source simulation tools for further development and collaboration with other researchers. The models and datasets used to create this dissertation are available at https://github.com/EnergyModels.

The organization of the dissertation is shown in Table 1-2. Chapters 2 through 5 each evaluate a single emerging energy technology. Chapter 2 presents a novel method for energy system planning that is used to evaluate the resilience of distributed electric grids. Chapter 3 evaluates sCO_2 power cycles for balancing deep deployment of solar and wind. Chapter 4 projects the system performance, cost and value to the grid for OCAES. Chapter 5 estimates the geospatial potential for OCAES in the northeastern United States. Chapter 7 then builds on the work of the previous chapters by using an energy system planning model to investigate the role of emerging technologies. Chapter 7 uses the analysis codes developed for Chapter 2 and represents distributed generation with rooftop solar. The energy system planning of chapter 7 also includes fossil generation with CCS (one type of sCO_2 cycle, Chapter 3), OCAES (Chapters 4 and 5) and BECCS (Chapter 6).

Table 1-1. Research questions addressed in this dissertation.

Question	Chapter	Primary Research Question
1	2	What is the impact of grid topology (distributed vs. centralized) and fuel mix (natural gas vs. natural gas, wind and solar) on costs, emissions and resilience?
2	3	How do existing and proposed advanced power cycles (sCO_2 power cycles) perform delivering load-balancing when integrated into a grid involving high deployment of solar PV?
3	4	What is the techno-economic performance of OCAES?
4	5	What is the geospatial potential of OCAES in the United States Mid-Atlantic?
5	6	What is the environmental impact of carbon capture and power plant technologies for BECCS?
6	7	What is the role of emerging technologies on decarbonization of the electric grid?

Table 1-2. Dissertation organization showing the research questions (Q) and corresponding chapter number (Ch).

<table>
<tr><th rowspan="2">Emerging Technology</th><th colspan="5">Analysis type</th></tr>
<tr><th>Technical performance</th><th>Economic performance</th><th>Life cycle assessment</th><th>Geospatial potential</th><th>Grid planning</th></tr>
<tr><td>Distributed electric grids</td><td></td><td></td><td></td><td></td><td>Q1 (Ch. 2) and Q6 (Ch. 7)</td></tr>
<tr><td>Advanced Fossil (sCO_2)</td><td colspan="2">Q2 (Ch. 3)</td><td></td><td></td><td rowspan="3">Q6 (Ch. 7)</td></tr>
<tr><td>Offshore Compressed Air Energy Storage (OCAES)</td><td colspan="2">Q3 (Ch. 4)</td><td></td><td>Q4 (Ch. 5)</td></tr>
<tr><td>Bioenergy with Carbon Capture and Storage (BECCS)</td><td>Q5 (Ch. 6)</td><td></td><td>Q5 (Ch. 6)</td><td></td></tr>
</table>

2 Extending energy system modelling to include extreme weather risks and application to hurricane events in Puerto Rico[1]

2.1 Summary

Energy system optimization models are used to examine different energy futures and draw insights that inform policy. I present an energy system optimization model that incorporates hurricane risks by combining storm probabilities with infrastructure fragility curves, and demonstrate its utility in the context of Puerto Rico, an island territory of the United States that had its energy system severely damaged by Hurricane Maria in 2017. The model assesses the potential to change grid architecture, fuel mix, and grid hardening measures considering hurricane impacts as well as climate mitigation policies. When hurricane trends are included, 2040 electricity cost projections increase by 32% based on historical hurricane frequencies and by 82% for increased hurricane frequencies. Transitioning to renewables and natural gas reduces costs and emissions independent of climate mitigation policies. This framework can be adapted to other contexts, enabling energy planners to explicitly consider extreme weather risks before making large infrastructure investments.

2.2 Introduction

In many regions of the world, extreme weather events such as hurricanes [51], floods, and wildfires [52] are increasingly impacting the provision of electricity through a centralized power grid. There is increasing evidence that the frequency and severity of these events is connected to changes in the climate system, suggesting this risk will only grow in the coming years [53]. Power grids are susceptible primarily because

---

[1] This chapter was adapted from: Bennett, J.A., Trevisan, C.N., DeCarolis, J.F., Ortiz-García, C., Pérez-Lugo, M., Etienne, B.T., Clarens, A.F., (2021). "Extending energy system modelling to include extreme weather risks and application to hurricane events in Puerto Rico", *Nature Energy*, 6, 240-249.

The published paper and Supplementary Information are available at https://www.nature.com/articles/s41560-020-00758-6 they rely on a centralized architecture that is dependent on a large network of overhead power lines that are vulnerable to weather extremes. A more decentralized grid would reduce the impact of single points of failure on the network [21], increase synergies with district heating [23], and reduce transmission losses [22]. Unfortunately, smaller thermal power plants typically have lower efficiencies and higher costs than larger counterparts [54]. These concerns about efficiency could be overcome by deploying increasingly low cost solar and wind generation, but high deployment of renewables requires storage that would increase costs (Figure 2-1). While *ad hoc* interventions to improve grid resilience have been proposed, these are generally expensive [55] or would increase emissions at a time of growing pressure to cut CO_2 emissions from the power sector [56].

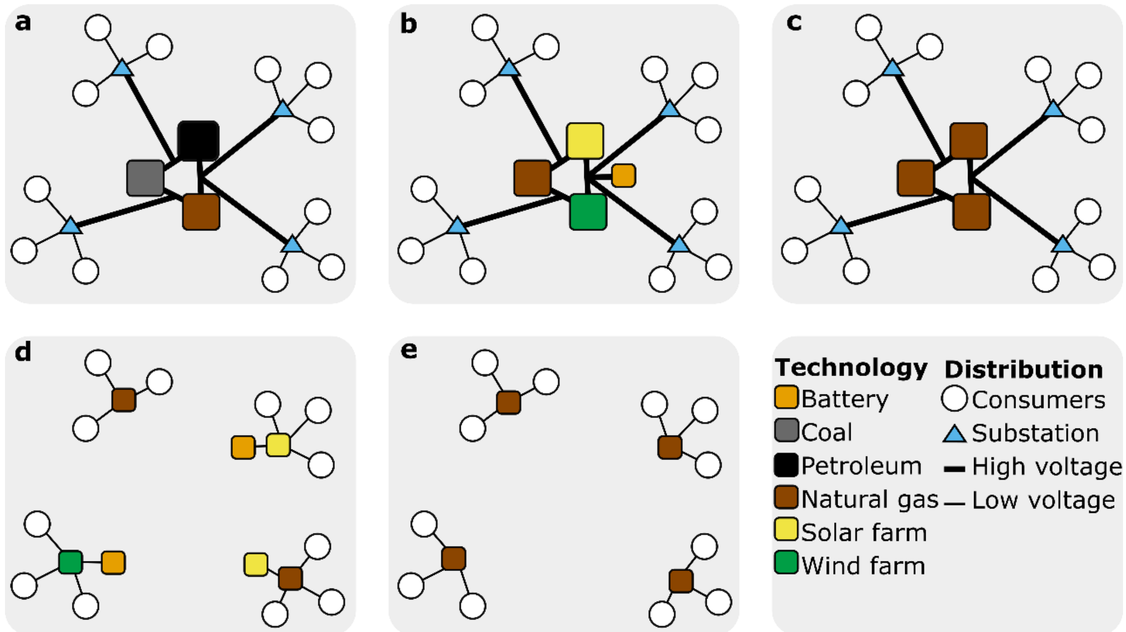

Figure 2-1. Stylized grid topologies reveal some of the choices in grid architecture and power generation facing planners. Here I consider five possibilities: a, business-as-usual (centralized with coal, petroleum and natural gas), b, centralized - hybrid (natural gas, solar and wind), c, centralized – natural gas, d, distributed – hybrid (natural gas, solar and wind), e, distributed – natural gas. High renewable energy deployment requires load-balancing from natural gas or battery storage [57]**. Not shown here is the option to bury power lines in regions subject to extreme weather.**

Quantitative evaluation of these competing objectives is typically performed using energy system optimization models (ESOMs) that use linear programming and stochastic optimization approaches to project power plant capacity investments and dispatch to meet demand over a given time horizon while minimizing cost [58]. ESOMs represent a critical tool to explore power plant investment decisions, including the identification of interactions that are often counterintuitive or difficult to project in the face of uncertainty (Figure 2-2). For example, McCollum et al. considered uncertainty in fuel prices [59] and Spyrou et al. and Patankar et al. considered the possibility of conflict in unstable political regions [60,61].

Recently, effects of climate change have been considered in ESOMs; for example, Perera et al. and Abdin et al. considered heat waves [62,63], Mukhi et al. examined stochastic linear programming to consider flooding uncertainty in Bangladesh [64], and Labriet et al. considered uncertainty of climate mitigation policies and emission impacts [65]. Newlun et al. used a mixed integer linear program to project capacity expansion in Puerto Rico assuming historic hurricane events repeated in a prescribed order once every 4 years and limited the consideration of damage to transmission and distribution lines [66]. However, prior to this study, the explicit consideration of extreme storms within a stochastic optimization framework has not been included in ESOMs, which limits the ability of the models to inform decision making under uncertainty about future storms.

Projecting the impact and cost of storms on energy systems has traditionally been carried out separately from energy system planning. For example, Nateghi et al. projected power outage durations due to hurricanes [67], Winkler et al. estimated storm damage using fragility curves [68], Ji et al. analysed the impact of Hurricane Sandy on New York [53], and Panteli and Mancarella assessed power system resilience [69]. These models provide high resolution details of hurricane impacts for a well-defined energy system, but are unable to help energy system planners project storm impacts for a future grid that does not yet exist.

Here, I develop a method to incorporate extreme weather events and the damage they inflict into ESOMs. The method can be adopted to various extreme weather events such as high winds, flooding, and fires. Here I demonstrate its utility for Puerto Rico’s electric grid considering high winds produced by hurricanes.

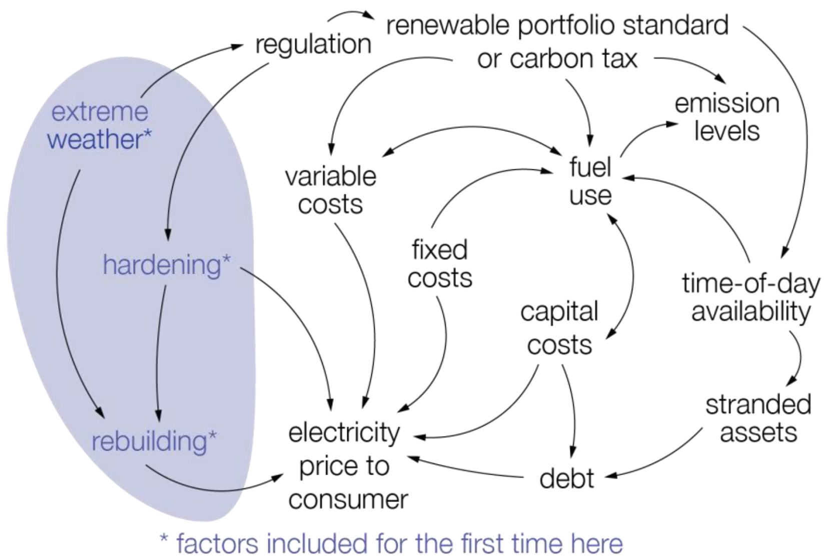

Figure 2-2. Interactions of electric grid planning options. Planners have a large number of factors to consider when selecting investment decisions, and the system-level interactions are not straightforward. This causal loop diagram shows some of the factors that are traditionally considered in these problems and the factors considered here including (1) extreme weather events (2) regulations intended to curb emissions and (3) the availability of renewable generation capacity. These factors have derivative impacts on stranded assets associated with premature retirement of high emissions technologies.

2.3 Puerto Rico and Hurricane Maria

Many of the grid fragility challenges faced by planners were highlighted by Hurricane Maria, which made landfall in Puerto Rico on September 20, 2017. By the end of that day, the Puerto Rico Electric Power Authority (PREPA) reported nearly 100% of their nearly 3.3 million customers without power [5]. Over the subsequent months, it would become the worst blackout in the history of the United States and one of the worst worldwide in terms of customer hours lost [70]. The extensive damage resulted in the majority of the island remaining without electricity for over 6 months [71]. While it is common to think of Maria as an isolated, worst case scenario, Puerto Rico has been hit directly or indirectly by thirteen named storms over the past thirty years [72] and a number of these have caused widespread damage. Maria was particularly destructive because the highest wind speeds were recorded near the population-dense regions surrounding the capital, San Juan (Figure 2-3). Power generation in Puerto Rico is centralized in five locations, so a few critical failures can trigger widespread power loss. Puerto Rico has 6,023 MW of generating capacity [73] and most of the electric infrastructure has exceeded its design life and needs modernization [74,75]. Moreover, because of its remote location, power on the island is very expensive. In 2016, 97% of power generation was produced using imported fossil fuels [76], leading to higher emissions and electricity costs when compared to the mainland United States [77]. However, Puerto Rico is rich in renewable energy resources. Figure 2-3e and 3f show the energy production potential from wind and solar, respectively. Utilizing a fraction of this potential would provide enough energy to power the island residents.

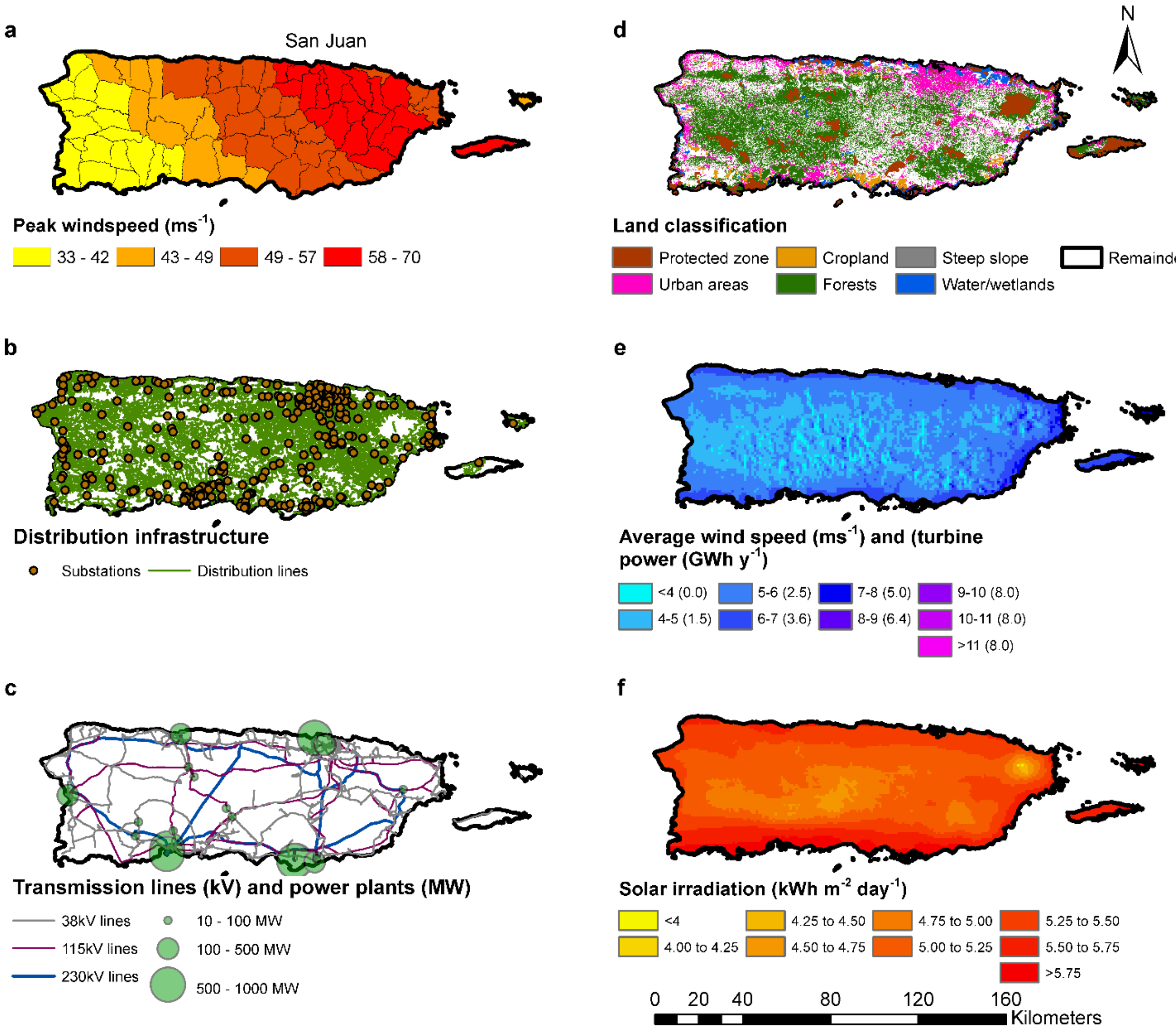

Figure 2-3. Hurricane Maria revealed the vulnerability of Puerto Rico's current electric grid. Here I present maps of a, peak wind speeds during the storm [78], b, distribution networks [79], c, transmission network with power plants [79], d, land classifications, highlighting areas that are excluded from consideration [80,81], e, average wind speeds [82] and corresponding electricity produced by a 2MW turbine in a year and f, average solar irradiation [83]. Data sources and methods used to produce these maps are described in the Methods section.

Puerto Rico is an ideal case study for exploring the effect of grid topology because it is isolated, heavily populated, and vulnerable to extreme weather. Puerto Rico lacks a neighbour with an electric grid that can provide backup or repair crews that can easily assist in times of crisis, and the power system is large enough that there are no silver bullets, e.g., switching to 100% hydropower. In 2019, the Puerto Rico Energy Public Policy Act was passed which included a renewable portfolio standard (RPS) setting 40% by 2025, 60% by 2040 and 100% by 2050 as well as retiring coal power generation by 2028 and goals for electricity to cost less than $0.20/kWh [84]. In addition, Puerto Rico faces economic hardships that make it representative of other regions with limited financial capacity to adapt to a changing climate. The large investment and corresponding long payback time of electric infrastructure also means that today's design decisions will lock Puerto Rican infrastructure in for decades amidst a rapidly changing energy landscape in which the prices of natural gas, renewable energy, and energy storage are decreasing rapidly [85].

2.4 Extending energy system modelling tools

Here I propose an energy system model that explicitly incorporates projected hurricane risks to inform investment decisions. I use the open source Tools for Energy Model Optimization and Analysis (Temoa) to examine grid design and operation over time [58], an ESOM model similar in structure to MARKAL/TIMES [86], OSeMOSYS [87], ReEDS [88] and IPM [89]. Temoa uses linear optimization of installed technology-specific capacity and dispatch to minimize costs subject to a range of a constraints, including time-of-day resource availability. This study considers, within an ESOM, the potential damage to infrastructure associated with future storm events and the impact those storms would have on investment decisions today. Cases representing policy decisions are simulated through a scenario tree using stochastic optimization (Figure 2-4) that delineates storms into three components: impacts, probability and severity. For this analysis, scenarios are defined as an individual path through the tree, and cases as all possible scenarios for a given set of conditions. Extreme weather impacts are based on the storm type. For a hurricane, most damage comes from high winds and/or flooding. To model the impacts of Hurricane Maria, I focused on high winds but the model is easily extended. The probability of a hurricane occurring was quantified probabilistically using historical data (detailed in Supplementary Note 6). I binned historical storms and their strength into three levels to simplify simulations. Severity was quantified in terms of peak wind speed. Over the past 25 years, Puerto Rico has experienced nine Category 1 hurricanes or tropical storms/depressions with an average peak wind speed of 10 m/s, two Category 2-3 hurricanes with an average peak wind speed of 51 m/s, and two Category 4-5 hurricanes with an average peak wind speed of 69 m/s [72]. Based on data for the past 25 years, I built a probabilistic distribution for the strongest storm to hit the island over 5-year intervals, which are the time periods represented within the model. The possibility that a Category 1 or lower storm will be the strongest in a future 5-year interval is 52%, the possibility that a Category 2-3 storm will be the strongest is 32%, and the probability that a Category 4-5 storm will be the strongest is 16% [72].

I incorporated a second level of uncertainty into the model by adjusting the hurricane probabilities based on the anticipated influence that climate change will have on storm frequency. Grinsted et al. has projected a 2-7 times increase in severe storm frequency for 1°C of warming [90], and Staid et al. considered adjusting historical storm frequencies by 0.5-4 times in projecting tropical cyclones in the United States [91]. Knutson et al. shows that projections of Category 4-5 storms are expected to increase 10% on average in the North Atlantic, but could be from -75% up to +697% [92]. To account for this increased frequency, I include an "increased storm frequency" case, which runs the model under constant future climate risks that assumes the probability of a Category 4-5 storm would triple to 48%, the chance of a Category 2-3 would remain at 32%, and a Category 1 would represent the remainder of occurrences.

A scenario tree was used to assess the possible combinations of storm events over a 25-year time horizon (Figure 2-4b). Each node represents a 5-year period. All scenarios start with no storm event (2016-20) and operate with infrastructure existing in Puerto Rico in 2016, including overhead power lines and predominantly fossil-fuel power plants. Scenarios then proceed to a branch with its assigned probability representing either a Category 1, 2-3 or 4-5 hurricane where average wind speeds are correlated to infrastructure damage. The ESOM then optimizes the operation of the remaining undamaged infrastructure and builds new infrastructure accordingly to meet electricity demand.

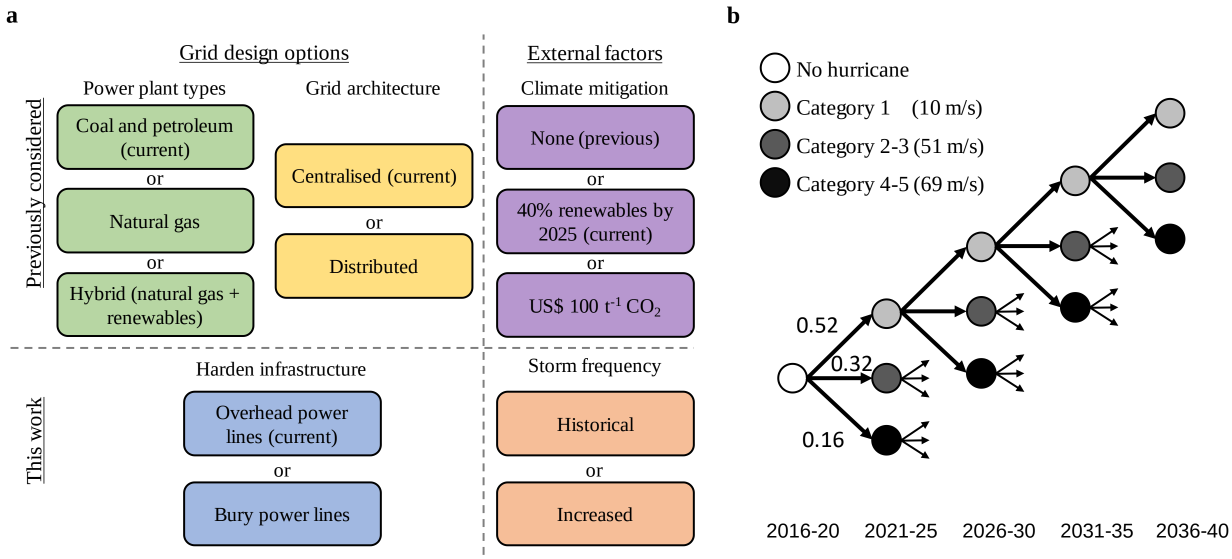

Figure 2-4. Overview of framework for grid planning with extreme weather. All stochastic optimization runs start with existing power plant capacity and build-out capacity from options available within each case to meet demand over a 25-year time horizon. a, Cases are developed for each permutation of the three grid design options (power plant types, grid architecture, and infrastructure hardening) and external factors (climate mitigation and storm frequency), as well as a case with all technologies available (no policy decision). b, Scenarios face varying storm severities every five-years throughout the time horizon. During the first time period there are no hurricanes and each subsequent period experiences a hurricane of three possible severity levels (Category 1, 2-3 or 4-5). The probability of no hurricane within a five-year period is sufficiently close to zero, so it was excluded. The probability of each severity level depends on the scenario's storm frequency (historical or increased); historical probabilities are illustrated above. There are 81 possible combinations of hurricanes associated with each case.

The damage caused by a storm is dependent on the fragility of infrastructure. A class of functions called fragility curves are used to estimate component damage based on a given threat. Several classes of grid fragility models have been developed including simulation-based, analytical, and statistical, each with different data requirements [93]. Here, a combination of historical and probabilistic fragility curves were selected to correlate storm wind speeds to infrastructure damage used in studies by Ouyang et al. [94], Winkler et al. [68], and Watson [95]. Projected storm wind speeds are mapped to the fragility curves to quantify the amount of damage, which is treated as unusable capacity. Figure 2-5 shows the relationship between wind speed and damage for a variety of components within the power grid. The impact of high winds varies with the type of infrastructure. The majority of power lines in Puerto Rico are overhead, making them very susceptible to hurricane Category 2-3 and higher wind speeds. The distribution lines are the most fragile component in the system, in line with findings from Ji et al. [53].

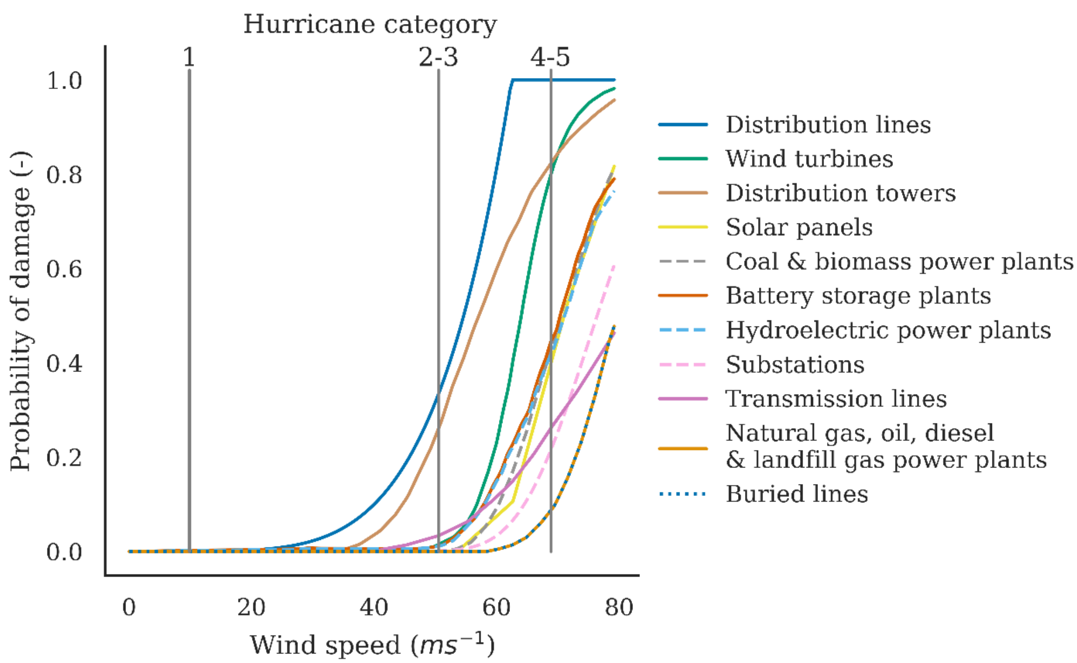

Figure 2-5. Technology fragility curves. Fragility curves for each technology show the amount of damage expected for each of the three hurricane severities possible in each model year. Storm damage is represented as a fraction of existing capacity that is no longer useable to meet demand.

2.5 Hurricane impacts on cost, emissions, and fuel use

Stochastic optimization was used to find the least cost means of providing electricity from all technologies, grid architectures, and grid hardening options considered here. Figure 2-6 presents electricity costs, emissions, and technology activity across nine cases representing different storm frequencies (none, historical and increased) and climate mitigation policies (no policy, US$ 100 t^{-1} CO_2, RPS including 40% by 2025 and coal retirement by 2028). Given the scenario tree shown in Figure 2-4, there are a number of conditional pathways based on the possible realized storms at each time stage. Thus, the results shown for 2036-2040 include 81 leaf nodes for each case considered. Adding hurricanes greatly increases cost projections. By 2040, cost projections under the RPS increase relative to the 'no storms' scenario on average by 32% for historical storm frequency and 82% for increased storm frequency, with maximum projected costs 153% increased. In all cases, projections of electricity costs (Figure 2-6a) show a short-term decrease, as the grid moves away from imported fossil fuels, only to rise over time, as future storms require that infrastructure be rebuilt following storms. The uncertainty of these forecasts increases over time, as the order and severity of hurricanes varies across scenarios. Scenarios with only Category 1 hurricanes result in the minimum values and those with only Category 5 hurricanes the maximum values; by 2040 there is two times difference. Increased storm frequency shifts the cost distributions upwards such that outlier conditions become the new average cost over the coming two decades. Emissions significantly decrease across all cases, most quickly under a carbon tax.

The investment decisions of the optimized case can be seen in Figure 2-6c, which shows the fuel use, grid architecture, and grid hardening measures (i.e. burying transmission and distribution lines) with and without climate mitigation policies. The fuel mix results suggest that the least cost option for Puerto Rico is to move rapidly away from coal and petroleum to solar, wind and natural gas for load balancing. Despite the potential for stranding assets, i.e., the premature retirement of power generation capacity due to fleet wide carbon constraints, all cases significantly reduce coal and petroleum usage by 2021-25. Implementation of the RPS and carbon tax reduces natural gas use in favor of wind.

Grid architecture was compared by grouping power plant activity based on architecture (centralized vs. distributed) and fuel type (fossil or renewable) in the middle row of Figure 2-6c. All variations start with the majority of fuel use coming from a centralized grid with predominantly fossil generation representing the current grid configuration. As storm frequency increases, the fraction of fossil fuel energy decreases and the grid tends to be built-back in a more distributed fashion. The trade-off of centralized and distributed fossil power can be attributed to a balance of lower cost and higher efficiency centralized natural gas plants coupled with storm-prone transmission systems. Conversely, centralized and distributed solar and wind power are both based off of modular utility-scale technology (i.e. single-axis tracking solar and 2.3 MW wind turbines), so they have the same installation costs, but only centralized has the transmission system. Under the presumed cost of buried lines, which is 14 times higher than overhead lines, their cost is not justified under the storm conditions modelled here (Figure 2-6c).

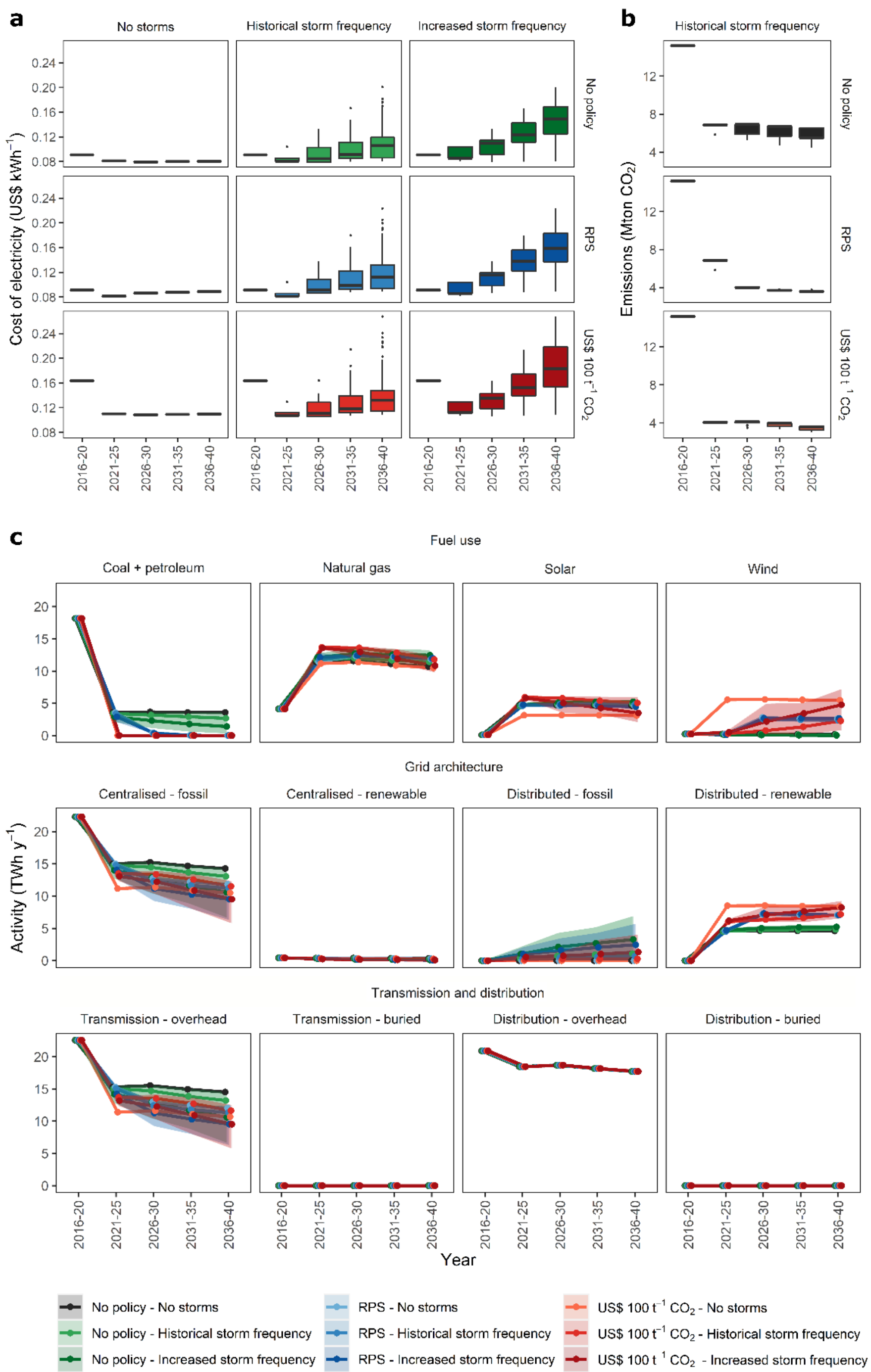

Figure 2-6. Projections of electricity costs, emissions and activity for stochastic optimization including reconstruction after severe weather events. Here I show a, electricity costs, b, emissions and c, activity when all technologies are available. Box edges (a and b) indicated the 25th and 75th percentiles, the box centre the median, and whisker edges represent the extent of the distribution with outliers indicated as points. Shading in c indicates the minimum and maximum values for each simulation. The carbon tax is included in the cost of electricity.

Five additional cases were considered to help understand model sensitivity and identify a suitable grid planning policy: (1) business-as-usual (centralized grid architecture with coal, petroleum and existing natural gas); (2) centralized grid architecture using natural gas and renewable power generation hybrids; (3) centralized grid architecture using natural gas power generation; (4) distributed grid architecture using natural gas and renewable power generation hybrids; (5) distributed grid architecture using natural gas power generation. To understand the economic and environmental trade-offs, Figure 2-7 presents costs and emissions for all cases considered with overhead power lines. I also show the impact of setting the RPS and a carbon tax. The RPS eliminates the business-as-usual and centralized/distributed natural gas cases.

Cost projections suggest that a business-as-usual strategy, which relies on a centralized electric grid fueled by petroleum and coal, will always result in the highest cost. The proposed alternatives to the current grid architecture will lower the cost of electricity. Further, it is not expected that the RPS will significantly increase costs. Increased storm frequency and the carbon tax shifts costs upward across all policies. The difference in anticipated electricity cost under historical storm frequencies is small between the centralized and distributed cases, but increases with storm frequency. As storm frequency increases, distributed electric grids begin to show decreased costs with less variance. This demonstrates that the benefits of distributed generation become apparent under increased storm frequencies when the cost of hurricane rebuilding is included. Based on existing fragility curves for solar panels and wind turbines, renewable energy generation is resilient, however future work could further refine fragility curves to be specific to Puerto Rico.

In line with the energy use, emission projections show that business-as-usual conditions always result in the highest emissions and costs. The 'all technologies' case always has the lowest emission levels suggesting that it is possible to significantly reduce emissions while having cost-competitive electricity prices. Storm frequency does not have a significant impact on emission levels, suggesting that less carbon intensive energy technologies are financially competitive even with increased severe weather events.

Emission differences between the centralized and distributed systems can be attributed to the higher efficiencies of centralized thermal power plants.

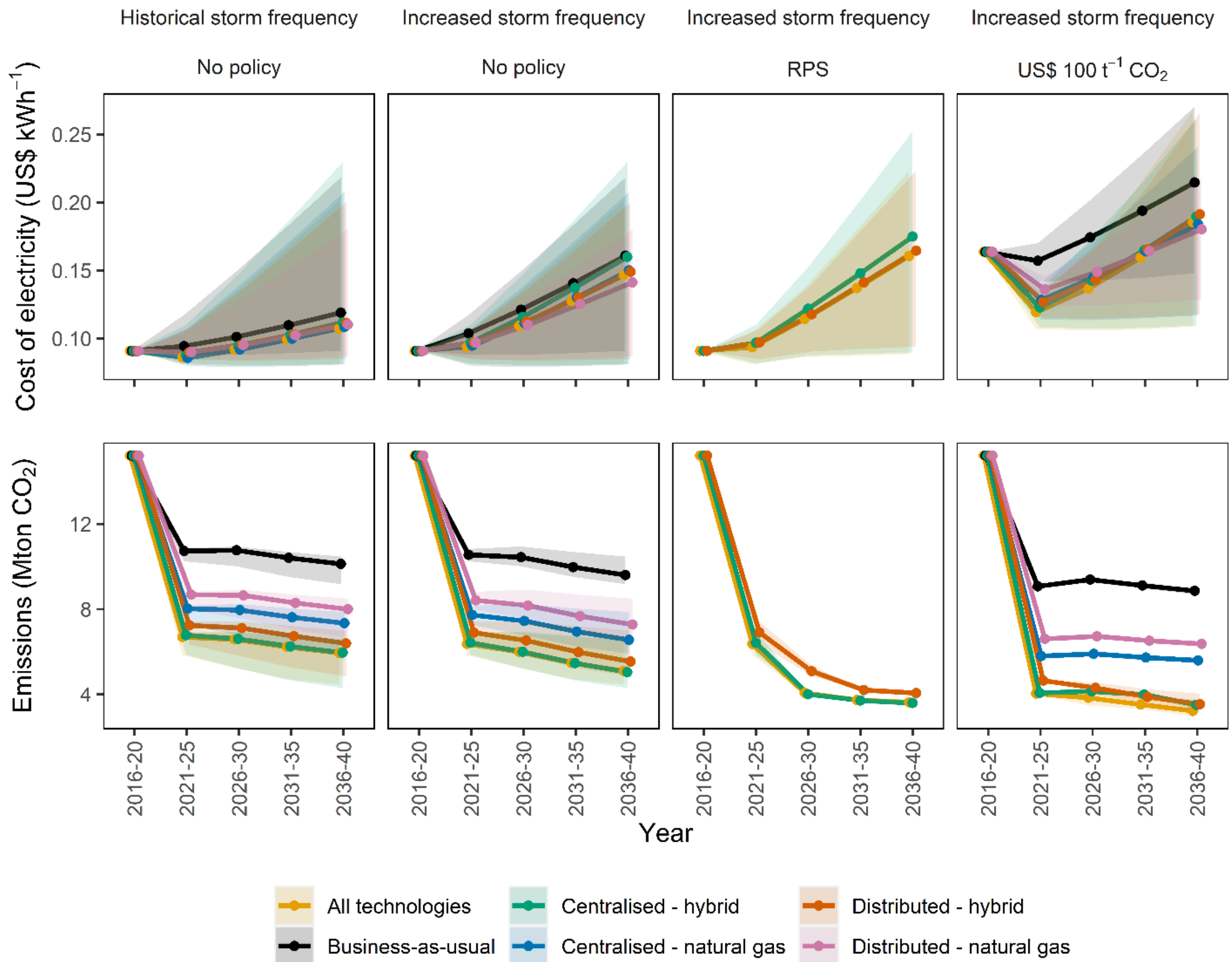

Figure 2-7. Projections of electricity costs and emissions for case-based simulations. Electricity costs and emissions are compared for cases with overhead power lines. Results are colored by combination of grid architecture and fuel mix, and then grouped by combinations of storm frequency (historical vs. a climate-induced increase in frequency) and renewable portfolio standard (none vs. 25% by 2025 with coal eliminated by 2028). Shading indicates the minimum and maximum levels projected across all scenarios within each case. The carbon tax is included in the cost of electricity.

2.6 Discussion and conclusions

Many regions of the world are vulnerable to extreme storms that may become more severe and frequent as a result of climate change. Here, I present an ESOM that explicitly incorporates the expected wind damage to electricity infrastructure caused by hurricanes to evaluate grid design alternatives. Puerto Rico, a hurricane prone territory of the United States, is grappling with how to make investments to modernize its electric power grid in the wake of a devastating 2017 hurricane. The results identify several planning alternatives that could reduce costs and improve resilience for the people of Puerto Rico. Transitioning to an electric grid fueled by a mix of natural gas and renewables significantly reduces costs and emissions, independent of the implementation of a 40% by 2025 renewable portfolio standard.

Under my assumptions about damage, distributed grid architectures cost less than centralized grids for increased storm frequencies. Further research into electric infrastructure fragility curves for ESOMs and consideration of spatially explicit topologies could provide additional insight, particularly for meshed transmission networks used in many regions The model does not consider the provision of the United States Stafford Act of 1988, which requires that infrastructure be replaced as it previously was before a storm [96], which makes it difficult for Puerto Rico to make their grid more resilient after a storm. The cost of power outages caused by hurricanes were also not considered in the model, and could be considered for future work. This modelling platform can be extended to other weather extremes by collecting event probabilities and fragility curves. This work suggests that energy planning decisions change when different climate scenarios are studied related to extreme weather and climate mitigation through either a carbon tax or RPS policy, which could result in less expensive and more resilient power systems.

2.7 Methods

2.7.1 Energy System Optimization Model

I used the open source Tools for Energy Model Optimization and Analysis (Temoa) to perform stochastic optimization. Because the model is open source, it enables third party replication of the results. The objective function of Temoa minimizes the present cost of total system-wide energy supply. The full algebraic formulation for Temoa is well-documented in Hunter et al. [58], with updates to the formulation provided in the model documentation [97]. Briefly here, the costs considered include capital costs, operation and maintenance (O&M) costs, and fuel prices, but excludes loan payments on capacity installed prior to the start of the model time horizon in 2016. New plants are purchased via a loan that lasts either the lifetime of the plant or 30 years, whichever is less, and with an interest rate equal to the model's discount rate of 9% [98]. The levelized cost of electricity is estimated by normalizing total annual costs by electricity demand.

Temoa performs capacity expansion over a set of user-defined future time periods that usually extend several decades into the future. For this work, the model time horizon starts in 2016 and extends to 2040 in five-year periods defined at 2016, 2021, 2026, 2031 and 2036. Stochastic optimization resolves hurricane uncertainty in the latter four periods. System level inputs are summarized in Supplementary Note 3.

The model optimizes a representative year within each time period, and therefore all years within the same time period are assumed identical. To capture sub-annual variations in energy supply and demand, each year is broken down into a set of seasons and times-of-day within each season, forming a set of time slices over which supply and demand must be balanced. Energy system optimization models must balance the number of time periods with computational run time. Teichgraeber et al. found that increasing the number of time periods improves the model accuracy, but that it is more important to include extreme time periods [99]. In this study, I use a capacity reserve margin to capture time periods of high demand and extreme weather events are considered in-between model years through stochastic optimization.

For a Caribbean island like Puerto Rico, seasonal variability is relatively small with two main seasons. To represent the variability of renewable resources, the model includes two typical days per year, one for the wet season, and one for the dry season. Each typical day is broken into 24 segments, to represent hourly wind and solar availability as well as electricity demand, which are estimated with historical data as described in the Supplementary Note 3. Upper bound capacity factors are included for solar and wind power plants, which ensure that generation within a given year is constrained. Here, I use forty-eight time segments (two days in twenty-four hour periods) to provide insight into renewable resource variations while balancing the computational demand of stochastic optimization to consider the probabilities of extreme weather events.

Our implementation of Temoa performs multi-stage stochastic optimization extending the two-stage cost optimization approach used by Mavromatidis et al. [100]. Across the model time horizon, different scenarios (i.e. pathways through the scenario tree) correspond to different combinations of three hurricane severities that can occur in each time period. Optimization is performed to decide how to rebuild the grid after hurricane damage. New generating capacity is built to compensate for capacity no longer available due to hurricane damage. Transmission towers, substations, distribution lines and distribution towers are also rebuilt in order to meet demand in future time periods. The model does not include specific network connections, so I do not evaluate reconstruction time or grid security metrics.

2.7.2 Electric Grid Characterization

GIS data from the Government of Puerto Rico was analyzed to tabulate the total length of transmission and distribution lines as well as number of substations, shown in Supplementary Table 1 [79]. For the energy system optimization model, it is assumed that this infrastructure will not be replaced, instead it would be repaired if there is damage from a hurricane. Repair costs along with typical pole spacing is from Ouyang et al. [94]. Substation repair cost is based on moderate damage.

The ESOM presented here considers the Puerto Rico electric grid in aggregate without an explicit spatial representation. Representing in aggregate reduces the computational demand. It is also appropriate, because the electric network topology in 10-20 years may be very different than today. In my model, power plants are linked in series with demand through transmission and distribution lines. Centralized power plants send electricity through the transmission lines and through substations before entering the distribution system, which consists of distribution towers and distribution lines. The inclusion of both distribution towers and lines allows the model to separately consider the extreme weather damages to both of these components. Distributed power plants bypass the transmission and substation components and send electricity directly into the distribution system. In addition to maintaining power generation capacity, the model also maintains sufficient transmission and distribution system capacity to deliver electricity. The model also has a reserve margin constraint to ensure that additional capacity exists in case of operational failures, further detailed in Supplementary Table 9.

2.7.3 Renewable Resource Evaluation

To provide a realistic limit of available solar and wind energy resources for the energy system optimization model, a GIS-based evaluation was performed, following an approach developed by the International Renewable Energy Agency (IRENA) [101]. This approach first determines land tracts that are viable for building wind and solar power plants. Digital elevation models (DEM) were used to calculate the slope of the land, and only areas with a slope less than 45 degrees were used. DEM data was taken from the HydroSHEDS dataset [102]. Next land cover data from the 0.5 km MODIS-based Global Land Cover Climatology dataset [80] was used to identify regions that were free of forest, cropland, waterbodies and urban development. The cropland restriction is only applied to solar resource potential, not wind. Protected zone data from [81] was used to exclude additional areas not suitable for development. After the exclusion zones were developed, wind and solar resources were combined with assumptions about spacing and efficiency to project the maximum yearly potential. Average wind speed data was taken from the DTU

Global Wind Atlas [82], and average solar (global horizontal irradiance) data was taken from SOLARGIS [83]. An empirical correlation from Hoogwijk et al. [103] was then used to estimate the yearly amount of electricity produced based on the average wind speed. The renewable resource evaluation model was implemented in a Python script for use with ArcMap v10.6 and is available for download at https://github.com/EnergyModels/RenewableResourceEval.

The total estimated wind resources are 20.9 TWh y^{-1} and total solar resources are 205 TWh y^{-1}. In an NREL study, it was estimated that Puerto Rico has the capacity potential for 0.84 GW (1.84 TWh y^{-1} at 25% capacity factor) of onshore wind power and 1.1 GW (2.11 TWh y^{-1} at 22% capacity factor) of solar power available [104], however it is not clear what method was used to make these estimates. For comparison, the 2016 power plant capacity of Puerto Rico was over 6 GW. Also, Puerto Rico's 2019 Integrated Resource Plan explored installing up to 4.1 GW of solar power [105]. Based on my estimates, Puerto Rico has adequate renewable energy potential to meet existing demand. These estimates were included in the energy system model as resource limits, shown in Supplementary Table 5.

2.7.4 Input Dataset for Puerto Rico

The general methodology for collecting data was to first collect data from Puerto Rico sources including PREPA [106] and PREC [76]. When Puerto Rico specific data was not available, data was taken from NREL [107], US EIA [108], and IEA-ETSAP [109]. When possible, the same source was used for the same type of data, i.e. the majority of new plant costs and capacity factors were taken from 2020 Mid projections from the NREL Annual Technology Baseline (ATB) [107].

The centralized and distributed power plants were selected to represent utility-scale installations of varying capacity. Centralized natural gas power plants were based on a 1 GW combined cycle plant, and a 500 MW open cycle plant to represent state-of-the-art utility-scale gas turbine technology. Distributed natural gas plants were based on a 200 MW combined cycle plant and a 100 MW open cycle plant to represent medium utility-scale gas turbine technology. Both centralized and distributed solar installations are simulated as utility-scale based on a 23 MW, single-axis tracking system. Similarly, centralized and distributed wind power is based on utility-scale 2.3 MW wind turbines in a 50-100 MW facility. Batteries are simulated as having 4 hours of storage [107]. It is expected that the installed capacity of solar and wind farms would be larger in the centralized case, but would still be classified as utility scale by the NREL ATB.

The model utilized fuel price rate increases based on price rate increases from the baseline projection by the US EIA [108]. Wind and solar capacity factors are from Puerto Rico's Integrated Resource Plan [105]. Model data is summarized in Supplementary Notes 2 and 3.

2.7.5 Model Verification

To verify the model results, fuel resources used in the first model year, 2016, were compared against actual usage recorded by the Autoridad de Energía Eléctrica in 2016 [76]. Cases are limited to using existing capacity in 2016. All projections of actual energy use are within 2.1 percentage points, as shown in the Supplementary Note 4.

2.7.6 Selection and Usage of Fragility Curves

Fragility curves for critical infrastructure were taken from a combination of historical and probabilistic fragility curves that correlate wind speeds to outages. Ideally, fragility curves would be specific to the region they are applied, but because no curves exist for Puerto Rico, a review of literature was used to find curves that fit best under similar conditions. Much of the infrastructure in Puerto Rico is aging - most of it has exceeded its design life [74,75]. Transmission line fragility curves were based on a computational analysis of United Kingdom transmission towers [110]. Fragility curves for the distribution towers and lines were based on work by Quanta Technology and also used by Ouyang et al. and Watson [94,95,111]. Substation fragility curves were based on HAZUS data for suburban terrain tabulated by Watson [95,112]. Solar panel fragility curves are based on a performance based approach by Goodman of a residential system [113] with a modification proposed by Watson [95] to better represent utility scale solar installations. Wind turbine fragility comes from an estimate of the impact of hurricanes on offshore wind turbines by Rose et al. [114]. These curves are based on hub height wind speeds of 90m, so a study by Franklin et al. was used to relate wind speeds at this height during a hurricane [115].

When fragility curves were unavailable for a type of power plant I followed Watson's use of building functions from HAZUS [95,112]. Based on Watson [95], natural gas and coal plants are represented by the HAZUS damage functions SECBM (Steel Engineered Commercial Building, 3-5 stories) and SECBH (Steel Engineered Commercial Building, 6 or more stories), respectively [95,112]. It is expected that oil, diesel and landfill gas plants are similar in size to natural gas plants, so SECBM was also used for these technologies. Biomass plants are expected to be similar in structure to coal plants, so SECBH was selected. The same family of HAZUS damage functions are used to represent hydro plants by CECBL (Concrete Engineered Commercial Building, 3-5 stories) and batteries by SECBL (Steel Engineered Commercial Building, 1-2 stories). Fragility curve values for each technology are tabulated for each storm condition in the Supplementary Table 14.

Fragility curves represent the failure probability of the *i*th component [94]. They assume that a piece of equipment is either useable or unusable. However, the ESOM is a linear program that does not track components individually. Instead, the ESOM determines the optimal capacity of a given technology. For example, 200 MW of gas turbines could refer to any number of plant configurations such as one 200 MW plant or two 100 MW plants. Therefore, I assumed that the fragility curve could be used to estimate the remaining operable infrastructure capacity following a hurricane,

$$X_{t,n} = X_{t,n-1} \cdot \left(1 - p_f(w_s)\right) \tag{2-1}$$

where $X_{t,n}$ is the operable capacity of technology t during the nth model year, $X_{t,n-1}$ is the operable existing capacity of technology t during the previous model year, p_f is the probability of failure from the fragility curve, and w_s is the peak hurricane wind speed of the nth model year. This approach assumes that all electrical infrastructure is identically and independently distributed with the probability of being unusable taken from the fragility curve. Because calculations are performed on a capacity basis instead of a component basis, it is possible that a fraction of a single power plant could be damaged. This outcome can be interpreted as the need for significant repairs in order to resume output at the original capacity. After the ESOM uses the fragility curves to assess the amount of capacity that is undamaged and still operable, it then finds the least cost means to meet demand, using the remaining operable capacity and deploying new capacity as required. With this simplified approach, within a given year, the model can choose to replace the amount of capacity that was damaged or build capacity of a different type. The model does not separately report costs for repairing damaged capacity from new capacity installations.

2.7.7 Benefits and Costs of Grid Hardening

I considered one form of grid hardening, burying power lines. Burying power lines has the benefit of greatly reducing susceptibility to wind damage. Therefore, I assumed that buried power lines would have a fragility curve equivalent with the most robust curve considered, which was the SECBH curves used to represent natural gas power plants.

Based on a report prepared by Hall for the Edison Electric Institute, burying transmission lines is estimated to cost 3,780 thousand US$ per km [116], or a total of 14 billion US$. In comparison, replacement costs from Ouyang et al. for downed transmission lines is 400 thousand US$ per pole [94], with poles spaced every 0.23 km [94] or a total of 6.4 billion US$ (2 times higher to bury). Burying distribution lines is estimated to cost 850 US$ thousand per km [116] or a total of 22 billion US$. In comparison, replacement cost for downed distribution lines (tower and conductor) is 4.0 US$ thousand per 0.042 km [94] or a total of 2.4 billion US$ (14 times higher to bury).

2.7.8 Data Availability

To enable replication of my work, the model, input dataset, and analysis code is open source and available for download at https://doi.org/10.18130/V3/QB0NPX. This includes the Python package and all scripts used to instantiate Temoa, run the analyses, and create the plots in this article, which are also available for download at https://github.com/EnergyModels/temoatools. All model inputs are summarized in Supplementary Notes 2 and 3.

2.8 Chapter Acknowledgements

Support for this work came from the University of Virginia Environmental Resilience Institute and the Rotating Machinery and Controls Laboratory. Thanks to Research Computing at the University of Virginia for providing computational resources and technical support that have contributed to the results reported within this publication. URL: http://rc.virginia.edu

2.9 Chapter Author contributions

J.B., C.T., J.D. and A.C. designed the research. J.B. and C.T conducted the literature review and data collection. J.B. performed the analysis. J.B. and A.C. created the figures. J.D. supported model development and implementation. C.G., M.L., and B.E. provided feedback on the scenarios and framing. J.B., J.D. and A.C. wrote the manuscript.

3 Feasibility of Using sCO_2 Turbines to Balance Load in Power Grids with a High Deployment of Solar Generation[2]

3.1 Summary

Solar photovoltaic power generation capacity is growing rapidly, increasing the need for dynamic load balancing when solar production dips. This balancing might be delivered using energy storage and/or advanced power generation cycles, that are compact, dynamic, and highly efficient, such as supercritical carbon dioxide (sCO_2) cycles. Here, the load balancing capability of a sCO_2 combined cycle plant was compared to open cycle and steam combined cycle gas turbines. A characteristic-based transient model was developed to evaluate the impact of machinery ramp rates, minimum part loads, and cycle efficiencies. High resolution demand and solar irradiance data from the University of Virginia, before and after installation of a major solar project, was used to represent low and high levels of solar deployment in the grid. The results suggest that under high deployment of solar power, sCO_2 cycles and steam combined cycle systems with ramp rates greater than 5.75%/min can balance load and provide comparable levelized costs of electricity ($0.057/kWh). Solar curtailment was driven by the minimum part load capabilities. A sCO_2 cycle with a minimum part load of 30% was predicted to have a curtailment of 15% in the high solar scenario without a battery, and 4% with a 30MWh battery.

---

[2] This chapter was adapted from: Bennett, J.A., Fuhrman, J., Brown, T., Andres, N., Fittro, R., & Clarens, A.F. (2019), Feasibility of Using sCO_2 Turbines to Balance Load in Power Grids with a High Deployment of Solar Generation, *Energy* 181(15), 548-560.

The published paper and supporting information are available at https://doi.org/10.1016/j.energy.2019.05.143

Table 3-1. Abbreviations.

CCGT	Combined Cycle Gas Turbine
CO_2	Carbon Dioxide
DHI	Direct Horizontal Irradiance
DNI	Direct Normal Irradiance
EIA	Energy Information Agency
GE	General Electric
GHI	Global Horizontal Irradiance
HRES	Hybrid Renewable Energy Systems
LCOE	Levelized Cost of Electricity
NREL	National Renewable Energy Laboratory
OCGT	Open Cycle Gas Turbine
O&M	Operation and Maintenance
PV	Photovoltaic
sCO_2	Supercritical Carbon Dioxide
UVA	University of Virginia
VPP	Virtual Power Plant

Table 3-2. Nomenclature.

A_2, A_1, A_0	Off-Design Efficiency Coefficients
C	Capacity
E	Energy
F	Fuel Costs
I	Investment Costs
L	Power Plant Load (%)
M	O&M Costs
N	System Lifetime
P	Power
$\dot{P}$	Ramp Rate
Q	Emissions factor
R	Discount rate
V	Present Value
ΔT	Model time step
η	Efficiency

Table 3-3. Subscripts.

B	Battery
D	Demand
F	Fixed
MAX	Maximum
MIN	Minimum
NG	Natural Gas Power Plant
NGLS	Natural Gas Power Plant Load Shed
PV	Photovoltaic
PVC	Photovoltaic Curtailment
REQ	Requested
V	Variable
Y	Year

3.2 Introduction

Natural gas and solar-based power production are the two fastest growing sources in many regions of the world. In the U.S. state of Virginia, installed natural gas capacity grew 47% over the past 5 years, and solar-based capacity grew from negligible levels to 406 MW, but the absolute installed capacity of solar photovoltaic (PV) power is still relatively small, accounting for only 0.35% of statewide consumption in 2017 [117] (Figure 3-1). The intermittent diurnal and weather-related fluctuations that are inherent in solar generation were thus easily absorbed by conventional fossil-based generation. At current growth rates, PV power production will require increased grid flexibility and storage to balance load variations inherent in its deployment [10]. As installed solar capacity grows, it will present a challenge for turbine based power to provide the rapid change in power output or ramp rates required to ensure grid stability. Huber et al. reviewed ramp rate needs in the European electric grids and found that deployment of renewable generation above 30% will dramatically change grid flexibility requirements [118]. Denholm et al. have shown that increasing solar deployment above 20% of yearly demand can result in unusable generation necessitating cutting back or curtailing of solar production [119].

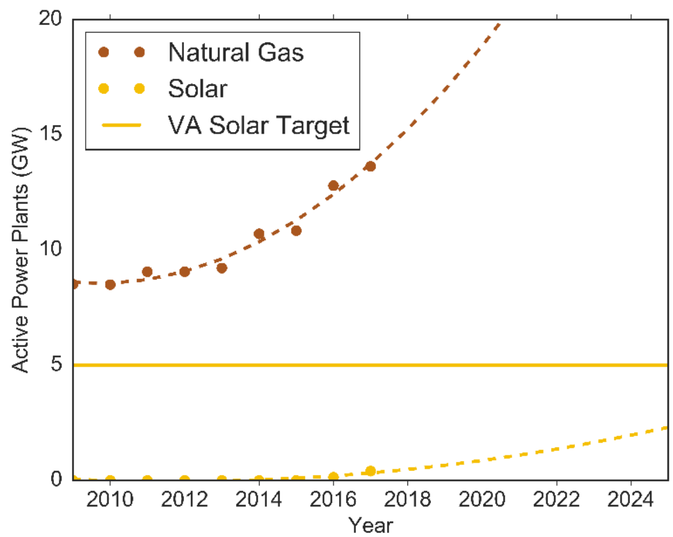

Figure 3-1. Deployment of utility natural gas and solar power plants in Virginia compared against solar deployment target [117,120].

Several groups have investigated changes in power plant generation in response to solar deployment. As solar deployment increases, the operating range of thermal power plants becomes important and is characterized by the minimum power output or minimum plant load. Denholm and Margolis scaled solar irradiance data from nine locations in the Texas electric grid and showed that some PV generation will become surplus after providing 4% of annual electricity demand assuming a minimum plant load of 35% [121]. Research into managing high deployment of renewable resources has been focused in the areas of hybrid renewable energy systems (HRES) and Virtual Power Plants (VPP). HRES are micro-grids that combine renewable and conventional power generation to meet demand either in stand-alone operation or grid-connected operation [122]. The VPP concept is based on the idea of operating and controlling a collection of distributed generators such as solar PV and energy storage as a single power plant [123]. VPP are connected to the greater electric grid, but focus on issues similar to HRES in terms of managing intermittent renewable resources [123]. Nostratabadi et al. provide a review of scheduling techniques including strategies to manage demand response, minimize emissions, and manage reactive power [124]. Bajpai and Dash provide a review of HRES modeling methods and show that conventional generation is usually limited to diesel generators and is represented by one or two equation models [122]. Dufo-Lopez et al. limit simulation of the diesel generation to fuel consumption [125]. Das et al. include diesel generators and micro gas turbines up to 65 kW and include efficiency corrections for ambient temperature and part-load operation, but do not include transient effects [126]. Kalantar and Mousavi simulated a hybrid system that included a 230 kW microturbine and used a physics-based system of equations to capture the dynamics of each system component [127]. These papers have been limited in the scale of power generation, and do not offer a flexible simulation strategy when the full system dynamics cannot be determined.

The most cost-effective and technically viable way to deliver solar load balancing will likely involve some combination of energy storage and advanced power generation with the capability to cycle rapidly [121]. The future of energy storage is focused on batteries, and to a lesser extent supercapacitors [128]. The principal drawback to using energy storage alone is that the costs of grid-scale batteries are prohibitively expensive and the charging and discharging cycles of batteries may be misaligned with variation in demand [14]. Increased solar deployment leads to the integration challenges of over-producing renewable electricity and reduced full-load hours for conventional power generation [129]. This creates a need for power plants that can start up rapidly and achieve high plant efficiencies across a range of operating conditions. Demand typically fluctuates by time of day and season resulting in a highly variable load balance as shown by the net power plant load based on PV generation and demand data for the University of Virginia (UVA) (Figure 3-2).

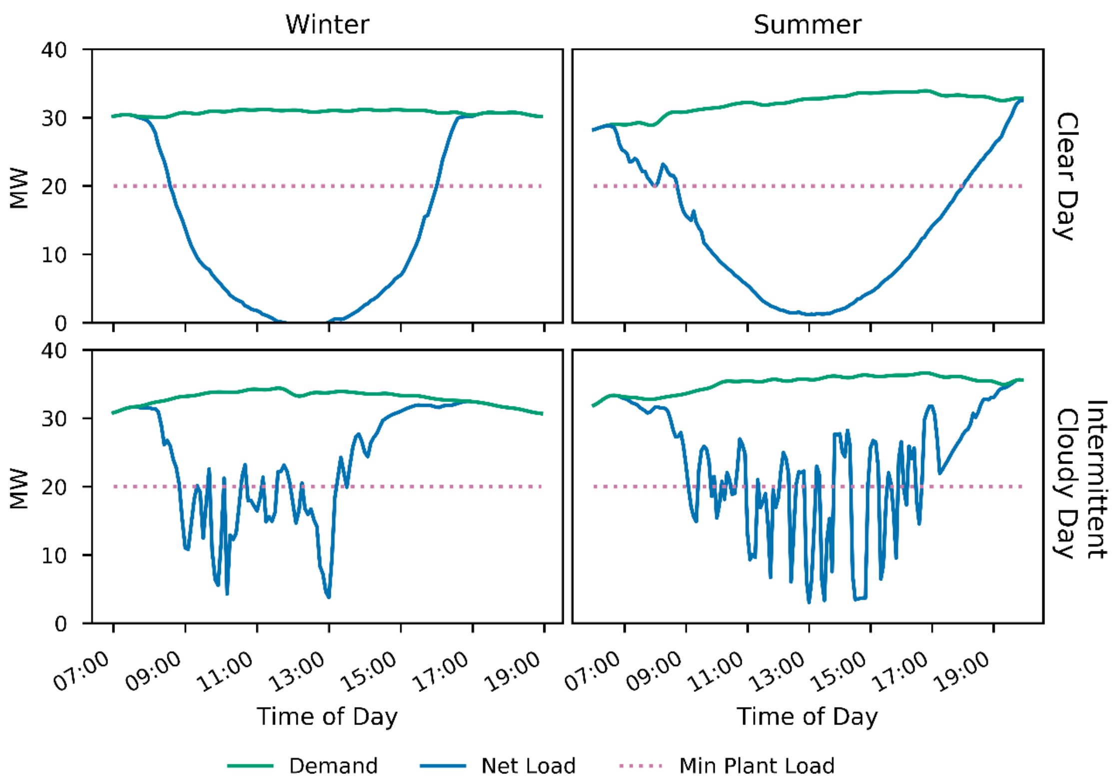

Figure 3-2. Characteristic power data from clear and intermittently cloudy days in the winter and summer are used to illustrate impacts of solar PV variability on net load for the University of Virginia.

Gonzalez-Salazar et al. provide a comparison of power plant flexibilities which show that responsive dispatchable generation are currently limited to open cycle gas turbines (OCGT) and combined cycle gas turbine (CCGT) power plants [13]. State-of-the-art OCGTs and CCGTs have much faster ramp rates and higher efficiencies than conventional simple steam turbines used in coal and nuclear power plants. Hydroelectric power plants are also a responsive generation (and storage) source, but limited in terms of geographic availability.

Supercritical carbon dioxide (sCO_2) power cycles are a promising alternative to the steam turbines used in CCGTs. In these cycles, CO_2 is used instead of steam as the working fluid. These cycles are expected to achieve rapid start-up and shutdown times in part because the turbines have physical footprints that are ten times smaller than conventional turbines [130]. They are also more efficient (system efficiencies greater than 50%) and potentially less expensive than conventional steam turbines. Several notable demonstrations of the sCO_2 cycle include 100 kW cycle [34], 250 kW cycle [35], and 1 MW turbine [36] tests, and a 10 MW cycle is currently under development [131]. These studies have demonstrated the on-design and off-design potential of these cycles to meet levelized cost of electricity (LCOE) targets, but have not yet proven transient capabilities of the cycles. sCO_2 cycles can be designed to operate using waste heat recovery (WHR), stored thermal fluids, biofuels, geothermal, or fossil fuel combustion [28]. Echogen Power Systems is focused on the WHR market, and while a number of waste heat sources exist, the most commonly utilized is gas turbine exhaust. In other words, Echogen's WHR design could replace a steam cycle in a combined cycle power plant. Currently, Echogen offers three WHR units; the EPS30[132], EPS35[133] and EPS100[134] which have power outputs of 1.35 MW, 1.8 MW and 8.6 MW, respectively. Each unit uses dry cooling technology thus no water is required for operation. The reduced size of the sCO_2 unit plus the elimination of water cooling auxiliary equipment reduces the overall system footprint by approximately 25% [135]. With less auxiliary systems and smaller turbine sizes, sCO_2 units are expected to start quickly. sCO_2 plant characteristics are compared against OCGT and CCGT in Figure 3-3 on the basis of plant size, start time, minimum plant load, and ramp rates. Faster ramp rates, indicated by larger circles in Figure 3-3B, are better suited for solar integration.

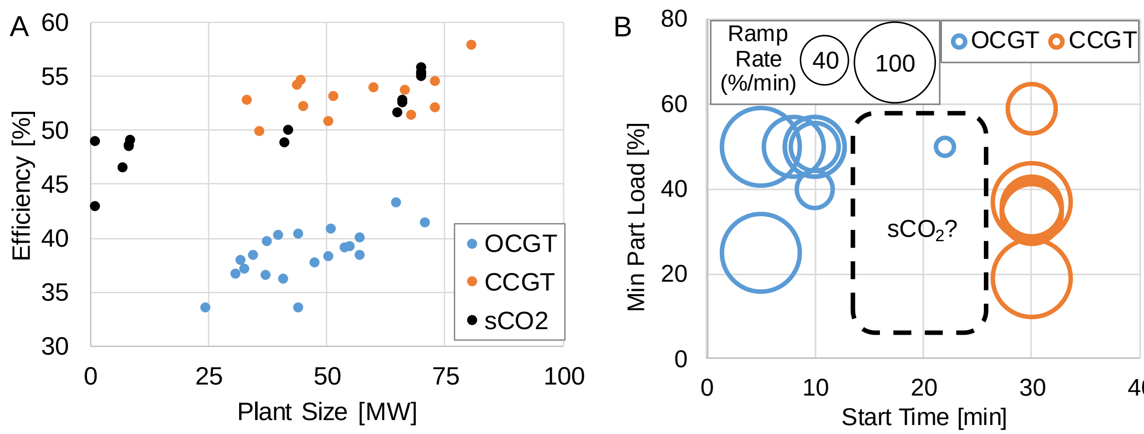

Figure 3-3. Grid balancing options for deep deployment of photovoltaic power production have a variety of tradeoffs including those between A) efficiency and plant size and B) minimum plant load and start time. sCO_2 cycles could represent an important bridge between efficient but slower combined cycle gas turbines and less efficient but quick starting open cycle gas turbines.

sCO_2 cycles present a number of challenges from a modeling perspective [39]. At the fluid level, the CO_2 properties can change very rapidly near the critical point, which many studies have found to be optimal compressor inlet conditions, and vary drastically between start-up conditions and full-power operation [130]. At the machine level, complex interactions between components exist which can result in non-linear responses unlike those of conventional turbines [136]. While the ongoing transient modeling work of sCO_2 cycles has provided important insight into how this class of turbine will behave [137] [138] [41], the recent modeling has yet to explore in aggregate how these power plants will perform as part of a dynamic grid with high renewable deployment.

Rooftop solar installations at the University of Virginia (UVA) account for 1.0% of peak demand (635 kW), representative of today's statewide deployment of solar power in Virginia. In late 2018, two solar farms came online (32 MW) which supply 20% of UVA's annual electricity demand and up to 63% of peak. Thus, UVA's demand and solar capacity are good surrogates for studying grid balancing under current and projected levels of solar deployment. The University made data available at temporal resolutions that enabled the modeling needed to understand how advanced turbines might be deployed to deliver grid balancing. Here, I investigate the ability of natural gas power plants to balance the load in an electric grid with increasing amounts of solar generation by combining the elements of measured data from UVA, the solar prediction library PVLib and the mathematical model BLIS, Balancing Load of Intermittent Solar as shown in Figure 3-4.

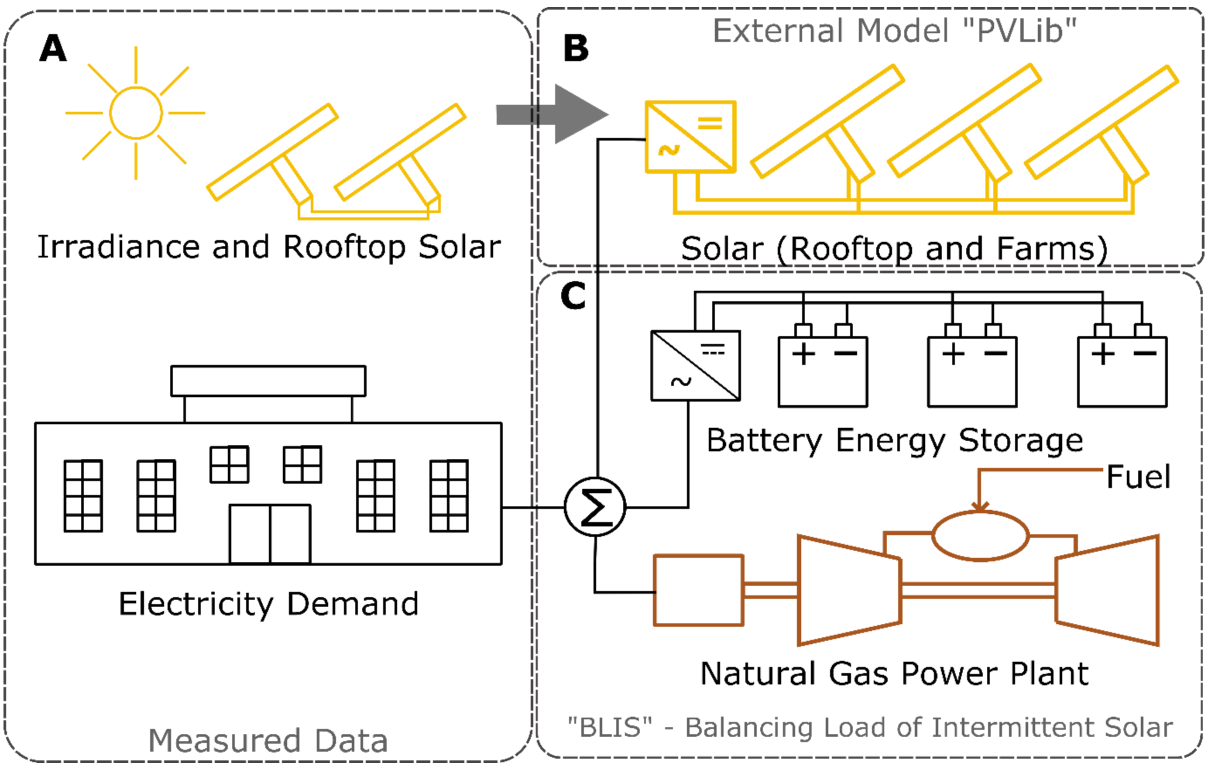

Figure 3-4. A) Measured data from UVA, B) Solar generation modeled using PVLib [139], and C) Mathematical model "BLIS" developed in this study.

The goal of this paper is to explore the ways in which sCO_2 cycles might be used to provide load balancing in a dynamic grid dominated by renewable energy production. A set of high-resolution generation and demand data and forecasting capabilities for the University of Virginia's microgrid was used to inform this analysis. This work seeks to answer two principal research questions. First, how do existing and proposed advanced power cycles perform for delivering load balancing when integrated into a grid involving high deployment of solar photovoltaic? Second, what sCO_2 power cycle characteristics are necessary for them to provide load balancing in a grid with high PV deployment?

This analysis seeks to fill several gaps in the existing literature. First, the effect of natural gas plant ramp rate, minimum plant load and efficiency were investigated for increasing solar. Second, sCO_2 turbines in combined cycle, which are just starting to enter the market, are compared against state-of-the-art OCGT and CCGT, providing insight into the future of the natural gas power market. Third, the methodology of this work improves upon prior HRES studies by introducing a characteristic-based model that includes power plant dynamics thus providing a more realistic power plant operation and relies on publicly available manufacturer specifications, making it more accessible for users to get model inputs. Fourth, the demand and solar data used are in fine enough intervals (5 minutes) to be useful for modern grid dispatch, represent production large enough to represent a small city, and small enough to allow analysis of a single power plant, to understand the implications of individual power plant requirements.

3.3 Methods

To understand the impact of power plant characteristics in grids with high solar deployment, a transient characteristic-based mathematical model was developed. The mathematical model was developed to rely on manufacturer advertised characteristics as inputs, such as ramp rate, max efficiency, and minimum plant load, for power plants. To make the simulations as realistic as possible, the model is designed to take one year of demand and solar irradiance data as inputs. The model operates on one-minute increments to make it useful to represent a power grid control scheme which increasingly occurs on 5 minute intervals [119]. Frequency control is omitted from the model. The mathematical model along with the solar and demand data are available for download as an open source Python package, entitled *blis* (Balancing Load of Intermittent Solar) at https://github.com/EnergyModels/blis.

3.3.1 Demand

Here, electricity demand data at a 5-minute temporal resolution was obtained from the UVA Facilities Management office for the period July 1, 2017 to July 1, 2018. The mathematical model ran on 1-minute increments; thus data was backfilled to provide a worst-case scenario with respect to changes in demand. For the time period investigated, UVA consumed 294 GWh with peak consumption at 51.3 MW. Based on EIA's average household electricity use, this is equivalent to roughly 28,000 typical American households [140] or 0.2% of Virginia's annual consumption [141].

3.3.2 Solar PV

UVA's installed rooftop solar capacity consists of approximately 0.635 MW of fixed tilt systems, or just over 1% of the peak electricity demand for the analysis period. Additionally, UVA has a power purchase agreement with two remote PV plants that came online late in 2018. These are single-axis tilt systems and have capacities of 17MW and 15MW, which represent 63% of the total university peak demand, and are expected to provide 20% of annual electricity demand.

To model the combined production of the solar PV systems at high temporal resolution over the full year, PVLib, an open source Python library developed by Sandia National Laboratory was used. Global horizontal irradiance (GHI), ambient air temperature, and windspeed data sampled every 4-8 minutes from a weather station installed on top of UVA's football stadium were used as model inputs [142]. During this time period, UVA experienced 169 sunny days, 75 cloudy days, and 121 days of intermittent clouds [143]. Solar angular position data at each timestep was obtained using NREL's solar position algorithm [144]. The GHI data was then decomposed into its direct normal (DNI) and diffuse horizontal (DHI) components using the Direct Insolation Simulation Code (DISC) model [145]. The single-axis tilt systems were assumed to be oriented facing due south and capable of backtracking to avoid shading. A module temperature loss coefficient of 0.47% $^{o}C^{-1}$ (for a standard PV module with a glass cover) was assumed, and a derate factor of 0.825 was applied to convert the peak AC capacity to a nominal DC capacity for the models [146]. While producing solar power from multiple locations attenuates some of the high frequency fluctuations in aggregated fleet production relative to a single location [147], it was assumed the large single axis tilt systems to be co-located with UVA's campus in order to magnify the effects of ramp rates. Production data for the rooftop solar systems (5 min resolution) and large PV plants (hourly resolution) were also provided by the UVA Facilities Management office and used to validate the model for the rooftop systems, with results shown in Appendix B.

The produced solar generation data sets were then analyzed to determine the corresponding ramp rate required by a natural gas and/or battery system to meet the demand. Figure 3-5 shows the distribution of net load ramp rates for every 5-minute period over the analysis timeframe with 1% and 63% solar deployment. The deep deployment of solar PV shifts the distribution to the right such that there are many more instances with high ramp rates. Few cases at 1% solar exist where ramp rates exceed 0.1 MW/min, however at 63% the probability of experiencing ramp rates above 1 MW/min are substantial.

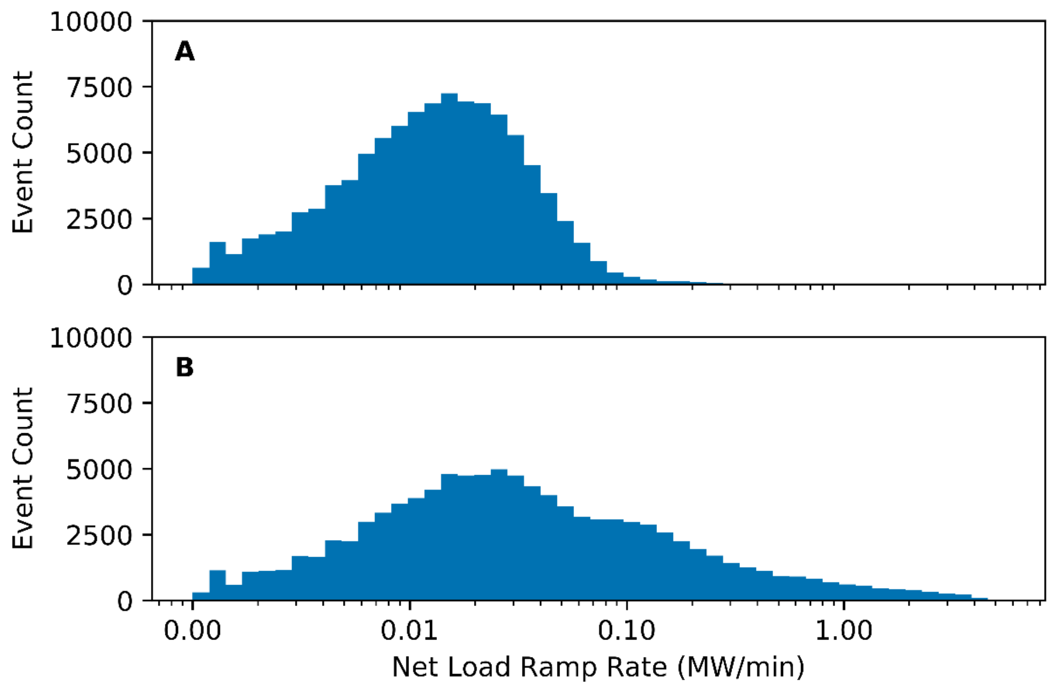

Figure 3-5. Histogram of ramp rate events with A) 1% solar deployment and B) 63% solar deployment.

3.3.3 Battery

The available battery discharge is calculated using the battery characteristics maximum discharge rate and time constant along with the current amount of energy stored

$$P_{B,OUT,MAX} = \min\,(P_{B,DESIGN}, \frac{E_B}{30\ \Delta\mathrm{T}}) \tag{3-1}$$

Where $P_{B,OUT,MAX}$ is the battery discharge available at the current time step, $P_{B,DESIGN}$ is the maximum allowable battery discharge rate, E_B is the energy stored in the battery at the current time step, ΔT is the time step. The dimensionless constant 30 is included to simulate a bumpless controller to ensure a smooth transition to other generation sources when the battery level is low. The available battery charge rate $P_{B,IN,MAX}$ is calculated as,

$$P_{B,IN,MAX} = \min\,(P_{B,DESIGN}, \frac{E_{B,MAX} - E_B}{\Delta\mathrm{T}}) \tag{3-2}$$

Where $E_{B,MAX}$ is the maximum battery storage level.

3.3.4 Power Plants

To simulate the three types of natural gas power plants being investigated, OCGT, CCGT and sCO_2, the mathematical model focused on four major characteristics: design efficiency, off-design efficiency curves, minimum load and ramp rate. To incorporate on-design and off-design efficiency, the efficiency η for load L is,

$$\eta = \eta_{NG,design} * (A_2 \cdot L^2 + A_1 \cdot L + A_0) \tag{3-3}$$

where $\eta_{NG,design}$ is the rated efficiency of the natural gas power plant and A_0, A_1, and A_2 are regression constants to represent off-design curves. Minimum plant load is enforced by limiting the requested plant load L_{REQ},

$$L_{REQ} = \max(L_{MIN}, L_{IDEAL}) \tag{3-4}$$

Where L_{IDEAL} is the ideal plant load which is calculated to optimize usage of the solar power plant and battery storage system by,

$$L_{IDEAL}\ (\%FL) = \frac{P_D - P_{B,OUT,MAX} - P_{PV}}{C_{NG}} * 100 \tag{3-5}$$

Where P_D is power demand and P_{PV} is PV power generation. To include the transient behavior of the power plant, the ramp rate is constrained by,

$$\left|\frac{C_{NG} \cdot (L - L_{REQ})}{\Delta \mathrm{T}}\right| \leq \dot{P}_{NG,DESIGN} \tag{3-6}$$

Where $\dot{P}_{NG,DESIGN}$ is the manufacturer rated ramp rate, C_{NG} is the capacity of the natural gas power plant, and ΔT is the time step.

3.3.5 Metrics

Modeling of power systems that includes a significant amount of renewable generation typically employs a number of metrics to quantify the flexibility of the power system to handle the variable nature of this resource [148]. Financial metrics are also important when modeling power systems, and therefore two costs were included in this model. In total, seven performance indices were selected to evaluate the performance of the natural gas power plants: curtailment, natural gas load shed, peak deficit, time of day emissions, yearly fuel costs, and LCOE. Solar curtailment is the fraction of solar power that is unused by the energy system.

$$Curtailment(\%) = \frac{\sum P_{PVC} \cdot \Delta T}{\sum P_{PV} \cdot \Delta \mathrm{T}} \tag{3-7}$$

Where P_{PVC} is the amount of solar power curtailed per time step. Natural gas load shed represents the amount of electricity produced by the natural gas power plant that must be curtailed due to excess supply that cannot be absorbed by the battery. It is normalized by the yearly demand,

$$Natural\ Gas\ Load\ Shed\ (\%) = \frac{\sum P_{NGLS} \cdot \Delta \mathrm{T}}{\sum P_D \cdot \Delta \mathrm{T}} \tag{3-8}$$

where P_{NGLS} is the amount of load shed per time step. The peak deficit represents that largest failure of the energy system with respect to being able to meet demand and is defined as,

$$Deficit(MW) = \max\left(P_D - P_{NG} - P_{PV} - P_B\right) \tag{3-9}$$

The time-of-day emissions represents the total amount of natural gas emissions during each hour weighted by the amount of demand in that hour, or,

$$Emissions(hr) = \frac{\sum \frac{P_{NG} \cdot \Delta \mathrm{T}}{\eta_{NG}}}{\sum P_D \cdot \Delta \mathrm{T}} * Q \tag{3-10}$$

where Q is the emission factor for natural gas, signifying the tons of carbon dioxide that are produced per thermal MW consumed.

3.3.6 LCOE

The mathematical model operates with one year's worth of data, thus by assuming that costs and operation are constant throughout the system lifetime, the Levelized Cost of Electricity [149], LCOE, was simplified to,

$$LCOE = \frac{\sum_{t=1}^{N} \frac{I_Y + M_Y + F_Y}{(1+R)^t}}{\sum_{t=1}^{N} \frac{E_Y}{(1+R)^t}} = \frac{I_Y + M_Y + F_Y}{E_Y} \tag{3-11}$$

where I_Y are investment costs in year Y, M_Y are O&M costs in year Y, F_Y are fuel costs in year Y, E_Y is the energy demand during year Y, R is the discount rate, and N is the life of the system. Investment costs are assumed to be financed thus, it is also a constant yearly value. The yearly investment cost is calculated by applying the Python numpy function pmt [150] to the present value, V, of the power plant,

$$V = C_{NG} * I_{NG} + C_{PV} * I_{PV} + C_B * I_B \tag{3-12}$$

The yearly O&M costs M_Y are calculated as,

$$M_Y = E_{NG} \cdot M_{V,NG} + C_{NG} * M_{F,NG} + C_{PV} * M_{F,PV} + C_B * M_{F,B} \tag{3-13}$$

where M_V and M_F are variable and fixed O&M costs, respectively.

3.3.7 Model Inputs

To find comparable performance statistics, a comprehensive review was performed of open cycle (OCGT) [151,152,161–164,153–160] and combined cycle (CCGT) [151,154–160,163,164] gas turbines sold by GE, Siemens and Mitsubishi Hitachi Power Systems for packages rated for 20 – 80 MW.

Approximately 15-20 configurations were found for both OCGT and CCGT, where both plant capacity and peak efficiency were reported. Off-design efficiency curves for OCGT and CCGT were obtained from the literature [165]. Each off-design curve was normalized to the peak efficiency, similar to that presented in [166], so that a unique efficiency curve could be generated for each peak efficiency used in subsequent simulations. Cost information was not readily available from manufacturers, so operation and maintenance data was obtained from EIA [167]. Open cycle cost data was taken for the LM2500, a 25MW gas turbine, using a price reported in [168]. The price for a combined cycle gas turbine was calculated using the GTW Handbook cost estimate based on a plant size of 51.3 MW [54].

Crespi et al. summarize studies predicting sCO_2 power cycle efficiencies, the few that focused on combined cycle applications did not vary with plant size [33], thus an average of the 4 cases found was used [169–173]. Only two part-load efficiency curves were found in the literature, one for the direct-fired Allam cycle [166] and one for concentrated solar power [174]. The curve for the Allam cycle was selected for this study, as it was expected that a natural gas fuel source would be more representative than a thermal solar application. Transient characteristics are unknown for sCO_2 power plants, so a uniform range of values were investigated. A larger range than CCGT was investigated for sCO_2 turbines as they have a much smaller rotor size, and may be able to react more quickly for the same power rating [30]. Walnum et al. included 60% as the minimum part-load for a combined cycle application [169]. This is on the high end of CCGT, so this was kept as the upper limit for the range investigated. Install cost and operation and maintenance (O&M) costs are based on [168]. Echogen's EPS100 [134] WHR unit uses dry cooling, thus they expect operational costs to be much lower than a CCGT system based on steam [135]. Echogen has not released price information, so operation and maintenance (O&M) costs, as well as installation costs are based on [168]. Power plant specific inputs are summarized in Table 3-4 and common inputs in Table 3-5. Note that variable O&M costs are excluded from PV and battery calculations, as the model did not track usage of these resources alone. For reference, EIA reports variable O&M costs of 0.0$/MWh for PV plants and 7.12$/MWh for battery storage [167].

Table 3-4. Power plant modeling inputs used in system-dynamics model with sources. Values reported are averages with minimum and maximum values shown in parenthesis.

	Name	**Open Cycle Gas Turbine**		**Combined Cycle Gas Turbine**		**Gas Turbine combined with sCO_2 Turbine**	
	Abbr.	**OCGT**		**CCGT**		**sCO_2**	
		Performance Characteristics					
Variable	Units	Estimate (+/-)	Reference	Estimate (+/-)	Reference	Estimate (+/-)	Reference
Max Plant Efficiency	(% LHV)	38.3 (33.5-43.3)	[151,152,161–164,153–160]	53.4 (49.9-58.0)	[151,154–160,163,164]	53.1 (43-59.1)	[169–173]
Off-Design Efficiency Coefficients (A2,A1,A0)	(-)	-1.09E-02 2.03 5.44	[165]	-6.94E-03 1.28 40.8	[165]	-5.60E-03 1.05 50.00	[166]
		Dynamic Characteristics					
Variable	Units	Estimate (+/-)	Reference	Estimate (+/-)	Reference	Estimate (+/-)	Reference
Hot Start-up Time	(min)	10.0 (5-22)	[151,152,161–164,153–160]	33.1 (30-55)	[151,154–160,163,164]	10.0	[175]
Minimum Plant Load	(% full load)	46.1 (25-50)	[151,152,161–164,153–160]	36.4 (19-59)	[151,154–160,163,164]	15-60	Assumption
Ramping Rate	(% full load/min)	72.8 (8.3-129.3)	[151,152,161–164,153–160]	64.9 (29.4-90.4)	[151,154–160,163,164]	30-110	Assumption
		Costs					
Variable	Units	Estimate (+/-)	Reference	Estimate (+/-)	Reference	Estimate (+/-)	Reference
Install	$/kW	750	[168]	1260	[54]	962	[168]
O&M Variable	$/MWh	3.54	[167]	3.54	[167]	8.00	[168]
O&M Fixed	$/kW/year	17.67	[167]	11.11	[167]	0.00	[168]

Table 3-5. Common power plant model inputs and assumptions.

Variable	Units	Value	Reference
Interest Rate	%	2.0	[168]
Timestep	min	1	Input
System Lifetime	years	20	[168]
Natural Gas Plant			
Plant Capacity	MW	51.3	Sized to peak demand
CO_2 Emissions	Metric ton/MWh	0.18	[176]
Fuel Cost	$/MWh	10.58	[177]
Battery			
Discharge Rate	MW/MWh	1.0	[178]
Efficiency	%	85.0	[14]
Initial Charge Cost	$/MWh	100.0	[179]
Install cost	$/kW	2067	[167]
O&M Fixed	$/kW/year	35.6	[167]
Solar PV			
Install cost	$/kW	2004	[167]
O&M Fixed	$/kW/year	22.02	[167]

3.3.8 Verification of Grid Operation

The model used in this study used a control strategy that first prioritizes use of solar power produced. It also slows the battery discharge with battery charge level to allow a smooth transition to the natural gas-powered cycle. Figure 3-6 verifies that the control strategy responded appropriately to the generation and demand on a representative sunny day. With a 30.0 MWh battery, there is not enough storage capability to permit shutting down the natural gas plant, thus it is cycled to balance the difference between solar generation and battery discharge to meet demand. As solar generation increases, the natural gas plant decreases its output until it reaches its minimum plant load, at which point the system begins to create more electricity than can be used. To handle excess, the first step is to charge the battery. The battery can only charge at 30 MW, so if necessary, curtailment is used to cut solar production. If any additional electricity remains then the natural gas load would be shed.

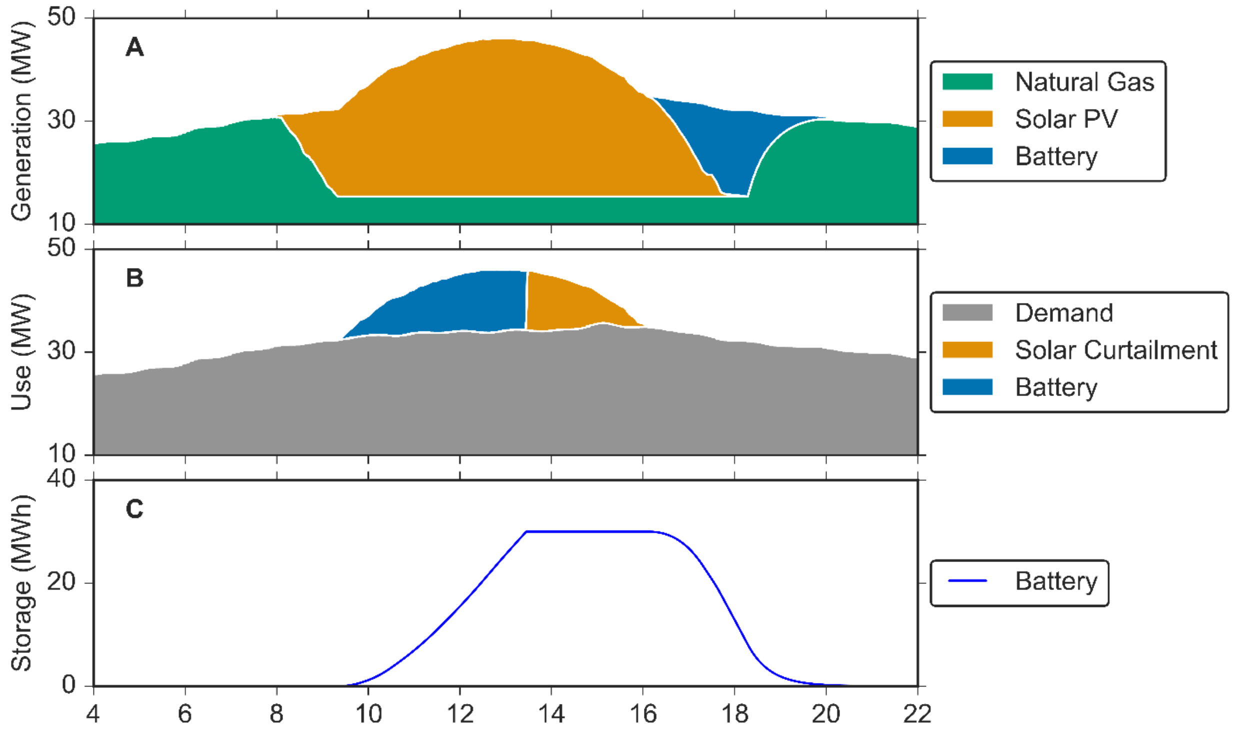

Figure 3-6. Operational control scheme for October 30, 2017 with 63% solar: A) Electricity generation by source, B) Electricity consumption by use, C) Battery charge level.

3.3.9 Scenarios

Three categories of simulations were performed, summarized in Table 3-6. First Monte Carlo simulations were used to compare the performance of sCO_2 plants with OCGT and CCGT for two levels of solar deployment (1% and 63%) and two levels of battery size (0 and 30 MWh). 100 iterations were performed per configuration. Next sCO_2 plants were studied in more detail to understand the impact of the ramp rate characteristic, while holding other plant characteristics constant. Lastly, the impact of battery size was investigated for three levels of minimum plant load, holding other characteristics constant for sCO_2 cycles.

Table 3-6. Scenarios.

#	Power Plant Types			Solar Capacities		Battery Capacity	Ramp Rate	Min Load
	sCO_2	OCGT	CCGT	0.6 MW (1 % Peak)	32.6 MW (63% Peak)	MW(MWh)	%	%
1	Y	Y	Y	Y	Y	0 and 30	NC	NC
2	Y			Y	Y	0 and 30	0 - 16	30
3	Y				Y	0 – 100	50	30,40,50

3.4 Results and Discussion

3.4.1 Levelized Cost of Electricity

The LCOE was calculated for each of the three cycle configurations modeled and the results are presented in Figure 3-7. The probability density functions for each turbine type are presented in four plots that show the impact of solar deployment and battery size. Results show that across all conditions, combined cycle (both CCGT and sCO_2) systems have considerably lower costs than open cycle gas turbines. The higher efficiency of the combined cycle systems is great enough that these systems generally produce electricity that is at least 0.005 \$/kWh less expensive than open cycle turbines. The OCGT LCOE results are driven by its lower efficiencies and corresponding higher fuel consumption. The addition of a battery (here assumed to be 30 MWh) increases the cost of electricity by 0.015 \$/kWh. The increase in LCOE when moving from 1% to 63% solar deployment is approximately 0.013 \$/kWh. The distributions for CCGT are the narrowest, which reflect the higher certainty associated with this well-established and commercialized technology. In contrast, sCO_2 results have longer tails associated with higher uncertainty in input parameters. While the distributions do hint at the potential for sCO_2 cycles to reduce LCOE relative to CCGTs, especially at higher solar deployment, current performance data suggest the impact of these advanced power cycles may be small from an overall systems perspective. To verify the model, LCOE predictions were compared to reports in the literature for sCO_2 cycles without solar or battery, which were found to be comparable to the estimates forecast in this model. Wright et al. report an LCOE of 0.029-0.034

$/kWh for a fuel cost of $10.2/MWh [172] and Persichilli et al. reports an LCOE for baseload operation from 0.05-0.06 $/kWh for a fuel cost of $12.2/MWh [135].

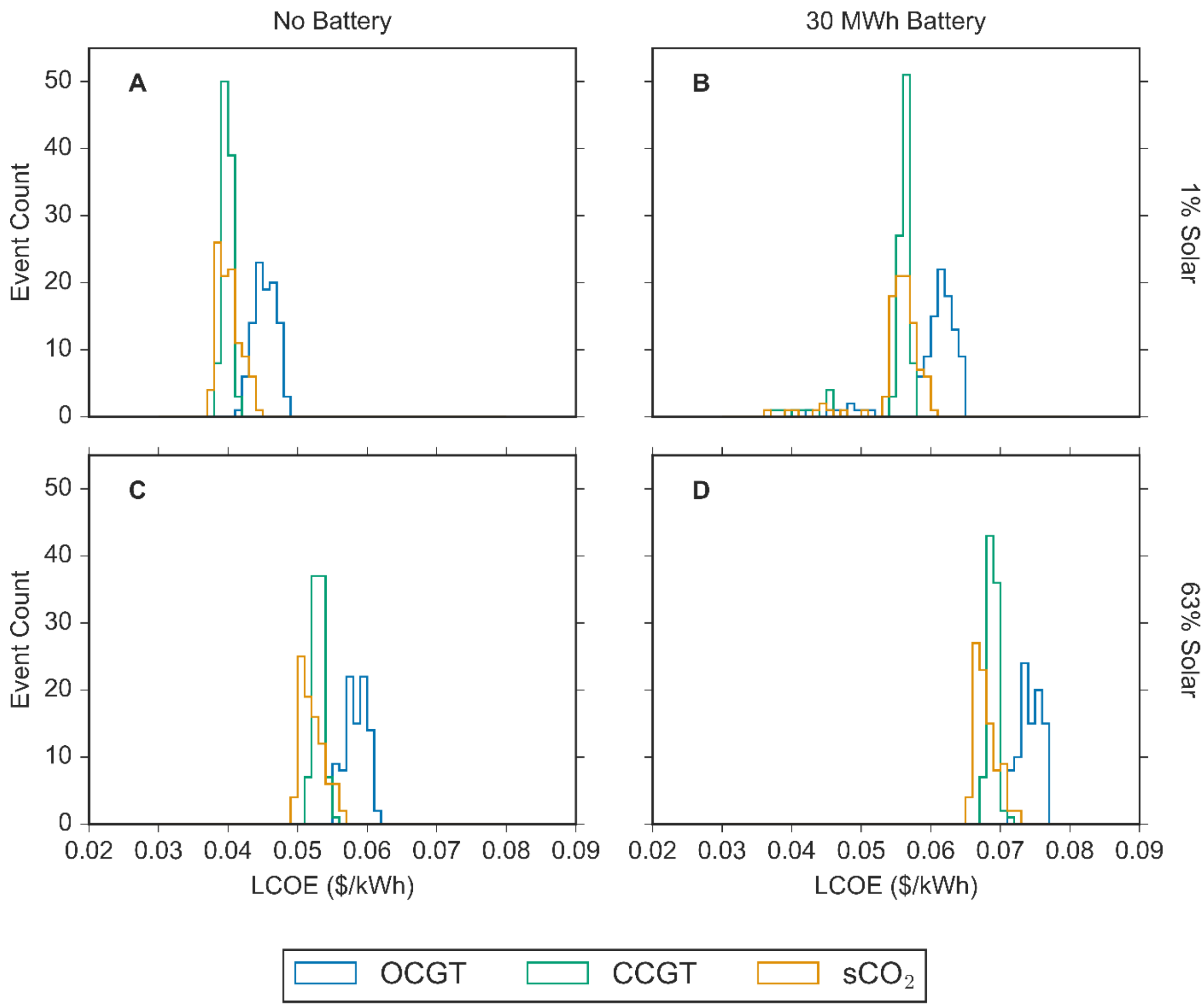

Figure 3-7. LCOE frequency of occurrence: A) 1% Solar with No Battery; B) 1% Solar with 30.0 MWh Battery; C) 63% Solar with No Battery; D) 63% Solar with 30.0 MWh Battery.

3.4.2 Time-of-Day Emissions

To understand the interaction of plant type, solar production, and battery storage on CO_2 emissions, a comparison was made on an hourly basis and weighted by demand (Figure 3-8). On the whole, CCGT had marginally lower emissions than sCO_2 cycles. sCO_2 cycles performed better at 63% solar and 30 MWh around mid-day which shows the impact of higher off-design efficiency. Emission levels of OCGT were consistently higher, even the addition of 63% solar and a 30 MWh battery did not reduce levels below CCGT and sCO_2 at 1% solar. The 95% confidence interval was largest for the 1% solar case with a battery which demonstrates that certain power plant characteristics enable higher battery utilization and thus lower emissions.

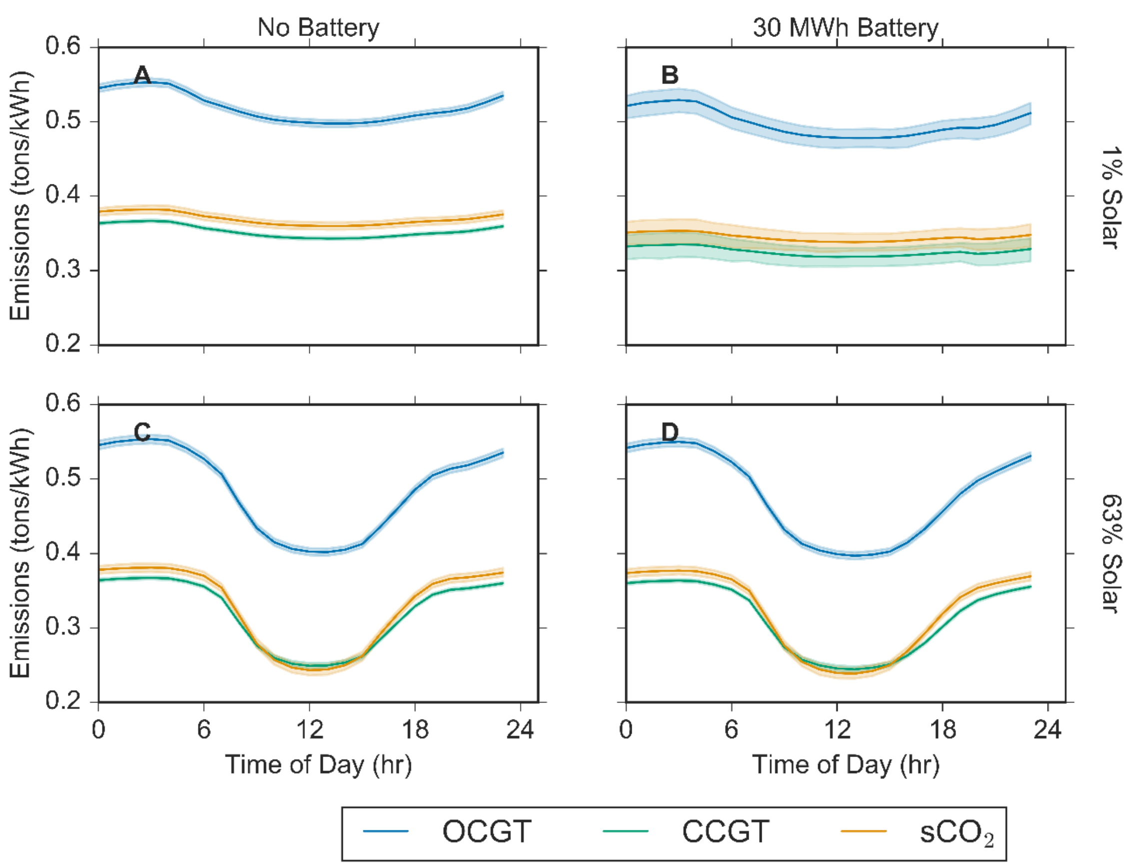

Figure 3-8. Annual time of day carbon dioxide emissions weighted by hourly demand shown with 95% confidence interval, A) 1% Solar with No Battery; B) 1% Solar with 30.0 MWh Battery; C) 63% Solar with No Battery; D) 63% Solar with 30.0 MWh Battery.

3.4.3 Solar Curtailment

Solar curtailment and natural gas load shed were quantified to determine how well the system utilizes electricity produced. The battery had a significant impact by greatly reducing the magnitude of solar curtailment occurring. Interestingly, sCO_2 cycles are shown to have higher curtailment than the other power sources. As previously demonstrated, sCO_2 cycle curtailment was driven by the minimum plant load, and of the plant types investigated, the largest range of minimum plant load was assumed for sCO_2 cycles due to the lack of real-world application data. Based on the control scheme used, load shedding only occurs when battery charging and solar curtailment are not available or insufficient. Figure 3-9B and D shows that only one configuration had any appreciable load shedding, and it was minimal. Based on Figure 3-9A, it is not a surprise that sCO_2 cycles are the cases that needed to use load shedding, as they also had the highest amount of solar curtailment.

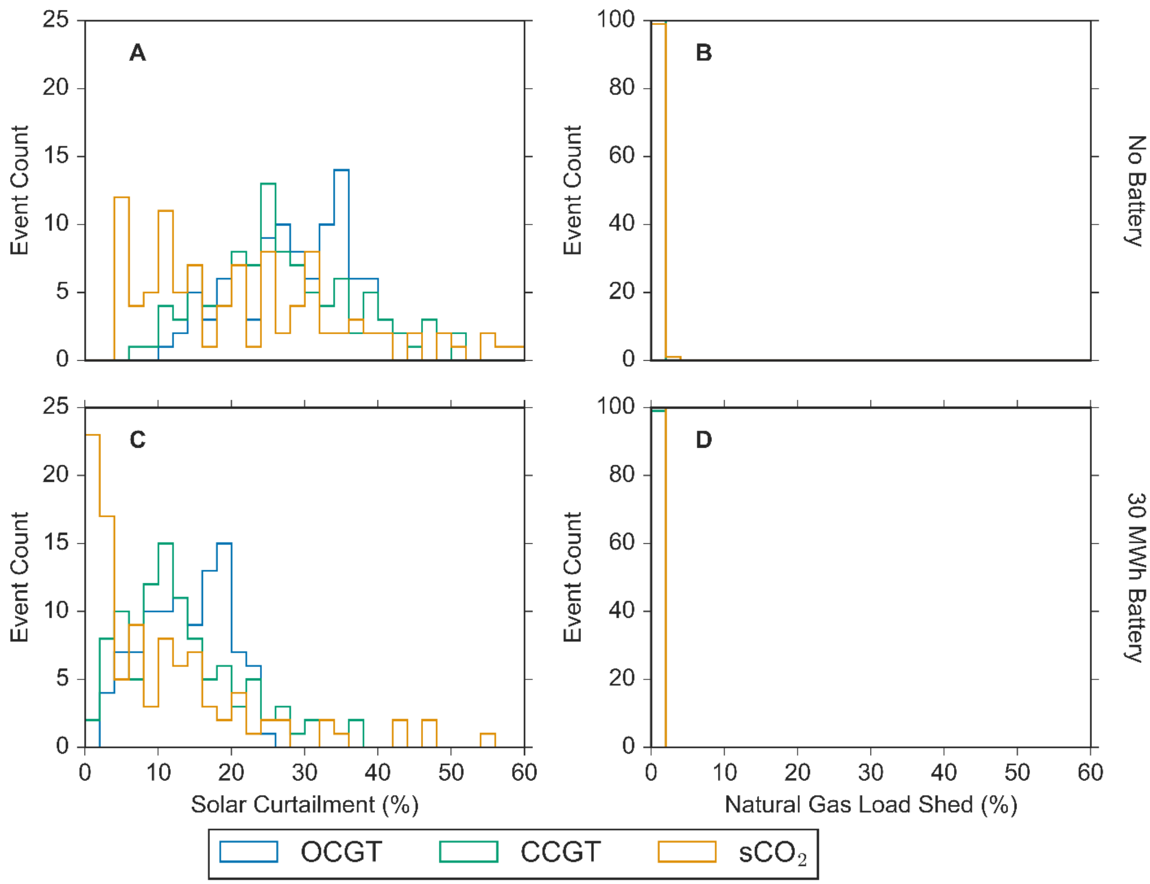

Figure 3-9. Percentage of energy wasted via solar curtailment (A and C) and natural gas load shed (B and D) for 63% solar without a battery (A and B) and with a 30 MWh battery (C and D). Distributions show frequency of occurrence from the 100 sample Monte Carlo simulation.

3.4.4 sCO_2 Cycle Sensitivity

To better understand which characteristics of the sCO_2 cycle are driving the trends, the effect of maximum efficiency, ramp rate and minimum load were quantified with respect to fuel cost and solar curtailment. Fuel cost provides an understanding of the financial impact and amount of natural gas being consumed while solar curtailment represents the system flexibility by showing what percentage of solar energy was not utilized during the year. Fuel cost and efficiency showed a very strong negative correlation

(Figure 3-10A) as expected. Fuel cost decreases with increased solar deployment and further with the use of battery storage. There is no apparent correlation between curtailment and either efficiency or ramp rate, which was unexpected. This suggests that the range of values considered are fast enough that it does not become a limiting characteristic. There is a weak positive correlation between the minimum load (Figure 3-10C) and fuel cost which demonstrates the inability of systems with higher minimum part loads to effectively balance solar power. This relationship is most apparent in Figure 3-10F, which shows a strong nonlinear correlation between solar curtailment and minimum part load. To have curtailment less than 2%, a plant needs a minimum part load of 55% for the 1% solar scenario and would need to be less than 15% for the 63% solar scenario. The addition of a 30.0 MWh battery relaxes the minimum part load needed to 25%, for the 63% solar deployment case. Only one CCGT was close to the minimum load required for 63% solar without a battery (with a minimum load of 18.9%) and none of the OCGT models reviewed would be capable of achieving this minimum load level. In addition to the changes in fuel cost and part load requirements, batteries may be needed to handle fluctuations on a less than 1-minute basis depending on the responsiveness of the power plant controls. The cost of a 30 MWh battery would be 60M$ at current market prices, which corresponds to ten years of fuel. However, a system with a peak demand of 51.3 MW can only be partially supplemented by a 30 MWh battery discharging at 30 MW.

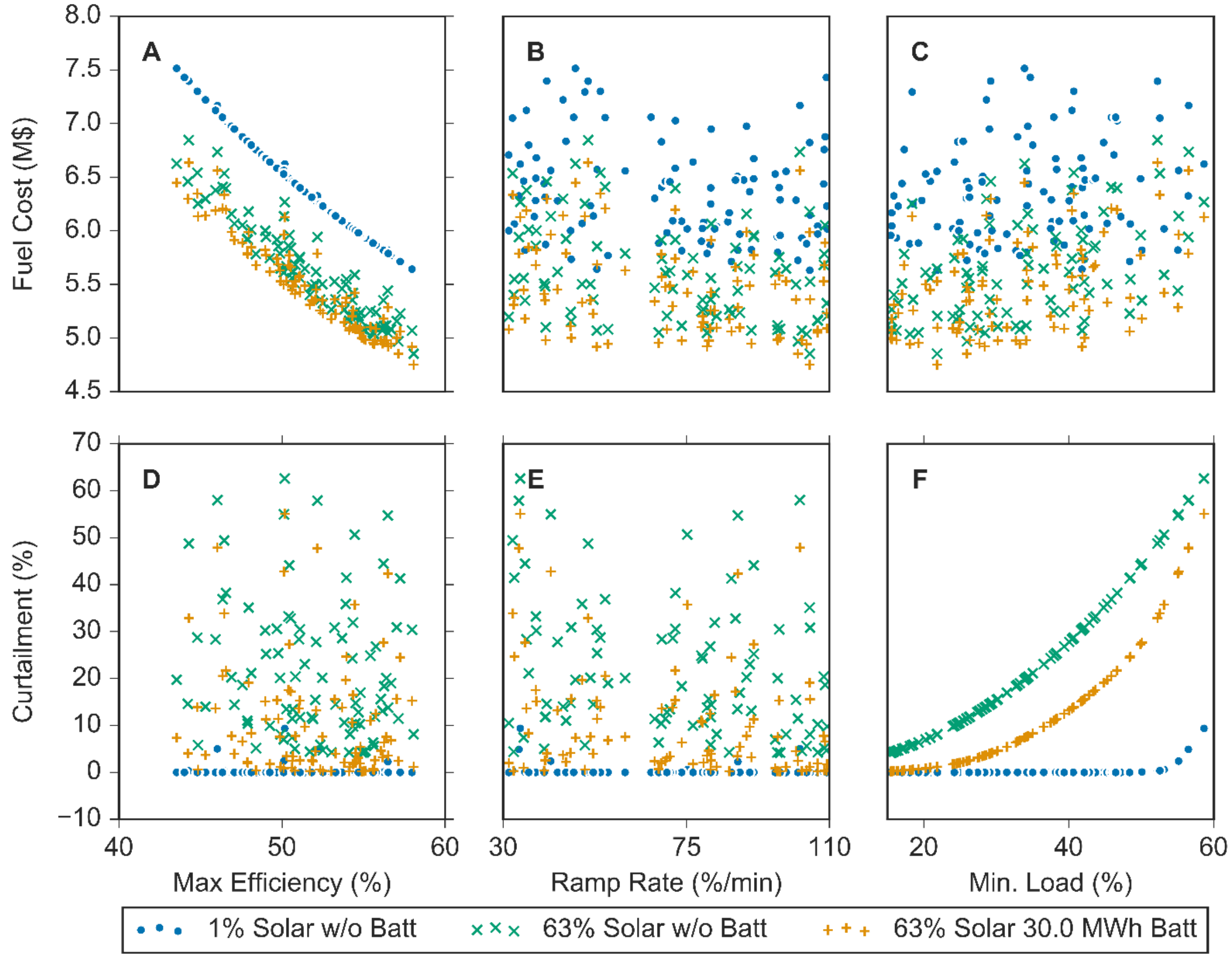

Figure 3-10. Sensitivity of sCO_2 plant inputs to fuel cost and solar curtailment A) Fuel cost vs. max efficiency, B) Fuel cost vs. ramp rate, C) Fuel cost vs. minimum load, D) Curtailment vs max efficiency, E) Curtailment vs. ramp rate, F) Curtailment vs. minimum load.

3.4.5 Impact of Ramp Rate

Although ramp rate was not found to have a significant impact on either LCOE or solar curtailment, it is expected that cycles with a slower ramp rate may be unable to respond to fluctuations in demand and solar supply. To determine what the critical values of ramp rate were, a sweep of simulations was performed on the baseline sCO_2 system using median values for efficiency and minimum part load while varying the ramp rate to compare against other generating technologies. Initial simulations analyzed ramp rates below 30% which was the low end of the Monte Carlo analysis, but results showed more interesting trends below 16%, which are presented in Figure 3-11 To analyze the impact of ramp rate, the maximum deficit was measured, which captures the maximum difference between demand and supply that neither the power plant, solar panels nor battery were able to meet. Figure 3-11 shows that the critical values of ramp rate are 3.25%/min, 5.75%/min and 4.75%/min, for the 1% solar, 63% solar without a battery and 63% solar with a 30.0 MWh battery cases, respectively. The addition of the battery decreases the critical ramp rate by 1%. Gonzalez-Salazar et al. presented a review of ramp rates for a variety of technologies which are overlaid for comparison and Nuclear power plants would be unable to handle the fluctuations of 63% solar, and coal plants would have to run at their limits which may be undesirable for long term operation [13]. Gonzalez-Salazar et al. also reported the ramp rate of CCGT to be 8%/min which is understood to represent a larger or older generation CCGT than those reviewed in this work [13].

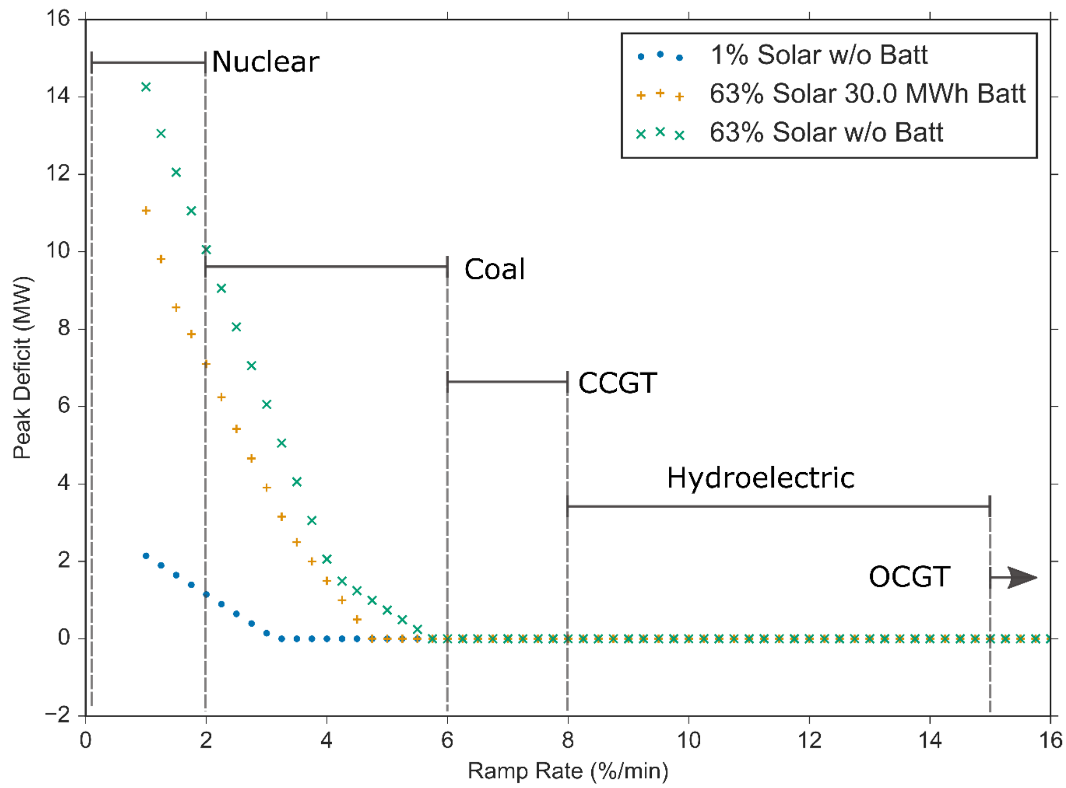

Figure 3-11. Sensitivity of energy system deficit to power plant ramp rate, technology characteristics from [13].

3.4.6 Impact of Battery Size

The results of the Monte Carlo simulations demonstrated that a 30 MWh battery would not completely prevent solar curtailment. For reference, a 90-kW/180-kWh zinc-bromine battery fits inside a 20-foot shipping container, and 168 of these batteries would be required to store 30 MWh [178]. This raised the question of how large a battery is necessary to prevent solar curtailment. To answer this question, baseline sCO_2 combined cycle efficiencies and ramp rates were held constant and a distribution of battery sizes from 1 to 100 MWh were analyzed at 63% solar deployment. Solar curtailment was previously shown to be a function of minimum plant load, therefore these simulations were repeated at three different minimum plant loads, 30%, 40% and 50% to represent the range currently available in CCGTs. Resulting curtailment, fuel cost and LCOE are shown in Figure 3-12. Figure 3-12A shows that in order to prevent more than 2% curtailment with a plant capable of 30% minimum load, a 48 MWh battery, expected to cost 96 M$, is needed [167], [178]. For a plant capable of 40% minimum load, twice the battery size would be required. And a plant with a 50% minimum load would require a battery greater than 100 MWh to prevent solar curtailment. The goal of preventing solar curtailment intuitively gives the impression that it will accompany a large reduction in fuel costs. However as shown in Figure 3-12B, fuel costs remain nearly constant because the majority of energy provided during the year still comes from natural gas, even with fully utilizing solar generation at 63% solar deployment. In order to meet demand completely with solar power, the solar capacity would need to be much larger than peak demand and accompanied by a large energy storage system. Despite fuel costs remaining constant, the LCOE experiences a linear increase as more batteries are added to the system.

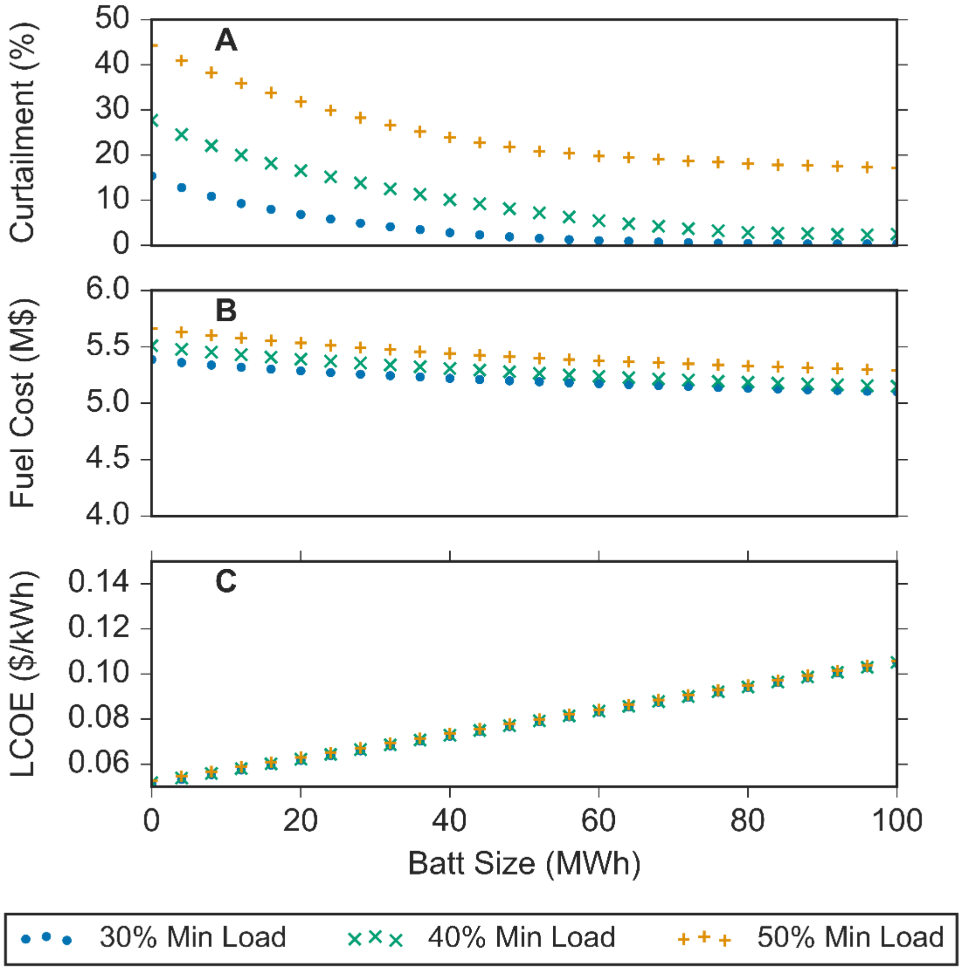

Figure 3-12. Impact of battery size on A) solar curtailment, B) fuel cost, and C) LCOE for a sCO_2 cycle with 63% solar deployment.

3.5 Conclusions

A power system analysis was performed to understand the ways in which load balancing can be delivered to a grid with deep deployment of solar power generation. Demand, solar irradiation and rooftop solar data were obtained from the University of Virginia and modeled to understand how increased solar deployment will impact the required performance characteristics of natural gas power plants providing grid balancing. The modeling suggests that state-of-the-art OCGT and CCGT are capable of providing the load balancing that would be needed in the system with high deployment (63% peak demand) of installed solar. CCGT operate with a much lower LCOE than OCGT due to their much higher efficiencies. It was shown that ramp rates of modern OCGT and CCGT are sufficient to keep up with solar generation ramp rates at 63% deployment whereas nuclear plants cannot and coal plants would be at their limits. Simulations of sCO_2 cycles operating in a combined cycle configuration with a gas turbine have shown that operating costs are expected to be comparable to CCGT, despite the promise of higher cycle efficiencies. In order to handle fluctuations in solar generation at 63% deployment without battery storage, sCO_2 cycles need to have ramp rates above 5.75% full load/min. To maximize their utility in grids with high solar deployment, sCO_2 cycles will need to operate with as low a minimum plant load as possible. This may be limited by the capabilities of the gas turbine it is combined with.

The results of this study suggest that in order to enable increased usage of solar PV, OCGT and CCGT designs should focus on lowering their minimum part load capabilities. For example, some manufacturers are combining two gas turbines with one steam turbine to allow the flexibility of two gas turbines while still achieving efficiencies of CCGT operation. It is expected that using smaller gas turbines in this configuration will reduce efficiencies, but expand the operational range. The fast start times, and high off-design efficiencies expected for sCO_2 cycles will be valuable as solar deployment increases. To gain a competitive edge over CCGT at low solar deployment, sCO_2 cycle research may consider focusing on reducing costs, both capital and operating. The results of balancing the solar generation have shown that a system with 63% solar deployment would require a large battery (48 MWh at 30% minimum load and 96 MWh at 40% minimum load) in order to avoid solar curtailment. Even with a battery this large, the majority of the electricity would come from burning natural gas. The model ran on a 1-minute interval and found that power plants operating with this degree of control would be able to adequately handle 63% solar deployment. Some degree of battery or capacitors may be necessary to handle fluctuations on the less than

1-minute interval in addition to the 30 MWh battery considered. As solar deployment continues to increase, the electric grid will increasingly rely on state-of-the-art natural gas fired plants to balance intermittent fluctuations. For the electric grid to operate completely on solar power the installed solar and storage capacity would need to far exceed what was modeled here. Such a transition will require natural gas power plants that in addition to having fast ramp rates will also require faster start-up times.

3.6 Chapter Acknowledgements

Thanks to the Rotating Machinery and Controls Laboratory at the University of Virginia, which supplied the funding for the worked described in this paper. Thanks to Ed Hall of UVA's Advanced Research Computing Service (ARCS) for his assistance with signal processing, University Facilities Management Department for providing the data, and Haley Neuhoff for her assistance with reviewing power plant and weather data

4 Techno-economic analysis of offshore isothermal compressed air energy storage in saline aquifers co-located with wind power[3]

4.1 Summary

Offshore wind power projects are increasingly attractive in many regions even though capacity is impacted by intermittency as it is with other renewable power sources. I examine balancing the intermittency with an Offshore Compressed Air Energy Storage (OCAES) system that combines near-isothermal compression and expansion processes via water spray injection with air storage in saline aquifers. Spray injection maintains the air at nearly constant temperatures to improve round-trip efficiency, and saline aquifers are abundant in near-shore environments at suitable depths. This techno-economic analysis estimates the efficiency, cost, and value of OCAES, and demonstrates it in the context of the Atlantic coast of the United States, for a wind lease near Virginia. The round-trip efficiency of the OCAES system is projected using a thermal fluid process model that accounts for machinery performance as well as geophysical subsurface characteristics and gradients. Cost estimates are based on combining axial gas turbine technology with water spray injection retrofits and drilling experience from the oil and gas industry. Value to the electric grid is quantified with a price-taker dispatch model that optimizes the value of delivered electricity. The results show that for the geophysical conditions considered, a 200 MW OCAES system is expected to have a round-trip efficiency of 77% and a capital cost of $1457/kW. When paired with a 500 MW wind farm, OCAES is able to increase revenue from $0.031/kWh, without storage, to $0.048/kWh. I also show that a 350 MW OCAES system with 168 hours of storage is able to make the wind farm power output constant with an LCOE of $0.22/kWh, 81% less than with 10-hour lithium-ion battery technology.

[3] This chapter was adapted from: Bennett, J.A., Simpson, J.G., Qin, C., Fittro, R., Koenig, G.M., Clarens, A.F., Loth, E. (2020), Techno-economic analysis of offshore compressed air energy storage in saline aquifers co-located with wind power. Manuscript submitted for publication.

4.2 Nomenclature

Table 4-1. Acronyms and Abbreviations.

CAES	Compressed Air Energy Storage
COVE	Cost of Valued Energy
DOE	Department of Energy
ICAES	Isothermal Compressed Air Energy Storage
LCOE	Levelized Cost of Energy
LMP	Locational Marginal Price
NREL	National Renewable Energy Laboratory
OCAES	Offshore Compressed Air Energy Storage
O&M	Operation and Maintenance
RPS	Renewable Portfolio Standard
RTE	Round-Trip Efficiency
VRE	Variable Renewable Energy

Table 4-2. Symbols.

A	Constant
AEP	Annual Energy Production
c	Specific heat
C	Cost
CC	Capacity Credit
CP	Capacity Payment
CR	Capacity Revenue
CRF	Capital Recovery Factor
D	Diameter
E	Energy demand
f	Friction coefficient
g	Gravitational constant
G	Hourly generation
h	Formation thickness
i	Real interest rate
k	Permeability
l	Length
$\dot{m}$	Mass flow rate
M	O&M costs
ML	Mass Loading
n	Polytropic exponent
N	Lifetime
p	Pressure
P’	Normalized spot market price
Q	Volumetric flow rate
R	Gas constant
Re	Reynolds number
r	Radius

T	Temperature
U	Mean flow velocity
v	Specific volume
V	Volume
w	Work
$\dot{w}$	Power
z	Depth
Z	Gas compressibility
γ	Specific heat ratio
ϵ	Roughness
η	Efficiency
μ	Viscosity
ρ	Density

4.3 Introduction

By 2050, solar and wind energy are projected to provide 30% of electricity generation in the United States and 50% in the world due to large reductions in capital costs combined with the establishment of policy incentives such as renewable portfolio standards (RPS) [180]. The intermittency of these Variable Renewable Energy (VRE) sources introduces grid integration challenges that require energy storage or fast-acting power plants for load-balancing [57]. Arbabzadeh et al. found that complementing renewables with energy storage will prevent curtailment and reduce the emissions of generating electricity [181]. However, the ability of VRE and energy storage to effectively mitigate climate change relies on cost improvements in energy storage, according to Braff et al. [182]. The most widely discussed energy storage technology is batteries because they are a proven modular technology with fast response times and high efficiency. However, the high costs [183], calendar and cycle life limitations [183], manufacturing and waste management environmental concerns [184], and the coupling of power output and energy stored [185] has led to a search for alternatives. Jafari et al. found short-term battery storage with offshore wind energy to be unprofitable based on data from 2010 to 2013; the breakeven price needed for batteries was below current cost of battery energy storage systems [186]. Energy storage technologies may need to be tailored to the region and installation location of the VRE production. For example, legislation passed in the United States for Virginia in 2020 and for New York in 2019 requires utilities to install 5.2 GW by 2034 and 9 GW by 2035 of offshore wind, respectively [187,188]. Co-locating these offshore wind farms with energy storage could smooth energy production and make the VRE dispatchable. The corrosive environment offshore is unsuitable for batteries but could be an opportunity for compressed air energy storage.

Compressed air energy storage (CAES) systems use electricity to pressurize and store air and then expand the air later to produce electricity at times in need of the generation. Combining wind power with CAES has been investigated as a way to meet baseload electricity demand [189] or even provide constant power [44]. Over 20 years ago, Seymour presented a concept of offshore compressed air energy storage

(OCAES) as storing air in an open-ended container at the bottom of the ocean and then piping the air back to an onshore expander [43]. Alternative air storage has been considered for OCAES, such as the use of underwater accumulators by Cheung et al. and Wang et al. [190–192]. Other forms of pressurized air storage for OCAES have been presented but not analyzed by Boehme et al. including floating sections of pipe, undersea caverns, and depleted gas reservoirs [193]. Mouli-Castillo et al. analyzed the potential of saline aquifers to store compressed air offshore of the United Kingdom for seasonal storage (multiple months) [46].

Saline aquifers or other porous media are advantageous offshore because they are geographically widespread and have a large capacity. There are many areas of overlap between subsurface saline aquifer formations and planned offshore wind farms for the eastern coast of the United States, as shown in Figure 4-1 for the Mid-Atlantic. Fukai et al. identified the Middle Cretaceous, Lower Cretaceous, and Upper Jurassic formations in the Mid-Atlantic, all strata in the Baltimore Canyon Trough, with a caprock suitable for pressurized storage [194]. Air storage has previously been considered in aquifers or other subsurface porous media for onshore applications as summarized by Li et al. [195]. Studies by Oldenburg and Pan, Guo et al. and others have performed two-dimensional multiphase numerical simulations of the porous media and wellbore [196–199]; however, these are computationally intensive and therefore limit the number of cases that can be considered. Other aspects of operating CAES in a porous media have included work by Sopher et al. that evaluated the total storage potential in Gotland, Sweden [200] and Yang et al. that examined daily, weekly, and monthly cycling of CAES in onshore aquifers [201]. As of 2020, no CAES plants are operating using a porous subsurface formation, such as a saline aquifer. The Iowa Stored Energy Park was a CAES plant planned to operate in an aquifer, but it was not ultimately built in part because the permeability was found to be insufficient late in the planning process [202].

Although OCAES faces the challenges of offshore installation costs and a corrosive environment, OCAES wells will have a higher formation pressure as compared to onshore, due to the hydrostatic pressure of being under the ocean, increasing the potential energy for the same amount of air stored. Using saline aquifers for CAES that are offshore will avoid concerns from adjacent landowners over induced seismicity [203,204]. It is also noted that monopile offshore wind turbine foundations are vulnerable to extreme earthquakes [205], thus co-locating with CAES would require additional review to make sure any risk of induced seismicity would not affect their structure.

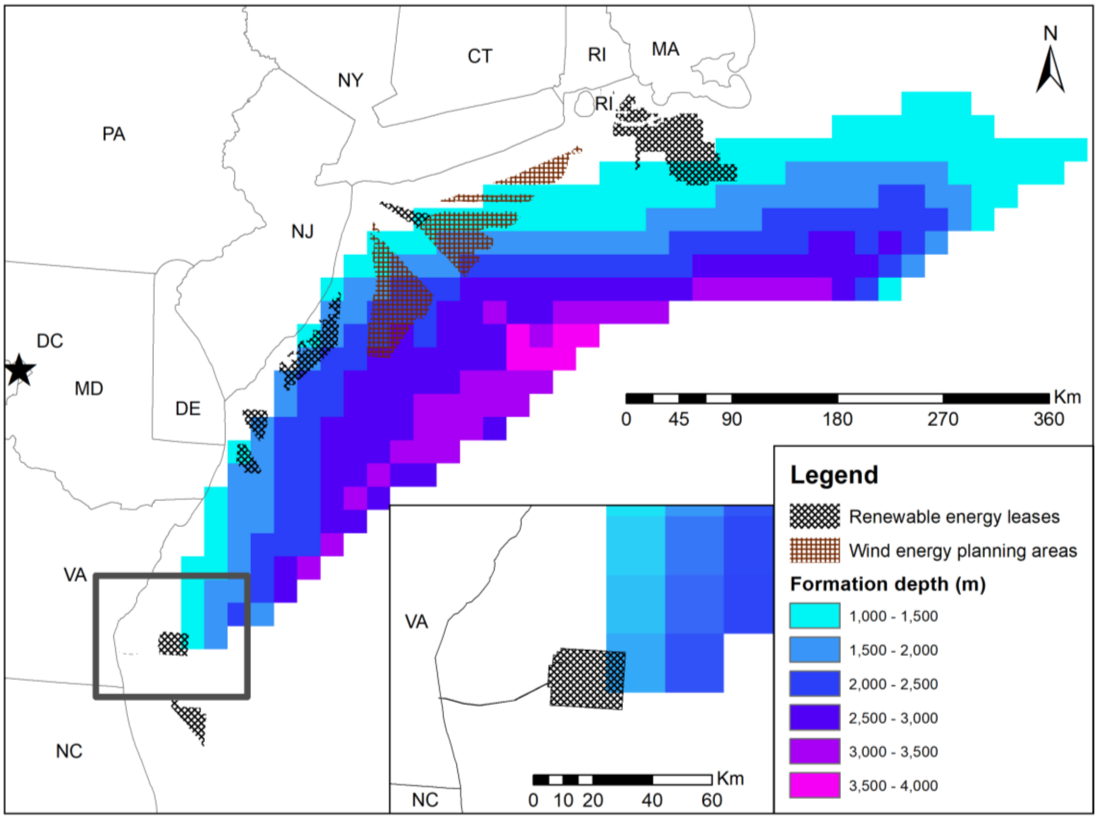

Figure 4-1. Comparison of offshore wind energy leases and underground saline aquifer formations. The inset shows Dominion Energy's renewable energy lease, which is the study area considered here. Lease data is from US Bureau of Ocean Energy Management [206]. The formation shown is the lower Cretaceous with data from Fukai et al. [194].

In addition to the type and location of the storage reservoir, CAES systems can also be classified by the type of thermodynamic cycle employed. Several thermodynamic cycles have been presented for OCAES, including diabatic, adiabatic, and isothermal. Conventional CAES uses a diabatic cycle, which requires combustion of a fuel such as natural gas before the expansion phase, and is used by the two utility-scale CAES plants in operation today: a 290 MW plant in Huntorf, Germany operated since 1978 and a 110 MW plant in McIntosh, Alabama operated since 1991 [14]. Mouli-Castillo et al. considered diabatic CAES in their study of OCAES in saline aquifers, but did not consider the need to meet or balance electricity demand [46]. Adiabatic CAES is the concept of capturing the heat of compression, storing it in thermal storage tanks, and re-using the heat in the expansion step. The development of adiabatic CAES has been limited by the need for a high-temperature thermal energy storage sub-system and a high-temperature electrically-driven compressor [42]. Isothermal CAES (ICAES) relies on near-isothermal compression and expansion processes, which eliminates the need for a heat source prior to the expansion process and is expected to have the highest round-trip efficiency (RTE) of CAES thermodynamic cycles [207]. In order to achieve a near-isothermal process, a large surface area is required to improve heat transfer during compression or expansion, which has been met through combinations of porous media [208], liquid pistons [207,209], and spray injection [210,211]. Injecting a small amount of atomized water droplets can provide a large surface area [212]; additionally, water has a large heat capacity to mitigate air temperature change. Water injection has also been demonstrated in a conventional solid piston for CAES [213], and is commonly used in industrial gas turbines [214] and aero engines [215] for the purpose of heat transfer enhancement. ICAES could be well-suited for OCAES because there is no need to burn fuel (as in diabatic CAES) or store heat for a long time (as in adiabatic CAES) offshore. Patil and Ro compared liquid piston-based ICAES systems storing air in an underwater container and found that round-trip efficiencies varied between 49% and 62% depending on the type of heat transfer enhancement used [207]. Li and DeCarolis performed a techno-economic analysis of OCAES that assumed a round-trip efficiency in the range of 70-80% for ICAES, but did not calculate the efficiency or consider the value of the electricity to the electric grid [44]. A comprehensive round-trip efficiency analysis has not been performed for ICAES in offshore saline aquifers.

In addition to considering the technical constraints of the storage system, it is important to analyze how the technology will be used and its economic trade-offs. Two ways energy storage is monetized are by spot market prices for energy sold to the grid and capacity value for guaranteed generation capacity. To capitalize on variable spot market prices, energy storage can implement energy arbitrage or time-shifting. Energy arbitrage involves buying energy when the spot market price is low and selling to the grid when the price is high to maximize revenue. With current energy storage technology, energy arbitrage revenue is not enough to offset the cost of storage in most markets [186,216]. Time-shifting is similar to energy arbitrage, but instead of buying electricity from the grid, energy storage is used to temporally decouple a generator from the grid and shift when energy is produced. Capacity markets provide another direct revenue source for energy storage but vary significantly by region [217]. In PJM, the regional transmission organization covering Virginia and several other Mid-Atlantic states, capacity payments are provided based on the Reliability Pricing Model, where power generators are paid for a commitment to provide electricity when needed by the electrical grid [217,218]. As VRE provides a larger share of the electrical grid, capacity prices are likely to rise and provide more revenue for energy storage systems.

The standard metric for comparing energy systems is Levelized Cost of Energy (LCOE), which normalizes annual costs by the annual energy produced [149]. Despite the many applications of energy storage, using LCOE to compare combined energy storage and generation systems will result in a no-storage solution because storage increases the cost of the system without increasing the amount of energy generated. A metric that includes the benefits and effects of adding storage is needed to evaluate systems with storage. A recent study by Simpson et al. proposed using the Cost of Value Energy (COVE) as an alternative metric that values energy based on when it is delivered to the electric grid [219]. COVE provides a single metric for optimization that includes both the cost of the system and a time-dependent value of energy, and therefore is a more accurate economic assessment than using just LCOE.

Various aspects of OCAES have been previously explored, but the optimal combination of storage medium, thermodynamic cycle, and operational timescale remains unknown. I hypothesize that an isothermal thermodynamic process combined with a saline aquifer will provide more value to the electric grid than Li-ion batteries. Near-isothermal compression and expansion processes are expected to have high efficiencies and require neither natural gas nor a separate thermal energy storage system. Saline aquifers confined by a caprock or impermeable layer are abundant in many coastal regions around the world, making this work broadly applicable to many regions. This paper aims to develop a methodology to assess the performance and value of OCAES for use with an offshore wind farm. I quantify the value of using OCAES for time-shifting with both LCOE and COVE. This is the first study to quantify the efficiency of an isothermal compressed air energy storage system using a saline aquifer for air storage. The framework presented here may be applicable to any site suitable for an offshore wind farm and adjacent to a saline aquifer. I demonstrate the methodology for the case of offshore Virginia because of significant potential related to the plans to install 5.2 GW of offshore wind by 2034 in leases that overlap the saline aquifers of the Baltimore Canyon Trough [187].

4.4 Methodology

To quantify the performance and economic value of OCAES, three models were developed and coupled. First, I formulated a thermal fluid process model to estimate the system Round-Trip Efficiency (RTE). Next, a cost model was created to estimate the capital costs. Finally, I developed an optimization model that uses the RTE and costs as inputs to quantify the value of OCAES to the electric grid. The interconnection of these models is shown in Figure 4-2.

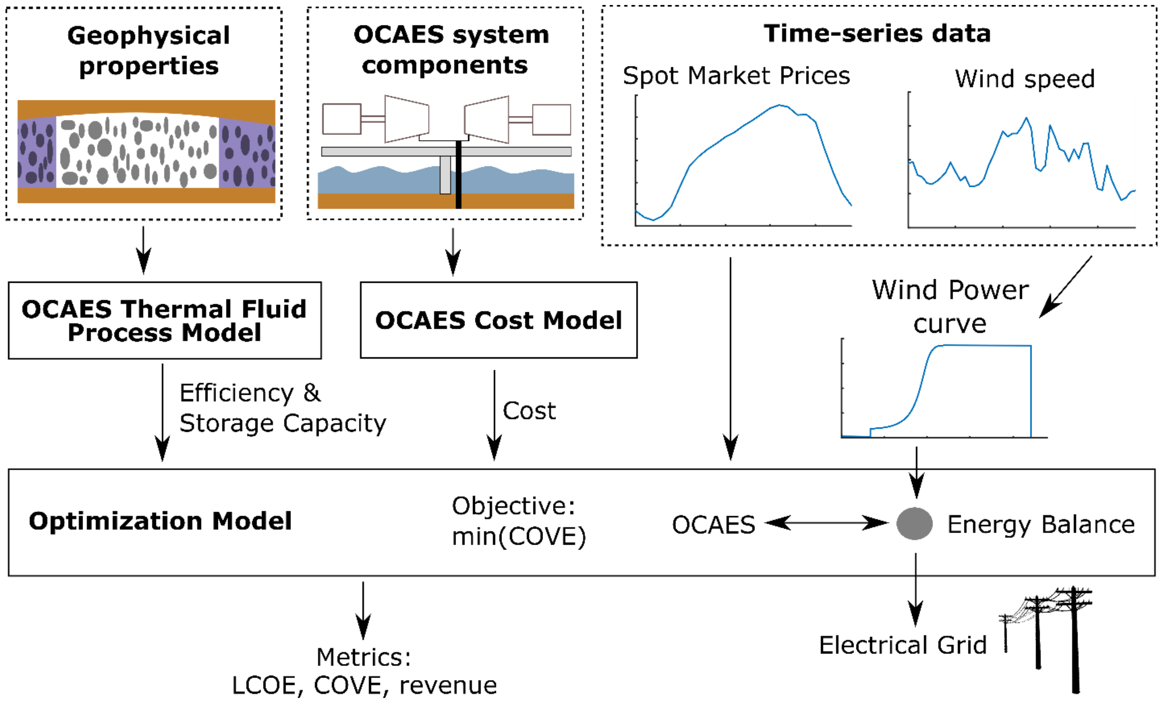

Figure 4-2. Optimization model system diagram where wind speeds and spot market prices are input from hourly datasets, efficiency, and storage capacity are input from the thermal fluid process model, and system cost is input from the cost model. The model then optimizes the hourly energy balance between wind power, OCAES, and the electrical grid over a year while minimizing COVE as the objective function.

4.4.1 Thermal fluid process model

The thermal fluid process model estimates the RTE of the OCAES system by simulating the performance of the major components and expected loss mechanisms. As shown in Figure 4-3, during charging, air at atmospheric temperature and pressure is compressed with a near-isothermal compressor (Comp.) with spray injection of desalinated water. The air then travels down the wellbore for which the pressure changes due to frictional losses and the change in gravitational potential. Next, the air exits a screened well and radially moves into the saline aquifer formation. Within the formation, the movement of air will result in pressure drops due to aerodynamic friction losses and the high pressure will lead to mass leakage due to the aquifer structure and permeability. During discharging, the air travels back through the aquifer formation and wellbore and is then expanded through a turbine (Turb.) with spray injection. The compression and expansion processes take place in 3-stages of machinery. Electrical losses in the motor and generator are also included as well as mechanical losses and pressure losses between machinery stages.

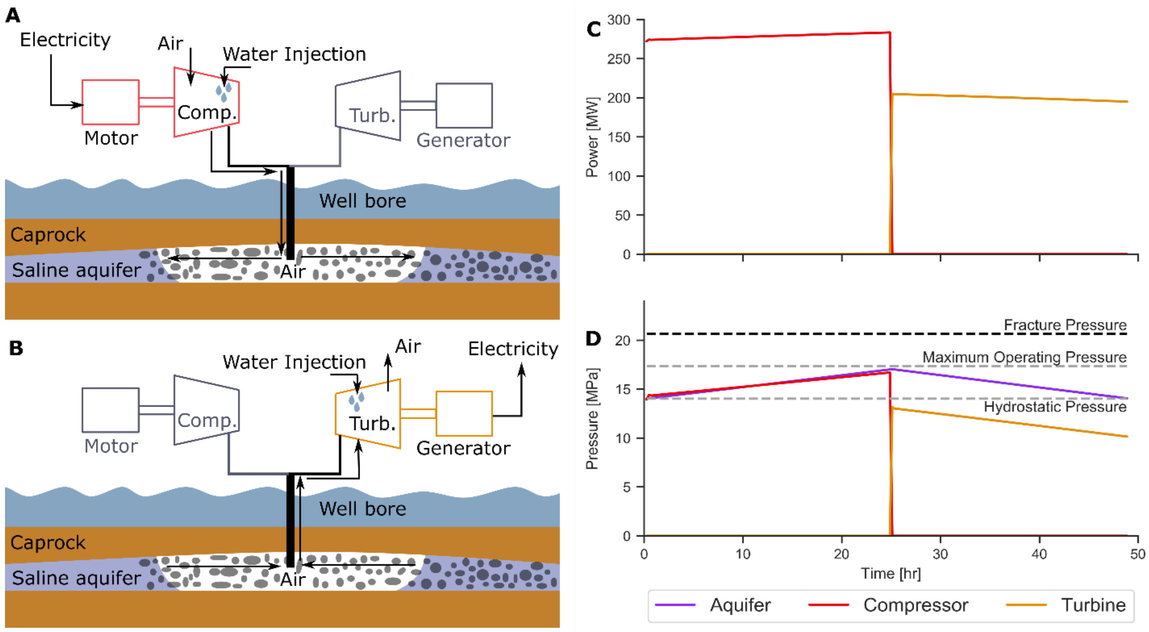

Figure 4-3. The thermal fluid process model estimates system round-trip efficiency by simulating air injection through a single charge (a) and discharge (b) cycle while calculating power inputs (c) and maintaining the aquifer pressure below the maximum operating pressure (d). Example simulation shown for a 200 MW, 24-hour duration system.

The thermal fluid process model uses empirical and physics-based relationships to assess a wide range of power capacities and storage durations. The model operates by simulating a single charge and discharge cycle, as shown in Figure 4-3. The operation cycle is dictated by the operating pressure range. The formation is simulated to start at hydrostatic pressure, and the pressure in the formation increases as air is injected until it reaches the maximum operating pressure, which is based on the expected fracture pressure with a safety factor. Geophysical and machinery parameters for the process model are summarized in Table 4-3.

Two other model inputs are radius of the air plume (formation volume occupied by air) and the mass flow rate. The model is run iteratively, varying the air plume radius and mass flow rate until it is sized at the intended power rating and storage duration. The primary output of the model is RTE. The geophysical parameters represent the conditions of the Lower Cretaceous formation in the Baltimore Canyon Trough, which is located under the Dominion Energy lease offshore Virginia (Figure 4-1) based on Fukai et al. [194].

Table 4-3. Summary of process model parameters.

Variable	**Value**	**Reference**
Geophysical Parameters (symbols)		
Depth and wellbore length (l)	1402 m	Fukai et al. [194]
Thickness	62.44 m	Fukai et al. [194]
Porosity	0.23	Fukai et al. [194]
Permeability (k)	38.67 mD	Fukai et al. [194]
Hydrostatic pressure	14.02 MPa	Fukai et al. [194]
Fracture pressure	20.66 MPa	Fukai et al. [194]
Fracture safety margin	0.5	Allen et al. [220]
Maximum Operating Pressure	17.34 MPa	Calculated
Formation temperature	42.87 °C	Calculated from [194]
Formation mass leakage	3.5%	Oldenburg and Pan [196]
Machinery Parameters		
Mass loading (ML) [Stage 1, Stage 2, Stage 3]	2, 1.5, 1.0	Assumption
Interstage pressure loss between stages	0.1 %	Assumption
Mechanical efficiency	99.0 %	Dixon and Hall [221]
Generator efficiency	98.9 %	Siemens [222]
Pump efficiency	75%	Assumption
Wellbore		
Inner Diameter (D)	0.41 m	Adams et al. [223]
Internal Roughness (ϵ stainless steel)	0.002 mm	White [224]
Atmospheric		
Sea-level Air Temperature	16.85 °C	NOAA [225]

4.4.1.1 Near-isothermal compression and expansion machinery

To provide sufficient storage capacity and power density for a wind farm, the compression and expansion system will need to handle high flow rates of air while compressing up to the formation pressure of 14 MPa. For example, at 300 MW, an air flow rate 825 kg/s is required. Depending on the design storage power, the system will likely involve multiple compressors in series and parallel to reach the desired compression ratio and flow rate. For example, a large flow rate axial compressor [226] followed by a smaller, high pressure axial or centrifugal compressor would be appropriate to reach the prescribed pressure ratio and flow rates.

No one has previously proposed performing isothermal compression with axial compressors. However, the same principle of water spray has been previously applied to piston compressors, where sufficiently small droplets and high mass loading can maintain a near isothermal environment while compressing or expanding the gas [213]. Water spray can be operated with axial compressors, although detailed concept design should be further explored in future research.

The high air flow rates for the upper end of OCAES power ratings considered herein will require even higher water flow rates and injection work. Cross-flow atomization has been shown to produce tiny drops while maintaining high mass flow rates [227] and thus will be used in the compression and expansion processes to meet the required mass loading and reduce injection work consumption. The water droplets generated by cross-flow atomization have tiny diameters, and the droplets can stay aloft and may carry over from one stage to the next. This can help to reduce the spray mass flow rate to a minimum of the highest mass loading stage; herein, the highest mass loading is in stage 1 with twice the air mass flow rate.

The spray system needed for isothermal compression will require a closed-loop clean water system. While minimal water loss to the air is expected, there will need to be a system for makeup water, likely via a desalination system for seawater.

The specific work of the near-isothermal machinery is represented as a polytropic process, which is expressed as,

$$w = \frac{n\,R\,T_1}{n-1}\left(1 - \left(\frac{p_2}{p_1}\right)^{\frac{n-1}{n}}\right) \tag{4-1}$$

where n is the polytropic exponent, R the gas constant, T_1 the temperature at state 1, p_1 the pressure at state 1, and p_2 the pressure at state 2. From Qin and Loth [210], the polytropic exponent for a near-isothermal spray injection process can be calculated as,

$$n = \gamma \cdot \frac{1+ML\,(c_d/c_p)}{1+k\cdot ML\,(c_d/c_p)} \tag{4-2}$$

where γ is the gas specific heat ratio (1.4 for air), c_d is the specific heat capacity of the droplets (water) and $c_p$the specific heat of the gas at constant pressure (air). The water Mass Loading, ML, for a continuous flow system is defined as,

$$ML = \frac{\dot{m}_{water}}{\dot{m}_{air}} \tag{4-3}$$

where $\dot{m}_{water}$ is the mass flow rate of water and $\dot{m}_{air}$ the mass flow rate of air [210]. Spray injection of water also requires pump work,

$$w_{pump} = \frac{v_1(p_2-p_1)}{\eta_{pump}} \tag{4-4}$$

where v_1 is the specific volume at the pump inlet, p_2 the pressure at the pump outlet, p_1 the pressure at the pump inlet, and η_{pump} the isentropic efficiency [228].

4.4.1.2 Wellbore

The air flow in the wellbore is assumed to be steady, incompressible and thus constant density along a streamline. The mean flow velocity of the compressed air in the wellbore is constrained to stay below 0.3 Mach to avoid compressibility effects and maintain the validity of equations shown here. Therefore, the mass flow rate is constrained based on the current air density in the system. The change in pressure due to a change in potential energy is calculated using Bernoulli's equation. Bernoulli's equation is then combined with the change in pressure due to viscous friction losses along the wellbore, resulting in equation 4-5,

$$p_1 - p_2 = \rho g(z_2 - z_1) + f\,\frac{l}{D}\frac{\rho U^2}{2} \tag{4-5}$$

where p_1 and p_2 are the pressures at the top and bottom of the well respectively, ρ is the density of the air going into the well, $z_1$and z_2 are the heights of the top and bottom of the wellbore respectively, D is the internal diameter of the wellbore, l is the length of the wellbore, and U is the average speed of the gas over the pipe cross-section. The friction coefficient f is found by iterating over equation 6, where ϵ is the pipe roughness and Re_D is the Reynolds number within the wellbore [229].

$$\frac{1}{\sqrt{f}} = -2\log\left[\frac{\epsilon/_D}{3.7} + \frac{2.51}{Re_D\sqrt{f}}\right] \tag{4-6}$$

Heat transfer along the wellbore is expected at the beginning of operation, but after many cycles the temperature in the adjacent formation is expected to stabilize and result in low heat loss [195,199]. Depending on the thermal diffusivity of the subsurface formation, pipe casing design and insulation may be important to reduce heat loss along the wellbore. Here, the insulation is assumed to be sufficient such that heat loss is negligible along the wellbore.

4.4.1.3 *Porous media aquifer formation*

The pressure drop in the aquifer formation is based on radial Darcy steady-state flow [200] and is calculated using,

$$Q = \frac{A\,k\,h\left(p_f^2 - p_w^2\right)}{\mu\,T\,Z\,\ln\left(\frac{r_f}{r_w}\right)} \tag{4-7}$$

where Q is the volumetric flow rate, k is the permeability, h is the aquifer height, p_f is the pressure at the formation edge, p_w the pressure at the wellbore, μ is the viscosity, Z is the gas compressibility factor, r_f is the radius of the formation, r_w the radius of the wellbore and A is a constant equal to 0.008834 m^2-cP-K/mD-MPa-s that combines π with unit conversions. The compressor outlet pressure is operated such that once the air has traveled through the wellbore and formation, it is the same pressure as the air in the formation. Injection of air into the aquifer will change the temperature of the formation over time [197] and may approach the injection temperature with frequent cycling [201]. Here, it is assumed that the air becomes the same temperature as the formation once it has traveled through the formation. For my simulations, the air injection temperature is higher than the formation temperature, so there is an implicit amount of heat lost. The amount of energy stored in the formation is represented as mass accumulation. Li et al. provide a review of other high-level methods to track energy stored in porous media [195]. The accumulated gas mass m, leads to an increased pressure, which is calculated using the ideal gas law,

$$p = \frac{m\,R\,T}{V} \tag{4-8}$$

where V is formation volume that is filled by the air (excludes any volume that is solid or liquid). Based on experience by Katz et al., the air plume is not expected to decrease in size if pressures are maintained above the initial reservoir pressure [230]. Additionally, the model includes a mass leakage rate of 3.5% based on Oldenburg and Pan [196].

4.4.2 Cost Model

The capital cost of the OCAES installation was estimated by considering the three main cost components to be the compression and expansion equipment, the well, and the offshore platform. The offshore wind farm costs are taken directly from the 2018 Cost of Wind Energy Review [231] for fixed bottom turbines.

4.4.2.1 Compression and expansion equipment

Due to the high design flow rates and high cost for space on an offshore platform, the first stages of compression and expansion will be done with axial compressors. Later stages may be completed with axial or centrifugal compressors but will be assumed to be axial for the purpose of the cost model. The cost for axial compressors and turbines (expanders) is based on gas turbine capital costs from the EIA 2020 Capital Cost and Performance Report [232]. The capital cost (excluding Owner's Cost) for 100 MW simple cycle aeroderivative gas turbines is $1050/kW, which includes the compressor, combustor, expander, generator, inlet filtration, and installation.

An additional motor is needed to run the compressor, and its cost (C_{motor}) is estimated based on Aminyavari et al. [233] as follows where $\dot{w}$, the power input work in units of kW, is related to cost in dollars as,

$$C_{motor}(US\$) = 26.18\ (\dot{w})^{0.95} \tag{9}$$

While the gas turbine capital cost estimate does include installation, the total cost of the compression/expansion system is increased by 15% to account for the complexities of installing this system offshore.

4.4.2.2 Isothermal retrofit cost

Many of the components included in the capital cost for a gas turbine are unnecessary or over-sized for the ICAES system, such as the oversized compressor or the turbine made to withstand high temperatures of combustion. It is assumed that the additional cost to retrofit the compressor and expansion system to be isothermal is covered by the unused parts in the gas turbine system.

The spray water system is designed as a closed-loop system, so the injected water needs to be collected, recycled, and supplied. The isothermal retrofit would also include an atomization system, which has a configuration of nozzles, pumps, and heat exchangers.

4.4.2.3 Drilling

For a conservative estimate, offshore well drilling costs were based on offshore CO_2 sequestration drilling cost estimates in the Pale Blue Dot report [234] previously used by Mouli-Castillo et al. [46] to estimate offshore diabatic CAES well costs. From the report, the median well cost for depths 700-3000 m was €7.2 million, which was then converted into 2020 USD as $8.6 million. Cost estimates are performed for one well.

This cost is significantly higher than other well cost estimates based on oil and gas drilling experience. For example, an estimated mid-range cost of $2 million for drilling the well was based on [235,236]. However, the cost of drilling for a CAES system is likely to be higher than traditional oil and gas drilling since the wellbore needs to be wider than standard sizes. For example, geothermal wells tend to have ~20 cm completion (internal) diameters and oil and gas wells tend to have ~12 cm completion diameters [237]. Oldenburg and Pan explored a 50 cm well diameter for CAES [196]. Adams et al. explored using wells with diameters up to 41 cm with depths as great as 5 km for geothermal applications [223], so I assumed a well diameter of 41 cm.

4.4.2.4 Offshore platform

The isothermal compression and expansion system will be located on an offshore platform, similar to platforms used for offshore substations. If the system is small enough, it may be co-located with the offshore wind farm substation platform. Cost estimates are performed assuming the OCAES system requires the construction of a separate platform, with costs based on offshore substations.

The area needed for the system was estimated based on square footage requirements for a gas turbine axial compressor first stage and centrifugal compressor second stage. A strong correlation between power and area was found by comparing the compression systems needed for set mass flow rates to the area of those systems. The area was then doubled to represent including the expansion system, and then doubled again account for maintenance access space based on spacing recommendations for an industrial gas turbine [226]. The cost for the platform was based on the NREL Balance of Station model documentation, which provides equations to estimate offshore substation cost based on substation mass [238]. That model was used in conjunction with an article detailing the London Array offshore wind farm substation [239], which provided an estimate for area to mass ratio. The final cost estimate used 250 MW of compression/expansion equipment to find an area and corresponding mass, and subsequently a cost. Based on cost estimates from BVG [240], an additional 29% cost was added for installation, resulting in a final cost for the offshore platform of $37.8 million.

4.4.2.5 *Other considerations*

Fixed and variable maintenance costs were applied to the OCAES system. Variable operating and maintenance (O&M) costs were estimated by starting with diabatic CAES variable O&M cost estimates [14,241], converting to 2020 USD, adding an estimated 20% increase for isothermal machinery maintenance [242], and finally adding an additional 100% for offshore maintenance costs, resulting in \$9.24/MWh. Fixed O&M costs were based on gas turbine O&M at \$16,300/MW-yr. [232].

Transmission lines from the wind farm (and offshore energy storage system) to shore could be adjusted in size to reduce cost or increase value to the system. This was done by Li and DeCarolis and Jafari et al. [44,186]. Instead, the OCAES system was treated as an addition to an existing wind farm, and thus transmission costs were not varied.

The lifetime of each loan and interest rate can significantly affect the annual cost projections for the system. The wind farm loan is annualized over 25 years with a 2.5% real discount rate (based on [231]), and the same lifetime and interest rate are applied to the OCAES system. A CAES system is expected to have a life of at least 20 years [14,44], and it is assumed to be 25 years to align with the wind farm.

Finally, the cost of electricity to fill the initial air plume in the saline aquifer before beginning operation of the OCAES system is not included. This cost is assumed to be negligible compared to capital costs when annualized over the expected lifetime of the system. Cost model inputs are summarized in Table 4-4.

Table 4-4. Summary of cost model parameters.

Variable	Value	References
Wind Farm		
Capital Cost	$4,444/kW	Stehly & Beiter [231]
Fixed O&M Cost (annual)	$129/kW	Stehly & Beiter [231]
Lifetime	25 years	Stehly & Beiter [231]
OCAES		
Isothermal compression/expansion equipment	$1,225/kW	Calculated from EIA [232], Aminyavari et al. [233]
Fixed O&M (annual)	$16.30/kW	Calculated from EIA [232]
Variable O&M	$0.00924/kWh	Calculated from Gu et al. [241], Luo et al. [14], Qin et al. [242]
Platform	$37.8M/platform	Calculated from Maness et al. [238], Froese [239]
Well	$8.6M/well	Calculated from Mouli-Castillo et al. [46], Pale Blue Dot Energy [234]
Lifetime	25 years	Assumption (same as wind farm)
Li-ion Battery (Benchmark)		
4-hour battery	$2,248/kW	Mongird et al. [183]
10-hour battery	$5,038/kW	Calculated from Mongird et al. [183]
Fixed O&M (annual)	$10/kW	Mongird et al. [183]
Variable O&M	$0.03/kWh	Mongird et al. [183]
Lifetime	10 years	Mongird et al. [183]
Economics		
Interest rate	5%	Stehly & Beiter [231]
Inflation rate	2.5%	Stehly & Beiter [231]

4.4.3 Battery Model

Li-ion battery storage will be used for comparison as it is currently the most common battery type installed for grid-scale energy storage [243]. The battery storage was assumed to be located onshore with either a 4-hour or 10-hour capacity, with 4-hour duration grid battery storage being used in multiple current installations and 10-hour duration relevant for comparison to OCAES. Based on the Department of Energy HydroWIRES report, the Li-ion battery storage was assumed to have a round-trip efficiency of 86%, a lifetime of 10 years, and a depth of discharge limit of 80% [183]. While the efficiency and capacity of batteries are likely to fade over time, these effects were not accounted for in the model used. Note that the low charge/discharge rate (e.g., C-rate [244]) of the system, with a maximum rate ¼ of the energy capacity (e.g., C/4), may result in a higher efficiency and longer lifetime, but those potential advantages were not considered. For financial analysis, the same interest rate as the wind farm is applied, but with a lifetime of 10 years.

Battery storage costs from the HydroWIRES report [183] were given for a 4-hour battery, with costs comparable to the median long-duration battery storage from the US EIA report on US Battery Storage Market Trends [243]. To better compare with an OCAES system, the cost of a 10-hour system was estimated by scaling up the costs of a 4-hour battery, and then the 80% depth of discharge limit was incorporated for both the 4-hour and 10-hour systems to find the cost of "working" power and energy rather than "nameplate" power and energy. Thus, for a working 400 MWh battery storage system, the corresponding nameplate cost would be for a 500 MWh system. This resulted in working costs of $5038/kW for a 10-hour system and $2248/kW for a 4-hour system.

4.4.4 Optimization model

Ultimately the value of energy storage is not based on its efficiency and capital cost alone, but rather its ability to balance the grid and shift the time when renewable generation is dispatched. An optimization model using linear programming was developed in Pyomo [245] to evaluate the value of OCAES to the electric grid. The model framework started with the optimization model presented by Li and DeCarolis [44] and extended the system boundary to include the price of electricity when selling to the grid. This enables time-shifting to sell wind energy when it is most valuable. This model is categorized as a "price-taker model" because it assumes that generation of energy from the proposed project will not affect energy prices. When wind energy makes up a small portion of the energy portfolio, this can be a reasonable assumption. However, as wind capacity for a reginal grid increases, energy prices would be expected to go down when wind energy production is high. In addition to the costs presented in Table 4-4, the model is also provided with one year of wind speed data off the Virginia coast from DOE BUOY data based on a 90 m wind turbine hub height [246] and day ahead hourly locational marginal prices (LMP) for Dominion's region in PJM [247]. The amount of wind energy is then estimated using the NREL 5 MW power curve [248], ignoring wind farm losses. The optimization model operates with perfect foresight and decides when to charge and discharge the OCAES system to minimize COVE. The amount of energy stored in the system is balanced, and the starting storage level in the system is a decision variable. The value of OCAES was measured with two metrics, LCOE and COVE. The Levelized Cost of Electricity [149], LCOE, can be simplified to,

$$LCOE = \frac{(C_{fixed} * CRF) + M_{fixed}}{AEP} + M_{var} = \frac{C_{total}}{AEP} \tag{4-10a}$$

$$\text{Real } CRF = \frac{i(1+i)^N}{(1+i)^N - 1} \tag{4-10b}$$

where C_{fixed} are the total capital costs, M_{fixed} are the annual fixed O&M costs, M_{var} are the variable O&M costs, AEP is expected annual energy production, and C_{total} is the total annualized cost. The Real Capital Recovery Factor (CRF) is used to annualize capital costs based on lifetime N and real interest rate i (discount rate less inflation rate) [231,249]. COVE is evaluated as,

$$COVE = \frac{C_{total}}{\int P\prime * G \, dt} \tag{4-11}$$

where P' is normalized spot market price and G is hourly generation, integrated over a year. While wind farm and energy storage size are specified in each simulation, hourly dispatch of the energy storage system is allowed to vary, affecting both the variable costs in the numerator and the weighted energy in the denominator. Due to this nonlinearity of COVE, the implemented objective function is to maximize the denominator of COVE, or the value of energy, to make it compatible with the linear program. This ignores the potential trade-off with variable O&M costs and assumes that those costs are small relative to the value gained by operating the energy storage system.

The revenue output from the optimization model includes electricity revenue from 2019 PJM spot market prices and capacity revenue. Capacity revenue (CR) is related to capacity value (CV) and capacity credit (CC) as follow.

$$CR = CV * CC * \left(\frac{365\ days}{yr}\right) \tag{4-12}$$

Capacity value is \$140/MW-day based on the 2021/2022 PJM capacity auction results [218]. The offshore wind farm was assumed to have a capacity credit in PJM of 20%, increased slightly from Byers et al. [217] to account for higher offshore wind capacity factors. Energy storage systems with storage capacity of 10 hours or greater received 100% capacity credit in PJM. Based on current PJM capacity requirements [250], the 4-hour battery system power was de-rated to reach 10 hours capacity, and thus received a capacity credit of 40%. The combined wind farm and energy storage capacity credit was limited to the 500 MW capacity of the wind farm transmission line.

A sample of the optimization model operation is shown in Figure 4-4. In this example, the algorithm identifies three local peaks in electricity prices around hours 15, 40 and 64. The storage system charges in the hours leading up to these peaks and then discharges at the peaks to maximize the value of electricity generated.

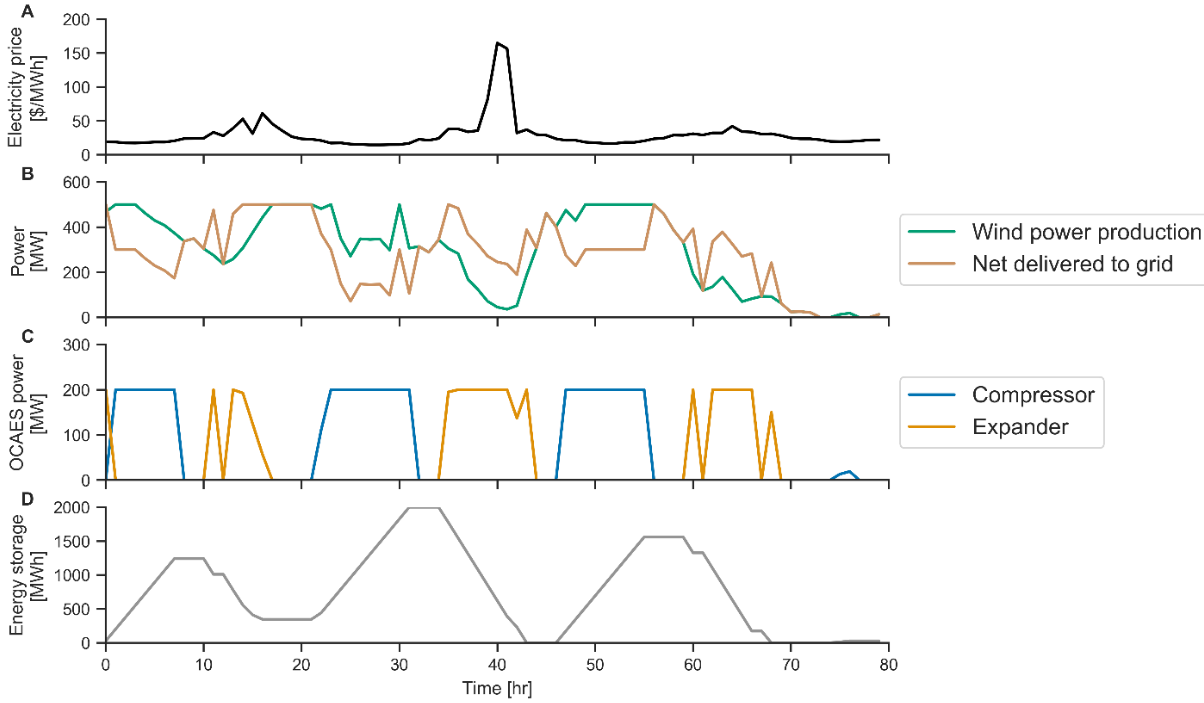

Figure 4-4. The optimization model minimizes the cost of valued energy (COVE) by storing wind power when electricity prices are low and selling it to the grid when prices are high. Shown for a 200 MW, 10-hour system.

4.5 Results and Discussion

4.5.1 Cost estimates

The total capital cost for an OCAES system with one well is shown in Figure 4-5 for varying power output. This cost is compared to the overall cost of a wind farm to illustrate the cost of storage relative to new generation. The cost of the OCAES system drops with increasing power because some costs are fixed for each well, such as drilling the well and building an offshore platform, while others vary directly with the power rating of the system, such as the compression and expansion machinery. The change in cost (in terms of $/kW) is small after 200 MW of power capacity. Capital costs are not annualized in Figure 4-5 and thus do not take into account the years of life expected. OCAES systems may be able to last through the entire lifetime of the wind farm. In comparison, Li-ion batteries are expected to be operational for 10 years or 3500 cycles [183], and would need to be replaced at least once during the lifetime of a wind farm. Battery storage costs $2,248/kW for a 4-hour system and $5,038/kW for a 10-hour system, while a 200 MW OCAES system is estimated to cost $1,457/kW. It is difficult for Li-ion batteries to compete on cost with OCAES in long-duration storage because of their inability to decouple energy and power. Albertus et al. has shown the importance of decoupling energy and power in their finding that long-duration storage will need significantly reduced energy capital costs with marginally reduced power capacity costs to be competitive with 100 hours of storage versus 10 hours of storage [251].

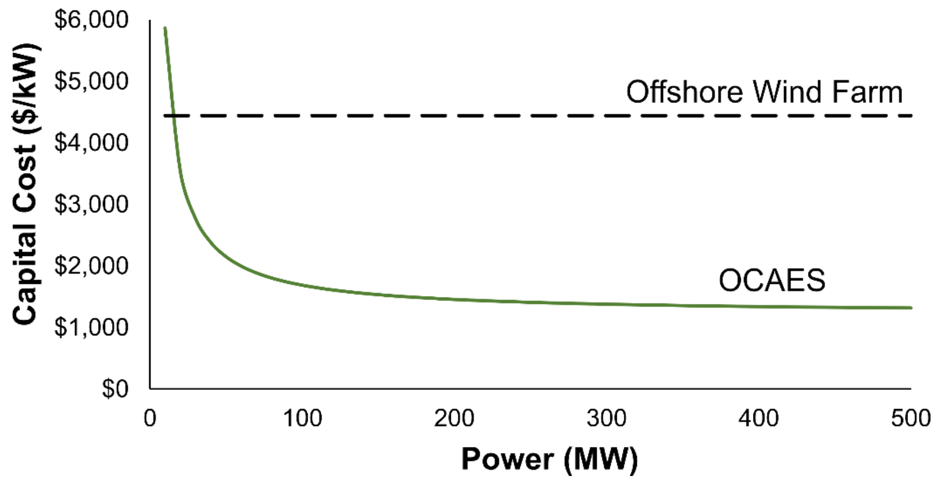

Figure 4-5. Capital cost vs. machinery capacity.

The distribution of annual costs for a 200 MW, 24-hour OCAES system ($21 M/yr in total) is shown in Figure 4-6. Estimated O&M costs are included based on an expected run time from the optimization model of 297,341 MWh/yr. The capital costs of the isothermal compression and expansion equipment contribute the most to the annual cost, but O&M costs are significant and should be considered in addition to capital costs when designing such a system.

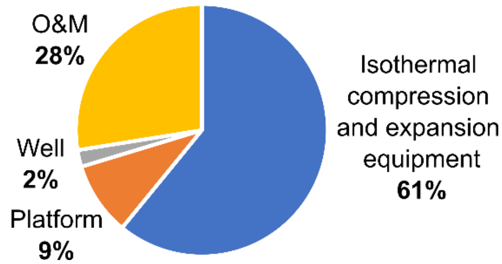

Figure 4-6. Breakdown of annual expected capital and operational costs for a 200 MW, 24-hour ICAES system.

4.5.2 Round-trip efficiency

Projected OCAES system round-trip efficiencies are shown in Figure 4-7 for a single well. Increasing the power rating requires higher injection flow rates and results in increased wellbore and aquifer frictional losses leading to decreased efficiencies. Power ratings above 400 MW are not shown because the injection pressure required to overcome frictional losses is so great that injection pressures would be larger than the maximum operating pressure of the formation as shown in Table 4-3 (including a safety factor with respect to the formation fracture pressure). The storage duration of the OCAES system is increased by expanding the radius of the air plume. The increased air plume radius results in increased frictional losses and decreased system efficiencies. The major losses for a 200 MW OCAES system are the near-isothermal system which is responsible for an 18-percentage point reduction. This is followed by air leakage and pipe friction, responsible for three percentage points each, and aquifer frictional losses at one percentage point. For comparison, the ICAES round-trip efficiency range is higher than that estimated by Patil and Ro [207] and in the same range as that estimated by Li and DeCarolis [44].

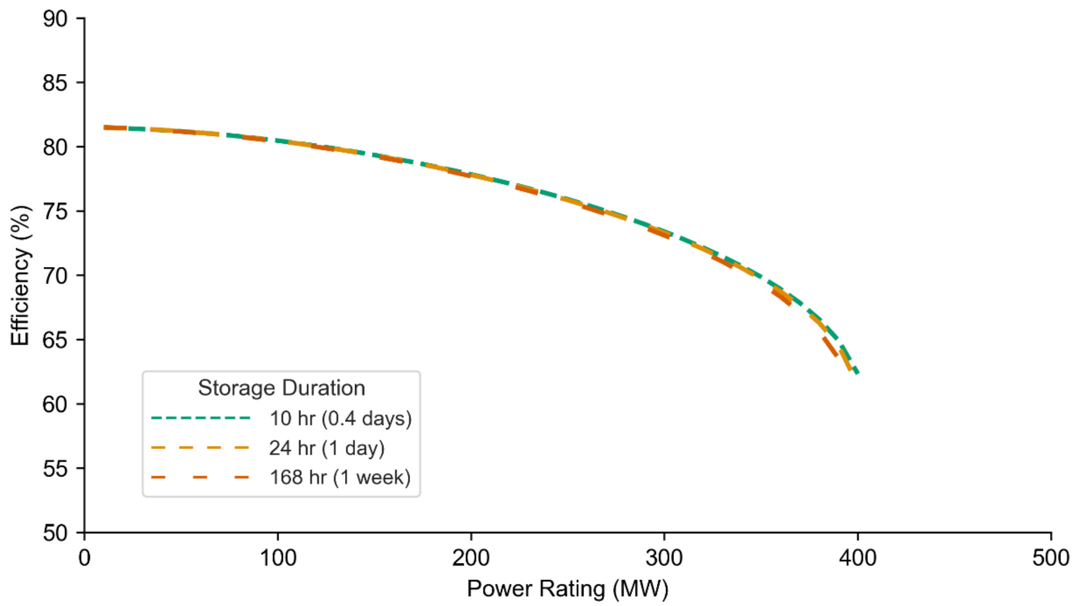

Figure 4-7. OCAES system sizing results using the performance model show the round-trip efficiency by power rating and storage duration.

4.5.3 OCAES value to the electric grid

To understand the value of OCAES to the electric grid, the dispatch model was run for two scenarios. Under the first scenario, the operation of the storage system was optimized for a fixed wind farm of 500 MW in order to minimize COVE over a range of energy storage power ratings. The purpose of this scenario was to simulate the wind farm and storage acting as a single entity selling to the electric grid. COVE is a more comprehensive approach to value the energy produced since LCOE does not consider the variability of prices. Figure 4-8 shows that adding storage significantly increased revenue over wind-only by up to 55% for one week (168-hours) of OCAES storage through a combination of capacity credits and shifting when generated electricity is sold to the grid. The LCOE of OCAES is 40% less than Li-ion batteries for 10-hour systems with 300 MW (3000 MWh) of storage (0.186 $/kWh vs. 0.113 $/kWh). With the given electricity market data, the revenue of wind is approximately one-third of the cost without storage;

therefore, offshore wind with or without storage is not able to break even with current costs. Optimal operation of the OCAES storage systems was able to maintain a COVE close to the original wind baseline despite the added cost of storage, while increasing the flexibility and dispatchability of the system. Storage currently does not provide a net profit based on spot price revenue and capacity payments (consistent with results from Jafari et al. in the PJM region [186]). However, price variations in the future are likely to grow (Virginia will have time of day pricing starting in January 2021 [252]) and may become negatively correlated with wind energy availability. This will effectively increase COVE for conventional wind farms, while plants with storage may be able to mitigate the effects of these negative correlations.

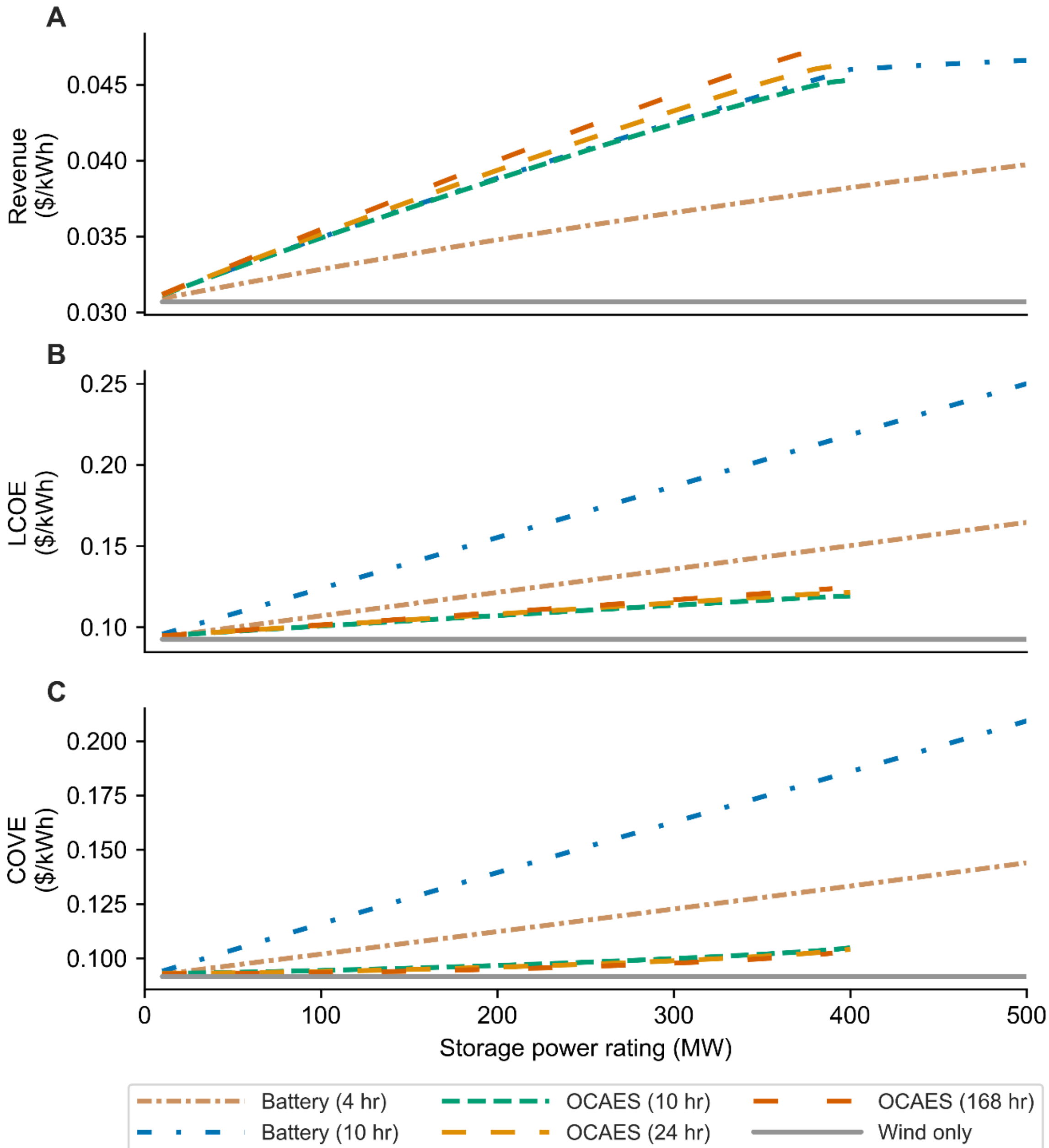

Figure 4-8. Comparison of battery and OCAES system capacity using 2019 day ahead prices on the basis of A) revenue, B) levelized cost of electricity (LCOE), C) Cost of Valued Energy (COVE).

The variability of wind combined with high levels of renewable deployment will result in high levels of curtailment without energy storage or increased grid flexibility as demonstrated by Denholm and Hand [10]. A second scenario was run to investigate the potential of relying on a wind farm with storage as a dispatchable power source. Under this scenario, the storage operation was optimized to maintain a constant amount of power delivered to the electric grid, again for a fixed wind farm size, to minimize COVE for a range of energy storage power ratings. Figure 4-9 shows that increasing storage duration results in higher possible constant dispatch power outputs and a much lower LCOE. Note that the LCOE in Figure 4-9 is influenced both by changes to the total system cost (based on storage technology) and by annual energy production (based on constant power output). The capacity factor of the wind farm is 46% for the given wind data, and thus 228 MW is the maximum constant power that could be delivered from the wind farm with perfectly efficient storage and infinite capacity. The storage options considered are only able to provide a fraction of that power at constant dispatch. Dispatchable wind power can cost as low as $0.224/kWh with OCAES for a week of storage at a storage rating of 350 MW, 81% lower than a 10-hour battery system. For comparison, the average July 2020 price of electricity in the US was $0.111/kWh, with maximum electricity prices at $0.261/kWh [253]. Therefore, 168 hours of OCAES storage is able to make wind dispatchable at a price worth considering in today's electric grid, though only in the most expensive of markets.

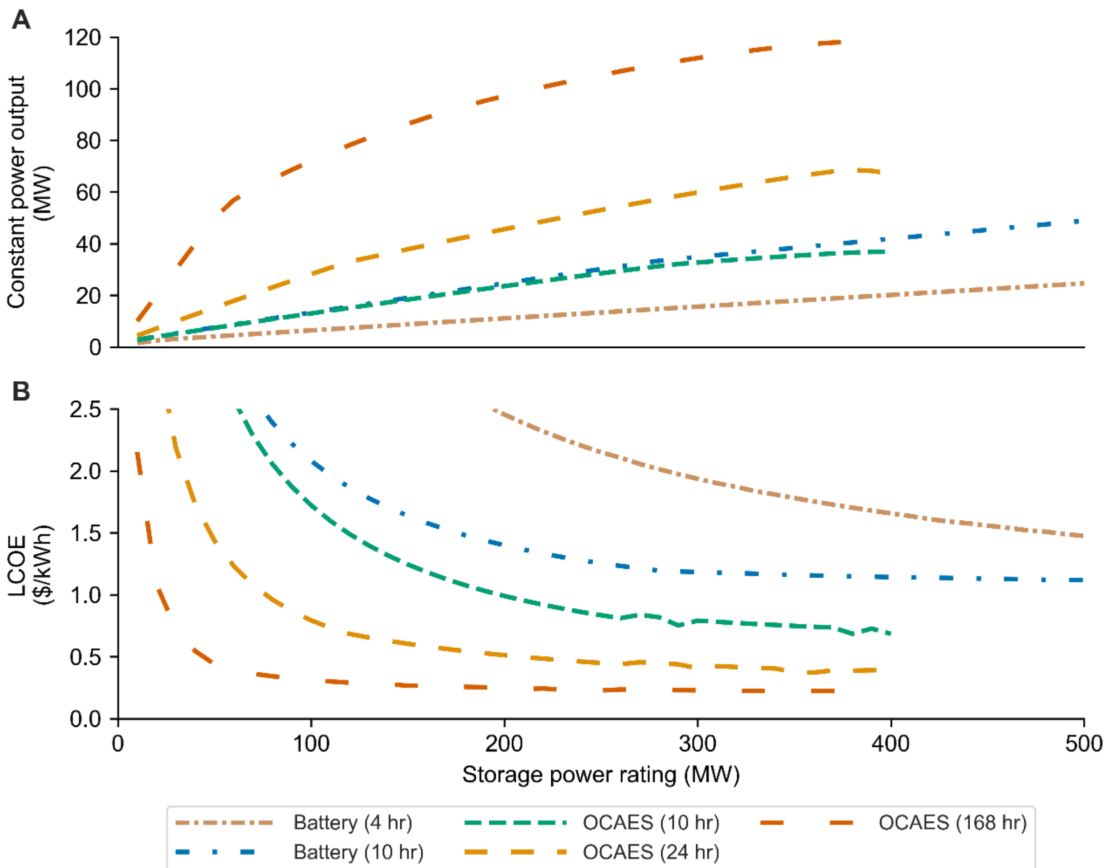

Figure 4-9. Comparison of battery and OCAES systems operating as dispatchable electricity generation using 2019 day ahead prices on the basis of A) constant power output to the electric grid, and B) levelized cost of electricity (LCOE).

4.6 Conclusions

Large-scale deployment of offshore wind energy will require energy storage for load-balancing to prevent curtailment. This study focused on the performance of a single-well compressed air energy storage system based on fixed geophysical parameters. When suitable geophysical conditions are present, offshore compressed air energy storage can provide the opportunity to co-locate energy storage with a wind farm. This study showed the engineering and economic viability of OCAES for 10+ hours of storage.

A thermal fluid process model was developed to estimate OCAES round-trip efficiencies based on given geophysical conditions. An OCAES system installed with geophysical parameters representative of the coast of Virginia is expected to have an efficiency between 61% and 82% depending on the energy storage capacity and power delivery rate. Efficiency decreases with increased power rating for a single wellbore due primarily to friction losses in the wellbore and aquifer.

This study estimated the capital costs to build and install an isothermal compressed air energy storage system using spray injection with air storage in a saline aquifer. The capital investment cost for a 10-hour 200 MW system is $1457/kW, half that of current Li-ion capital costs. Additionally, OCAES is expected to have an operational lifetime on the timescale of a wind farm, much longer than Li-ion batteries. The availability of OCAES does not lower either LCOE or COVE compared to the baseline, but does increase participation in the capacity market.

To quantify the value of OCAES to an offshore wind farm, a price-taker dispatch model was used. The model was optimized to decrease the cost of valued electricity (COVE), similar to LCOE. Based on hourly spot market prices from 2019 and a year of wind speed data, I estimated that OCAES will increase the revenue of an offshore wind farm by as much as 55%. Note that COVE results are likely to improve in the future as increased wind penetration in the electricity grid is expected to increase spot market price variability and thus increase the value of time-shifting. Additionally, increased capacity prices would help the OCAES system break even. I also investigated producing wind energy at regular dispatch of a constant output with energy storage and found that OCAES costs are 79% lower than Li-ion battery storage.

4.7 Chapter CRediT authorship contribution statement

Jeffrey Bennett: Conceptualization, Methodology, Software, Formal analysis, Data Curation, Writing – Original draft preparation, Visualization. **Juliet Simpson:** Conceptualization, Methodology, Formal analysis, Data Curation, Writing – Original draft preparation, Visualization. **Chao Qin:** Conceptualization, Methodology, Writing – Review & Editing. **Roger Fittro:** Conceptualization, Methodology, Writing – Review & Editing. **Gary Koenig:** Conceptualization, Methodology, Writing – Review & Editing. **Andres Clarens:** Conceptualization, Methodology, Writing – Review & Editing. **Eric Loth:** Conceptualization, Methodology, Writing – Review & Editing, Project administration.

4.8 Chapter Acknowledgments

Support for this work came from the University of Virginia School of Engineering and Applied Science, the David and Joy Peyton Fellowship, and the National Science Foundation Graduate Research Fellowship Program under Grant No. 1842490. Any opinions, findings, and conclusions or recommendations expressed in this material are those of the authors and do not necessarily reflect the views of the National Science Foundation. I would like to acknowledge Laura Keister and Neeraj Gupta from Battelle for sharing the geophysical parameters of the Baltimore Canyon Trough. I also acknowledge Binghui Li and Joseph DeCarolis for sharing the optimization model they created at NC State University. The authors acknowledge Research Computing at The University of Virginia for providing computational resources and technical support that have contributed to the results reported within this publication. URL: http://rc.virginia.edu

4.9 Data Availability

The thermal fluid process model and optimization models were created in Python 3 and are available for downloaded at https://www.github.com/EnergyModels under the *caes* and *OCAES* repositories.

5 Isothermal Compressed Air Energy Storage Capacity of Offshore Saline Aquifers[4]

5.1 Summary

Plans for offshore wind energy has led to a search for energy storage technologies able to provide temporal balancing of electricity generation and demand. Offshore compressed air energy storage (OCAES) is a nascent energy storage option that uses saline aquifers as storage reservoirs and isothermal thermodynamic cycles to inject and extract air. Here, I present a method to assess the round-trip efficiency of OCAES when considering the uncertainty of geophysical parameters and machinery performance using the Baltimore Canyon Trough off the coast of the Mid-Atlantic United States as a case study. My results show that OCAES round-trip efficiencies of 60-62% could provide 23.6 TWh of storage in water depths less than 60 m. I also identify permeability and thickness as critical subsurface parameters, and show the need to develop isothermal cycles at the commercial scale. At a projected $61/kWh, isothermal OCAES compares well against current energy storage technologies.

5.2 Introduction

The growth in wind and solar energy production, both of which generate intermittently, will require increased grid flexibility to reliably meet electricity demand [10,254]. Grid flexibility could include fast-acting power plants [57] or demand response [10], however many regions expect to rely primarily on energy storage [187,255]. Initially, short duration storage, such as 4-hour lithium-ion batteries, are expected to have the largest impact [256]; however, as the amount of variable renewable energy grows, long duration energy storage will also be needed [251]. Batteries have fixed ratios of power capacity and energy storage making them costly to scale to long duration storage. Dowling et al. has shown that long duration storage (greater than 10 hours) is expected to lower electricity costs with high renewable installations [15]. As

[4] This chapter was adapted from: Bennett, J.A., Fitts, J.P., Clarens, A.F. (2021), Isothermal Compressed Air Energy Storage Capacity of Offshore Saline Aquifers. Manuscript in preparation.

governments with offshore access, such as Virginia and New York, develop plans for multi-GW offshore wind farms [187,188], they will need to determine the most suitable long duration energy storage technology to temporally balance generation and demand. High real estate prices on the United States eastern coast, especially near New York City, could motivate energy storage to be located offshore. Co-locating long duration energy storage with offshore wind presents an opportunity to share transmission, permitting, planning and construction vessel costs. Although the corrosive offshore environment is very challenging for some energy storage technologies such as batteries, the offshore environment could be manageable for offshore compressed air energy storage (OCAES) with proper air inlet filtration, as used extensively for machinery in the oil and gas industry.

OCAES plants can be categorized based on both the type of thermodynamic cycle used and the type of storage (Figure 5-1). Whether onshore or offshore, compressed air energy storage (CAES) systems operate by storing compressed air in subsurface formations and later expand the air through a turbine to produce electricity when generation is required. Two utility-scale onshore CAES plants; a 321 MW plant located in Huntorf, Germany and a 110 MW plant in McIntosh, Alabama, combine a diabatic cycle with a salt cavern for storage [42]. Diabatic cycles have low round-trip efficiencies and require a fossil fuel to operate, so they emit carbon dioxide [42]. Further, salt caverns are not geographically widespread, so this combination of CAES is limited [45]. Schmidt et al. found conventional, onshore diabatic CAES to be competitive in only a few long duration storage applications [257].

Recent advancements in adiabatic and isothermal thermodynamic cycles for CAES show the opportunity for increased round-trip efficiencies and warrant new investigations into its potential for offshore. Adiabatic cycles and isothermal thermodynamic cycles are expected to have higher round-trip efficiencies than diabatic cycles and they also do not require fossil fuels (Figure 5-1B and C). The development of adiabatic cycles has been limited by the high temperature components [42], and was found by Beuse et al. to not be competitive with other energy storage technologies [258]. Isothermal cycles use a heat transfer enhancement to achieve near-isothermal compression and expansion, such as, spray injection [210,213,259], wire mesh [260], and aqueous foam [261]. While bench-scale experiments have shown promising potential at low pressure ratios [213,259–261], uncertainty remains in the performance of isothermal cycles at the high pressure ratios required for CAES at a commercial scale. I use an uncertainty analysis to project the system performance based on the range of anticipated isothermal cycle performance.

There is growing interest in considering geological alternatives to salt caverns for CAES. Succar et al. suggested exploring the potential for abandoned oil and gas wells (Figure 5-1G) [45]. Mouli-Castillo et al. explored the use of saline aquifers in combination with a diabatic thermodynamic cycle [46]. When a saline aquifer is used for air storage, the air displaces the brine and creates an air plume. Another advantage of saline aquifers is that the storage duration can be increased without altering the machinery or wellbore, only by injecting more air and increasing the size of the air plume. The performance and capital costs of an OCAES system using saline aquifers combined with isothermal cycles has previously been estimated for a single site by the authors [262]. CAES using saline aquifers has faced limited deployment due to unsuitable subsurface conditions. For example, the Iowa Stored Energy Park was planned to provide 270 MW of storage using a sandstone aquifer but due to geologic site conditions, including low permeability, it was abandoned [202]. When evaluating the use of saline aquifers for CAES, it is necessary to consider the uncertainty of the subsurface conditions. Fukai et al. recently assessed saline aquifers in the Mid-Atlantic United States continental shelf as a CO_2 storage resource and made available the subsurface properties as part of a project for the United States Department of Energy [194]. Here, I explore the storage potential for OCAES in the United States Mid-Atlantic using saline aquifers and isothermal thermodynamic cycles (Figure 5-1C and F).

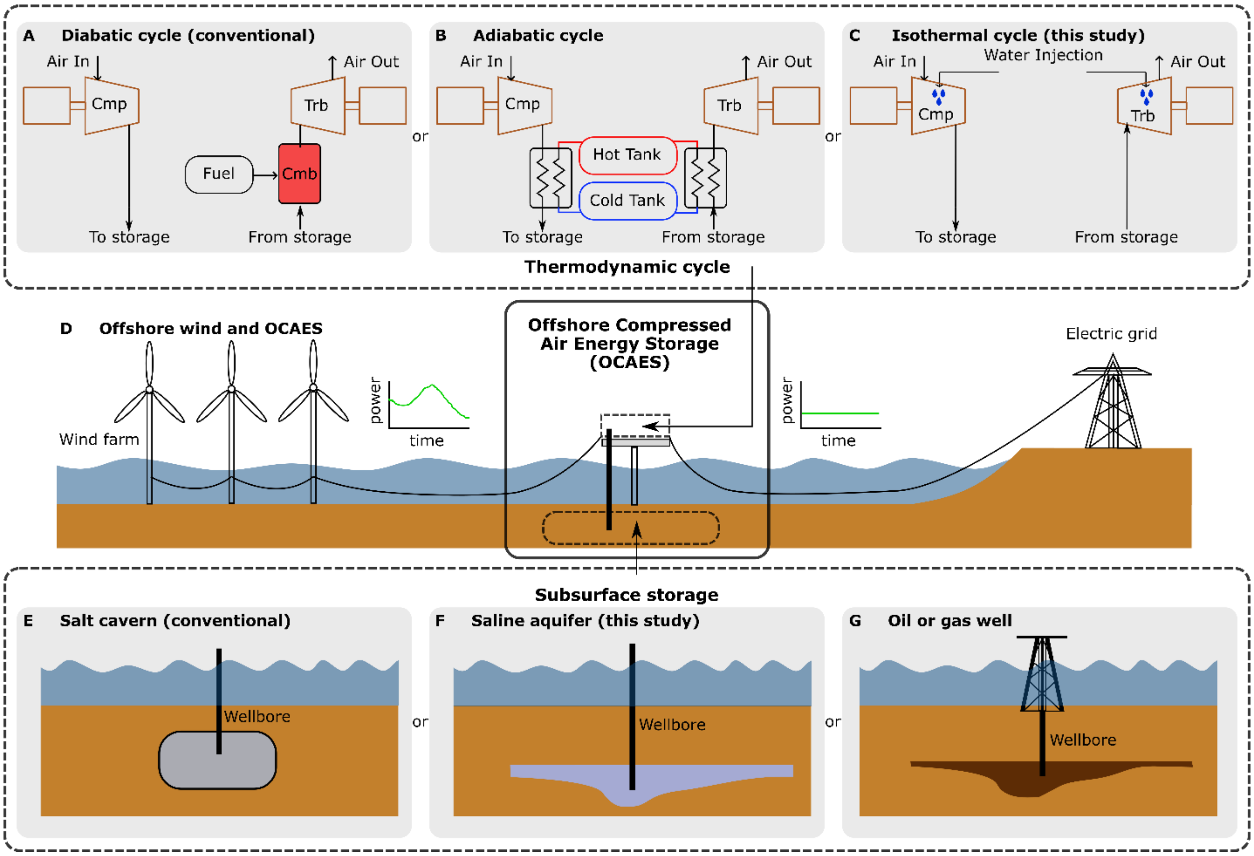

Figure 5-1. Offshore compressed air energy storage could be co-located with offshore wind (D) and used to be balance the intermittent generation. Offshore compressed air energy storage systems combine a thermodynamic cycle (A, diabatic, B, adiabatic, C, isothermal) with subsurface storage (E, solution mined salt cavern, F, saline aquifer, G, abandoned oil or gas well).

The uncertainty and geospatial heterogeneity of subsurface properties is expected to have a large impact on system performance and economics. For example, Pollack and Mukerji performed a techno-economic analysis of enhanced geothermal systems and found that considering uncertainty resulted in a 66% lower net present value [263]. Here, I consider the Baltimore Canyon Trough, a geologic formation that contains three sandstone saline aquifers with potential to be viable storage formations; Middle Cretaceous, Lower Cretaceous and Upper Jurassic (Figure 5-2A and B). The study by Fukai et al. estimated the depth, thickness, porosity, and permeability for 20 km by 20 km parcels of these three saline aquifers below the continental shelf [194]. Estimates are based on a limited number of well logs, such that the coarse resolution leaves the potential for unaccounted heterogeneities, as found in related studies [264]. Bowen et al. found in the Mount Simon sandstone formation that porosity varied both laterally and with depth due to facies, composition and diagenetic modifications such as clay mineral precipitation and iron oxide cementation [265]. Medina et al. used a curve fit to relate permeability to porosity measurements in the Mount Simon basin with a least squares fit of 41% [266]. Fukai et al. performed a similar curve fit for the Baltimore Canyon Trough with a least squares fit of 16 to 58%, depending on the formation [194]. Other sources of subsurface uncertainty that would influence storage performance include the aquifer temperature and pressure.

Here, I present a method to evaluate OCAES performance considering the uncertainty of the subsurface and machinery performance, and use the results to identify optimal locations and potential storage capacity (Figure 5-2C). The modeling framework could be applied anywhere, and here I demonstrate it for the United States Mid-Atlantic. First, I sized a 200 MW, 24-hour duration OCAES system for each parcel in the Baltimore Canyon Trough. Next, I performed an uncertainty analysis on the system and quantified its round-trip efficiency and storage duration. The uncertainty analysis used Monte Carlo sampling to consider the uncertainty of subsurface parameters (porosity, permeability, depth, thickness, temperature, fracture pressure, aquifer pressure, and air leakage) and machinery performance (polytropic index). A sample output of the OCAES system model which calculates the performance of a single charge and discharge cycle is shown in Figure 5-2D.

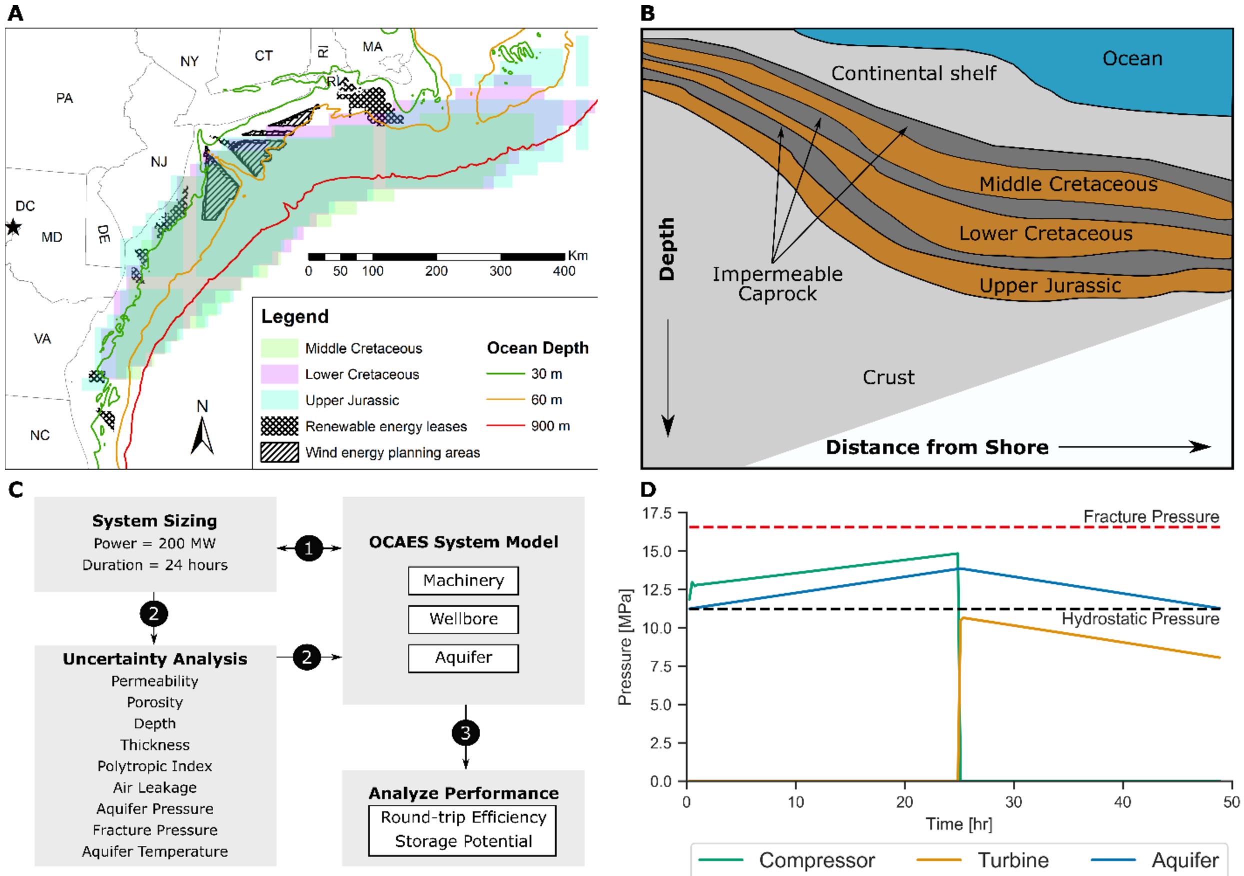

Figure 5-2. To explore the potential of offshore compressed air energy storage, I studied the A) Baltimore Canyon Trough (BCT), a subsurface formation along the coast of the northeastern United States. B) A cross-section of the BCT based on Miller et al. [267]**. C) An overview of the simulation process that incorporates geophysical and machinery uncertainty. First (1) a 200 MW, 24-hour system is iteratively sized using the OCAES system model. Second (2) The sized system undergoes an uncertainty analysis. Finally (3), the efficiency and storage potential are analyzed. D) A sample output from the thermal fluid process model used for the simulations. In A), Formation data is from Battelle** [194,268]**, lease data from the Bureau for Ocean Energy Management [206], ocean depth from NOAA Office for Coastal Management** [269]**, and state boundaries from the US Census** [270]**.**

5.3 Results

5.3.1 Vast OCAES Energy Storage Potential

Figure 5-3 illustrates the total storage potential of OCAES in the Baltimore Canyon Trough based on round-trip efficiency and water depth. This estimate conservatively assumes that 10% of the brine in the saline aquifer would be displaced by air for OCAES systems, to limit installations to locations with a caprock structure conducive to trapping air. Water depth is expected to be a major cost driver, with depths less than 60 m suitable for fixed bottom structures [269], whereas depths greater than 60 m will require more advanced and expensive wind turbine foundations, such as a floating platform. The total storage potential in water less than 60 m was found to be 23.6 TWh with a round-trip efficiency (RTE) of 60-62% and 858 TWh with an efficiency of at least 50%. The highest efficiency sites in less than 60 m water depth were found closest to New Jersey with efficiencies up to 61%. To put this storage potential in perspective, there are currently 0.000124 TWh of battery storage installed in the United States [243]. The 2020 Net-Zero America Interim report by Larson et al. projects that up to 1.24 TWh (190 GW with an average duration of 7-hours) of grid battery capacity will be needed in the United States by 2050 [271]. The OCAES storage potential is nineteen times this projected battery capacity. If commercialized, OCAES is more likely to be limited by the amount of nearby wind turbines than subsurface capacity.

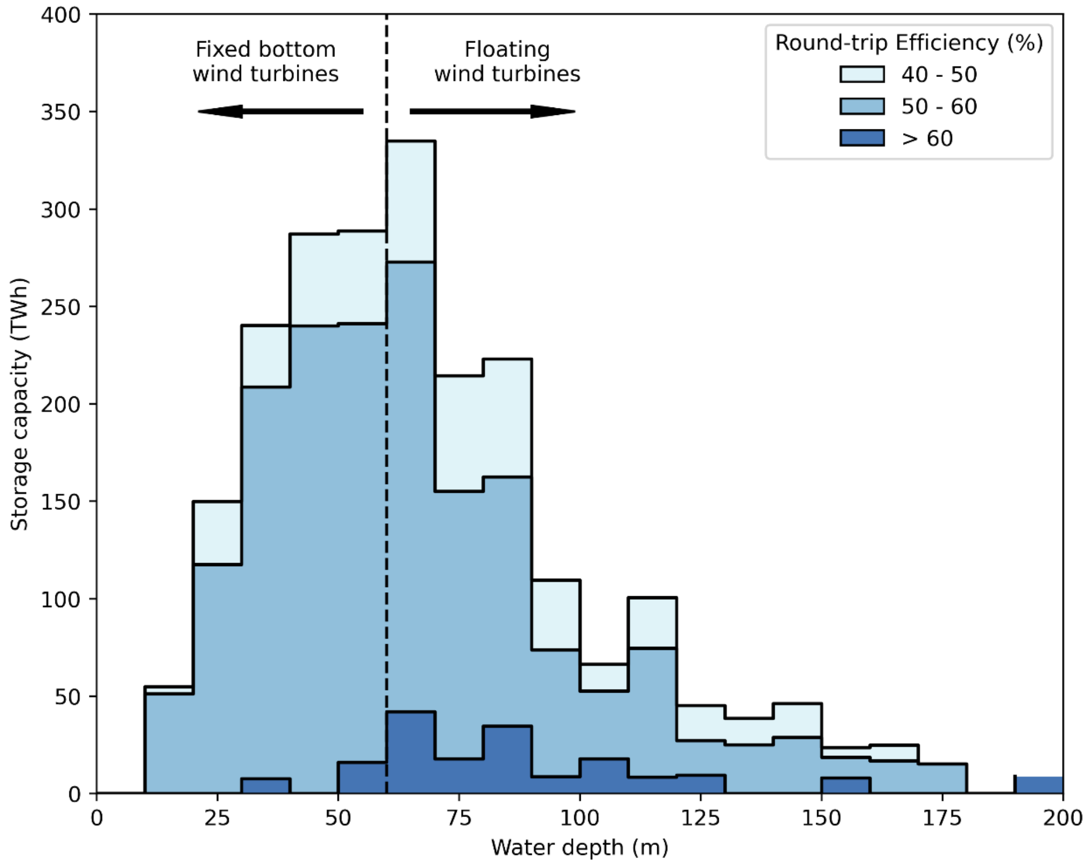

Figure 5-3. Estimate of total storage potential in the Baltimore Canyon Trough by water depth and round-trip efficiency. This figure highlights the maximum water depth currently accessible to fixed bottom offshore wind turbines, where OCAES is envisioned to be co-located [269]**. Deeper waters require floating structures which are more expensive, but there are many high efficiency OCAES sites in water depths greater than 200 m. Round trip efficiency estimates are the average results from the Monte Carlo simulation.**

5.3.2 OCAES Compares Well Against Other Energy Storage Technologies

Our results show very large capacity for OCAES in near shore saline aquifers even with uncertainty in the subsurface and machine performance. It can be challenging to valorize energy storage technologies because the traditional energy system metric of levelized cost of electricity (LCOE) will always increase when storage is added. Table 5-1 presents a comparison of OCAES with other energy storage technologies on the basis of capital costs normalized by power and energy ratings. The OCAES configuration I present, isothermal OCAES, does not operate with CO_2 emissions, although all energy technologies generate some amount of CO_2 emissions during their construction [56]. The CO_2 emissions presented in Table 5-1 only includes those generated during normal operation. To compare the different lifetimes of energy storage, I also show costs on an energy basis normalized by expected lifetime. On this basis, CAES is the least expensive. I assumed a lifetime of 25 years for the OCAES plant to match the expected lifetime of the co-located wind farm, although the OCAES machinery may operate much longer. For comparison, Ziegler et al. project that energy storage costs less than $20/kWh would be competitive with a nuclear fission plant [254]. Unlike Li-ion batteries or conventional CAES plants using a salt cavern of a fixed size, the storage duration of an OCAES system using a saline aquifer can be increased without any structural modifications; simply by injecting more air into the aquifer. An OCAES system with 72-hour storage duration would then cost $20/kWh.

Table 5-1. Comparison of offshore CAES to other energy storage technologies. The calculations of the expected operational emissions are presented in Appendix C. The capital costs for the operating CAES systems are taken from Beuse et al. and are meant to represent the cost of installing this technology today [258]**. The Li-ion battery capital cost are moderate 2021 projections from the 2020 NREL Annual Technology Baseline** [8]**.**

Technology (-)	Operational CO_2 emissions (gCO2/kWh)	Storage duration (hours)	Round-trip efficiency (%)	Lifetime (years)	Capital cost		
					Power ($/kW)	Energy ($/kWh)	Energy /lifetime ($/kWh-year)
Li-ion Batteries	0	4 [8]	75 – 97 [14], 85 [8], 95 [258]	15 [8]	1365 [8]	341	22.8
Vanadium Flow Batteries	0	24**	65 – 85 [14], 74 [258]	19 [258]	7533 [258]	314	16.5
Pumped hydro	0	24**	70 - 87 [14]	60 [258]	1691 [258]	70	1.2
Supercapacitor	0	1 [42]	84 - 97 [14]	20 [14]	275 [14]	275	13.8
Operating CAES (Huntorf, Germany)	290	2 [42]	42* [42]	60 [258]	1317 [258]	659	11.0
Operating CAES (McIntosh, USA)	212	24 [42]	54* [42]	60 [258]	4507 [258]	188	3.1
Diabatic OCAES	212	830 [46]	54 - 59* [46]	40 [46]	9191 [46]	11	0.3
Isothermal OCAES (this study)	0	24	Up to 62% in shallow ocean	25 [262]	1457 [262]	61	2.4

*Efficiency for diabatic systems includes the heat input of natural gas. **The duration is assumed to be 24 hours to be comparable to Isothermal OCAES.

5.3.3 Opportunities for OCAES Across the Baltimore Canyon Trough

Figure 5-4 shows the mean round-trip efficiency (RTE) from the uncertainty analysis results across the Baltimore Canyon Trough (BCT). There is a wide range of results, with some locations having a mean RTE up to 62.2%, and others less than 10%. Some combinations of geophysical parameters require an injection pressure greater than the maximum operating pressure which is assigned an efficiency of zero, lowering the mean RTE. Within the BCT, the Lower Cretaceous is the most suitable for OCAES with a majority of the formation having a mean RTE greater than 40%. However, all sites with an efficiency greater than 60% and in water depths less than 80 m are in the Upper Jurassic (Table 5-2). In general, the Middle Cretaceous and Upper Jurassic formations have limited locations with a high RTE. Also shown in Figure 5-4 are the renewable energy leases and wind energy planning areas from the Bureau of Ocean Energy Management [206]. My results show that regions identified by Fukai et al. to have high CO_2 storage potential [194], are generally suitable for OCAES with an expected RTE greater than 30%. I expect that RTE numbers would be lower for alternative CAES systems such as diabatic or adiabatic, however this will depend on the isothermal machinery performance. I project that all Mid-Atlantic states adjacent to the Baltimore Canyon Trough (Virginia, Maryland, Delaware, New Jersey, New York, Rhode Island, and Massachusetts) can access ample OCAES capacity with an RTE greater than 50% within 60 m water depth and 100 km of shore.

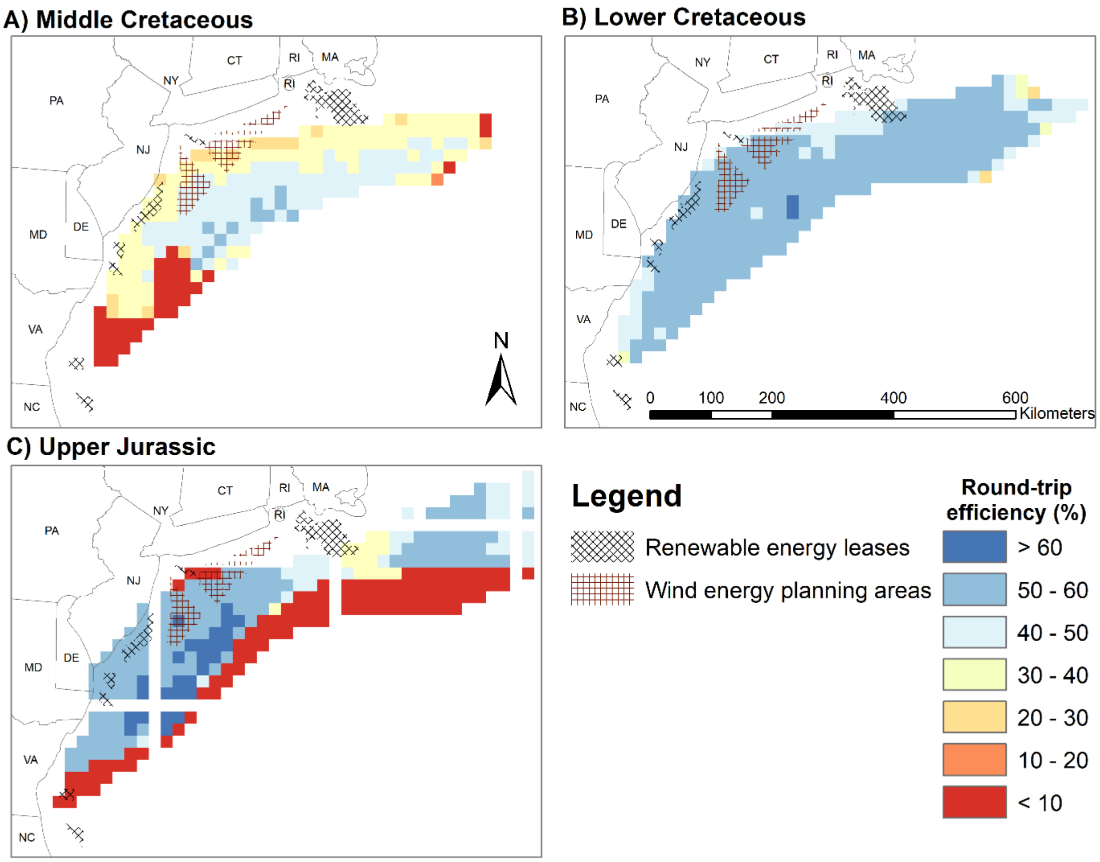

Figure 5-4. **Mean round-trip efficiency (RTE) for OCAES in the Baltimore Canyon Trough based on 100 Monte Carlo simulations per location representing the expected distribution of geophysical conditions. A) Middle Cretaceous (average depth 1800 m), B) Lower Cretaceous (average depth 2110 m), C) Upper Jurassic (average depth 2960 m).**

Table 5-2. Sites with the highest round-trip efficiency expected for OCAES sorted by water depth.

Water depth (m)	Distance to shore (km)	Round-trip efficiency (%)	Nearest State (-)	Formation (-)	Permeability (mD)	Thickness (m)	Porosity (-)	Formation depth (m)
38	54	60.7	New Jersey	Upper Jurassic	217	704	0.25	3177
51	86	61.0	New Jersey	Upper Jurassic	63	596	0.22	3791
53	89	60.9	New Jersey	Upper Jurassic	66	1017	0.22	3760
61	94	61.5	New Jersey	Upper Jurassic	90	1096	0.23	3856
62	97	60.6	Maryland	Upper Jurassic	57	399	0.22	4135
63	108	60.4	New York	Upper Jurassic	126	544	0.24	3489
68	82	61.9	Maryland	Upper Jurassic	60	355	0.22	3880
69	112	60.4	New Jersey	Upper Jurassic	72	1200	0.22	4537
78	121	60.9	New Jersey	Upper Jurassic	422	411	0.27	3921
80	118	60.4	New Jersey	Upper Jurassic	59	404	0.22	4090

5.3.4 Permeability and Thickness are Critical Parameters

Next, I investigated the relationships between geophysical parameters and RTE. I hypothesized that porosity and permeability would be the most important geophysical parameters, however I found that permeability and thickness had the largest impacts. Figure 5-5 shows the relationship between permeability and thickness for all of the Monte Carlo simulation results grouped by formation. These results demonstrate general threshold values for permeability and thickness of 10 mD and 10 m, respectively. Permeability and thickness values less than the threshold tend towards a RTE less than 10% and above the threshold to RTE greater than 50%. Porosity is often correlated to permeability [194]. It might be possible to have successful operation of very thin formations with very high permeability, however this could be challenging to drill. These results demonstrate the importance of selecting sites with adequate permeability and thickness which must be verified through seismic studies and pump tests.

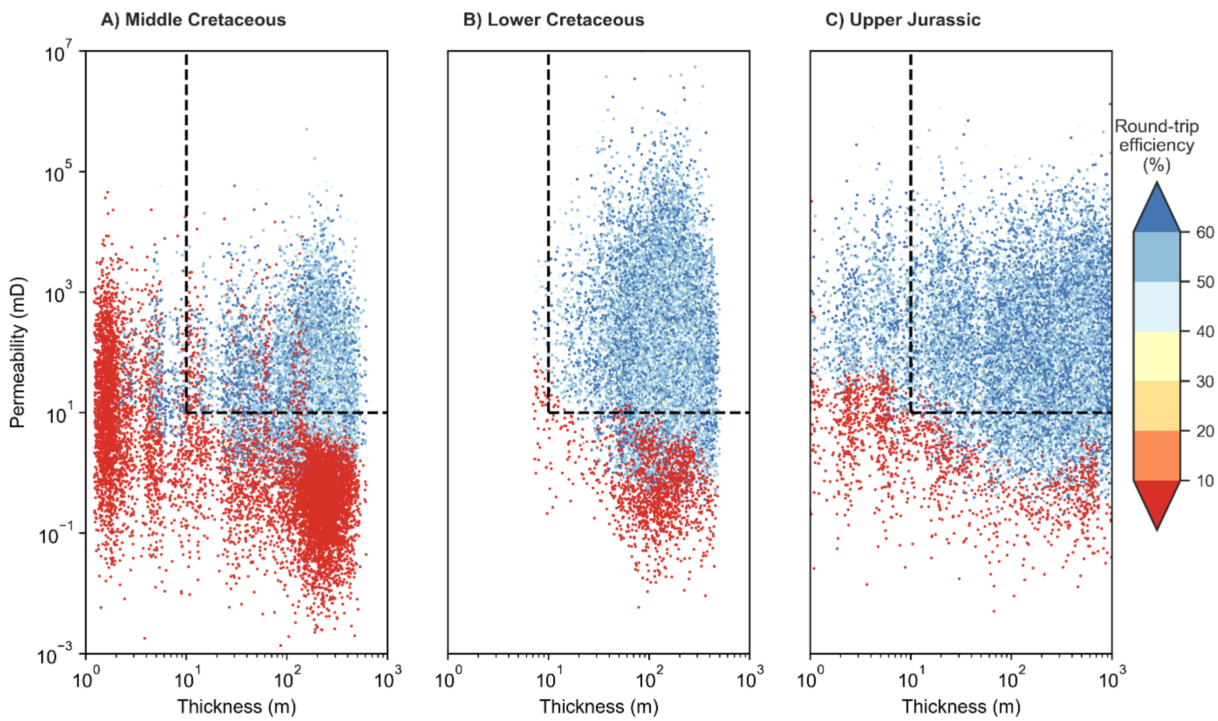

Figure 5-5. Permeability and thickness have a disproportionately large impact on the success of the OCAES system.

5.3.5 Machinery Performance, Formation Depth and Air Leakage Impact Round-trip Efficiency

After determining the permeability and thickness threshold values required for successful operation, I wanted to understand which parameters led to highly efficient systems. Figure 5-6 explores the relationship between system parameters and RTE for Monte Carlo simulations within the Upper Jurassic formation. The strongest correlations were with polytropic index, air leakage and depth. The polytropic index determines the amount of heat transfer during compression and expansion with a value of 1 representing an ideal isothermal process and 1.4 an adiabatic process. The next generation isothermal cycle analyzed here, benefits from a low polytropic index, as shown by round-trip efficiencies greater than 70% for a polytropic index of 1.06. RTE exhibits a negative correlation with air leakage which is understandable as the compressor work to inject the lost air is wasted energy. A positive correlation between RTE and depth suggests that moving to a deeper formation would be advantageous. A deeper location has a higher storage pressure which translates to reduced mass flow rates and therefore lower friction losses for the same power rating. Disadvantages of a deeper location include increased drilling costs and the challenge of performing isothermal heat transfer enhancements at higher pressures. The Middle Cretaceous and Lower Cretaceous formations exhibit similar trends.

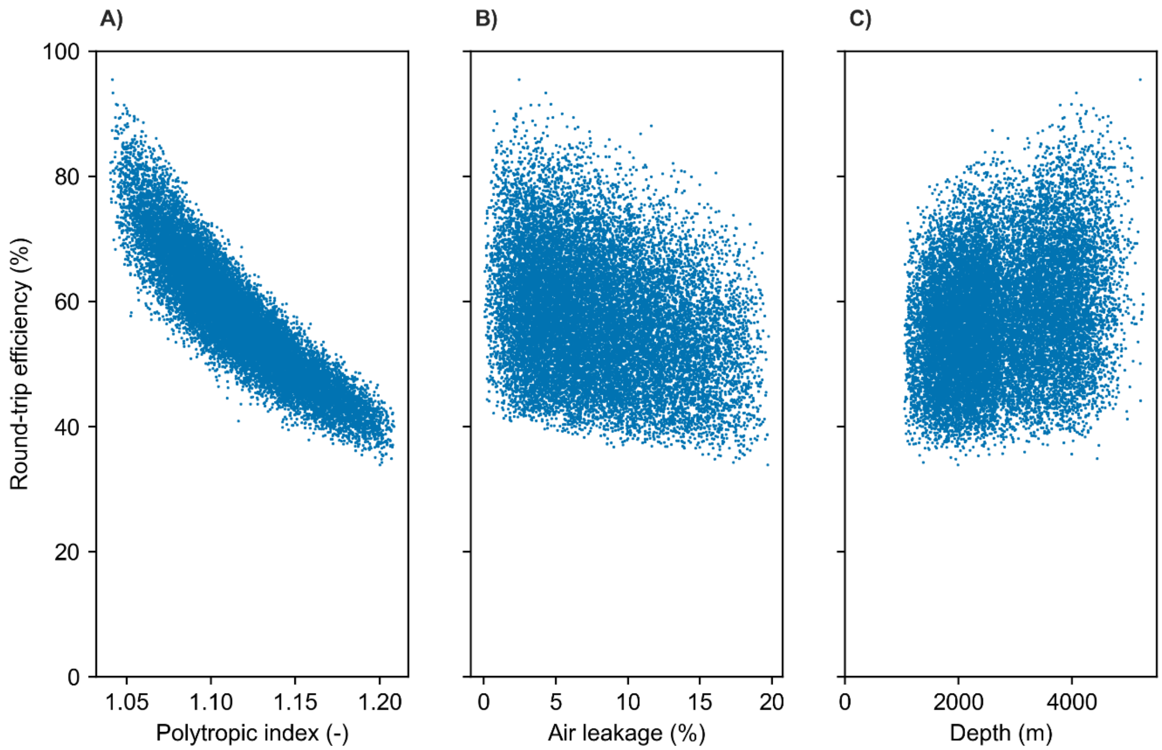

Figure 5-6. Investigating the impact of uncertain machinery and subsurface variables on round-trip efficiency. A) polytropic index representing machinery performance, B) air leakage to represent uneven saline aquifer morphology and C) depth. Each point represents one Monte Carlo run for one location in the Upper Jurassic formation within the Baltimore Canyon Trough. The range of values investigated for each parameter is further explained in Table 5-3.

5.4 Discussion

This study presented a method to estimate the performance and storage potential of OCAES systems using isothermal thermodynamic cycles and saline aquifers. I used the approach to evaluate the potential of OCAES in the Baltimore Canyon Trough off the coast of the northeastern United States. I estimate that 23.6 TWh of storage with a round trip efficiency of at least 60% are within water depths less than 60 m. This is nineteen times the battery storage projected for the United States by 2050 [271], and the water depth is suitable to pair with fixed bottom offshore wind turbines. I also found that OCAES systems with an RTE greater than 50% are possible within 60 m water depth and 100 km of shore for all U.S. Mid-Atlantic states adjacent to the Baltimore Canyon Trough.

By exploring the uncertainty of geophysical conditions and machinery performance, I identified the critical parameters for high efficiency operation. The aquifer permeability and thickness are the most limiting geophysical parameters; below 10 mD and 10 m, respectively, the system will not operate. Independent of the subsurface, the performance of the isothermal machinery is critical. Other important factors that need to be considered for economic feasibility include the water depth and distance to shore. The method presented here can be adapted to other world regions after collecting measurements of subsurface conditions.

The geophysical data used for this analysis was based on square grids of 20 km by 20 km; future research is needed to characterize prospective high efficiency OCAES sites in detail. Measurements (such as pump tests and high-resolution seismic surveys) to identify the permeability, aquifer thickness and determine the shape of the subsurface including anticlines and synclines would be valuable to determine the full techno-economic potential. Expanding the open source NATCARB data set would be advantageous to making the information widely available [272]. Future research is also needed to demonstrate the performance of isothermal machinery at high pressure ratios and an industrial scale, including part-load operation and start-up times to understand integration potential with offshore wind.

5.5 Experimental Procedures

5.5.1 Data and Software Availability

The model and analysis scripts were developed in Python 3 using the open source libraries CoolProp [273], pandas [274], Numpy [275], Seaborn [276], Matplotlib [277], and Joblib [278]. The model and data are available at https://www.github.com/EnergyModels/caes.

5.5.2 Method Overview

To understand the impact of uncertainty on the OCAES potential, I used a deterministic thermal fluid process model to estimate the viability and round-trip efficiency under fixed geophysical, machinery and engineering parameters. First, I used the model to determine the mass flow rate and well radius necessary for the intended storage duration and power rating. Next, I compiled distributions of geophysical and machinery parameters to represent the system uncertainty. I then performed an uncertainty analysis using Monte Carlo sampling. An overview of the method is shown in Figure 5-7. I applied the method to the Baltimore Canyon Trough as a case study.

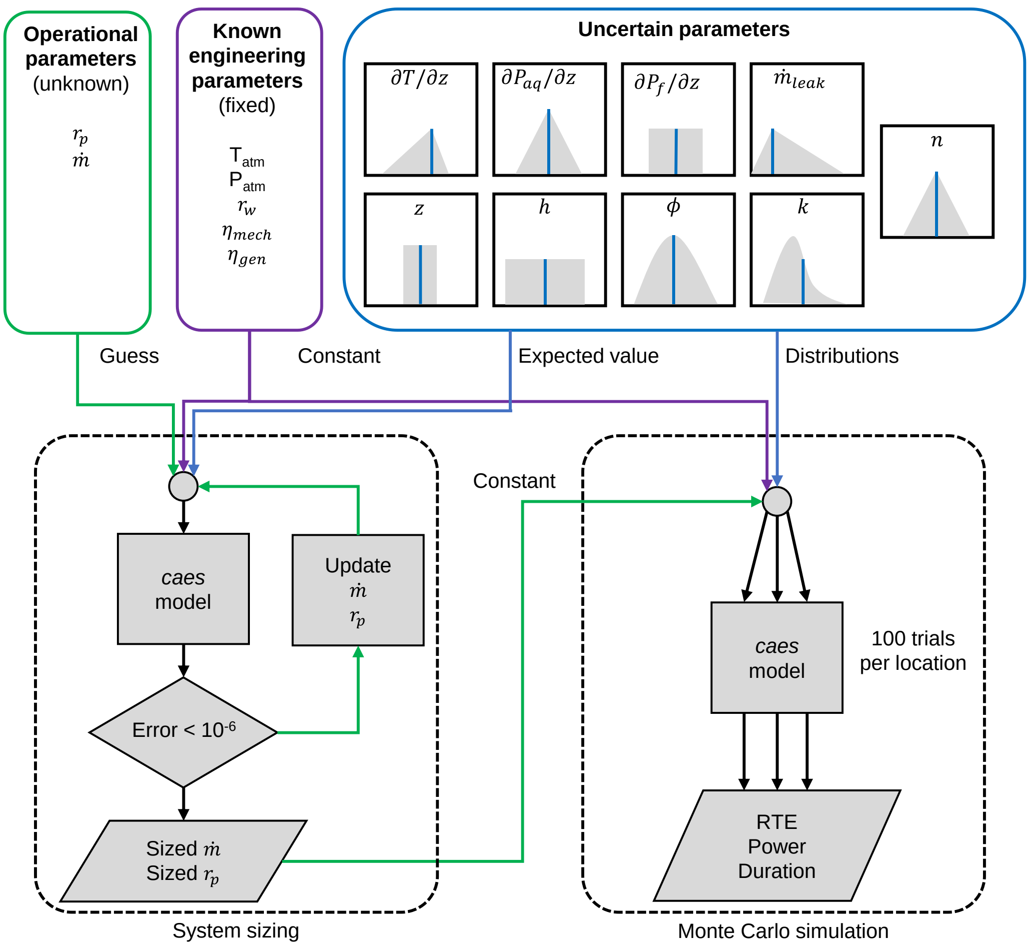

Figure 5-7. Overview of computational strategy to first size the system to reach 200 MW and 24 hours in duration before applying the Monte Carlo distributions of uncertain geophysical parameters.

5.5.3 Study Area

The Baltimore Canyon Trough (BCT) was characterized by the Mid-Atlantic U.S. Offshore Carbon Storage Resource Assessment Project (MAOCSRAP) as reported by Fukai et al. and Battelle et al. [194,268]. Using the historical data, MAOCSRAP estimated the depth, thickness and porosity at 300 grid points for three formations in the BCT including the Middle Cretaceous, Lower Cretaceous and Upper Jurassic [194,268]. Permeability was estimated at each location using a curve fit, however the curve had a correlation coefficient between 16% and 58% depending on the formation [194].

5.5.4 OCAES System Model

A thermal fluid process model of the OCAES system was used that represents the major components including aquifer, wellbore, and machinery. The model was first developed for Chapter 4, and for this study was updated to represent the machinery using a polytropic index, further detailed in the Supplemental Information [262]. The model tracks the temperature, pressure and mass flow rate at each location. The thermal fluid process model simulates a single cycle of charging and discharging. Simulations operate with a fixed mass flow rate and the total amount of air injected depends on the initial aquifer conditions and maximum operating pressure. Charging and discharging are each simulated in 100 timesteps to capture the varying work required at different pressures. An overview of the model equations is presented in the Supplemental Information.

5.5.5 System Sizing

Each location in the BCT was sized for a 200 MW, 24-hour duration OCAES system. The sizing represents an engineering firm designing and building the machinery to operate at a range of pressures at the design mass flow rate. It also includes fixing the air plume radius, which represents a pre-determined spacing between wells. If only a single well were installed, then this could be adjusted on site.

5.5.6 Uncertainty Analysis

To represent the uncertainty in the subsurface, each geophysical and machinery parameter was represented with a distribution as shown in Table 5-3. Geophysical parameters were grouped into those that apply to the entire BCT, general, and location-specific parameters that are based on their spatial position. General parameters used the same distribution across the BCT.

Table 5-3. Uncertainty distributions used in the Monte Carlo sampling.

Variable	Distribution	Mean Value	Distribution Parameters
General Parameters			
Polytropic index	Triangle	1.1	Minimum: 1.04 [259] Maximum: 1.21 [213]
Temperature gradient	Triangle	23 °C/km [268]	Minimum: 16 °C/km [268] Maximum: 24 °C/km [268]
Aquifer pressure gradient	Triangle	10.0 MPa/km [268]	Minimum: 9.42 MPa/km [268] Maximum: 11.1 MPa/km [268]
Fracture pressure gradient	Uniform	14.703 MPa/km [194,268]	Minimum: 13.6 MPa/km [268] Maximum: 15.8 MPa/km [268]
Air leakage	Triangle	3.5 % [196]	Minimum: 0% Maximum: 20%
Location-specific Parameters			
Depth	Uniform	Location specific [194]	+/- 10%
Thickness	Uniform	Location specific [194]	+/- 20%
Porosity	Normal [279]	Location specific [194]	Variance of 0.05% [279]
Permeability	Lognormal [279]	Location specific [194]	Variance of 2.448 [279]

5.5.6.1 Machinery Parameters

A variety of heat transfer enhancements have been tested for near-isothermal processes including spray injection [210,213,259], wire mesh [260], hollow spheres [280], and aqueous foam.[261] Based on a review summarized in Appendix C, a triangle distribution of polytropic indices between 1.04 and 1.21 were used.

5.5.6.2 General Geophysical Parameters

Variations in the geothermal gradient have previously been considered by Liu and Zhang which considered a gradient between 25 °C/km and 50 °C/km [281]. Battelle et al. found a range of geothermal gradients between 16 °C/km and 24 °C/km with an average of 23 °C/km and attributed the differences to variations in seawater depth and being near oceanic crust [268]. I applied a triangle distribution to represent the range of values found in the BCT. Battelle et al. found a very high correlation between aquifer pressure gradient with depth, therefore a triangle distribution was used to include the range of values while heavily weighting the expected value of 10 MPa/km [268]. Allen et al. have shown that the threshold pressure (difference between aquifer pressure and fracture pressure) depends on the rock type [220]. Conservative relationships use a threshold pressure maximums of 5 to 6.6 MPa, but they can be as high as 20.7 MPa

[220]. A uniform distribution was selected for the fracture pressure gradient based on sensitivity study by Battelle et al. that considered fracture gradients of 13.6, 14.7 and 15.8 MPa/km [268].

The model always starts with an air plume at the initial aquifer pressure that is not recovered during normal operation. Air leakage represents the amount of air injected during normal operation that is not recoverable. Oldenburg and Pan estimated a 3.5% air leakage for a compressed air energy storage system using a saline aquifer based on numerical reservoir simulations [196]. In comparison, the Huntorf CAES plant that operates with a salt cavern also requires 3.5% make-up air [196]. Succar and Williams also present a ranking criteria for aquifer suitability for CAES, that ranks sites with no leakage as shown by pumped tests to be the most suitable [45]. I used a triangular distribution for air leakage centered at 3.5% based on Oldenburg and Pan, and extended the distribution to 0% as a best cast and 20% as a worst case.

5.5.6.3 Location-specific Parameters

Location-specific parameters used results from the MAOCSRAP as the expected value. Based on the subsurface heterogeneity, variations in depth and thickness are expected, however due to limited data, these parameters were represented with uniform distributions. It is more common to vary porosity and permeability in studies that consider subsurface uncertainty. Pollack and Mukeriji varied porosity uniformly from 5% to 30% and permeability uniformly from log(0 mD) to log(5 mD) [263]. Jung et al. varied permeability +/-50% and also performed a sensitivity study that varied +/- permeability an order of magnitude [282]. Here I based distributions for porosity and permeability on the characterization of the Mount Simon sandstone formation by Barnes et al. [279], because the BCT formations are also sandstone. Barnes et al. used a normal distribution for porosity with variance of 0.05% and a lognormal distribution for intrinsic permeability with a variance of 2.448 mD [279]. I applied the same distributions as Barnes et al. while drawing the mean value from the MAOCSRAP.

5.6 Chapter Acknowledgements

I would like to acknowledge the financial support of the David and Joy Peyton Fellowship. I would like to acknowledge Laura Keister and Neeraj Gupta from Battelle for sharing the geophysical parameters of the Baltimore Canyon Trough and Research Computing at The University of Virginia for providing computational resources and technical support that have contributed to the results reported within this publication. URL: http://rc.virginia.edu

5.7 Author Contributions

J.B.: Conceptualization, Methodology, Software, Formal analysis, Data Curation, Writing – Original draft preparation, Visualization. **J.F.**: Conceptualization, Methodology, Writing – Review & Editing. **A.C.**: Conceptualization, Methodology, Writing – Review & Editing, Project administration.

6 Life Cycle Meta-Analysis of Carbon Capture Pathways in Power Plants: Implications for Bioenergy with Carbon Capture and Storage[5]

6.1 Summary

Bioenergy with carbon capture and storage (BECCS) is one possible approach to decarbonization by reducing atmospheric carbon dioxide levels at large scale. To support sustainable decarbonization, this study evaluates the environmental impacts of leveraging existing power plants for BECCS. I performed a life cycle meta-analysis of eight carbon capture technologies, including five previously simulated only for coal and natural gas, for both steam cycle and integrated gasification combined cycle (IGCC) power plants. I found that IGCC plants offer the best balance of negative emissions, energy return on investment (EROI) and low water use irrespective of capture technologies. However, current coal IGCC plants tend to be large whereas biomass-fired power plants are often small and distributed in the landscape, because of the distributed nature of the fuel. Steam cycle plants had larger negative emissions, but also lower EROI, and so blending with coal may be necessary to achieve a suitable EROI. Steam cycles were sensitive to capture technology type, and results found membrane and calcium looping capture technologies offer a balance between negative emissions, EROI and water use when fired using coal-biomass blends. These results suggest that steam-powered plants may be the most desirable candidates to support early-stage deployment of BECCS.

[5] This chapter was adapted from: Bennett, J.A., Abotalib, M., Zhao, F., Clarens, A.F. (2020), Life Cycle Meta-Analysis of Carbon Capture Pathways in Power Plants: Implications for Bioenergy with Carbon Capture and Storage. Manuscript submitted for publication.

6.2 Chapter Nomenclature

Table 6-1. Acronyms and Abbreviations.

BECCS	Bioenergy with Carbon Capture and Storage
CaL	Calcium Looping
CC	Carbon Capture
CCS	Carbon Capture and Storage
CL	Chemical Looping
EROI	Energy Return on Investment
EU	Energy Use
FU	Functional Unit
GWP	Global Warming Potential
HHV	Higher Heating Value
IGCC	Integrated Gasification Combined Cycle
LCA	Life Cycle Assessment
LHV	Lower Heating Value
MDEA	Methyl Diethanolamine
MEA	Monoethanolamine
MWe	Megawatt electric
NET	Negative Emission Technology
NGCC	Natural Gas Combined Cycle
NIST	National Institute of Standards and Technology
NG	Natural Gas
SEWGS	Sorption Enhanced Water Gas Shift
US	United States
WTP	Well-to-pump
WTW	Well-to-wheels
WU	Water Use

Table 6-2. Symbols.

D	Distance traveled
I_{CC}	Impact of Carbon Capture
I_{FP}	Impact of Fuel Production and Transport
I_{PG}	Impact of Power Generation
I_{SP}	Impact of Solvent Production
I_{ST}	Impact of Solvent Transport
$\dot{m}_{CO_2}$	CO_2 flow rate
$\dot{m}_{CO_2,B}$	CO_2 flow rate of baseline GREET plant
$\dot{m}_S$	Solvent Mass consumption rate
q_{FUEL}	Fuel specific emission rate
WU	Water Use
$\dot{W}$	Plant Power Output
$\dot{W}_{CMP}$	Compressor Power
β	Carbon Capture Rate
Δh	Enthalpy change
$\Delta\eta$	Total efficiency reduction
$\Delta\eta_{CC}$	Efficiency reduction due to CC
$\Delta\eta_{CMP}$	Efficiency reduction due to compression power
η_{PP}	Power Plant Efficiency without CC
$\eta_{PP,B}$	Baseline Power Plant Efficiency without CC
η_{PP+CC}	Power Plant Efficiency with CC

6.3 Introduction

The 2°C target of the 2015 Paris Climate Agreement requires that nations drastically reduce their CO_2 emissions [283]. Achieving these reductions as nations move towards decarbonization will likely require the adoption of Negative Emission Technologies (NETs) [284]. NETs are a group of technologies under development that actively reduce the amount of carbon dioxide (CO_2) in the atmosphere via direct air capture using chemical separations, enhanced weathering of silicate materials, and bioenergy with carbon capture and storage (BECCS). Direct air capture consumes energy to separate CO_2 from the air before storing it in the subsurface and enhanced weathering accelerates the rate of carbon mineralization in rocks [19]. Unlike other NETs, the BECCS power plant concept combines the storage of CO_2 with electricity production, and is based on a number of separately proven technologies: biomass-fired power plants are already in use and several existing demonstration-scale power plants actively capture and store CO_2 [48].

6.3.1 Concept and status

In BECCS power plants, perennial (for example, switchgrass) or woody (for example, pine) bioenergy crops are grown, harvested, and transported to a power plant where it is burned to generate electricity. Whereas in a conventional biomass-fired power plant, the carbon in the biomass is re-released to the atmosphere resulting in net positive CO_2 emissions across the life cycle, because of the gross emissions from biomass cultivation and power production [285]. BECCS power plants capture CO_2 at the power plant, and then store it in the deep subsurface, which creates the potential for net negative life cycle emissions [47].

There are currently two BECCS power plants in operation, the Drax pilot plant in North Yorkshire, United Kingdom and the 50 MWe (MW electric) Mikawa Power Plant in Omuta, Japan; both are retrofitted coal power plants [49,50]. BECCS has not been deployed in the United States (US) for power generation, however there are five facilities that combine ethanol production from biomass with carbon capture and storage [286].

Selecting the type of power plant and capture technology to use for BECCS requires balancing costs and environmental impacts. Fajardy et al. also examined the economic impact of BECCS and found that wide spread deployment would not be detrimental to agricultural commodity prices [287]. Emenike et al. performed a techno-economic analysis of BECCS and found that the break-even price depends on both the biomass feedstock and power plant type [288]. For fossil fuel fired power plants, a meta-analysis of carbon capture costs by Akbilgic et al. found the major driving factors to be capital costs and efficiency penalty [289]. With so many existing fossil-fuel power plants and so few operational BECCS power plants, questions remain over the optimal carbon capture technology for retrofitting existing power plants with respect to environmental impacts.

6.3.2 Environmental impacts of BECCS

Environmental impacts can be quantified with life cycle assessment which Stavrakas et al. and others assert is necessary to confirm that BECCS power plants have net negative emissions [48]. Global warming potential (GWP) is the most commonly used metric for quantifying the equivalent amount of CO_2 emissions [290]. Mac Dowell and Fajardy have highlighted a paradox that less efficient BECCS power plants result in more negative CO_2 emissions [291]. This is attributed to the fact that a less-efficient plant requires more biomass to produce the same amount of electricity, so it stores more CO_2. This was re-affirmed in a study by Cumicheo et al. that compared combining biomass and natural gas fuel sources which also found that plants that fired biomass alone had the largest negative emissions [292].

BECCS projects will also be evaluated on the basis of other environmental impacts such as water use, and energy use to support sustainable operation. Thermal power plants have large water demands, which is a concern because Gosling and Arnell and others have projected water scarcity to increase with climate change [293]. One motivation to deploy a BECCS power plant is that it offsets fossil electricity production, so minimizing energy use is important to maximize electricity outputs. Hetland et al. found that the low initial efficiencies of bioenergy plants combined with the efficiency penalties of carbon capture could jeopardize the commercial viability of BECCS [294].

Increasingly, energy return on investment (EROI) is also being used to evaluate novel energy generation pathways [295]. EROI is defined simply as the ratio of energy produced to energy consumed. While an EROI of 1 would be energetically balanced (energy in equals energy out), King and van den Bergh suggest that an EROI of 3 would be insufficient for an affluent society, and that present society relies on EROIs greater than 20 [296]. In contrast, Sgouridis et al. found that fossil power plants with carbon capture (CC) have EROIs of 6.6 to 21.3, and Moeller and Murphy found unconventional gas in the Marcellus Shale to have an EROI of 10.72 [295,297]. A comparison of biomass feedstocks on EROI performed by Fajardy and Mac Dowell found EROIs ranging from 0.5 to 5.7 [298]. EROI has direct implications for the economic viability of a technology, particularly those that generate or consume energy. For example, Heun and Wit found that there is a high probability of increased oil prices when EROI drops below 10 [299]. There is a research need to concurrently consider trade-offs between GWP, EROI, water use and energy use for the sustainable operation of BECCS.

6.3.3 BECCS power plant configurations

A growing body of literature is exploring some of the life cycle dimensions of BECCS power plant configurations. Existing BECCS Life Cycle Assessment (LCA) studies have considered the role of biomass feedstocks including biomass residue [300], wood [285,301–305], switchgrass [306], straw [304] and crops [304,306]. Many of these studies exclusively considered co-firing biomass with coal; for example, Schakel et al. compared co-firing coal with a 30% blend of biomass in large plants but did not consider biomass-dedicated plants [304]. These studies have primarily focused on two types of power plants; the steam or Rankine cycle based on burning pulverized coal and the integrated gasification with combined cycle (IGCC) which combines a gas turbine and steam cycle [307]. Supercritical carbon dioxide power cycles have also been considered as an alternative to steam and IGCC [308].

Only a limited number of carbon capture technologies have been considered in the life cycle assessment literature for the context of BECCS power plants: amine-based, oxy-fuel and Selexol [285,300–306]. CO_2 capture at the power plant occurs following either post-combustion i.e., removal of CO_2 after the fuel is burnt in air or pre-combustion i.e., first converting the fuel into a mixture of hydrogen and CO_2, followed by CO_2 capture. The most common type of carbon capture is performed via chemical sorption using amine-based solvents such as monoethanolamine (MEA) or methyl diethanolamine (MDEA). Amine-based capture has been considered for BECCS power plants in a number of studies [285,300–303]. In oxy-fuel carbon capture, the fuel is burned in pure oxygen obtained from the cryogenic distillation of air, which creates a pure CO_2 stream, eliminating the need to separate the flue gas following combustion. Herron et al. and Falano et al. analyzed oxy-fuel for BECCS power plants and found that auxiliary power requirements increase greatly, primarily due to the air separation [285,305]. Selexol is a type of physical solvent that relies on the physical sorption of CO_2 to the solvent [309]. Schakel et al. and Black et al. evaluated Selexol for BECCS power plants [304,306]. Black et al. noted that a 300-500 MWe plant would be logistically constrained to operating with 66% biomass by weight, because there would not be enough biomass available [306]. Schakel et al. found that pre-combustion with Selexol was more favorable than amine-based with respect to net negative emissions [304].

The life cycle assessment literature for carbon capture from fossil fuel power plants is much more extensive. Cúeller-Franca and Azapagic compared 27 different carbon capture approaches using life cycle meta-analysis and found that oxy-fuel had the lowest GWP [310]. In addition to considering amine-based [311,312], oxy-fuel [312] and Selexol [312], recent fossil fuel studies have highlighted five emerging carbon capture technologies: ammonia [313], chemical looping [314], calcium looping [313–316], membrane [317] and sorption enhanced water gas shift [311]. Ammonia is an alternative choice for chemical sorption to replace amine-based solvents [313]. Chemical looping (CL) is similar to oxy-fuel in that fuel is combusted in pure oxygen but uses a metal oxide such as an oxide of iron or copper to produce oxygen instead of air separation [318]. Calcium looping (CaL) is an emerging carbon capture technique in which calcium oxide (CaO) reacts with CO_2 to create calcium carbonate ($CaCO_3$), which is subsequently heated to release the CO_2 and recycle the calcium [319]. Membrane-based capture uses physical separation typically with advanced materials such as polymers, palladium, and ceramics [318]. Another recently considered capture technology is sorption enhanced water gas shift (SEWGS) which is a pre-combustion carbon capture technology based on using pressure swing adsorption to produce syngas [311]. The development of advanced carbon capture technologies for fossil fuel power plants asks whether these could lead to BECCS configurations with reduced environmental impacts.

6.3.4 Need for harmonization

Comparing carbon capture technologies for power plants is challenging because of differences in modeling assumptions and system boundaries [320]. Corsten et al. performed a review of existing LCAs and highlighted differences in the inclusion or exclusion of CO_2 transport and storage within power plant life cycle boundaries [321]. Heath and Mann have shown that harmonization of system boundaries and inputs is necessary to make life cycle assessment studies directly comparable [322]. Additionally, challenges exist for comparing carbon capture technologies for different fuels. Vasudevan et al. highlighted that accounting must be done for differences in exhaust CO_2 partial pressures [323]. These studies have shown the importance of harmonizing system boundaries and model inputs while accounting for differences in exhaust gas composition, however a methodology to combine these steps has not been demonstrated.

6.3.5 Siting challenges and opportunities

Siting a BECCS power plant is challenging because it must be near energy crop feedstocks, a geologic formation suitable for CO_2 storage, and electricity infrastructure. Baik et al. performed a comparison of crops and storage locations in the US and found that transportation barriers and unsuitable storage reduce the negative emission potential of BECCS by 73% [324].

Even though BECCS power plants have not been deployed in the US to date, there are currently 22 biomass-fired power plants with a capacity of at least 10 MWe, with the largest having a capacity of 113 MWe (Figure 6-1A) [325]. There are also 32 biomass-fired power plants in the US with a capacity less than 10 MWe [325]. Biomass transportation costs increase with plant capacity due to increased fuel consumption [326,327]; thus, bioenergy plants are typically much smaller than their fossil fuel counterparts [108]. Another challenge with biomass is its seasonal availability [328].

In contrast to the US biomass-fired power plant infrastructure, there are hundreds of coal and natural gas power plants (Figure 6-1B, C). If US policies were to shift towards large deployment of low carbon fuels, this could leave many stranded assets in the form of existing coal and natural gas power plants. Stranded assets are infrastructure investments that become uneconomic to operate and must close before they reach the end of their design life due to a change in the regulatory environment [329]. In the US, the location of many coal and natural gas plants overlaps with the location (Figure 6-1D) of much of the biomass resources suggesting there may be opportunities to retrofit some of these ageing power plants for BECCS. For example, the recent conversion from coal to biomass for 4 units built in the 1960-70's at the Drax Power Plant is also expected to extend the lifetime and had a total cost of 964 million USD (730 million pounds) or 365 USD/kW [330,331]. Converting a coal power plant to biomass requires biomass-dedicated covered storage and conveying systems as well as combustor modifications [332]. Although a major investment, the Drax Power Plant conversion is equivalent to approximately 8% of the anticipated capital costs for a new biomass-fired power plant [8]. Co-firing with coal is another option that can lead to higher power plant efficiencies as compared with firing biomass alone [328]. Further analysis is required to understand whether it is better to retrofit existing power plants, or to a construct a state-of-the-art BECCS power plant.

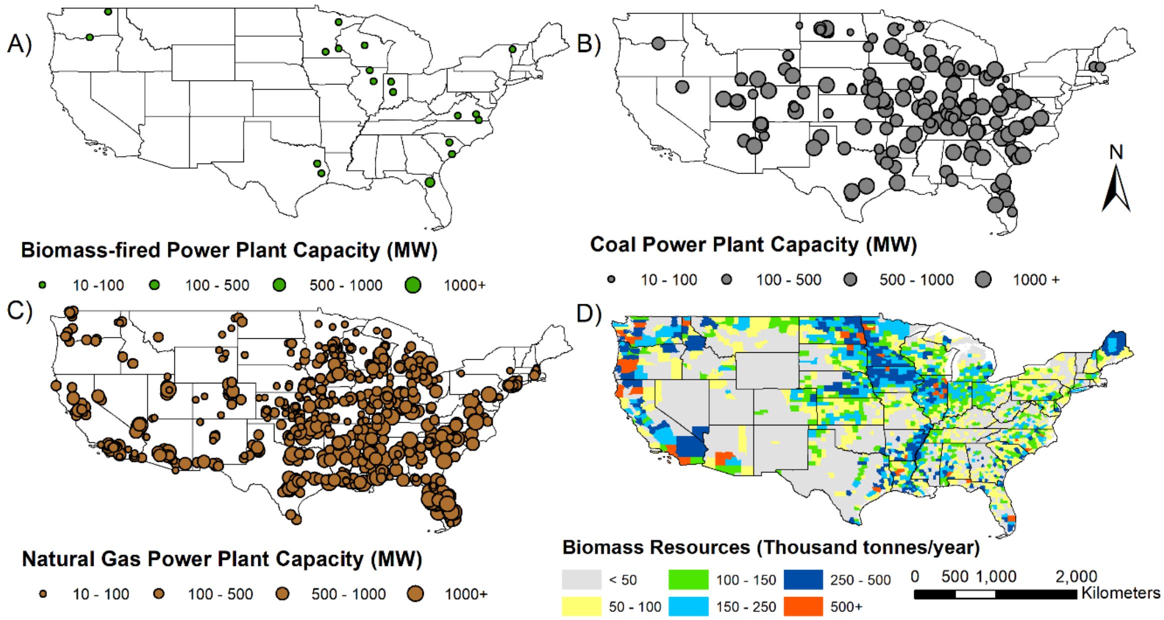

Figure 6-1. A comparison of existing A) biomass-fired, B) coal, C) natural gas electric utility power plants, and D) total biomass resources in the United States illustrates the opportunity to convert existing fossil power plants to bioenergy [325,333]**.**

6.3.6 Study overview

The goal of this study is to support electric grid decarbonization by identifying carbon capture technologies with minimal environmental impacts for retrofitting coal power plants into BECCS power plants. I use a meta life-cycle-assessment methodology to compare the environmental impact of emerging carbon capture technologies with carbon capture technologies previously considered for BECCS power plants. Specifically, I analyze, for the first-time, ammonia, chemical looping, calcium looping, membrane and sorption enhanced water gas shift for retrofitting existing steam and IGCC power plants into BECCS power plants. To consider these emerging technologies, I developed a method to harmonize and apply carbon capture technologies from one power plant to another, and made the model publicly available. In order to sustainably decarbonize the electric grid, negative emissions need to be balanced with other environmental impacts, so I investigate trade-offs with energy use, water use and EROI. I also used my model to consider trade-offs in burning biomass with and without coal. Using these results, I explore the potential to retrofit existing coal and natural gas power plants in the United States for BECCS.

6.4 Methodology

A comparative life cycle meta-analysis was performed by combining the harmonization approach outlined in Heath and Mann [322] with a BECCS performance projection. Harmonization was necessary because my review of recent published studies included LCAs as well as techno-economic and thermodynamic-based analyses found varying model inputs, system boundaries, and fuel inputs. For this meta-analysis I selected published studies from 2012-2019 that had similar system boundaries and provided the capture rate (percent of CO_2 captured) as well as the power plant efficiency before and after the addition of carbon capture. From the studies I also extracted the CO_2 outlet pressure and whether the efficiency was based on the Higher Heating Value (HHV) or Lower Heating Value (LHV) of the fuel. A summary of the literature is shown in Table 6-3 with full model inputs presented in Appendix D.

Table 6-3. A summary of the literature review highlights the number of data points used in addition to an overview of model parameters. Some of the studies used were meta-analyses or contained analyses of multiple plant configurations, therefore each data point refers to a unique combination of a power plant with and without carbon capture.

	Data points (-)					All Fuel and Power Plant Combinations		
Fuel	**Biomass**	**Coal**		**Natural Gas**	**All**	**Capture rate (%)**	**Outlet Pressure (MPa)**	**Efficiency Reduction (%)**
Power Plant	**Steam**	**Steam**	**IGCC**	**NGCC**	**All**			
Amine-based	1	2	6	6	15	88.3 – 90.5	11.0 – 20.2	5.1 – 6.8
Ammonia			1		1	85.0	12.0	8.1
CaL		3	9		12	77.0 – 92.7	10.0 – 15.0	3.5 – 11.6
CL		1			1	99.5	12.0	6.2
Membrane			2		2	90.0	15.0	5.6 – 5.9
Oxy-fuel	1		6		7	90.0 – 98.0	11.0 – 15.3	8.3 – 9.9
Selexol		4			4	90.0	15.3 – 20.2	7.1 – 12.0
SEWGS				2	2	85.7 – 91.1	11.0	12.1 – 12.5

The published studies were harmonized by using common model inputs and compensating for differences in the system boundary. Specifically, the studies were harmonized to have a common compressed CO_2 outlet pressure of 15.3 MPa, which was the most common in Rubin et al. [312]. Next, an efficiency reduction parameter was calculated based on power plant efficiencies before and after carbon capture that accounted for differences in fuel inputs, which enabled projecting the capture technology performance for BECCS. Environmental impacts for each configuration were calculated by applying the efficiency reduction to the common model inputs. Capture rates were not harmonized.

6.4.1 Model inputs

To compare combinations of capture technologies and power plant configurations, life cycle inventory data and power plant performance data was taken from the 2019 version of the Greenhouse gases, Regulated Emissions, and Energy use in Transportation Model (GREET) using the target year 2020 [334]. The power plant data is summarized below in Table 6-4. Additional GREET data for fuel gathering including biomass cultivation, amine production and transportation is shown in Table 6-5. All simulations use switchgrass as a representative biomass source. Switchgrass is similar in its cultivation and combustion to straw or corn stover and was included in GREET.

Table 6-4. Processed "Non Distributed - U.S. Mix" Power Plant Data from GREET 2019, with target year 2020 [334]**. Raw data and calculations are shown in Appendix D.**

Power Plant Type	Biomass (IGCC)	Biomass (Steam)	Coal (IGCC)	Coal (Steam)	NG (NGCC)
GREET Process	Electricity: Switchgrass IGCC Power Plant*	Electricity: Switchgrass (Steam Turbine) Power Plant	Electricity: Coal-Fired (IGCC Turbine) Plant	Electricity: Coal-Fired (Steam Turbine) Plant	Electricity: NG-Fired (Combined-cycle Gas Turbine) Plant
Type	Well-to-pump	Well-to-pump	Well-to-pump	Well-to-pump	Well-to-pump
Functional Unit	kWh	kWh	kWh	kWh	kWh
Efficiency (fr)	0.45	0.25	0.39	0.38	0.60
Well-to-use					
GWP (g CO_2eq)	63.96	77.76	931.72	956.77	402.29
Energy Use (MJ)	0.33	0.59	0.19	0.20	70.52
Water Use (l)	0.09	1.68	1.51	1.65	0.67
Onsite					
CO_2 (g)	813.17	1457.47	875.25	898.26	337.72
GWP (g CO_2eq)	22.90	3.85	878.69	902.35	338.24
Energy Use (MJ)	0.00	0.00	0.00	0.00	0.00
Water Use (l)	1.38*	1.51	1.38	1.52	0.60

*GREET did not include Onsite water use for biomass IGCC so I assumed it to be the same per kWh as coal IGCC

Table 6-5. Processed Fuel Gathering, Chemical Production, and Transport Data from GREET 2019, with target year 2020 [334]**. Raw data and calculations are shown in Appendix D.**

Product	Biomass	Coal	Methyl Amine	Natural Gas	Transport
GREET Product	Switchgrass Production for Ethanol Plant	Coal for Power Plants	Production Pathway for Methyl Amine	NA NG from Shale and Regular Recovery for Electricity Generation	HD Truck: Combination Short-Haul CIDI - Low Sulfur Diesel
Type	Well-to-pump	Well-to-pump	Well-to-pump	Well-to-pump	Well-to-wheels
Functional Unit	MJ	MJ	g	MJ	tonne-km
Well-to-use					
GWP (g CO_2eq)	5.13	5.74	2.66	10.68	70.84
Energy Use (MJ)	0.04	0.02	0.07	0.09	0.92
Water Use (l)	0.011	0.014	0.002	0.011	0.064

6.4.2 System boundary

Recent carbon capture studies of coal and natural gas plants consider system boundaries that include fuel gathering through compression of CO_2 at the power plant, thus I used the same boundary (Figure 6-2). Cúellar-Franca and Azapagic report that infrastructure production had a negligible impact on life cycle GWP for a carbon capture and storage project comparing pulverized coal, IGCC, and combined cycle gas turbine power plants [310]. BECCS power plants are not expected to be significantly different in construction from this set of power plants, thus the construction phase of the life cycle was excluded from the analysis. For the analysis it was assumed that solvent would need to be transported 100 km.

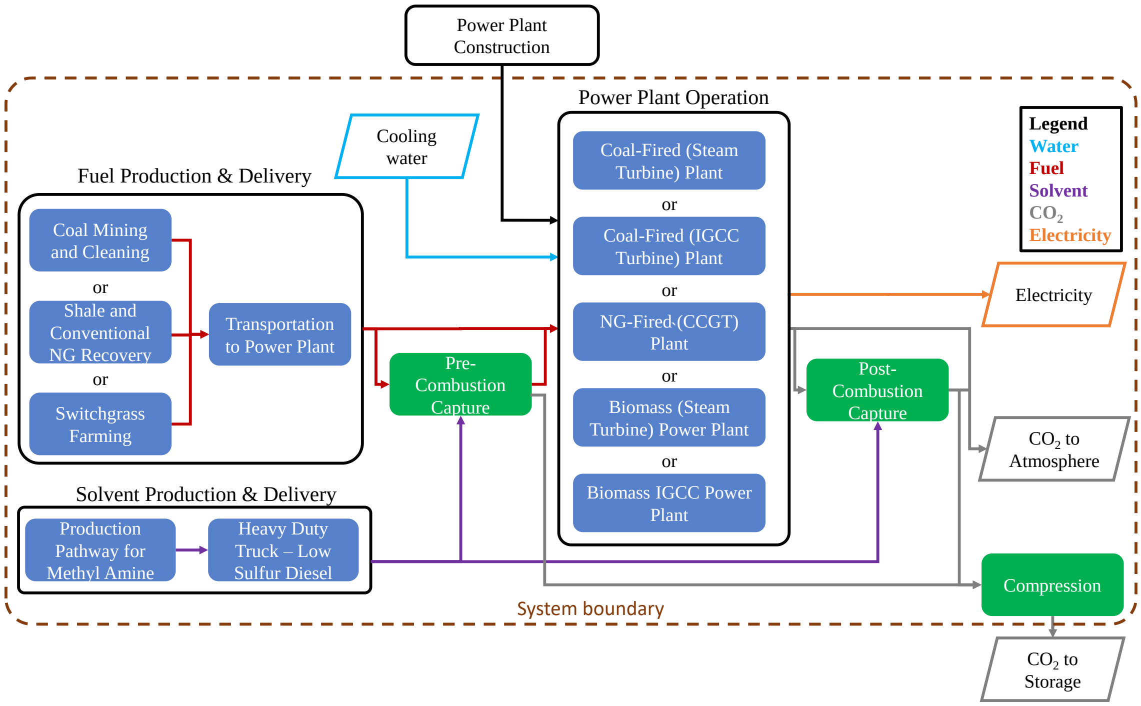

Figure 6-2. The system boundary of the life cycle assessment was selected to include upstream impacts of fuel gathering through compression of CO_2 at the power plant. The energy stored in the fuels i.e., due to photosynthesis is excluded from the system boundary.

Based on my review of solvent consumption (Table 6-6), an average consumption of 1.76 kg/tonne CO_2 was calculated and assumed for all amine-based systems using a generic MEA [335–337]. This is a conservative assumption for MEA systems with new products such as KS-1 advertising reduced degradation [338]. Based on Pehnt and Henkel, it was assumed that Selexol consumption was negligible [336].

Table 6-6. Solvent Consumption of Power Plants with Carbon Capture from Literature.

Study [-]	Solvent [-]	Consumption [kg / tonne $_{CO2}$]
Koorneef et al., 2008 [335]	MEA	2.34
Pehnt and Henkel 2009 [336]	MEA	1.50
Pehnt and Henkel 2009 [336]	Selexol	0.00
Giordano et al., 2018 [337]	MEA	1.44

6.4.3 Efficiency reduction

An efficiency reduction parameter $\Delta\eta$ was developed to provide a universal method to account for the change in power plant efficiency due to the implementation of a carbon capture technology. Once calculated, it is applied to the GREET baseline power plant efficiencies, $\eta_{PP,B}$,

$$\eta_{PP+CC} = \eta_{PP,B} - \Delta\eta \tag{6-1}$$

to calculate the efficiency of the power plant with carbon capture η_{PP+CC}. It is nontrivial to compare the impact of carbon capture systems across the literature because few assumed the same operating conditions and outlet pressure. To make studies comparable, I focused on the reduction in plant efficiency due to carbon capture $\Delta\eta_{CC}$,

$$\Delta\eta_{CC} = \eta_{PP} - \eta_{PP+CC} \tag{6-2}$$

where η_{PP} is the efficiency of the power plant without carbon capture and η_{PP+CC} the efficiency of the power plant with carbon capture. The majority of studies reported efficiencies on a LHV basis, however some also used HHV. Where applicable, efficiency reductions were corrected using values from Table 6-5. In addition to different operating conditions, studies also varied the CO_2 outlet pressure of the capture system. To harmonize results, an efficiency correction was developed for differences in compression work $\Delta\eta_{CMP}$,

$$\Delta\eta_{CMP} = \frac{\dot{W}_{CMP}}{\dot{W}} \tag{6-3}$$

where $\dot{W}_{cmp}$ is the compressor power, and $\dot{W}$ the plant power.

$$\dot{W}_{CMP} = \frac{\dot{m}_{CO_2}.\Delta h}{\eta_{isen}} \tag{6-4}$$

where $\dot{m}_{CO_2}$is the mass flow rate of carbon dioxide, Δh is the enthalpy change using real gas properties from NIST miniREFPROP [339] using the Span and Wagner equation of state [340] assuming a starting temperature of 25 °C and outlet pressure of 15.3 MPa which was the most common in the review by Rubin et al. [312] and η_{isen} an isentropic efficiency of 80% [315]. The CO_2 flowrate of the compressor is evaluated as,

$$\dot{m}_{CO_2}. = \beta \cdot q_{FUEL} \cdot \frac{\dot{W}}{\eta_{PP+CC}} \tag{6-5}$$

where β is the rate of carbon capture, and q_{FUEL} the fuel specific carbon dioxide emission rate. Equations 6- through 6-5 can then be combined to,

$$\Delta\eta_{\text{CMP}} = \frac{\dot{W}_{CMP}}{\dot{W}} = \frac{\dot{m}_{CO_2}.\Delta h}{\dot{W}} = \frac{q_{FUEL} \cdot \beta \cdot \Delta h}{\eta_{PP+CC}} \tag{6-6}$$

The total efficiency reduction $\Delta\eta$ is then computed as,

$$\Delta\eta = \Delta\eta_{CC} + \Delta\eta_{CMP} \tag{6-7}$$

Predicting the efficiency reduction for another fuel type, here biomass, requires consideration of the exhaust gas CO_2 concentration, which is highly correlated with capture energy requirements. A proportional correction was developed to predict the efficiency reduction for using biomass $\Delta\eta_{biomass}$,

$$\Delta\eta_{biomass} = \left(\frac{q_{FUEL}}{q_{FUEL,biomass}}\right) \cdot \Delta\eta \tag{6-8}$$

Fuel-specific emission factors derived from GREET 2019 are shown in Table 6-7.

.

Table 6-7. Emission factors and ratio of higher heating value (HHV) to lower heating value (LHV) by fuel source, derived from GREET 2019 [334]**.**

Fuel	Emission Factors [g CO_2/MJ]	HHV/LHV ratio [-]
Switchgrass	101.43	1.11
Coal	94.82	1.11
Natural Gas	56.29	1.14

6.4.4 Environmental impacts

For this analysis, I considered four environmental impacts: global warming potential (GWP), energy use (EU), water use (WU) and energy return on investment (EROI). GWP calculations are made on a 100 year basis and are from GREET [334]. Literature was reviewed to select the functional unit for the impacts. In Cúellar-Franca and Azapagic's review of CCS technology studies, 1 kWh was the most common functional unit [310]. Schakel et al.'s LCA of a power plant co-fired with biomass and coal also used a functional unit of 1 kWh [304]. Therefore, a functional unit of 1 kWh of produced electricity was selected to be consistent with similar LCAs to enable comparisons of results. The process of calculating the environmental impacts is based on scaling the baseline power plant environmental impacts from GREET with the efficiency reduction parameter and the addition of solvent production if applicable. The detailed process of calculating the environmental impacts using the efficiency reduction parameter is shown in Appendix D.

6.5 Results and Discussion

6.5.1 GWP vs. EROI

Figure 6-3 presents system global warming potential and energy return on investment for each BECCS configuration considered here. The ideal power plant would have high EROI and low GWP which corresponds to the bottom right corner of the figure. Instead of identifying a single best configuration, I see a Pareto front representing the trade-off between EROI and GWP. Some power plant configurations in the bottom left-hand corner of the plot (for example, steam power plants burning only biomass and capturing CO_2 with amine-based scrubbers) have high rates of CO_2 removal, but these power plants have very low EROI that could influence the economic competitiveness of the plants. Conversely, power plants in the upper right-hand corner of the plot (for example, steam power plants burning only coal and capturing CO_2 using calcium looping) have very high EROI but are net carbon positive. The power plants located in the elbow of the curve present a balance between GWP and EROI.

The inset (Figure 6-3B) provides a higher resolution depiction of the power plant configurations with this balance. The results suggest that IGCC plants that burn biomass or a blend of coal and biomass provide the most balance between EROI and GWP. However, steam-based co-firing of coal and biomass provides EROI values that are almost as high as IGCC plants with biomass, particularly for those plants that deploy membrane or calcium-looping based separation. In all cases, NGCC plants are dominated, so regardless of preference for EROI or GWP, there are better options.

Chemical looping (CL) based separation produces the best EROI and GWP results with SEWGS, CaL and Selexol following close behind. Amine-based steam cycles offer the lowest GWP at the expense of the lowest EROI. Conversely, IGCC plants with a 50% blend of biomass and coal offer the highest EROI with net negative emissions. Negative GWP only occurs for power plants that use 100% biomass or a 50% blend of biomass and coal, as would be expected. I explored additional co-firing fractions and found that EROI did not vary significantly between 25% and 50% co-firing (see Appendix D for more detail). For comparison, corn ethanol CCS is projected to have an EROI of 1.54 and sugarcane ethanol an EROI of 3.89 based on Cheng et al [341]. I also verified GWP and EROI results by comparing my results with estimates reported in the literature, as shown in Table 6-8.

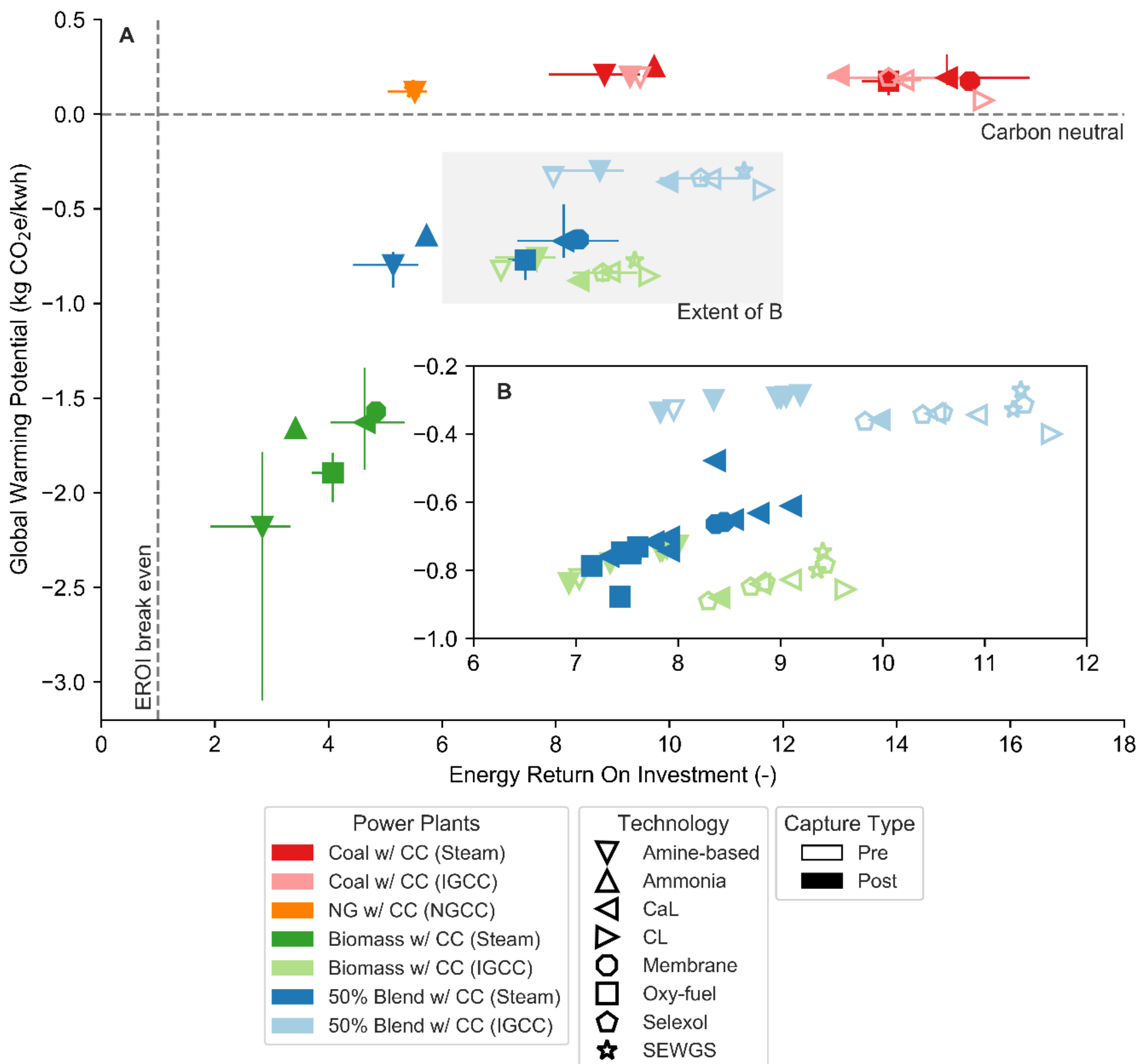

Figure 6-3. Comparison of GWP vs. EROI for power plants equipped with carbon capture. Negative GWP (indicated by horizontal dashed line) is necessary for lowering atmospheric CO_2 levels and EROI values greater than one (vertical dashed line) indicate energetically balanced processes. 50% Blend refers to 50% biomass and 50% coal by mass.

Table 6-8. Verification of EROI and GWP outputs.

	EROI (-)		GWP (kg CO_2eq/kWh)	
Technology	[296]	This study	[56]	This study
Coal with CC	9 – 13	7.9 – 16.3	0.079 – 0.147	0.100 – 0.314
NGCC with CC	4 – 7	5.0 – 5.7	0.063 – 0.097	0.11 – 0.14
Biomass with CC	N/A	1.9 – 9.6	-1.490 – -0.368	-3.096 – -0.725

Table 6-9 presents the two capture technologies with the highest EROI for each plant that burns or partially burns biomass. Full results for all configurations including minimum and maximum values as well as results for fossil-fuel power plants are provided in Appendix D. The configurations are ordered from highest to lowest EROI. As EROI decreases from within these select results, GWP decreases and water use increases.

Table 6-9. Leading biomass configurations based on EROI. The mean performance of biomass power plants with carbon capture is shown in terms of GWP, EROI, and WU (water use). Pre/post indicates whether it is pre- or post-combustion capture. Blend refers to 50% biomass and 50% coal by mass.

Power Plant Type	Capture Type	Pre/Post	EROI [-]	GWP [kg CO_2/kWh]	WU [l/kWh]
Blend (IGCC)	CL	Pre	11.65	-0.40	1.73
Blend (IGCC)	SEWGS	Pre	11.31	-0.30	1.79
Biomass (IGCC)	CL	Pre	9.64	-0.86	1.69
Biomass (IGCC)	SEWGS	Pre	9.39	-0.77	1.73
Blend (Steam)	Membrane	Post	8.41	-0.66	2.02
Blend (Steam)	CaL	Post	8.14	-0.67	2.09
Biomass (Steam)	Membrane	Post	4.83	-1.57	2.13
Biomass (Steam)	CaL	Post	4.64	-1.63	2.24

6.5.2 Water use

In Figure 6-4, water use is compared against EROI for both pre-combustion and post-combustion capture technologies. The bar at the bottom of each panel reports the average switchgrass cultivation water use for a steam-power plant fueled using biomass based on GREET data for a 25% efficient plant without carbon capture. This value is presented to illustrate just how much of the overall life cycle water burdens are attributed to power plant cooling and CCS. Each family of power plant results has an optimal carbon capture technology that achieves low water use and high EROI. Thus, if water use and EROI were the only metrics of interest, neither would have to be compromised. In general, IGCC plants were found to have a lower water use and higher EROI than steam cycle counterparts for the same fuel. Pre-combustion capture technologies for IGCC biomass had higher EROI and similar water use to the post-combustion alternatives. The leading IGCC biomass configuration used an average of 1.69 l/kWh with chemical looping having an EROI of 9.6. The leading biomass with steam plants used membrane capture technology and achieved a water use of 2.13 l/kWh and EROI of 4.8. Blending with coal improves EROI (1-2 points) over pure biomass for IGCC, but greatly improves it for steam (4-5 points) with similar water use. The leading blend with steam used post-combustion membrane capture and had a water use of 2.02 l/kWh and EROI of 8.4.

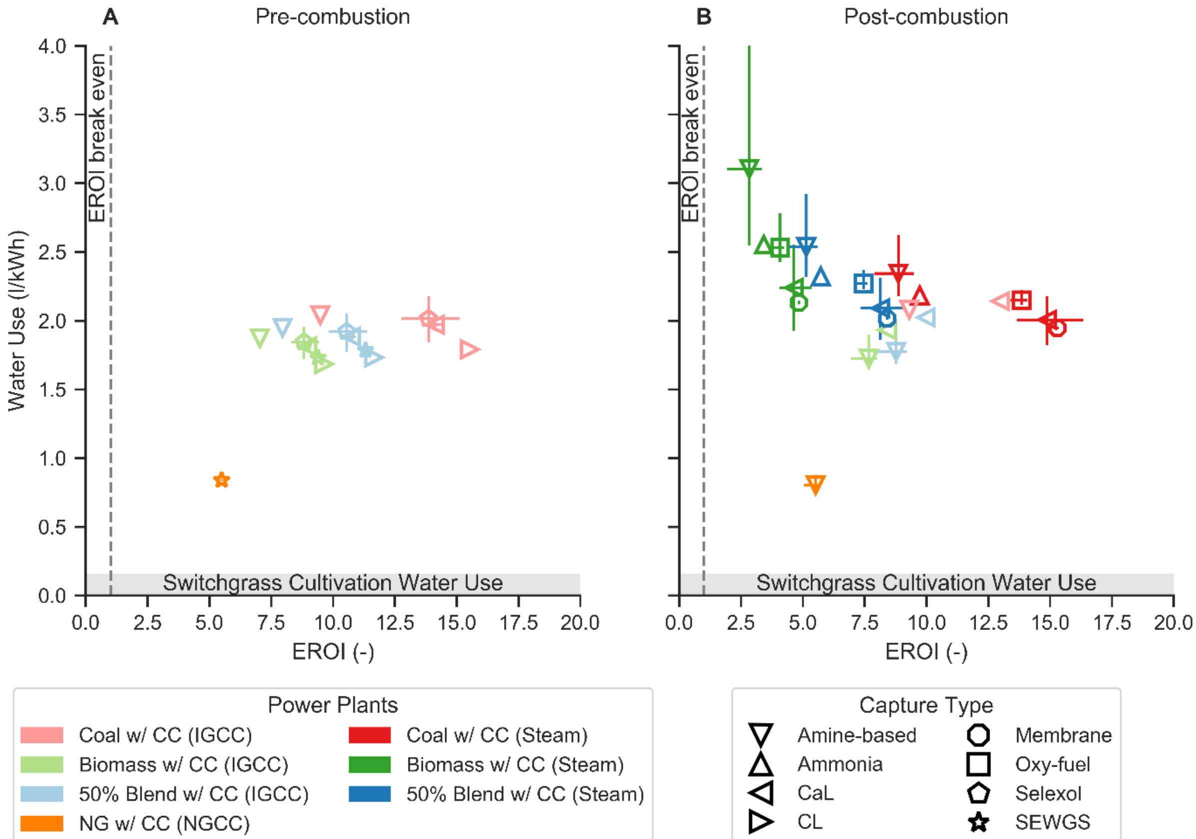

Figure 6-4. Water use vs. EROI is compared for a) pre-combustion and b) post-combustion configurations. Here oxy-fuel is included in post-combustion. Blend refers to 50% biomass and 50% coal by mass. Switchgrass Cultivation Water Use refers to the water use for a steam cycle plant fueled with switchgrass based on GREET data for a 25% efficient plant without carbon capture [334]**.**

6.5.3 Life cycle stage analysis

To identify which life cycle stages were driving the results for biomass-based configurations, I performed a life cycle stage analysis (Figure 6-5). If GWP were the only consideration, then biomass with steam would be the best option. With respect to energy use, IGCC plants consume much less energy than steam cycles. The best water use cases are comparable between steam and IGCC, however some steam capture technologies have very high water use (amine-based). There is little variation across capture technologies for IGCC plants. Most impacts were dominated by a single life cycle stage: GWP by carbon capture, energy use by carbon capture, and water use by power generation (cooling). This identifies where research is needed to improve a particular environmental impact. Solvent production and transportation were found to have negligible impacts. The GWP of fuel production and transport for biomass was negligible based on GREET data when compared with negative emissions.

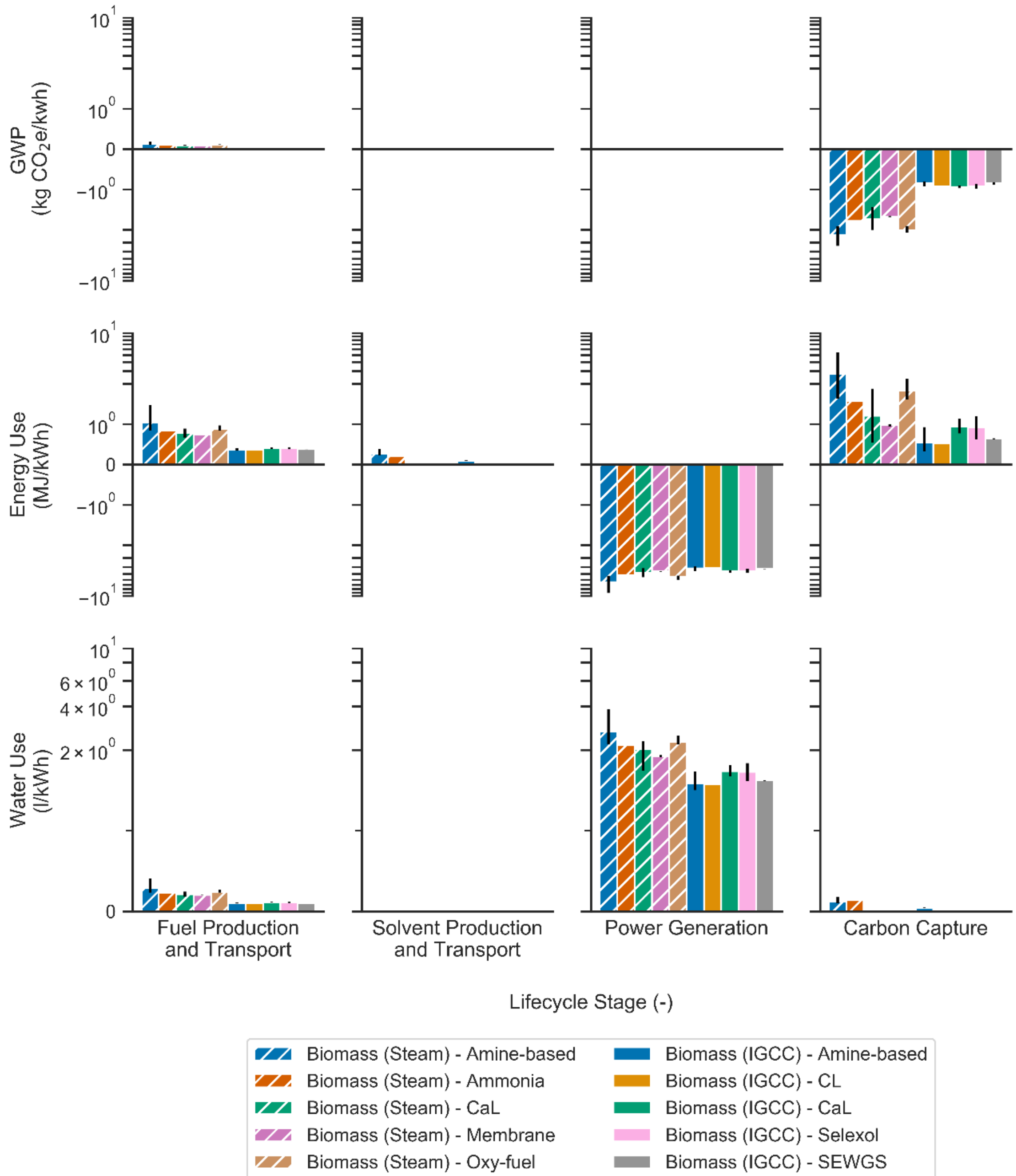

Figure 6-5. A life cycle stage analysis of biomass power plants identifies the stages with the most impact for further improvement and to help identify the optimal configuration.

EROI is often correlated to cost, so my identification of IGCC as having a balance between EROI and GWP is reaffirmed by a recent report for the state of California, which identifies IGCC as a cost-effective option for negative emissions [342]. Although IGCC appears to be the leading option for BECCS, with respect to retrofitting it is a different story. Based on EIA data, there is currently only one operational IGCC plant in the United States with a rated capacity of 756 MWe [343]. The limited deployment of IGCC plants to date is based on technical and economic challenges associated with the technology. Another plant started in Kemper County, Mississippi with a planned capacity of 582 MWe was abandoned due to cost overruns [344]. Therefore, the conversion of existing power plants to BECCS is more likely to take place at coal plants that operate using steam cycles. Patrizio et al project that repurposing coal power plants for BECCS and replacing coal plants beyond their design life with natural gas will create 22,000 jobs in the United States [345]. Additional workforce training would be necessary if BECCS were to be deployed using IGCC configurations, due to the limited experience managing and staffing these kinds of facilities. In theory, it could also be possible to convert a natural gas combined cycle plant by adding a gasification system, but this would be a very large additional infrastructure investment. Additional concerns of retrofitting existing large capacity fossil fuel power plants are the transportation costs and logistics required to provide sufficient feedstock [326,327]. This is further challenged by the need to be located near a suitable CO_2 storage site [324]. Belmont has highlighted other challenges of the potential for combustion-based BECCS in the United States including slow increase in baseload power plants, inconsistent regulatory policies and staying competitive with current natural gas prices [346].

6.5.4 Impact of capture technology characteristics

Each capture technology has a number of unique characteristics in my analysis including efficiency reduction ($\Delta\eta$), capture rate (β), and solvent consumption. To understand how these characteristics were driving the results previously shown in Figure 6-3 through Figure 6-5, I took a detailed look at the impact of efficiency reduction and capture rate on GWP, EROI, and water use in Figure 6-6. Solvent consumption was not included because it was found to have a negligible impact.

Figure 6-6 shows that chemical looping is advantageous due to its high capture rate combined with a low efficiency reduction. Most studies published to date assume a capture rate of 90%, which is why many of the results are clustered in that range. Steam plants have significantly lower GWP compared to IGCC plants independent of efficiency reduction and capture rate, due to a much lower starting power plant efficiency (45% versus 25%). Although carbon capture results in an efficiency reduction, when accounting for the differences in CO_2 concentration in the feedstock, BECCS plants have lower efficiency reductions and thus higher power plant efficiencies than coal or natural gas power plants with carbon capture. Within steam plants, amine-based separations have the lowest GWP, followed by oxy-fuel due to the highest efficiency reductions. IGCC plants have similar GWP across configurations.

IGCC plants have much higher EROI values than steam plants. Of capture technologies, amine-based processes have the lowest EROI which is correlated with large efficiency reductions. For water use, IGCC has lower water use than steam plants, which can also be correlated to the efficiency reduction. IGCC has similar water use levels across configurations. Water use for steam plants however is a function of efficiency reduction, with more water used by less efficient plants. Large efficiency reductions are associated with lower GWPs. Modest negative correlation was found between capture rate and GWP and no strong correlation between capture rate and EROI.

Figure 6-6 also confirms the paradox that low efficiency power plants result in the largest negative emissions [291]. This is based on the fact that CO_2 capture rates are directly proportional to biomass consumption. A less efficient plant requires more biomass to produce the same amount of electricity so it stores more CO_2. However, my analysis shows that this comes at the cost of high water use and a low EROI.

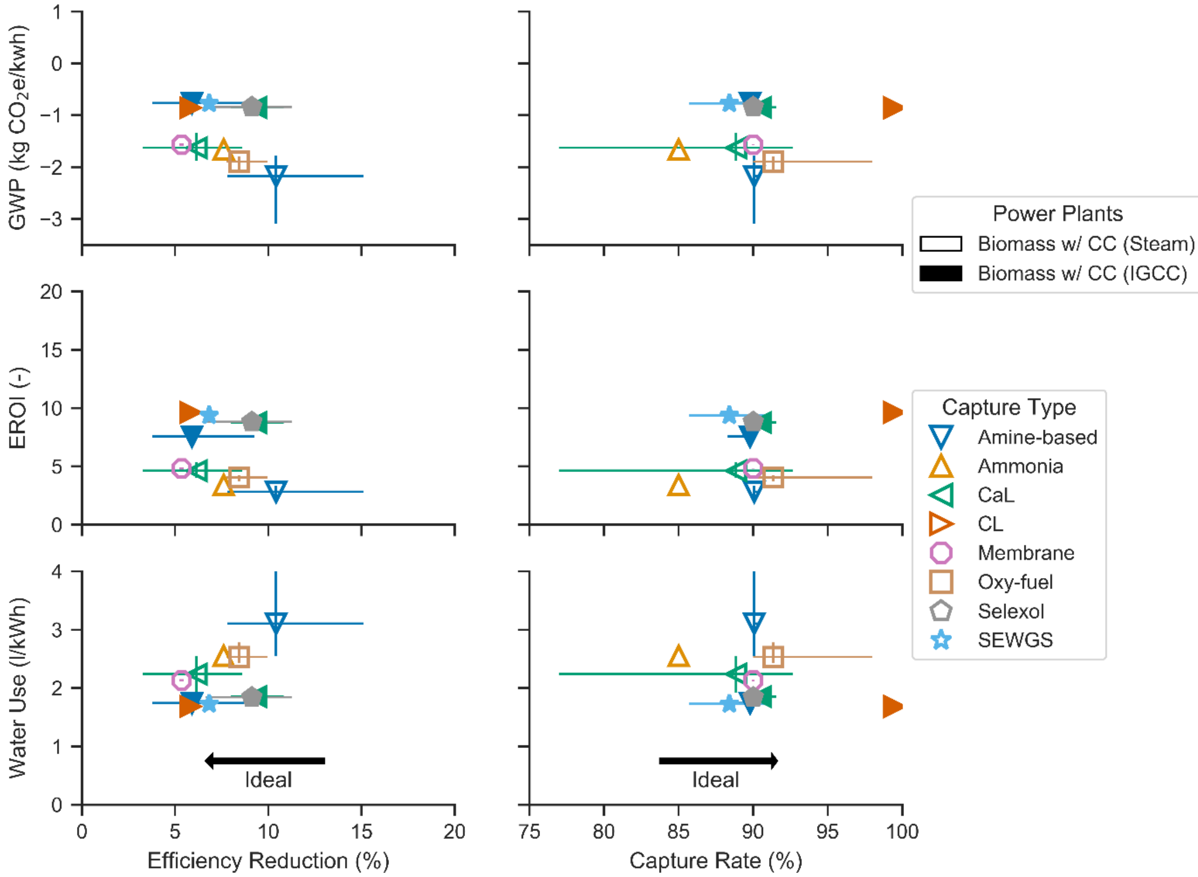

Figure 6-6. The meta-analysis model relies heavily on two inputs, capture technology efficiency reduction and capture rate. Here they are compared against GWP, EROI and water use to better understand the influence of these parameters.

6.5.5 Other considerations

In this study, I applied equal weight to the metrics of GWP, EROI, energy use and water use. However, in practice, the selection of the optimal BECCS power plant configuration for sustainable decarbonization will require weighting these metrics with respect to regional goals and impacts. For example, environmental constraints such as water availability or carbon emission regulations will vary by region. If the primary goal is net zero emissions by mid-century, then the focus will be on maximizing negative emissions, regardless of the resulting EROI. Alternatively, climate mitigation measures such as carbon pricing or cap and trade systems will reinforce the need for negative emissions while creating trade-offs with economic value. BECCS power plants could be used primarily for power production, however due to their increased water use and decreased EROI compared to fossil fuel power plants, the success of BECCS power plants is expected to rely on successfully providing negative emissions. Future work can further consider metric weighting in a system analysis.

6.6 Conclusions

Negative emission technologies are necessary for achieving carbon neutrality goals and stabilizing atmospheric CO_2 levels. Bioenergy with carbon capture is expected to be an important source of negative emissions that could leverage existing power plant infrastructure. Detailed comparisons of carbon capture technologies with biomass were previously limited to only a few different types of power plant capture technologies. Here I harmonized carbon capture estimates from fossil fuel studies to forecast the emissions factors from biomass plants, and compare life cycle impacts across operational configurations. The results reveal important trade-offs between global warming potential and energy return on investment for different power plant and carbon capture configurations. IGCC plants were found to have higher EROI values while still achieving negative emissions which makes them the best candidate for conversion. However, IGCC plants are typically very large and bioenergy plants tend to be small. Further, the US currently has only one IGCC plant which is in stark contrast with hundreds of steam plants currently operating. Transitioning to low-carbon fuels would leave existing fossil-fuel power plants as stranded assets, because they will no longer be economically viable to operate. Many of the existing steam plants are in close proximity to biomass sources. Successful BECCS operation will also require close proximity to suitable carbon storage sites.

Chemical looping was found to be marginally better than other capture technologies for IGCC, however future work could consider infrastructure and operational costs. Biomass plants operating with a steam cycle and amine-based capture technologies were found to have the lowest GWP but this was accompanied by significant increase in water use and low EROI. Retrofitting steam plants to burn biomass will likely require blending with coal to achieve negative emissions along with a suitably high EROI. Steam cycles were more sensitive to capture technologies than the IGCC power plant configurations. Steam-based coal plants with membrane or calcium looping-based separations performed almost as well as IGCC, especially when the plants burned a blend of coal and biomass.

6.7 Chapter Acknowledgements

I would like to acknowledge the Rotating Machinery and Controls Laboratory at the University of Virginia, which provided financial support for JB. Also, thanks to Immanuel Ndumbe for his work developing plotting scripts.

6.8 Data Availability

The model and analysis programs are available for download at http://www.github.com/EnergyModels/BECCS-LCA-MetaAnalysis. The model was created in Excel 2016, data analysis performed in R version 4.02 [347] using dplyr [348] and readxl [349], and plotting performed in Python 3.7.6 [350] using numpy [275], pandas [351], matplotlib [277], seaborn [352] and xlrd [353].

7 The Role of Long Duration Storage and Negative Emissions in Meeting Decarbonization Goals at the Regional Scale

7.1 Summary

This chapter uses an energy system optimization model to evaluate the role of the emerging technologies considered in this dissertation by projecting their deployment in the grid planning of Virginia. Virginia has targeted decarbonization by 2050, therefore I explore the impact of grid planning with long duration storage (i.e. offshore compressed air energy storage), negative emission technologies (i.e. bioenergy with carbon capture and storage), fossil infrastructure (i.e. sCO_2 power cycles with carbon capture and storage), and distributed generation (i.e. rooftop solar). The results show that including long duration storage and negative emission technologies in decarbonization planning results in 31% lower 2050 electricity costs. I also show that the deployment of OCAES depends on its cost, but that BECCS will be deployed based on biomass availability. Rooftop solar is only installed after utility scale solar has reached its limit and natural gas with CCS is deployed when available.

7.2 Introduction

In order to limit the world to 2° C of warming, countries need to go above and beyond their original targets for the 2015 Paris Agreement [283]. While many countries are planning for decarbonization by 2050 [1], some countries (i.e. Finland [354]) and institutions (i.e. University of Virginia [355]) also aim to be fossil-free. In the United States, energy sector planning is led by the Energy Information Agency (EIA), however their modeling only incorporates established and close to market energy technologies into their planning through 2050 [356]. As countries plan for electric sector decarbonization, they need to consider emerging energy technologies such as long duration energy storage, and negative emission technologies. Long duration energy storage technologies capable of storing energy for more than 10 hours has been shown by Dowling et al. to reduce costs in comparison with batteries [15]. Negative Emission Technologies

(NETs) actively reduce atmospheric CO_2 concentrations and are relied on by Integrated Assessment Models (IAM) that project future CO_2 concentrations [357]. Although some institutions are moving away from fossil fuels, the EIA Annual Energy Outlook projects increased consumption of petroleum and natural gas [356]. Natural gas has been presented as a bridge fuel, however Zhang et al. has shown that it could offset benefits by preventing earlier deployment of low-emission technologies [358]. Here, I explore the effects of long duration storage, negative emission technologies, and fossil infrastructure on the regional decarbonization of the electric sector using Virginia as a case study.

7.2.1 Long duration storage

Transitioning the electric sector to be carbon-neutral will rely heavily on variable wind and solar power, which in turn will depend on energy storage to balance intermittent generation. Lithium-ion batteries are the most commonly discussed energy storage technology; however, they have fixed ratios of power and energy [185] that do not work well for long duration storage. Although a range of energy storage technologies exist [14], energy systems are expected to rely on long duration storage, which commonly refers to energy storage with a duration greater than 10 hours [251]. Two examples of long duration energy storage technologies are offshore compressed air energy storage (OCAES), and vanadium flow batteries (VFB). OCAES has been evaluated for the United Kingdom by Mouli-Castillo [46] and North Carolina by Li and DeCarolis [44]. In this dissertation, OCAES has been explored for Virginia and is projected to cost \$1457/kW (less than Lithium-ion), with a round-trip efficiency of 70% for 200 MW, 24-hour storage [262]. Virginia does not have the geology for onshore compressed air energy storage [45]. VFB are a next generation battery design that overcomes the challenges of traditional batteries by decoupling the energy storage from the power conversion components [14]. VFB have recently been demonstrated at the 15 MW scale with 4 hours of storage [359]. Although it is expected that energy systems will rely on long duration storage, the EIA currently only includes 4-hour lithium-ion storage [356]. Therefore, I explore the role of OCAES, and VFB as examples of long duration emerging technologies in energy system planning.

7.2.2 Negative emission technologies

Negative Emission Technologies (NETs) are a group of technologies that actively reduce atmospheric carbon dioxide levels. Two commonly discussed NETs are Bioenergy with Carbon Capture and Storage (BECCS) and Direct Air Capture (DAC). BECCS refers to the conversion of crops such as wood or switchgrass to energy and to store the CO_2 generated in the process [19]. The two BECCS power plants in operation are retrofitted coal plants; a pilot scale power plant in the United Kingdom, and a 50 MW in Japan plants [49,50]. One challenge with BECCS, and all NETs, is to ensure that the lifecycle emissions of the technology are in fact negative [48]. Since BECCS is still in the development phase, a variety of BECCS power plant configurations have been evaluated (Chapter 6) [308,360]. DAC is an alternative NETs that uses either chemical or physical processes to remove CO_2 from the air [19]. A number of DAC demonstration plants are in operation with capture capacities up to 1000 tonne CO_2/year [19] Although the cost of DAC is currently high, Keith et al. project costs could get as low as 94$/t-CO2 [361]. The EIA currently does include NETs in the United States energy system plan, so I evaluate the role of BECCS and DAC to explore the potential impact for this group of technologies.

7.2.3 The role of natural gas

The need to decarbonize has led to developments in carbon capture and storage for fossil fuel power plants that enables the majority of the CO_2 generated to be captured and stored in the ground. Natural gas in particular has been presented as a bridge fuel because it produces fewer CO_2 emissions as compared to petroleum and coal. With the shale gas revolution, natural gas has also led to reduced energy prices and a shift from coal generation to natural gas power plants [362]. Advances in natural gas power plants, such as supercritical CO_2 power cycles [28] and in particular the Allam cycle have led to capture levels near 100% [32]. Supercritical CO_2 cycles were explored for their ability to provide balancing to renewable energy deployment in Chapter 3 [57]. Although natural gas has been presented as a cleaner fuel, there is a large body of evidence that shows concerns over methane leakage and water contamination [363]. The persistent low price of natural gas provides an apparent justification for continued investment in gas-fired generation, but the potential for economic stranding of these new assets (power plants that become uneconomical to operate before the end of their design life) is high, as states announce aggressive decarbonization plans [11]. Therefore, in this study, I also examine the issue of whether or not to continue building new natural gas power plants, alongside the decision about the deployment of new storage and carbon capture technologies in decarbonizing electricity sectors.

7.2.4 Hypotheses, research questions and contributions

I investigate the role of long-duration storage (OCAES and VFB), negative emission technologies (BECCS, DAC) and the role of new fossil infrastructure. I hypothesize that long duration storage (LDS) and negative emission technologies (NETs) will enable a faster and less expensive transition to decarbonization. I also evaluate the decision whether or not to build new fossil fuel infrastructure based on power sector monetary costs. To explore the effects of LDS and NETs, I use Virginia as a case study. In 2021, Virginia established a legal mandate for the decarbonization of its electric sector by 2050 [187].

7.3 Methods

7.3.1 Energy System Optimization Model

7.3.1.1 Tools for Energy Model Optimization and Analysis

To explore the role of emerging energy technologies I used an energy system optimization model (ESOM) calibrated for Virginia. The ESOM was created using the Tools for Energy Model Optimization and Analysis (Temoa). Temoa is an open source, ESOM that projects power plant deployment and operation to meet demand while minimizing costs [58]. Temoa has been used to project energy system planning from the national [364] to the state level (Chapter 2) [365].

7.3.1.2 Virginia model

Virginia is used as a case study because it is similar to many locations in that it experiences four seasons, and has limited renewable energy resources. As shown in Figure 7-1, I simulated Virginia with six representative seasons. In addition to the standard calendar seasons, two synthetic seasons were added, to also account for times of year with limited solar and wind resources. Although Virginia does not have the largest solar resource potential [366], solar deployment has increased from 139 MW in 2016 to 626 MW in 2019 [367]. Utility-scale wind has not yet been installed onshore in Virginia. Virginia had 12 MW of offshore wind in place at the end of 2020 [368], and the 2020 Virginia Clean Economy Act requires the addition of over 5 GW of offshore wind capacity by 2035 [187]. Here, I assume that offshore wind beyond 5 GW would take the form of floating wind turbines based on Shobe et al. [369]. With respect to biomass availability, 3.87% of electricity produced in Virginia in 2019 was from biomass [370], which equates to 52.6 PJ of biomass fuel assuming a power plant efficiency of 25% [8]. In comparison, based on the NREL biofuels atlas, there is an estimated 78 PJ of biomass fuel currently available in Virginia [371,372].

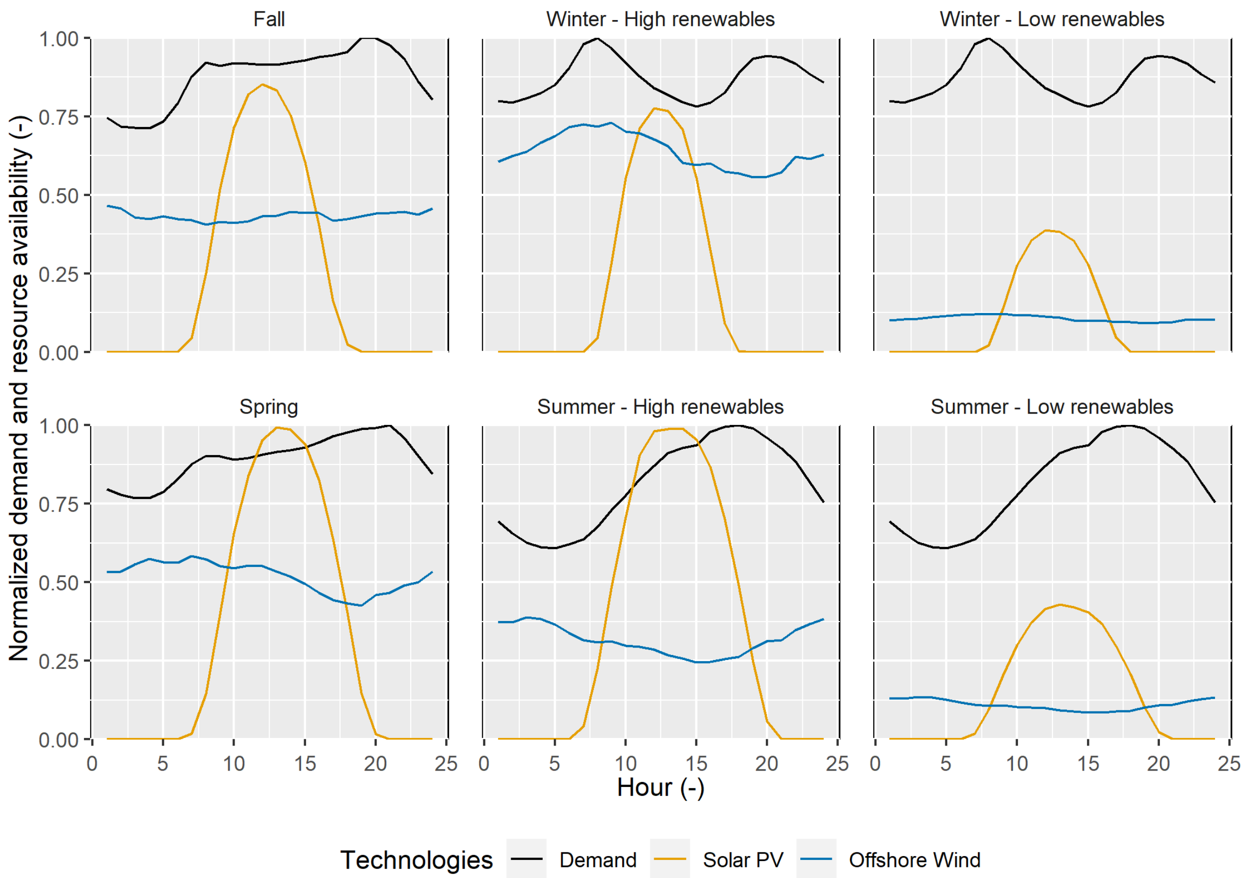

Figure 7-1. Wind and solar resource availability and electricity demand by time of day and season. To represent the variability in wind and solar resources and demand, the model used six representative seasons. The Fall and Spring seasons each constitute 25% of the year, the high renewable seasons each 20% of the year and the low renewables seasons 5% of the year [248,373–375]**.**

7.3.2 Technology cost projections

7.3.2.1 Established technologies

Temoa performs a least-cost optimization; therefore, the cost of technologies will determine their deployment and operation. For more established and common technologies, I used cost projections based on moderate estimates from the NREL Annual Technology Baseline (ATB) [8]. Due to the uncertainty of the future costs and performance of direct fired sCO_2 power plants with CCS, I evaluated natural gas power plants with CCS from NREL ATB as a surrogate. Direct fired sCO_2 power plants are expected to have higher system efficiencies and higher capture rates, so if natural gas with CCS is found to be competitive, than it can be expected that if direct fired sCO_2 cycles are commercialized with a similar cost, then they too, would be competitive. When technology costs were not available in the ATB, I used estimates from the EIA Annual Energy Outlook [356]. For pumped hydro I used estimates from Beuse et al. [258] and Luo et al. [14]. Power plant and energy storage installation costs are presented in Figure 7-2 along with fuel costs. Additional details such as operating and maintenance costs are presented in Appendix E.

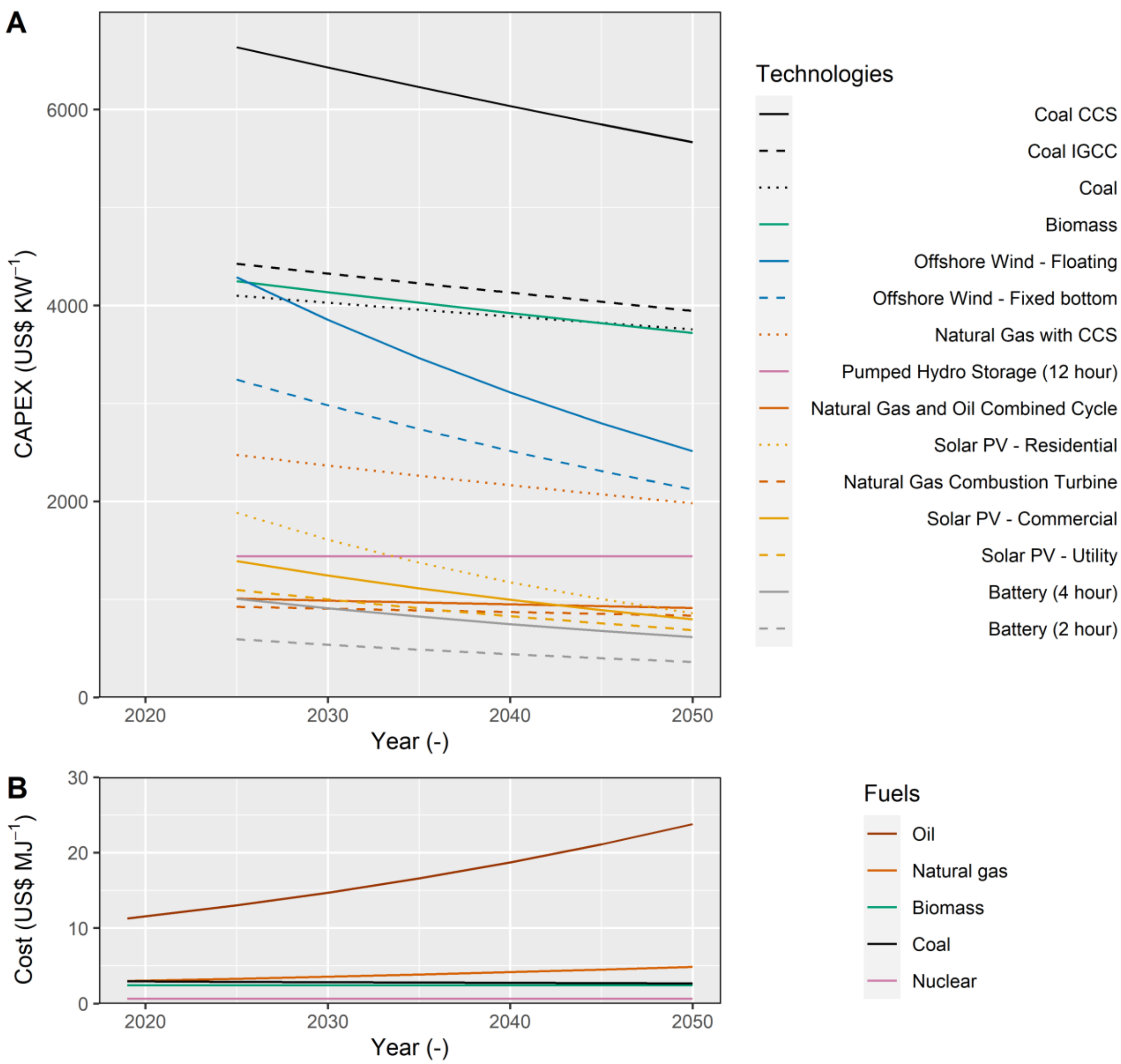

Figure 7-2. a) Technology capital costs and b) fuel price projections until 2050. Technologies from the NREL ATB follow the moderate price projection [8]**.**

7.3.2.2 Long duration storage and negative emission technologies

The future cost of long duration storage and negative emission technologies is considerably less certain than for established energy technologies. For this study, I surveyed the literature and found a range of cost estimates for the LDS and NETs considered here. A summary of the low and high cost estimates are shown in Table 7-1. I used Monte Carlo sampling with uniform distributions to investigate the uncertainty of the technology capital costs. I assumed that the operation and maintenance costs, both fixed and variable, would remain constant. Additional details on the representation of each technology are presented in Appendix E.

Table 7-1. Investment costs of the long duration storage and negative emission technologies considered in this study. Additional details regarding the calculations of the low and high cost are provided in Appendix E.

Category	Technology	Low Cost	High Cost
Long Duration Storage (LDS)	Offshore Compressed Air Energy Storage (OCAES), 24-hour duration	$1457/kW [262]	$9191/kW [46]
	Vanadium Flow Batteries (VFB), 10-hour duration	$1820/kW [376]	$3781/kW [258]
Negative Emission Technology (NET)	BioEnergy with Carbon Capture and Storage (BECCS)	$4781/kW [285] ($571/t CO2/year)	11714 $/kW [287] ($1400/t CO2/year)
	Direct Air Capture (DAC)	$795/t CO2/year [361]	$1150/t CO2/year [361]

7.3.3 Scenarios

To evaluate the impact and need for long duration storage and negative emission technologies, I simulated scenarios over a range of planning options. The scenarios were developed around three decisions: the use of LDS/NET (long duration storage and negative emission technologies), the building of fossil fuel infrastructure and the biomass resources available for the energy sector. First, I developed energy planning scenarios with and without LDS/NET. For the Monte Carlo sampling, I made 100 random draws from the uniform-cost distributions for each of the emerging technologies (Table 7-2). Scenarios that did not include LDS/NET had constant model inputs, therefore only one iteration was necessary for these simulations. I repeated this analysis for two scenarios differing only by whether they did or did not allow new fossil fuel power plants. Lastly, I developed scenarios that either limited biomass consumption for power generation to current levels or allowed it to double. A doubling of biomass is meant to represent the higher limit estimated based on data from NREL in combination with policies to increase biomass production. All scenarios were simulated over the same time horizon from 2018 to 2050. Decarbonization in Virginia is expected to be challenging because electricity demand is expected to increase due to plans for data centers in Virginia [369]. Therefore, each scenario also used the same electricity demand and emission limit leading to decarbonization in 2050 (Figure 7-3).

Table 7-2. Overview of cases studied.

Scenario	Biomass Conditions	Long Duration Storage and Negative Emission Technologies (LDS/NET)	New Fossil Infrastructure	Iterations
Without Emerging Tech - With New Fossil	Current, Double	No	Yes	1
Without Emerging Tech - Without New Fossil	Current, Double	No	No	1
With Emerging Tech - With New Fossil	Current, Double	Yes	Yes	100
With Emerging Tech - Without New Fossil	Current, Double	Yes	No	100

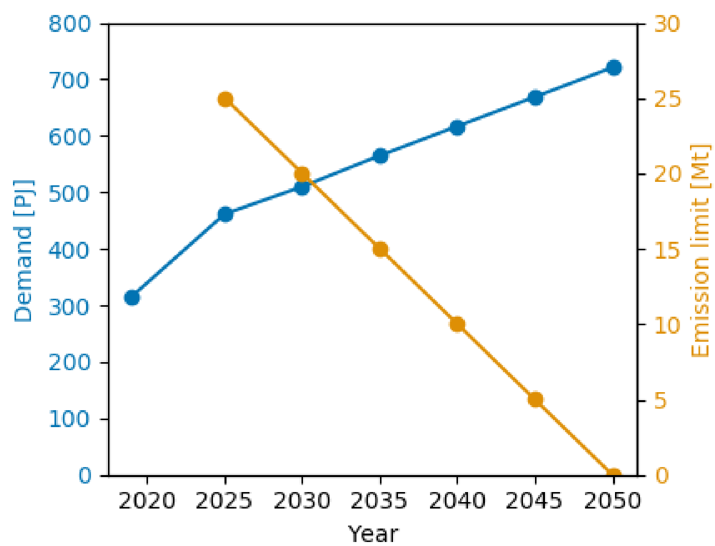

Figure 7-3. Decarbonization emission timeline and projected electricity demand.

7.4 Results and Discussion

7.4.1 Cost projections

Figure 7-4A shows the projected annual cost of electricity for each scenario. With and without long duration storage (LDS) and negative emission technologies (NET) follow a similar trend until 2050. In 2050, the average cost without LDS/NET is between 28% and 45% higher, highlighting the value of LDS/NET. The narrow range of the simulations with LDS/NET suggests that the price is less important than the unique function that long duration storage and negative emission technologies can perform. 2050 costs without LDS/NET are lower without new fossil infrastructure, whereas with LDS/NET the costs are lower with new fossil infrastructure. All simulations followed the emission constraint (Figure 7-4B), showing that decarbonization is not faster with LDS/NET, although it is less expensive. Figure 7-4C shows the capacity investments made in wind, solar, natural gas and batteries. The most notable difference is in batteries. Without LDS/NET, the average investment in batteries is up to 270% higher at current biomass levels, and up to 213% higher with doubled biomass.

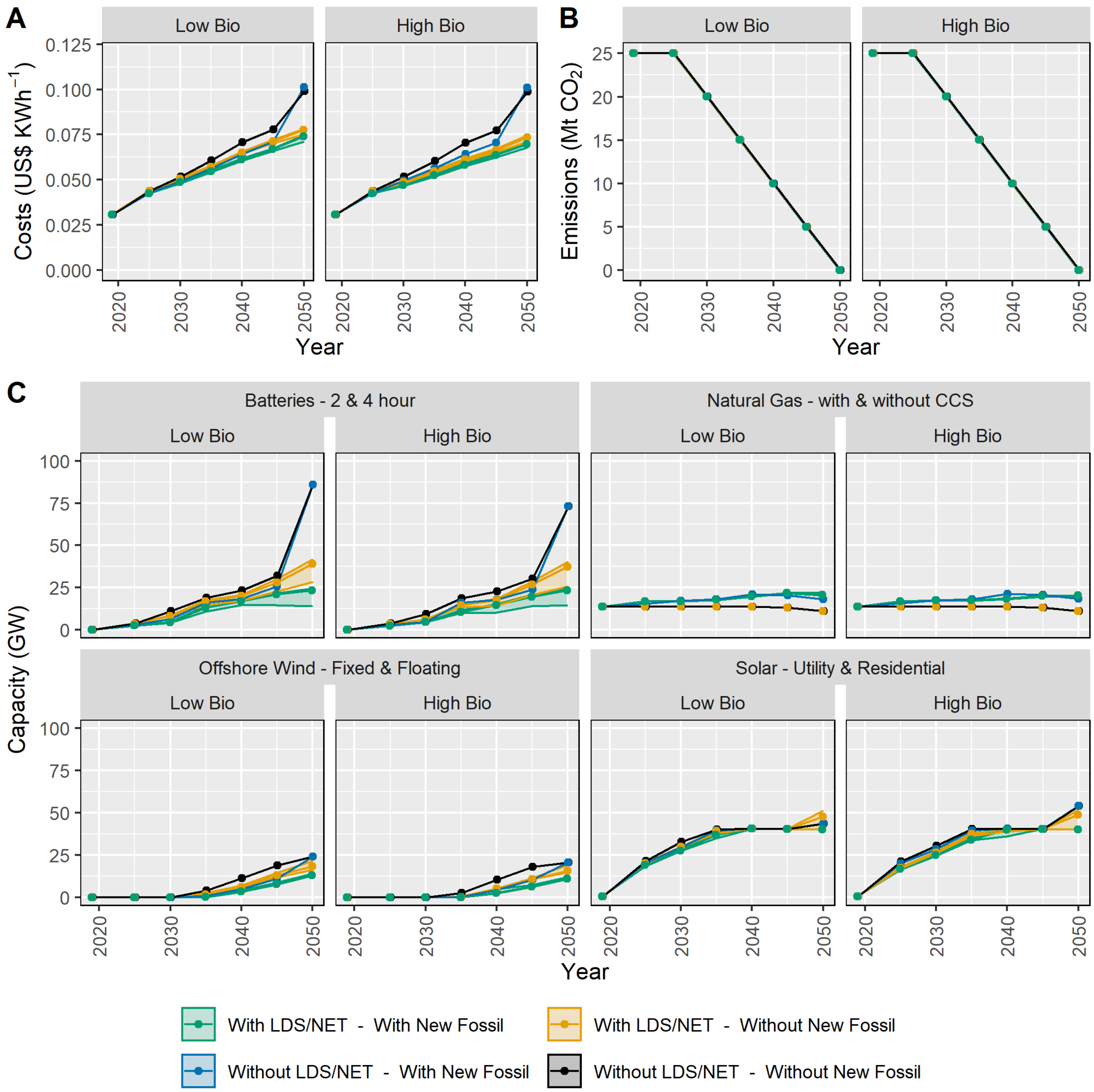

Figure 7-4. Projections of A) cost of electricity, B) emissions and C) capacity of wind, solar, batteries and natural gas.

7.4.2 Projected technology operation

Figure 7-5 shows the annual activity of power plants, energy storage, and negative emissions technologies with current biomass resources. The majority of batteries installed have 4-hour durations, and although simulations without LDS/NET have much higher deployment, the usage of the battery systems is similar. Natural gas remains an important fuel source across the scenarios. Simulations that can build new fossil infrastructure invest in carbon capture and storage, however without a negative emission technology, fossil with CCS must by retired by 2050 to comply with the decarbonization requirement. The relative usage of biomass and BECCS is low in comparison to the others, showing that it is not a large source of power generation. The lower costs of utility solar lead to it being fully utilized before distributed solar becomes the optimal choice. This shows that without incentives or extreme events (Chapter 2), higher-cost distributed generation has a lower value in a capacity expansion planning. All simulations that have access to fossil with CCS use it, showing the benefit of further developing these technologies (i.e. sCO_2 power cycles). However, without negative emission technologies, decarbonization cannot include fossil with CCS. The usage of DAC refers to the amount of natural gas consumed for operation, with operation increasing after 2035. Flow batteries and commercial solar are not shown because they are not deployed in any of the scenarios. The overall trends remain the same for doubled biomass levels.

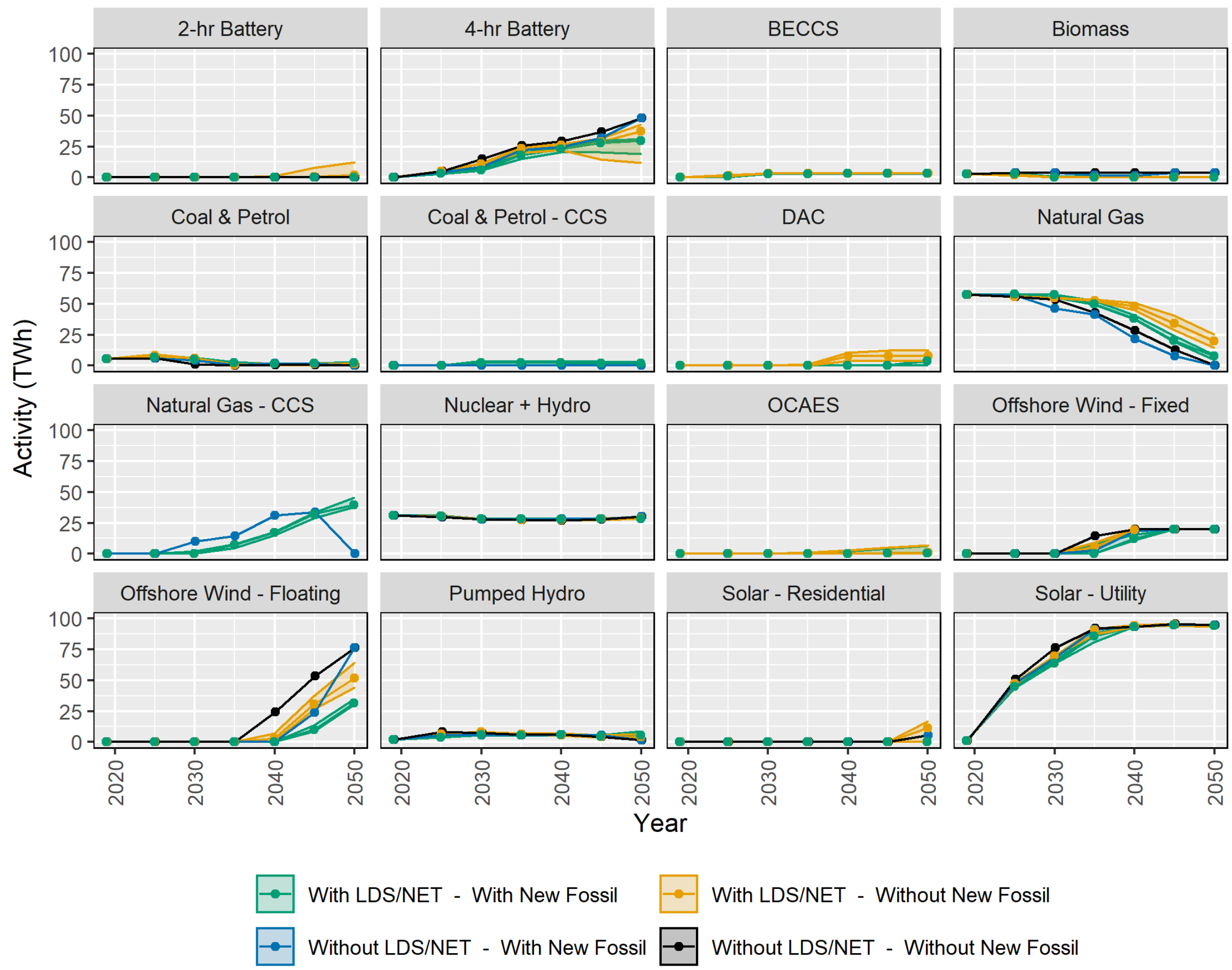

Figure 7-5. Activity transition with current biomass resource available. The activity of DAC refers to the heat content of natural gas consumed.

7.4.3 Long duration storage

Figure 7-6 shows the projected deployment of batteries and OCAES as a function of OCAES cost. At costs lower than $3200/kW, OCAES is competitive (dashed line), reaching a peak deployment of 6.4 GW. Once OCAES is competitive, there is a shift in battery deployment where 2-hour batteries start being used in place of 4-hour batteries. This demonstrates that the long duration storage of OCAES pairs well with the short duration storage of a 2-hour battery. At the lowest OCAES price without new fossil infrastructure, the combined energy storage capacity (batteries and OCAES) is 32 GW, as compared to 40 GW when OCAES is expensive. In general, the installation trends are similar regardless of either the biomass availability or the option to build new fossil, except when it comes to 4-hour batteries. When OCAES prices are above \$3200, the 4-hour battery deployment is 67% higher without new fossil versus with new fossil. Across all simulations pumped hydro is always built to the maximum available (300 MW new and 3200 existing).

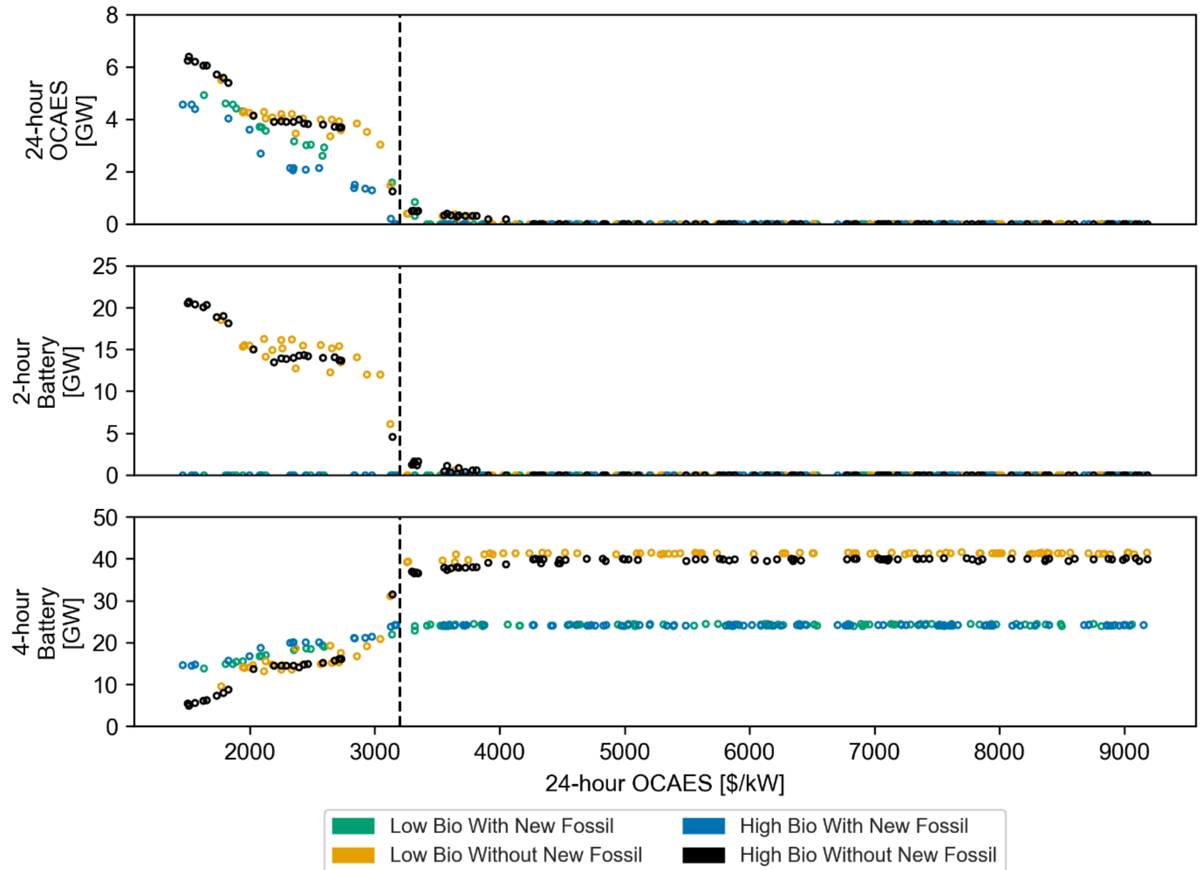

Figure 7-6. Projected 2050 capacity of OCAES and battery technologies.

7.4.4 Negative emission technologies

The deployment of negative emission technologies is shown Figure 7-7 against the capital costs. The results show that the deployment of BECCS is nearly always at a maximum and is independent of the cost of either BECCS or DAC. Compared to other power plants, the capital costs of BECCS are high and the efficiencies are low. Therefore, the high deployment of BECCS regardless of cost shows that it is most valued for its negative emission potential. A techno-economic analysis of BECCS by Mac Dowell and Fajardy suggested that low cost, low efficiency BECCS is preferred over high cost, high efficiency BECCS [291]. Here, I show the cost of BECCS is less important than its function. DAC is only deployed when the biomass availability remains at current levels. As expected, more DAC is deployed at lower costs. Below \$1025/t-CO_2/year, DAC is deployed at higher levels without new fossil than with new fossil. This is because simulations that are able build new fossil utilize CCS plants. For comparison, Section 45Q of the United States Tax Code will credit up to \$50/t CO_2 for injection into the subsurface [377].

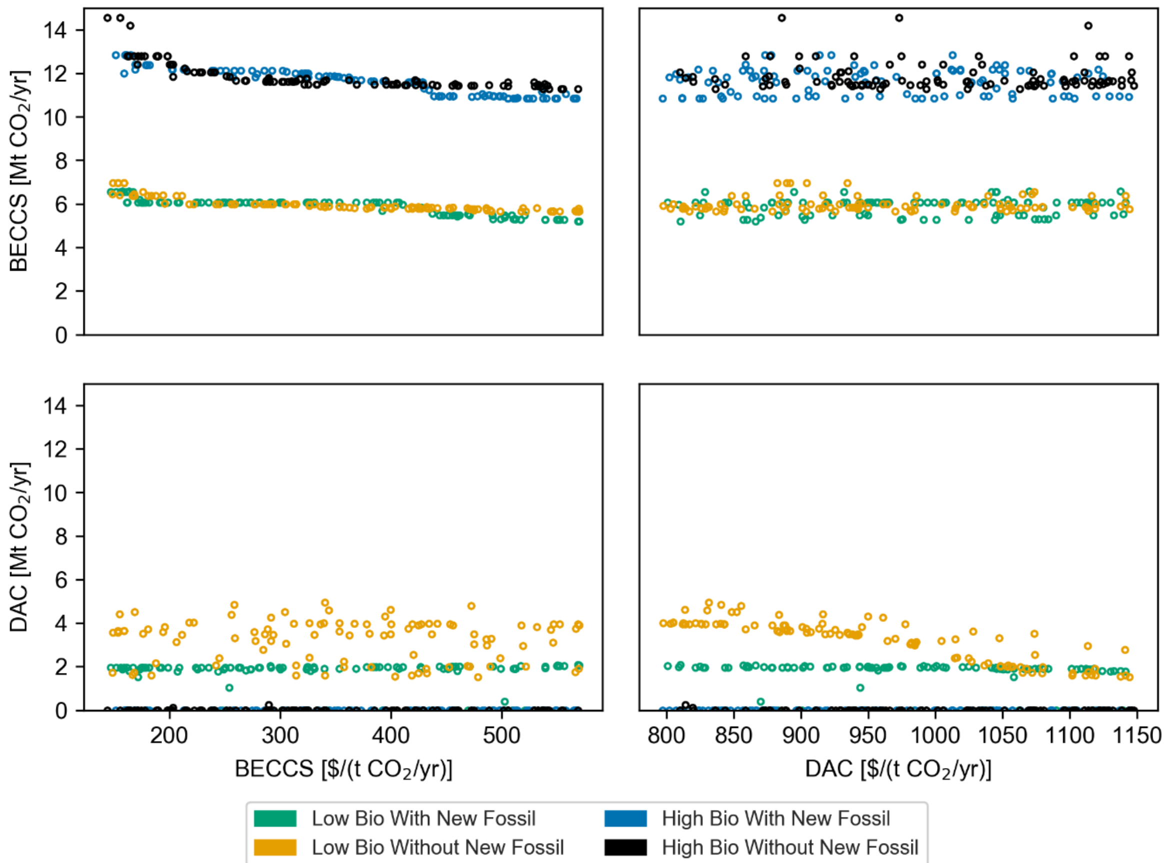

Figure 7-7. Projected 2050 capacity of negative emission technologies.

7.5 Conclusions

This study examined the value of long duration storage and negative emission technologies in regional energy system planning for decarbonization. Decarbonization is realized across all planning decisions including whether or not to build long duration storage (LDS), negative emission technologies (NETs), new fossil infrastructure, or to increase the amount of biomass available for the energy sector. Although there is high uncertainty in the future costs of LDS and NETs, together they are able to significantly reduce electricity costs in 2050. Choosing to build new fossil infrastructure reduces annual costs during the transition due to natural gas with CCS, but results in higher 2050 costs. This suggests that commercialization of direct fired sCO_2 power plants with CCS would also be deployed, and therefore should be evaluated further. The amount of biomass available also did not greatly impact costs, but when BECCS is deployed, this resource was primarily used for BECCS over conventional biomass energy. This suggests that more in-depth assessments should be performed to determine the amount of biomass available for BECCS in Virginia. DAC deployment also depends on biomass availability; when it remains low, DAC is installed to provide the negative emissions in place of more BECCS. With respect to long duration storage, pumped hydro was built to its limited potential of 300 MW, flow batteries were not used, and large amounts of OCAES were used to provide balancing of offshore wind. Although distributed generation was available in the form of rooftop solar, this resource was rarely selected due to its higher price, this shows that without an impetus in planning for extreme events, distributed generation will not be selected.

In this study, I assumed that 5.2 GW of fixed bottom offshore wind could be developed, and any additional wind development would be built as floating offshore wind. Floating offshore wind depends on a number of technological advancements, so future work should also consider the potential for onshore installations in Virginia.

Future work should also compare the impact of high and low pricing pathways for long duration storage and negative emission technologies to further investigate their impact on future energy technology investments. Long duration storage could be paired with a large deployment of renewables and negative emission technologies with fossil with CCS, but it is expected that these pathways are highly dependent on future costs.

8 Conclusions and Future Work

8.1 Conclusions

This dissertation investigated the role of emerging technologies in the transition to a decarbonized electric grid. The four technologies considered were distributed electric grids, supercritical CO_2 power cycles, offshore compressed air energy storage (OCAES) and bioenergy with carbon capture and storage (BECCS). Each was found to provide value to a decarbonized electric grid. This section summarizes the main contributions of this dissertation by revisiting the primary research questions of Chapter 1.

1) *What is the impact of grid topology (distributed vs. centralized) and fuel mix (natural gas vs. natural gas, wind and solar) on costs, emissions and resilience?*
   - To answer this question, I developed a novel methodology that enabled explicit consideration of extreme weather events in energy system planning.
   - I found that distributed grid architectures are less expensive when considering the risk of increased hurricane frequency.
   - A grid based on renewables and natural gas reduces costs and emissions independent of climate policy.
   - Including the expected impact of hurricanes enables grid planners to understand the trade-offs between the high capital costs of grid hardening measures with reduced repair costs after future storms.

2) *How do existing and proposed advanced power cycles (sCO_2 power cycles) perform delivering load-balancing when integrated into a grid involving high deployment of solar PV?*

- To evaluate this question, I developed a novel characteristic-based transient model to understand the impact of ramp rates, part-load operation and power plant efficiency.
- I found that existing and advanced natural gas power plants with ramp rates greater than 5.75%/min are well-suited to balance high solar power deployment
- This study focused on sCO_2 power cycles in combined cycle (i.e. replacing the steam cycle in a combined cycle natural gas turbine) and found that this configuration does not provide significant advantages over conventional natural gas combined cycle power plants. However, the wide range of applications possible for sCO_2 cycles, and the ability of direct-fired cycles to provide storage-ready CO_2 led to further examination of its potential in Chapter 7.

3) *What is the techno-economic performance of OCAES?*

- Using a thermal fluid process model, I projected that OCAES can have round-trip efficiencies up to 77% off the coast of Virginia.
- OCAES is expected to cost less than batteries at $1457/kW for a 200 MW system.
- A system that combines offshore wind with OCAES is expected to provide dispatchable power at $0.22/kWh.

4) *What is the geospatial potential of OCAES in the United States Mid-Atlantic?*

- There is the potential for 24 TWh of OCAES in the Mid-Atlantic with round-trip efficiencies greater than 60% and in water depths less than 60 m (suitable for fixed bottom wind turbines).
- For comparison, this is nineteen times the battery storage projected for the United States by 2050.
- There is even more storage potential further offshore with round-trip efficiencies greater than 60%.

5) *What is the environmental impact of carbon capture and power plant technologies for BECCS?*

- A life cycle assessment identified Integrated Gasification and Combined Cycle (IGCC) power plants with chemical looping as offering a balance of negative emissions, water use and energy use.
- The United States experience with IGCC power plants is limited with only one plant in operation, therefore BECCS plants are more likely to adopt steam cycle plants, perhaps by retrofitting existing coal power plants.
- Membrane and calcium looping capture offer balanced environmental impacts with steam cycles.
- If the primary goal of BECCS is negative emissions, then amine-based carbon capture offers the largest negative emissions, at the expense of large water use and energy use.

6) *What is the role of emerging technologies on decarbonization of the electric grid?*

- 2050 electricity costs are projected to be up to 31% less expensive when including emerging technologies as demonstrated through studying the build-out of Virginia's electric grid.
- Residential solar (i.e. distributed generation) was built out when new fossil infrastructure was not permitted and after utility scale solar had reached its maximum potential.
- Natural gas with CCS (i.e. direct fired sCO_2 with carbon capture and storage), is deployed whenever new fossil infrastructure is allowed.
- Using Monte Carlo sampling, I demonstrated that OCAES is deployed when capital costs are less than $3200/kW ($1457/kW was projected in Chapter 4).
- BECCS was always deployed when available, despite the wide range of costs investigated ($4781/kW to $11714/kW), demonstrating its high value to a decarbonized electric grid.

8.2 Future Work

Distributed electric grids and micro-grids are commercialized technologies with limited deployment. I found that they are economically beneficial when considering risks not included in traditional electric grid planning. Therefore, future research is needed to incorporate more extreme events into electric grid planning so that planners can better understand the value of these technologies.

Two versions of sCO_2 power cycles were considered in this dissertation, combined cycle (Chapter 3) and direct-fired with CCS (Chapter 7). Both are being demonstrated in the United States at the writing of this dissertation. When operating in combined cycle, I did not see a clear advantage for sCO_2 over conventional natural gas plants. However, direct-fired sCO_2 plants with CCS are expected to be highly valued in a decarbonized electric grid by providing low-carbon emitting generation. Next steps for direct-fired sCO_2 power cycles would be to evaluate their transient performance and use this data to update their performance in dispatch and capacity expansion models.

OCAES is the least developed technology investigated in this dissertation. I presented a novel concept that combined isothermal cycles and aquifer storage. In order for OCAES to be successful, the performance of isothermal cycles needs to be investigated at the pressure ratios needed for OCAES. The previous failure of CAES in aquifers for Iowa requires a proof-of-concept demonstration.

The two BECCS plants currently in operation are expected to help gain confidence in the technology, however future research is still needed. Membrane and calcium looping capture technologies showed reduced environmental impacts therefore, they need to be demonstrated at large scale in order to encourage their use in future power plants. Another challenge for BECCS is to better understand the availability of biomass. I found in Chapter 7 that BECCS deployment is limited by the biomass available.

Appendix A: Supplementary Information for Chapter 2 - Extending energy system modelling to include extreme weather risks and application to hurricane events in Puerto Rico

An energy system optimization model (ESOM) of Puerto Rico was built by reviewing existing infrastructure, resource availability and variations in electricity demand.

Supplementary Note 1: Electric grid Characterization

The total length of transmission and distribution lines as well as the number of substations shown in Table A-1 is from PREPA's operational profile [73]. Infrastructure spacing and repair costs were taken from Ouyang et al. [94] with substation costs selected to represent severe damage. The existing capacity of transmission, substation and distribution infrastructure was estimated as the capacity required by the ESOM to operate during the first model year. Cost inputs to the ESOM were in the units of \$/kW, therefore an average capacity-based repair cost was calculated as,

$$Capacity - based\ repair\ cost = \frac{Quantity \cdot \frac{1}{Component\ Spacing} \cdot Component\ Repair\ cost}{Existing\ capacity} \tag{A-1}$$

where quantity is either the length of transmission and distribution lines, or number of substations. Component spacing refers to the distance between transmission and distribution poles. Component spacing is not applicable to substations so a value of 1 is used. Component repair cost refers to the cost to repair either a transmission pole, substation, distribution tower or distribution span after a hurricane. This capacity-based repair cost is included in Table A-8 as the investment costs for electric grid infrastructure.

Table A-1. Electric Grid Characterization.

System	Quantity	Component Spacing	Component Repair Cost (k$)	Entire System Repair Cost (M$)	Existing Capacity (MW)	Capacity-based Repair Cost ($/kW)
Transmission	3,988 km[73]	0.23 km/ pole [94]	400/pole [94]	6,936	3080	2252
Substations	279 stations[73]	-	5,500/station [94]	1,535	3068	500
Distribution towers	50,670 km[73]	0.042 km/ pole [94]	2.5/pole [94]	3,016	2853	1057
Distribution lines	50,670 km[73]	0.042 km/span [94]	1.5/span [94]	1,810	2853	634

Supplementary Note 2: Technology representation

Technology model inputs are summarized below in Tables A-2 through A-8 with corresponding references. In addition to the costs shown in Table A-2, the investment cost of natural gas ports was also included. Puerto Rico currently has one natural gas import terminal, that prior to Hurricane Maria connected two tankers per month to provide 159 MMcf d^{-1} [378] or 1.92 GW. A recent study projected the cost to install a new gas port in Puerto Rico which would have cost US 382 M$[379] for a capacity of 500 MMcf d^{-1} [380] or 6.04 GW. Therefore, an investment cost of US 63.3 M$/GW was used for additional capacity.

Table A-2. Fuel Costs and CO_2 Emission.

Fuel	Variable Cost					CO_2 Emission activity		Carbon Tax (US \$100 tonne^{-1})
	2016		Yearly Increase		2041			
-	US M$/PJ	Ref.	%	Ref.	US M$/PJ	kton/PJ	Ref.	US M$/PJ
Biomass	5.70	[381]	0.72	[108]	6.82	0.00	Assumed to be carbon neutral	0.0
Coal	4.03	[382]	-0.16	[108]	3.87	90.37	[176]	9.04
Diesel	11.46	[382]	0.23	[108]	12.14	69.34	[176]	6.93
Hydro	0.00	N/A	N/A	N/A	0.00	0.00	N/A	0.0
Landfill Gas	0.00	N/A	N/A	N/A	0.00	39.51	[176]	3.95
Oil	7.19	[382]	1.20	[108]	9.70	67.58	[176]	6.76
Natural Gas	7.62	[382]	1.14	[108]	10.12	50.30	[176]	5.03
Solar	0.00	N/A	N/A	N/A	0.00	0.00	N/A	0.00
Wind	0.00	N/A	N/A	N/A	0.00	0.00	N/A	0.00

For data from the NREL ATB[107], 2020 pricing with Biomass power plants as “Dedicated – Mid”, Coal plants are represented as “Coal-new-HighCF-Mid”, Solar as “Utility PV – Los Angeles – Mid”, Hydro Electric as “NPD 4 - mid”, Natural Gas Open Cycle as “Gas-CT-HighCF-Mid”, and Natural Gas Combined Cycle as “Gas-CC-HighCF-Mid”. Investment costs are taken as the CAPEX costs in the NREL ATB[107]. Battery storage is represented as having 4 hours of storage available, based on the pricing from the NREL ATB[107]. For data from the EIA[383], new diesel and oil power plants are represented by “Conv gas/oil combined cycle (CC)”.

Table A-3. Power Plant Investment, Fixed and Variable Costs.

Technologies	Investment Cost		Fixed Cost		Variable Cost	
-	US$/kW	Ref.	US$/kW	Ref.	US M$/PJ	Ref.
Existing Centralized Power Plants						
Coal	N/A	-	75.97	[382]	1.92	[382]
Diesel	N/A	-	19.60	[382]	2.84	[382]
Diesel Combined Cycle	N/A	-	24.63	[382]	0.99	[382]
Heavy Fuel Oil Combustion Turbine Type 1	N/A	-	30.57	[382][379]	0.60	[382]
Heavy Fuel Oil Combustion Turbine Type 2	N/A	-	34.31	[382]	0.72	[382]
Heavy Fuel Oil Combustion Turbine Type 3	N/A	-	45.56	[382]	1.03	[382]
Hydro Electric	4022	[107]	43.00	[107]	0.00	[107]
MSW - Landfill Gas	N/A	-	425.38	[383]	2.63	[383]
Natural Gas Combined Cycle	N/A	-	18.10	[382]	0.00	[382]
Solar Photovoltaic Plant	N/A	-	13.00	[107]	0.00	[107]
Wind On-Shore	N/A	-	42.00	[107]	0.00	[107]
New Centralized Power Technologies						
Battery	1284	[107]	32.10	[107]	0.00	[107]
Biomass	3908	[107]	112.00	[107]	1.67	[107]
Coal	3981	[107]	33.0	[107]	1.39	[107]
Diesel Combined Cycle	999	[383]	11.33	[383]	1.00	[383]
Oil Combined Cycle	999	[383]	11.33	[383]	1.00	[383]
Natural Gas Combined Cycle	613	[54]	11.00	[107]	0.83	[107]
Natural Gas Open Cycle	188	[54]	12.00	[107]	1.94	[107]
Solar Photovoltaic Plant	1075	[107]	13.00	[107]	0.00	[107]
Wind On-Shore	1528	[107]	42.00	[107]	0.00	[107]
New Distributed Power Technologies						
Battery	1284	[107]	32.10	[107]	0.00	[107]
Biomass	3908	[107]	112.00	[107]	1.67	[107]
Natural Gas Combined Cycle	861	[54]	11.00	[107]	0.83	[107]
Natural Gas Open Cycle	305	[54]	12.00	[107]	1.94	[107]
Solar Photovoltaic Plant	1075	[107]	13.00	[107]	0.00	[107]
Wind On-Shore	1528	[107]	42.00	[107]	0.00	[107]

In Table A-4, "MSW – Landfill Gas" is assumed to have the same capacity factor and expected lifetime as Biomass. All new combined cycle plants are assumed to have the same capacity factor and expected lifetime, based on Natural Gas Combined Cycle power plants.

Table A-4. Power Plant capacity factors, efficiencies and expected lifetime.

Technologies	Capacity Factor		Efficiency		Expected Lifetime	
-	%	Ref.	%	Ref.	Years	Ref.
Existing Centralized Power Plants						
Coal	91.4	[106]	34.8	[382]	75	[107]
Diesel	76.0	[106]	29.9	[382]	50	Still active
Diesel Combined Cycle	80.0	[106]	40.0	[382]	50	Still active
Heavy Fuel Oil Combustion Turbine Type 1	89.0	[106]	35.3	[382]	55	Still active
Heavy Fuel Oil Combustion Turbine Type 2	58.0	[106]	34.6	[382]	65	Still active
Heavy Fuel Oil Combustion Turbine Type 3	78.5	[106]	34.1	[382]	65	Still active
Hydro Electric	28.0	[105]	36.8	[167]	100	[107]
MSW - Landfill Gas	56.0	[107]	19.0	[383]	45	[107]
Natural Gas Combined Cycle	93.0	[106]	45.5	[382]	55	[107]
Solar Photovoltaic Plant	22.0	[105]	36.8	[167]	30	[107]
Wind On-Shore	25.0	[105]	36.8	[167]	30	[107]
New Centralized Power Technologies						
Battery	50.0	N/A	85.0	[107]	15	[107]
Biomass	56.0	[107]	25.3	[107]	45	[107]
Coal	85.0	[107]	38.8	[107]	75	[107]
Diesel Combined Cycle	87.0	[107]	51.7	[383]	55	[107]
Oil Combined Cycle	87.0	[107]	51.7	[383]	55	[107]
Natural Gas Combined Cycle	87.0	[107]	62.12	[54]	55	[107]
Natural Gas Open Cycle	30.0	[107]	42.34	[54]	55	[107]
Solar Photovoltaic Plant	22.0	[105]	36.8	[167]	30	[107]
Wind On-Shore	25.0	[105]	36.8	[167]	30	[107]
New Distributed Power Technologies						
Battery	50.0	N/A	85.0	[107]	15	[107]
Biomass	56.0	[107]	25.3	[107]	45	[107]
Natural Gas Combined Cycle	87.0	[107]	54.17	[54]	55	[107]
Natural Gas Open Cycle	30.0	[107]	37.11	[54]	55	[107]
Solar Photovoltaic Plant	22.0	[105]	36.8	[167]	30	[107]
Wind On-Shore	25.0	[105]	36.8	[167]	30	[107]

Table A-5. Power Plant Ramp Rates, Capacity and Activity Limits

Technologies	Ramp Rate		Max Capacity		Max Activity	
-	[Fr/Hr]	Ref.	[MW]	Ref.	[TWh/yr]	Ref.
Existing Centralized Power Plants						
Coal	0.01	[382]	N/A	-	N/A	-
Diesel	1	[382]	N/A	-	N/A	-
Diesel Combined Cycle	0.93	[382]	N/A	-	N/A	-
Heavy Fuel Oil Combustion Turbine Type 1	0.67	[106,382]	N/A	-	N/A	-
Heavy Fuel Oil Combustion Turbine Type 2	0.73	[106,382]	N/A	-	N/A	-
Heavy Fuel Oil Combustion Turbine Type 3	0.92	[106,382]	N/A	-	N/A	-
Hydro Electric	N/A	-	102.7	[104]	N/A	-
MSW - Landfill Gas	N/A	-	N/A	-	N/A	-
Natural Gas Combined Cycle	N/A	-	N/A	-	N/A	-
Solar Photovoltaic Plant	N/A	-	N/A	-	N/A	-
Wind On-Shore	N/A	-	N/A	-	N/A	-
New Centralized Power Technologies						
Battery	N/A	-	N/A	-	N/A	-
Biomass	N/A	-	290	[104]	N/A	-
Coal	0.01	[382]	N/A	-	N/A	-
Diesel Combined Cycle	0.93	[382]	N/A	-	N/A	-
Oil Combined Cycle	0.93	[106,382]	N/A	-	N/A	-
Natural Gas Combined Cycle	1	[106,382]	N/A	-	N/A	-
Natural Gas Open Cycle	N/A	-	N/A	-	N/A	-
Solar Photovoltaic Plant	N/A	-	N/A	-	205	Model
Wind On-Shore	N/A	-	N/A	-	20.9	Model
New Distributed Power Technologies						
Battery	N/A	-	N/A	-	N/A	-
Biomass	N/A	-	290	[104]	N/A	-
Natural Gas Combined Cycle	1	[106,382]	N/A	-	N/A	-
Natural Gas Open Cycle	N/A	-	N/A	-	N/A	-
Solar Photovoltaic Plant	N/A	-	N/A	-	205	Model
Wind On-Shore	N/A	-	N/A	-	20.9	Model

Capacity credits in Table A-6 are based on 2020 values from a Temoa model of the United States electric grid [364] where solar farms are represented by E_SOLPVCEN_N (existing solar PV plant), wind farms by E_WND_R (existing wind plant), hydro electric by E_HYDCONV_R (existing conventional hydroelectric power plant), coal power plants by E_COALSTM_R (existing coal steam power plant), biomass plants, including landfill gas, by E_BIOIGCC_N (new BioIGCC plant), battery storage by E_BATT (battery storage), combined cycle power plants by E_NGACC_R (existing natural gas combined cycle power plant) and remaining fossil fuelled power plants by E_NGACT_N (existing natural gas combustion turbine power plant).

Table A-6. Power Plant Capacity Credits, used in Reserve Margin Calculations.

Technologies	Capacity Credit	
-	[Fr]	Ref.
Coal	0.9	[364]
Diesel	0.91	[364]
Diesel Combined Cycle	0.95	[364]
Heavy Fuel Oil Combustion Turbine Type 1	0.91	[364]
Heavy Fuel Oil Combustion Turbine Type 2	0.91	[364]
Heavy Fuel Oil Combustion Turbine Type 3	0.91	[364]
Hydro Electric	0.95	[364]
MSW - Landfill Gas	0.95	[364]
Natural Gas Combined Cycle	0.95	[364]
Solar Photovoltaic Plant	0.29	[364]
Wind On-Shore	0.36	[364]
Battery	0.75	[364]
Biomass	0.95	[364]
Coal	0.9	[364]
Diesel Combined Cycle	0.95	[364]
Oil Combined Cycle	0.95	[364]
Natural Gas Combined Cycle	0.95	[364]
Natural Gas Open Cycle	0.91	[364]
Solar Photovoltaic Plant	0.29	[364]
Wind On-Shore	0.36	[364]
Battery	0.75	[364]
Biomass	0.95	[364]
Natural Gas Combined Cycle	0.95	[364]
Natural Gas Open Cycle	0.91	[364]
Solar Photovoltaic Plant	0.29	[364]
Wind On-Shore	0.36	[364]

Table A-7. Power Plant Existing Capacity by Year Installed.

Technologies	50-54	55-59	60-64	65-69	70-74	75-79	95-99	00-04	05-09	10-14	15-Pres	Ref.
Existing Centralized Power Plants (MW)												
Coal	0.0	0.0	0.0	0.0	0.0	0.0	0.0	454.0	0.0	0.0	0.0	[73]
Diesel	0.0	0.0	0.0	0.0	378.0	0.0	247.5	0.0	220.0	0.0	0.0	[106]
Diesel Combined Cycle	0.0	0.0	0.0	0.0	0.0	592.0	0.0	0.0	440.0	0.0	0.0	[106]
Heavy Fuel Oil Combustion Turbine Type 1	0.0	0.0	0.0	0.0	900.0	0.0	0.0	0.0	0.0	0.0	0.0	[106]
Heavy Fuel Oil Combustion Turbine Type 2	0.0	0.0	170.0	410	410.0	0.0	0.0	0.0	0.0	0.0	0.0	[106]
Heavy Fuel Oil Combustion Turbine Type 3	0.0	170.0	200.0	632.0	0.0	0.0	0.0	0.0	0.0	0.0	0.0	[106]
Hydro Electric	34.0	0.0	0.0	0.0	0.0	0.0	0.0	0.0	0.0	0.0	0.0	[105]
MSW - Landfill Gas	0.0	0.0	0.0	0.0	0.0	0.0	0.0	0.0	0.0	0.0	2.4	[384]
Natural Gas Combined Cycle	0.0	0.0	0.0	0.0	0.0	0.0	0.0	507.0	0.0	0.0	0.0	[73]
Solar Photovoltaic Plant	0.0	0.0	0.0	0.0	0.0	0.0	0.0	0.0	0.0	22.1	30.0	[106,384]
Wind On-Shore	0.0	0.0	0.0	0.0	0.0	0.0	0.0	0.0	0.0	102.0	0.0	[384]

Transmission, substation, and distribution losses are based on International Energy Agency Energy Technology Systems Analysis Program (ETSAP) [109]. Transmission losses are based on 100 km of distance and a loss rate of 7%/1000 km [109]. The values of existing capacity and expected lifetime were selected so that the model would start with sufficient capacity for operation, and that rebuilding of these systems was limited to damage from hurricanes (Table A-8). The assumed year built was selected so that new capacity does not need to be added unless there is hurricane damage. The assumed life was selected so that the purchase of new equipment is paid back on a 30-year basis, similar to most power plants. Repair from hurricane damage is represented by the investment cost which is based on Table A-1, normalized by the existing capacity. Investment costs for underground transmission and distribution lines are based on average conversion costs for suburban areas [116] to capture the mix of development areas in Puerto Rico. Operational maintenance is based on 2014-2015 costs [385], normalized by demand expected in the first model year [379].

Table A-8. Transmission System Loss, Lifetime and Costs. Assumptions denoted by "Asm.".

Technologies	**Loss**		**Existing Capacity and Expected Lifetime**				**Investment (Repair) Cost**		**Variable Cost**	
-	%	Ref.	MW	Built	Life	Ref.	US$/kW	Ref.	US M$/PJ	Ref.
Transmission Lines	0.7	[109]	3080	2015	30	Asm.	2252	Calc.	0.86	[385]
Buried Transmission Lines	0.7	Asm.			30	Asm.	4868	Calc.	-	Asm.
Substations	0.4	[109]	3068	2015	30	Asm.	500	Calc.	-	-
Distribution Towers	0.0	Asm.	2853	2015	30	Asm.	1057	Calc.	-	Asm.
Distribution Lines	7.0	[109]	2853	2015	30	Asm.	634	Calc.	1.15	[385]
Buried Distribution Lines	7.0	Asm.			30	Asm.	15084	Calc.	-	Asm.

Supplementary Note 3: Electricity demand and system parameters

The model includes two typical days per year, one for the wet season, and one for the dry season. Each typical day is broken into 24 segments, to represent each hour of the day and the corresponding wind and solar availability [98] and electricity demand [384,386–388] are prescribed based on historical data as shown in Figure A-1. System level inputs are summarized in Table A-9, and electricity in Table A-10. The basis for the reserve margin is a 6.2% difference between peak demand in the model versus historical data [384,386–388], plus an additional 30% of planning capacity reserves based on the 2019 Integrated Resource Plan [105]. Reserve margins might differ in practice based on electric grid configurations (i.e. centralized vs. decentralized), however this is not typically captured in ESOMs and could be investigated by other types of models. The 2016-20 value for demand is from a 2017 PREPA study [379] and the remaining projected demand values from the 2019 Integrated Resource Plan [105].

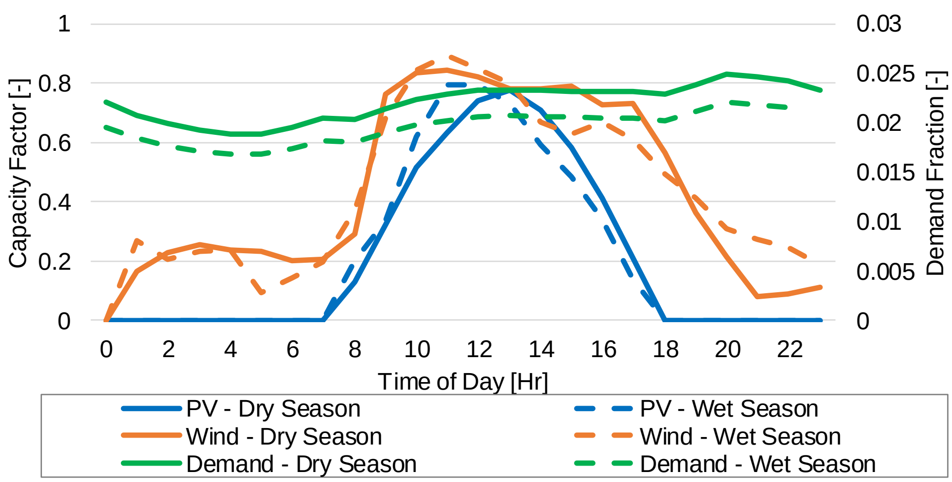

Figure A-1. To capture seasonal and daily variations, the energy system model was provided with solar and wind capacity factors [98] and demand [384,386–388] **in hourly increments.**

Table A-9. Puerto Rico Electric System Inputs.

Parameter	Value	Ref.
Model time horizon [years]	25	User defined
Seasons	2	User defined
Times of day	24	User defined
Discount Rate	0.09	[98,105]
Reserve Margin	36.2%	[384,386–388]

Table A-10. Yearly Demand Projection [105,379] **and Renewable Portfolio Standard (RPS) [84].**

Year [-]	2016-20	2021-25	2026-30	2031-35	2036-40
Demand [PJ]	75.24	66.49	67.28	65.32	63.75
RPS	0%	0%	40%	40%	40%

Supplementary Note 4: Model verification

To verify the model, fuel resources used in the first model year, 2016, were compared against actual usage recorded by the Autoridad de Energía Eléctrica in 2016 [76], shown in Table A-11.

Table A-11. The energy system model was validated by comparing the results of the first model year (2016) to actual fuel consumption in 2016.

	% of Total Electricity Production	
Energy Source	**2016 Actual** [76]	**2016-20 Model**
Petroleum + Diesel	61.8	63.9
Natural Gas	18.5	18.2
Coal	17.2	16.0
Hydroelectric	0.5	0.4
Wind	1.3	1.0
Solar PV	0.6	0.4
Other Renewable	0.2	0.1

Supplementary Note 5: Grid topology cases

Cases were selected to represent the two scales of topology being proposed by PREPA, and are shown in Table A-12. The cases with centralized grid topologies maintain the existing grid structure. The distributed topologies represent a system that relies only on the distribution network, thus spreading power generation throughout the municipalities.

Table A-12. Cases considered to evaluate the impact of grid topology and power plant types. This table reveals which power plant options were available in each case.

Case	Grid Architecture	New Installation Options								
		Renewable Fuel				Fossil Fuel (imported)				Storage
		Biomass	Hydro	Solar	Wind	Coal	Diesel	Oil	Natural Gas	Batteries
All technologies	Not fixed	X	X	X	X	X	X	X	X	X
Business-as-usual	Centralized		X			X	X	X		
Centralized – hybrid	Centralized	X	X	X	X				X	X
Centralized – natural gas	Centralized		X						X	
Distributed – hybrid	Distributed	X	X	X	X				X	X
Distributed – natural gas	Distributed		X						X	

Supplementary Note 6: Hurricane damage value estimation

Historical hurricane data from NOAA was reviewed for occurrences where the eye of the storm was within 65 nautical miles of striking Puerto Rico since 1979, which is the closest range that includes 2017 Hurricane Irma [72]. The maximum windspeed and category shown is within range of Puerto Rico.

Table A-13. Forty years of hurricanes within 65 nautical miles of Puerto Rico.

Year	Name	Max. Category	Max. Windspeed (knots)	Max. Windspeed (mph)
1979	Frederic	Tropical Storm	45	51.8
1979	Claudette	Tropical Depression	30	34.5
1981	Gert	Tropical Storm	50	57.5
1984	Klaus	Tropical Storm	45	51.8
1988	Chris	Tropical Depression	30	34.5
1989	Hugo	Category 3	110	126.6
1995	Marilyn	Category 2	95	109.3
1996	Hortense	Category 1	70	80.6
1998	Georges	Category 3	100	115.1
2000	Derby	Category 1	65	74.8
2004	Jeanne	Tropical Storm	60	69.0
2007	Noel	Tropical Depression	25	28.8
2007	Olga	Tropical Storm	40	46.0
2008	Fay	Tropical Depression	30	34.5
2011	Irene	Category 1	60	69.0
2014	Bertha	Tropical Storm	40	46.0
2015	Erika	Category 1	45	51.8
2017	Irma	Category 5	150	175.6
2017	Maria	Category 5	135	155.4

The historical hurricane data was analyzed to find the probability of the maximum strength storm and average windspeed that would occur within a given five-year period (Figure A-2). Analysis was performed over ranges of the past 25, 30, 35, and 40 years. The start year of the analysis was varied to avoid influence of the start year, thus the error bars showing variation. The number of scenario branches considered in the model was limited to three in order to balance computational resources. The first branch, named category 1 was created to capture instances of no hurricane, tropical depressions, tropical storms and category 1 hurricanes. A second branch included category 2 and 3 hurricanes, and a third branch for category 4 and 5 hurricanes. This recategorization is shown in Figure A-3.

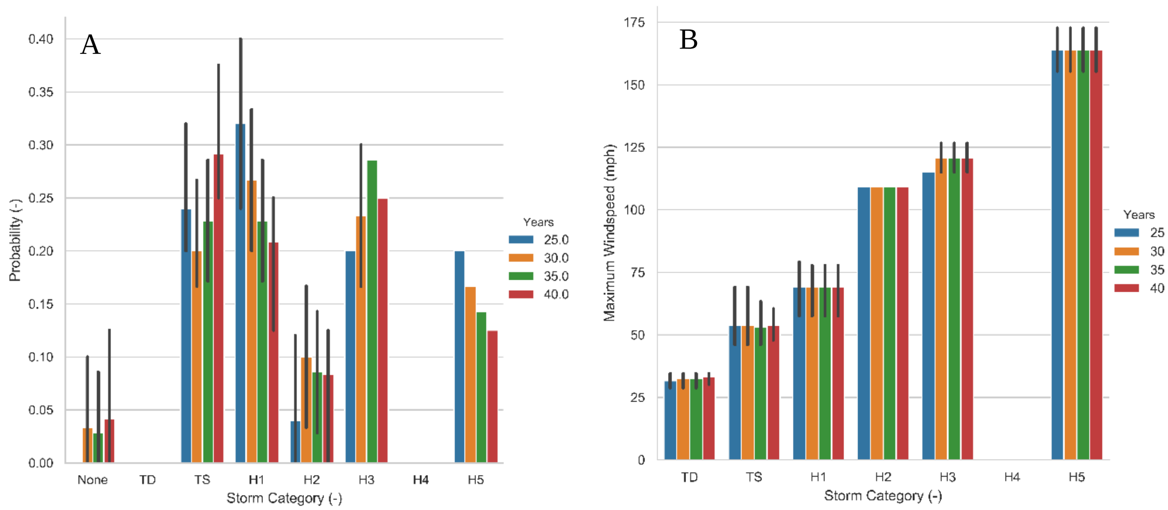

Figure A-2. Historical A) storm probability and B) average storm windspeeds based on 5-year increments (TD – Tropical Depression, TS- Tropical Storm, H# - Category # Hurricane).

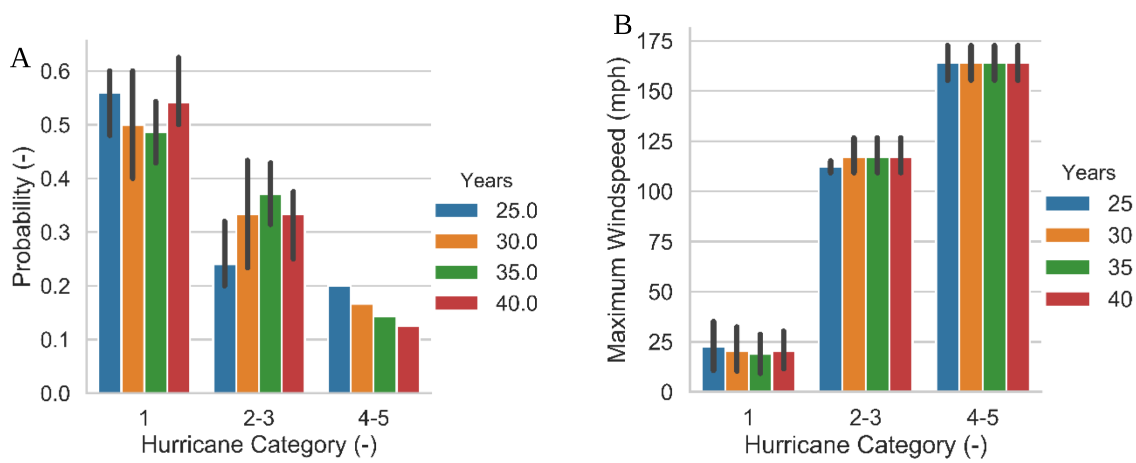

Figure A-3. The historical storm data was binned into three representative groups and displayed by A) storm probability and B) average storm windspeeds based on 5-year increments.

Table A-14 summarizes the projected undamaged capacity for each technology based on the fragility curves.

Table A-14. Fraction of undamaged capacity for technologies based on representative hurricane categories.

Technology	Ref.	Hurricane Category (windspeed) 1 (10 m/s)	2-3 (51 m/s)	4-5 (69 m/s)
Distribution lines	[111]	1.000	0.666	0.000
Wind turbines	[114]	1.000	0.985	0.201
Distribution towers	[111]	1.000	0.739	0.177
Solar panels	[95,113]	1.000	1.000	0.602
Coal & biomass power plants	SECBH [95,112] Severe	1.000	1.000	0.573
Battery storage plants	SECBL[112] Severe	0.998	0.989	0.554
Hydroelectric power plants	CECBL[112] Severe	0.998	0.989	0.582
Substations	Suburban[95]	1.000	0.999	0.785
Transmission Lines	[110]	1.000	0.967	0.739
Natural Gas, Oil, Diesel, and Landfill Gas (Open Cycle and Combined Cycle)	SECBM [95,112] Severe	1.000	1.000	0.913
Buried lines	SECBM [112] Severe	1.000	1.000	0.913

Supplementary Note 7: New and repaired capacity projections

The inclusion of storm damage in my model is represented as capacity that is damaged and inoperable. The model is not required to repair the damaged infrastructure, instead it starts with the undamaged capacity and then builds any new capacity required to meet demand for the lowest cost. This formulation does not distinguish between new capacity additions and capacity that is being repaired. For some storms, the amount of damage is quite low. For example, a Category 1 hurricane damages 0.2% of the hydroelectric capacity (see Table A-14). So, it is possible that a small amount of new capacity will be added to reach the 102.7 MW capacity limit shown in Table A-5.

An example of capacity installations for a stochastic simulation is shown in Figure A-4 for the case with all technologies without a climate mitigation policy. Figure A-5 is shown to summarize capacity installations across all cases presented in this study. The installations per time period represent the total amount of capacity added in the 5-year time periods considered in this study. For example, 1.5 GW of gas turbine capacity would be interpreted as a number of gas turbine power plants that total 1.5 GW within a 5-year period. For comparison, recent EIA data shows that California installed 6 GW of solar power in 4 years and North Carolina installed 2.9 GW of solar power in 4 years [389].

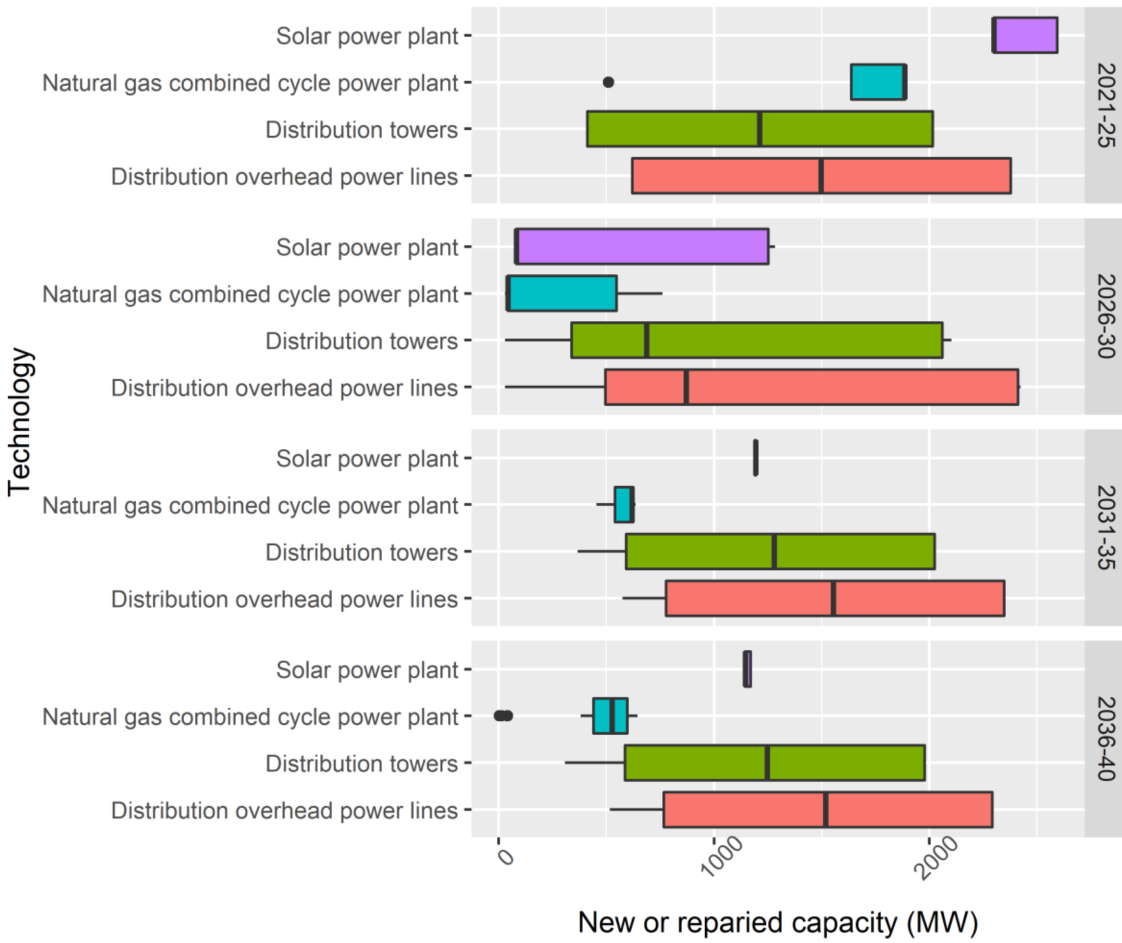

Figure A-4. Non-zero capacity installations for the 'all technologies' case without a climate mitigation strategy. No capacity installations were allowed during the first model time period of 2016-2020.

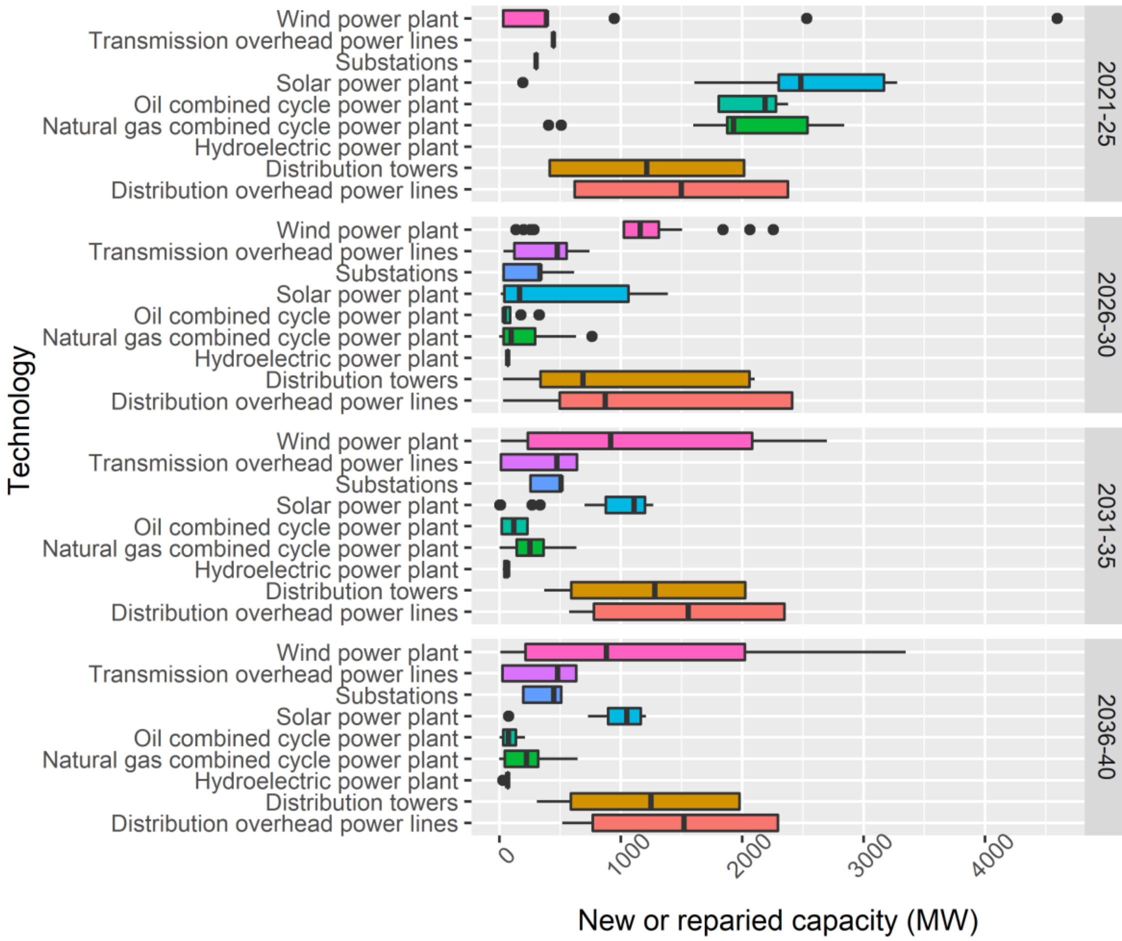

Figure A-5. Summary of non-zero capacity installations across all stochastic optimization cases presented in this study. No capacity installations were allowed during the first model time period of 2016-2020.

Supplementary Note 8: Tabulated cost results

Tabulated cost of electricity projections for Figure 2-6A are presented in Table A-15 and for Figure 2-7 in Table A-16.

Table A-15. Cost of electricity ($/kWh) for All Technologies Case, graphically presented in Figure 2-6A.

Storm frequency	Climate mitigation policy	Quantity	2016-20	2021-25	2026-30	2031-35	2036-40
None	No policy	Deterministic	0.091	0.081	0.080	0.080	0.081
	RPS	Deterministic	0.091	0.081	0.086	0.087	0.088
	US$ 100 t^{-1} CO_2	Deterministic	0.164	0.110	0.109	0.109	0.110
Historical storm frequency	No policy	Minimum	0.091	0.081	0.080	0.080	0.081
		Mean	0.091	0.086	0.092	0.099	0.107
		Maximum	0.091	0.104	0.134	0.167	0.201
	RPS	Minimum	0.091	0.081	0.086	0.087	0.089
		Mean	0.091	0.086	0.098	0.107	0.117
		Maximum	0.091	0.104	0.137	0.180	0.223
	US$ 100 t^{-1} CO_2	Minimum	0.164	0.107	0.106	0.107	0.109
		Mean	0.164	0.112	0.118	0.127	0.137
		Maximum	0.164	0.130	0.164	0.214	0.267
Increased storm frequency	No policy	Minimum	0.091	0.081	0.080	0.080	0.081
		Mean	0.091	0.094	0.109	0.127	0.147
		Maximum	0.091	0.104	0.134	0.167	0.201
	RPS	Minimum	0.091	0.081	0.086	0.087	0.089
		Mean	0.091	0.094	0.114	0.137	0.161
		Maximum	0.091	0.104	0.137	0.180	0.223
	US$ 100 t^{-1} CO_2	Minimum	0.164	0.107	0.106	0.107	0.109
		Mean	0.164	0.119	0.137	0.159	0.185
		Maximum	0.164	0.130	0.164	0.214	0.267

Table A-16. Mean cost of electricity ($/kWh) for cases graphically presented in Figure 2-7.

Storm frequency	Climate mitigation policy	Case	2016-20	2021-25	2026-30	2031-35	2036-40
Historical storm frequency	No policy	All technologies	0.091	0.086	0.092	0.099	0.107
		Business-as-usual	0.091	0.094	0.101	0.110	0.119
		Centralized-hybrid	0.091	0.088	0.094	0.103	0.112
		Centralized - natural gas	0.091	0.086	0.092	0.100	0.108
		Distributed - hybrid	0.091	0.090	0.096	0.103	0.111
		Distributed - natural gas	0.091	0.090	0.095	0.102	0.110
Increased storm frequency	No policy	All technologies	0.091	0.094	0.109	0.127	0.147
		Business-as-usual	0.091	0.104	0.121	0.141	0.161
		Centralized - hybrid	0.091	0.097	0.116	0.137	0.160
		Centralized - natural gas	0.091	0.095	0.111	0.130	0.150
		Distributed - hybrid	0.091	0.097	0.112	0.130	0.149
		Distributed - natural gas	0.091	0.097	0.110	0.125	0.141
	RPS	All technologies	0.091	0.094	0.114	0.137	0.161
		Centralized - hybrid	0.091	0.097	0.122	0.148	0.175
		Distributed - hybrid	0.091	0.097	0.118	0.141	0.165
	US$ 100 t^{-1} CO_2	All technologies	0.164	0.119	0.137	0.159	0.185
		Business-as-usual	0.164	0.157	0.174	0.194	0.215
		Centralized - hybrid	0.164	0.123	0.143	0.165	0.190
		Centralized - natural gas	0.164	0.128	0.145	0.164	0.184
		Distributed - hybrid	0.164	0.127	0.143	0.165	0.191
		Distributed - natural gas	0.164	0.136	0.149	0.164	0.180

Supplementary Note 9: Computational resources

The stochastic simulations were performed on University of Virginia's High-Performance Computing System, Rivanna. Each of the stochastic optimization simulations required 4-9 hours to run on 8 cores or 33-72 CPU-hours. Simulations were performed using Python 2.7 and Gurobi 9.0.1 from a Linux environment. More information about Rivanna can be found at https://rc.virginia.edu.

Appendix B – Supporting Information for Chapter 3 - Feasibility of Using sCO_2 Turbines to Balance Load in Power Grids with a High Deployment of Solar Generation

Models and Data

The source code and data used to perform this study has been archived and is available for download at https://doi.org/10.18130/V3/IKPFBV. Additionally, the most recent version of the BLIS model is available at https://github.com/EnergyModels/blis.

Rooftop solar validation

PVLib solar predictions were validated by comparing against production data for the rooftop solar systems (5 min resolution) provided by the UVA Facilities Management office, as shown in Table B-1.

Table B-1. Validation metrics for rooftop PV systems

Rooftop Array	Peak Capacity	r^2	% Diff (Cumulative)
1	10 kW	0.95	-5.0
2	126 kW	0.88	-15.0
3	15 kW	0.91	-13.0
4	224 kW	0.92	3.0
5	140 kW	0.94	3.0

Appendix C – Supporting Information for Chapter 5 - Saline Aquifer Suitability for Long Duration Offshore Compressed Air Energy Storage

Nomenclature

Acronyms and Abbreviations

CAES	Compressed Air Energy Storage
NOAA	National Oceanic and Atmospheric Administration
OCAES	Offshore Compressed Air Energy Storage
PM-CAES	Porous Media Compressed Air Energy Storage
RTE	Round-Trip Efficiency

Symbols

h	Formation thickness
k	Permeability
$\dot{m}$	Mass flow rate
M	Mass
n	Polytropic index
N	System life
p	Pressure
Q	Volumetric flow rate
r	Radius
R	Gas constant
SF	Safety Factor
T	Temperature
V	Volume
w	Specific work
V	Volume
z	Depth
Z	Gas compressibility
μ	Viscosity
ϕ	Porosity

Thermal fluid process model

Estimating subsurface conditions

In the absence of site-specific measurements, empirical relations are used to estimate the temperature and pressure of the saline aquifer prior to air storage. The geothermal gradient is used to estimate the temperature T_{aq}, of the aquifer,

$$T_{aq} = \frac{\partial T}{\partial z} \cdot z + T_0 \tag{C-1}$$

where $\frac{\partial T}{\partial z}$ is the geothermal gradient, z is the aquifer depth and T_0 is the geothermal intercept. Based on Battelle et al., the geothermal intercept was calculated to be 10.62 °C [268]. The initial pressure of the aquifer, P_{aq}, is represented as,

$$p_{aq} = \frac{\partial p_{aq}}{\partial z} \cdot z \tag{C-2}$$

where $\frac{\partial p_{aq}}{\partial z}$ is the aquifer pressure gradient, and z is the aquifer depth. The composition of materials in overlying formations varies therefore an empirical relation is preferred over the hydrostatic pressure of water alone. An impermeable caprock overlying the saline aquifer is necessary to contain the air. The composition and thickness of the caprock will determine the maximum air pressure that it can contain. The pressure at which the caprock will fracture, p_f, is estimated as,

$$p_f = \frac{\partial p_f}{\partial z} \cdot z \tag{C-3}$$

where $\frac{\partial p_f}{\partial z}$ is the fracture pressure gradient, and z is the aquifer depth. A factor of safety is used to minimize the risk of fracture. The maximum operating pressure, p_{max}, allowed during operation is defined as,

$$p_{max} = p_{aq} + SF \cdot \left(p_f - p_{aq}\right) \tag{C-4}$$

where SF is the safety factor.

Air storage

The injected air is expected to radially spread into a plume in the saline aquifer. It is assumed that the air becomes the temperature of the aquifer upon injection. Based on Katz et al.'s work with underground gas storage, it will take months to years to develop the air plume in a saline aquifer, but once developed, it is expected to maintain its volume as long as the plume pressure is greater than the aquifer [230]. This is reiterated by Oldenburg and Pan explaining that water movement after initial injection is expected to be limited to vaporization [196]. The development of the air plume is a complex phenomenon that depends on the formation thickness, slope of the caprock, and buoyancy forces. Studies such as Nordbotten and Celia have projected the plume development for CO_2 with a level caprock [390] and Guo et al. and Oldenburg and Pan estimated the plume development for air with an assumed formation thickness and caprock slope [196,199]. Other studies such as Li et al. have considered the influence of changing the well screening height, which found that increased well screening is advantageous [391]. Katz et al. presented several simple methods to estimate the plume shape including as a disk when the thickness of the aquifer is limiting and as a hemisphere when the aquifer thickness is very large [392]. Here, I represent the air plume as a disk with volume V_p,

$$V_p = \pi \cdot r_p^2 \cdot h_{plume} \cdot \phi \tag{C-5}$$

where r_p is the plume radius, h is the plume thickness, and ϕ is the porosity. In order to also capture the possibility that the aquifer thickness is not limiting, leading to a hemisphere-like plume, h_{plume} is defined as the lesser of the aquifer thickness, h, and the plume radius. The simulation is initialized with an established air plume at the aquifer pressure and temperature based on Equations C-1 and C-2. As air is injected into the aquifer, energy is stored as accumulated mass. The pressure of the plume, p_p, is estimated using the ideal gas law,

$$p_p = \frac{m \cdot R \cdot T_{aq}}{V_p} \tag{C-6}$$

where m is the total mass of air in the aquifer and R is the gas constant. Depending on the temperature of the injected fluid, it is expected that the aquifer temperature will change over time, such as shown by Guo et al. [197]. This model simulates one cycle; therefore, the temperature is assumed to be constant.

Aquifer friction losses

As the air travels through the aquifer, it will experience resistance to the porous medium and undergo friction losses. It is assumed that the air will uniformly travel radially throughout the air plume. The thermal fluid process model uses a form of the radial Darcy-flow equation from Sopher et al. [200] to represent the aquifer friction losses for a given volumetric flow rate, Q,

$$Q = \frac{8.834 \cdot 10^{-3} k \cdot h\left(p_p^2 - p_w^2\right)}{\mu \cdot T_{aq} \cdot Z \cdot \ln\left(\frac{r_p}{r_w}\right)} \tag{C-7}$$

where k is the permeability (mD), h is the aquifer height (m), p_p is the pressure at the air plume edge (MPa), p_w the pressure at the wellbore (MPa), μ is the viscosity (cP), Z is the compressibility (-), r_p is the radius of the plume (m), and r_w the radius of the wellbore (m). With the substitution of the continuity equation, Equation 7 is rearranged to solve for pressure drop. Air fluid properties including viscosity, density and compressibility are calculated with CoolProp [273]. Previous PM-CAES studies have considered a range of diameters and flow rates. Oldenburg and Pan used a 0.5 m wellbore, with a depth of 720 m with a flow rate of 54-209 kg/s [196]. Yang et al. used a 0.2 m well diameter, 200 m depth and for the plume development, a flow rate from 2 to 5 kg/s [201]. Here I assume a well diameter of 0.41 m, based on the enhanced geothermal study by Adams et al. [223]. Figure C-1 illustrates the impact of permeability and flow rate on the expected pressure loss in Equation C-7.

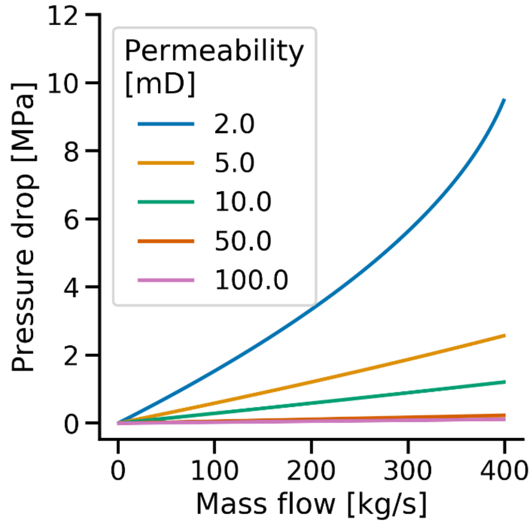

Figure C-1. Aquifer pressure drop expected for air at 12 MPa and 35 °C in an aquifer 50 m thick, well diameter of 0.41 m and plume radius of 100 m.

Air leakage

In addition to friction losses, it is expected that some quantity of injected air will not be recoverable. If the air is injected into an anticline, then it is expected that a larger portion of air will migrate away from the plume. An air leakage term is incorporated into the model to capture this effect. Due to the lack of CAES plants in porous media, Oldenburg and Pan assumed a mass leakage of 3.5% which is based on the Huntorf, Germany CAES plant in a solution mined salt cavern [196].

Near-isothermal machinery

Compression and expansion processes for isothermal CAES systems are commonly represented analytically as polytropic processes. Polytropic processes are quasi-equilibrium and take the form,

$$pV^n = constant \tag{C-8}$$

where p is pressure, V is volume and n is the polytropic index [228]. The polytropic index is process dependent. A polytropic index of 1 is an idealized isothermal process and an index equal to the ratio of specific heats (1.4 for air) is an adiabatic process. The work of the near-isothermal machinery in the thermal fluid process model is represented as a polytropic process which is expressed as,

$$w = \frac{n\,R\,T_1}{n-1}\left(1 - \left(\frac{p_2}{p_1}\right)^{\frac{n-1}{n}}\right) \tag{C-9}$$

where w is the specific work, T_1 the temperature at state 1, p_1 the pressure at state 1, and p_2 the pressure at state 2. Near-isothermal compression and expansion processes use heat transfer enhancements to reduce the polytropic index. It is desirable to reduce the polytropic index because it results in less work for the same pressure rise.

Wellbore

The wellbore is represented with the Bernoulli equation to include changes in gravitational potential and friction losses based on the well casing roughness [229].

Metrics and sizing

The primary metric of the thermal fluid process model is round-trip efficiency (RTE).

$$RTE = \frac{\sum w_{expansion}}{\sum w_{compression}} \tag{C-10}$$

Other model outputs include storage duration and average power output. For a given set of geophysical parameters, the output power is dependent on the mass flow rate, and the storage duration on the plume radius. The focus of this study is on an OCAES system with an output power of 200 MW and 24-hour duration storage that uses a single wellbore. In order to size a system at this rating, the model was run iteratively, varying mass flow rate and plume radius until both output power and duration converged with an error less than 1e-6.

Fixed model inputs

A summary of fixed model inputs is shown in Table C-1.

Table C-1. Summary of fixed model parameters.

Variable	**Value**	**Reference**
Geophysical Parameters		
Safety Factor	0.5	Allen et al. [220]
Machinery Parameters		
Mechanical efficiency	99 %	Dixon and Hall [221]
Generator efficiency	98.9 %	Siemens [222]
Wellbore		
Diameter	0.41 m	Adams et al. [223]
Roughness (stainless steel)	0.002 mm	White [224]
Atmospheric		
Temperature	16.85 °C	NOAA [225]

Review of Polytropic indices

I reviewed near-isothermal simulations and experiments and summarized the resulting polytropic indexes in Table C-2. Zhang et al. [213] and Patil et al. [259,261] did not directly report the polytropic index and instead presented the isothermal efficiency which was defined in these studies as,

$$\eta_{isothermal} = \frac{\ln(P_r) - 1 + \frac{1}{P_r}}{\frac{P_r^{\left(\frac{n-1}{n}\right)} - 1}{n-1} + P_r^{-\frac{1}{n}} - 1 + (P_r - 1)\left(P_r^{-\frac{1}{n}} - \frac{1}{P_r}\right)} \tag{C-11}$$

where P_r is pressure ratio. For these results, the polytropic index was computed based on the given isothermal efficiency and pressure ratio.

Table C-2. Review of studies that examined the effect of machine type and near-isothermal enhancements on the polytropic index.

Study	Study Type	Machine Type	Heat Transfer Enhancement	Pressure Ratio	Polytropic Index
Park et al. [393]	Experiment	Liquid piston compressor	n/a	2.2	1.25
Ramakrishnan et al. [280]	Experiment	Liquid piston compressor	n/a	2	1.15
Ramakrishnan et al. [280]	Experiment	Liquid piston compressor	n/a	5	1.09-1.17
Patil and Ro [207]	Experiment	Liquid piston compressor	n/a	6	1.14
Dolatabadi et al. [394]	Experiment	Liquid piston compressor	n/a	5	1.19
Ramakrishnan et al. [280]	Experiment	Liquid piston compressor	Hollow spheres	2	1.08
Ramakrishnan et al. [280]	Experiment	Liquid piston compressor	Hollow spheres	5	1.07-1.9
Qin and Loth [210]	Computational Fluid Dynamics	Liquid piston compressor	Spray injection	10	1.05-1.3
Li [Reference 23 in [213]]	Experiment	Reciprocating compressor	Spray injection	-	1.161
Patil et al. [260]	Experiment	Liquid piston compressor	Wire mesh	2.8	1.08-1.12
Patil et al. [259]	Experiment	Liquid piston compressor	Spray injection	2.5	1.04*
Patil et al. [261]	Experiment	Liquid piston compressor	Aqueous foam	2.5	1.07*
Zhang et al. [213]	Experiment	Reciprocating expander	Spray injection	10	1.21*
*Calculated using equation 13					

Estimating Storage Potential

The thermal fluid process model was used to calculate the round-trip efficiency for a 200 MW, 24-hour duration OCAES systems for each of the three formations (Middle Cretaceous, Lower Cretaceous and Upper Jurassic) for each GIS cell. The total energy storage available per GIS cell, S, was calculated as

$$S = E\frac{A}{\pi r^2} \tag{C-12}$$

where E is the energy storage per OCAES system, A is the aquifer area available, and r is the radius of the OCAES system's air plume within the saline aquifer system. Details on the calculation of E and A are shown below in Table C-3. The OCAES air plume radius is unique to each GIS site based on the subsurface conditions.

Table C-3. Summary of parameters used to calculate the storage duration available per location in the Baltimore Canyon Trough.

OCAES System Size	
Power rating	200 MW
Storage duration	24 Hours
E, Energy storage	4800 MWh
GIS Cell details	
GIS cell size	19.79 km x 19.79 km [194]
GIS cell area	391 km^2
Available for OCAES	10%
A, Area available for OCAES	39.1 km^2

Estimating Emissions

Table C-4 presents a calculation of the specific emissions from the diabatic CAES systems compared in Table 5-1.

Table C-4. Diabatic CAES system specific emissions.

	Huntorf, Germany	**McIntosh, USA**	**Mouli-Castillo (Mid-range)**
Electricity output [kWh]	1 [42]	1 [42]	8.82e9 [46]
Fuel costs [pounds]	-	-	3.97e8 [46]
Cost of fuel [pound/MMBtu]	-	-	11.25 [46]
Fuel input [kWh]	1.6 [42]	1.17 [42]	1.03e10
Fuel specific emissions [gCO_2/MBtu]	53.07 [176]	53.07 [176]	53.07 [176]
Fuel specific emissions [gCO_2/kWh]	181.08	181.08	181.08
Fuel emissions [gCO_2]	289.7	211.9	1.87e12
System specific emissions [gCO_2/kWh]	289.7	211.9	212.3

Full Monte Carlo Simulation Results

The full results of the Monte Carlo simulations are presented in Figure C-2.

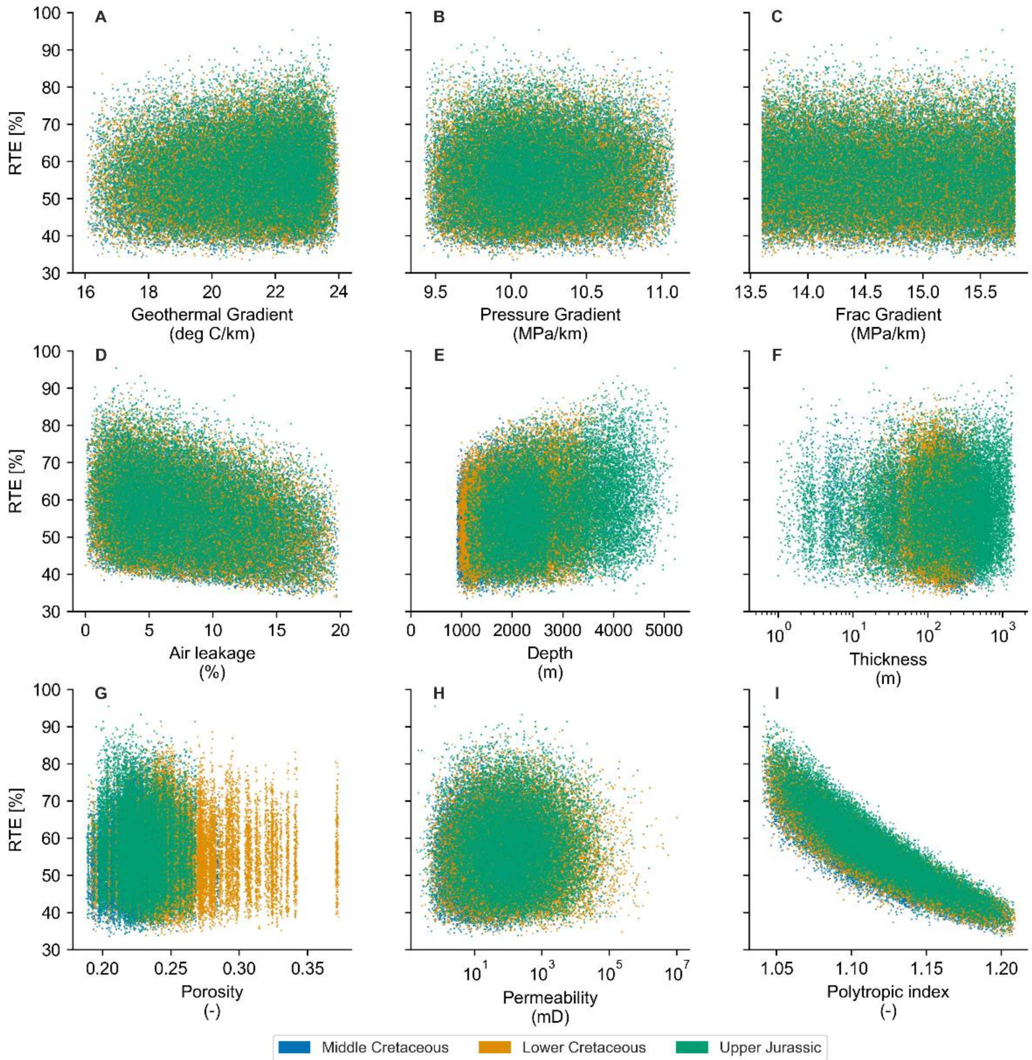

Figure C-2. Monte Carlo simulation results show the impact of the nine uncertainty variables on the round-trip efficiency.

Water Depth vs Distance to Shore

Figure C-3 shows the water depth and distance to shore for sites with a mean RTE of at least 50%. Most regions in the Baltimore Canyon Trough show a similar trend in increasing water depth as moving away from shore that steeply decreases around 100 to 150 km when dropping off the continental shelf. The exception to this is a bifurcation for Massachusetts primarily near Cape Cod. To highlight the most realistic OCAES sites, Figure C-3B shows locations with depths less than 60m and less than 100 km from shore. Sites with an OCAES RTE greater than 50% are expected for all Mid-Atlantic states examined here.

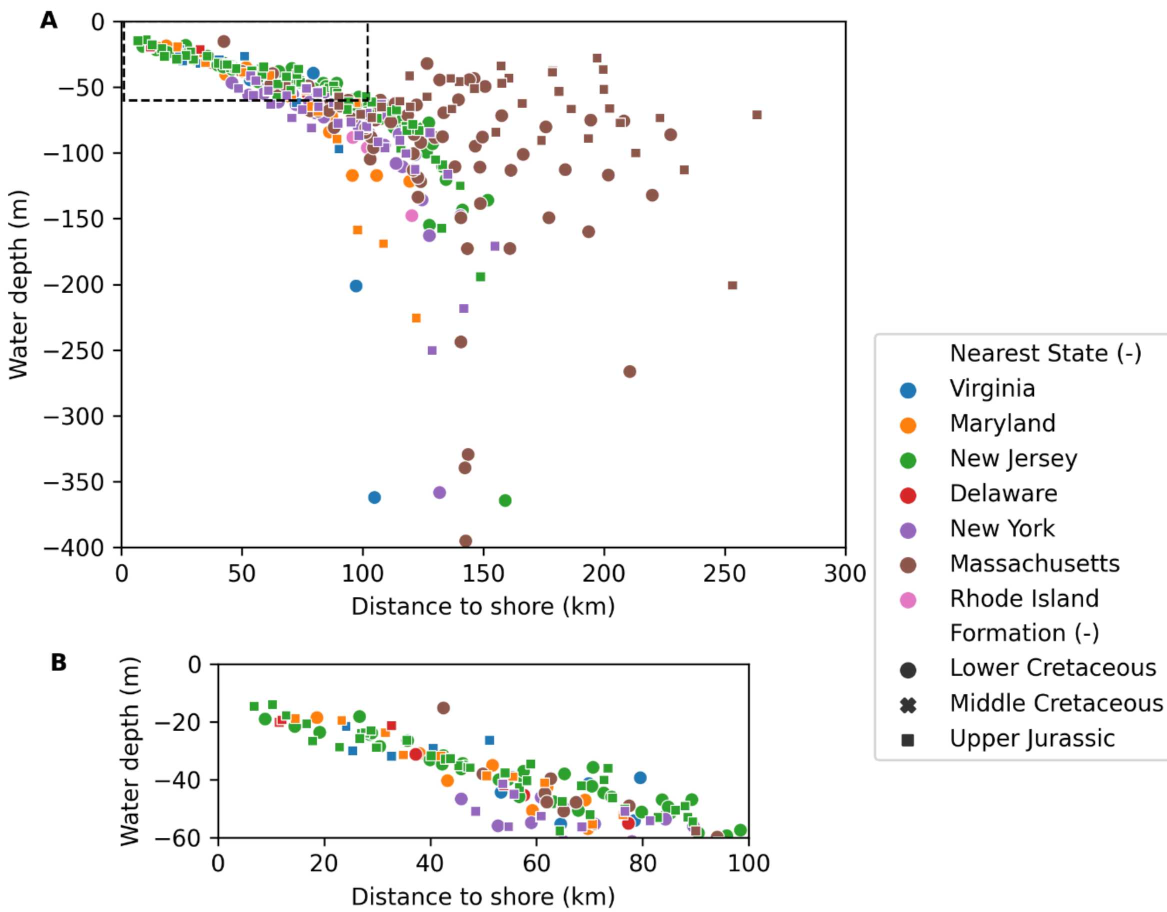

Figure C-3. Comparison of distance to shore and water depth for sites identified with a mean OCAES RTE of at least 50%.

Model sensitivity

A sensitivity study was performed in order to compare the impact of geophysical parameters against engineering design variables. For this analysis, simulations were run where one model input was perturbed at a time, either increased or decreased by 10%. All model inputs other than polytropic index were investigated because it was previously demonstrated to have a large impact in Figure 5-6. Figure C-4 shows the impact of model inputs that affected the RTE by at least 0.01 efficiency points. The efficiency of the baseline scenario was 62.6% and is based on the PJM analysis location. In addition to the geophysical parameters which have already been shown to have a significant impact on RTE, I see that atmospheric conditions are very important. This analysis assumed a constant atmospheric temperature and pressure, corresponding to the average conditions off the coast of Virginia. In reality, these results show that the RTE will change seasonally with the air temperature. Several engineering parameters are also important including the wellbore radius as well as the generator and mechanical losses.

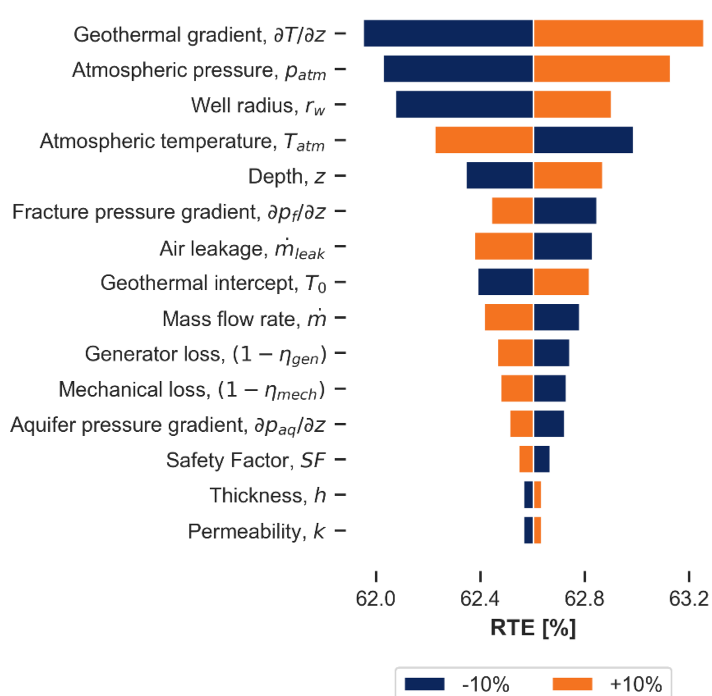

Figure C-4. Model sensitivity study for parameters with that affected RTE by at least 0.01 %.

Appendix D – Supporting Information for Chapter 6 - Life Cycle Meta-Analysis of Carbon Capture Pathways in Power Plants: Implications for Bioenergy with Carbon Capture and Storage

Literature Inputs

The technical data from literature used in this study are summarized in Table D-1 through Table D-4.

Table D-1. Performance of integrated gasification combined cycle coal power plants with carbon capture and compression from literature.

Publication	Case	–Capture Type	η_{PP}	η_{PP+CC}	HHV or LHV	Capture Rate	Outlet Pressure (MPa)
Cormos et al., 2018 [395]	Case 1a vs. Case 1b	Amine-based (Post, MDEA)	46.05	36.03	LHV	90.00	12.00
Cormos et al., 2018 [395]	Case 1a vs. Case 1c	Amine-based (Pre, MDEA)	46.05	36.59	LHV	90.00	12.00
Cormos et al., 2018 [395]	Case 1a vs. Case 1d	CaL (Post)	46.05	34.35	LHV	90.00	12.00
Cormos et al., 2018 [395]	Case 1a vs. Case 1e	CaL (Pre)	46.05	36.10	LHV	90.00	12.00
Petrescu and Cormos, 2017 [314]	Case 1 vs Case 2	CaL (Pre)	45.09	36.44	LHV	91.56	12.00
Petrescu and Cormos, 2017 [314]	Case 1 vs Case 3	CL (Pre, iron-based)	45.09	38.76	LHV	99.45	12.00
Rubin et al., 2015 [312]	USDOE 2013	Selexol (Selexol, Pre)	39.00	32.60	HHV	90.00	15.30
Rubin et al., 2015 [312]	USDOE 2013	Selexol (Selexol, Pre)	39.70	31.00	HHV	90.00	15.30
Rubin et al., 2015 [312]	USDOE 2013	Selexol (Selexol, Pre)	42.10	31.20	HHV	90.00	15.30
Rubin et al., 2015 [312]	GCCSI 2011	Selexol (Selexol NS, Pre)	41.10	32.00	HHV	90.00	20.20

Table D-2. Performance of pulverized coal power plants with carbon capture and compression from literature.

Publication	Case	Capture Type	η_{PP}	η_{PP+CC}	HHV or LHV	Capture Rate	Outlet Pressure (MPa)
Rubin et al., 2015 [312]	ZEP 2011	Amine-based (Post, Adv.amine)	44.20	36.50	HHV	90.00	11.00
Rubin et al., 2015 [312]	GCCSI 2011	Amine-based (Post, Amine)	39.10	27.20	HHV	90.00	20.20
Rubin et al., 2015 [312]	IEAGHG 2014	Amine-based (Post, Cansolv)	42.30	33.80	HHV	90.00	11.00
Rubin et al., 2015 [312]	USDOE 2013	Amine-based (Post, Econ FG+)	39.30	28.40	HHV	90.00	15.30
Cormos et al., 2018 [395]	Case 2a vs. Case 2b	Amine-based (Post, MDEA)	43.33	34.29	LHV	90.00	12.00
Petrescu et al., 2017 [313]	Case 1 vs 2	Amine-based (Post, MDEA)	43.33	34.29	LHV	90.49	12.00
Petrescu et al., 2017 [313]	Case 1 vs 3	Ammonia (Post)	43.33	35.09	LHV	85.00	12.00
Ozcan et al., 2015 [315]	Case A	CaL (Ca-Cu, Post)	40.10	35.60	LHV	90.00	15.00
Ozcan et al., 2015 [315]	Case D	CaL (Ca-Cu, Post)	40.10	36.60	LHV	90.00	15.00
Ozcan et al., 2015 [315]	Case E	CaL (Ca-Cu, Post)	40.10	34.80	LHV	90.00	15.00
Cormos et al., 2018 [395]	Case 2a vs. Case 2c	CaL (Post)	43.33	35.91	LHV	90.00	12.00
Ortiz et al., 2016 [316]	N/A	CaL (Post)	33.50	28.00	HHV	77.00	10.00
Ozcan et al., 2015 [315]	Case A	CaL (Post)	40.10	31.60	LHV	90.00	15.00
Ozcan et al., 2015 [315]	Case D	CaL (Post)	40.10	32.30	LHV	90.00	15.00
Ozcan et al., 2015 [315]	Case E	CaL (Post)	40.10	30.90	LHV	90.00	15.00
Petrescu et al., 2017 [313]	Case 1 vs 4	CaL (Post)	43.33	35.91	LHV	92.66	12.00
Kotowicz and Bartela, 2012 [317]	Fig. 4	Membrane (Post)	48.78	42.92	LHV	90.00	15.00
Kotowicz and Bartela, 2012 [317]	Fig. 6	Membrane (Post)	48.78	43.18	LHV	90.00	15.00
Rubin et al., 2015 [312]	USDOE 2010	Oxy-fuel	38.70	31.00	HHV	90.80	15.30
Rubin et al., 2015 [312]	USDOE 2010	Oxy-fuel	38.90	30.10	HHV	90.60	15.30
Rubin et al., 2015 [312]	EPRI 2011	Oxy-fuel	39.00	31.50	HHV	90.00	15.30
Rubin et al., 2015 [312]	EPRI 2011	Oxy-fuel	39.00	31.50	HHV	90.00	15.30
Rubin et al., 2015 [312]	EPRI 2011	Oxy-fuel	39.00	31.00	HHV	98.00	15.30
Rubin et al., 2015 [312]	IEAGHG 2014	Oxy-fuel	42.20	34.10	HHV	90.00	11.00

Table D-3. Performance of natural gas combined cycle power plants with carbon capture and compression from literature.

Publication	Case	Capture Type	η_{PP}	η_{PP+CC}	HHV or LHV	Capture Rate	Outlet Pressure (MPa)
Rubin et al., 2015 [312]	IEAGHG 2012	Amine-based (Post, Adv.amine)	53.20	47.00	HHV	90.00	11.00
Rubin et al., 2015 [312]	USDOE 2011	Amine-based (Post, Econamine FG+)	50.50	42.90	HHV	90.00	15.20
Rubin et al., 2015 [312]	Rubin and Zhai 2012	Amine-based (Post, Econamine FG+)	50.00	42.60	HHV	90.00	13.70
Rubin et al., 2015 [312]	USDOE 2013	Amine-based (Post, Econamine FG+)	50.20	42.80	HHV	90.00	15.20
Gazzani et al., 2013 [311]	MEA	Amine-based (Post, MEA)	58.34	45.06	LHV	88.30	11.00
Rubin et al., 2015 [312]	IEAGHG 2012	Amine-based (Post, MEA)	53.20	46.10	HHV	90.00	11.00
Gazzani et al., 2013 [311]	SEWGS Case 4	SEWGS (Pre)	58.34	46.18	LHV	85.70	11.00
Gazzani et al., 2013 [311]	SEWGS Case 5	SEWGS (Pre)	58.34	45.78	LHV	91.10	11.00

Table D-4. Performance of biomass power plants with carbon capture and compression from literature.

Publication	Case	Capture Type	η_{PP}	η_{PP+CC}	HHV or LHV	Capture Rate	Outlet Pressure (MPa)
Herron et al., 2012 [285]	100% Poplar (P.N.1 vs P.A.1)	Amine-based (Post, Econamine FG+)	35.80	22.60	HHV	90.00	15.30
Herron et al., 2012 [285]	100% Poplar (P.N.1 vs P.O.1)	Oxy-fuel	35.80	27.10	HHV	90.00	15.30

GREET Data

To compare combinations of capture technologies and power plant configurations, life cycle inventory data and power plant performance data was taken from GREET 2019 using target year 2020 [334].

Select data from the GREET model requires pre-processing because the model did not track energy use directly. GREET does track the amount of fossil and non-fossil energy used, thus to calculate the well-to-use energy use (EU) for a given product or process, it was defined as,

$$EU = Non\ Fossil\ Energy + Fossil\ Energy \tag{D-1}$$

The fuel gathering processes in GREET contains the energy content of the fuel produced, thus an additional equation was developed for this case,

$$EU_{fuel} = Non\ Fossil\ Energy + Fossil\ Energy - 1MJ \tag{D-2}$$

Similarly, power plants include the energy content of the fuel as energy used, thus an additional equation was developed for this case,

$$EU_{power\ plant} = \begin{cases} Non\ Fossil\ Energy + Fossil\ Energy - 1MJ, & for\ Well - to - use \\ 0, & for\ onsite \end{cases} \tag{D-3}$$

Onsite energy use impacts of the power plant only track fuel used in GREET, thus the special case of zero shown. A summary of the GREET data used in the model is shown below in Table D-5 and D-6.

Table D-5. "Non Distributed - U.S. Mix" Power Plant Data from GREET 2019, with target year 2020 [334]**. (WTP – well-to-pump, FU – functional unit, GWP – global warming potential, EU – energy use and WU – water use).**

Power Plant Type		Biomass (IGCC)	Biomass (Steam)	Coal (IGCC)	Coal (Steam)	NG (NGCC)
GREET Process		Electricity: Switchgrass IGCC Power Plant*	Electricity: Switchgrass (Steam Turbine) Power Plant	Electricity: Coal-Fired (IGCC Turbine) Plant	Electricity: Coal-Fired (Steam Turbine) Plant	Electricity: NG-Fired (Combined-cycle Gas Turbine) Plant
Type		WTP	WTP	WTP	WTP	WTP
FU		kWh	kWh	kWh	kWh	kWh
Efficiency (fr)		0.45	0.25	0.39	0.38	0.60
Data - Well to use (used for baseline comparison)						
CO_2 (g)		834.74	1496.30	889.21	912.59	367.57
CO_2 Biogenic (g)		-813.58	-1464.45	-0.02	-0.02	-0.01
GHG-100 (g CO_2eq)	**A**	63.96	77.76	931.72	956.77	402.29
Non Fossil Energy (MJ)	**B**	8.01	14.41	0.01	0.01	0.00
Fossil Energy (MJ)	**C**	0.32	0.57	9.42	9.67	76.52
Water Total (cm^3)	**D**	89.91	1676.00	1506.35	1654.20	668.54
Data – Onsite						
CO_2 (g)	**E**	813.17	1457.47	875.25	898.26	337.72
CO_2 Biogenic (g)		-813.56	-1464.41	0.00	0.00	0.00
GHG-100 (g CO_2eq)	**F**	22.90	3.85	878.69	902.35	338.24
Fuel Use (MJ)	**G**	8.00	14.40	9.23	9.47	6.00
Water Cooling (cm^3)	**H**	0.00	1514.17	1377.89	1522.47	601.19
Calculations - Well to use						
GWP (g CO_2eq)	**=A**	63.96	77.76	931.72	956.77	402.29
EU (MJ)	**= B + C – G**	0.33	0.59	0.19	0.20	70.52
WU (cm^3)	**= D + H**	89.91	1676.00	1506.35	1654.20	668.54
Calculations – Onsite						
CO_2 (g)	**= E**	813.17	1457.47	875.25	898.26	337.72
GWP (g CO_2eq)	**= F**	22.90	3.85	878.69	902.35	338.24
EU (MJ)	**= -3.60**	-3.60	-3.60	-3.60	-3.60	-3.60
WU (cm^3)	**= G**	1377.89	1514.17	1377.89	1522.47	601.19

*GREET did not include Onsite water use for biomass IGCC, assumed to be the same per kWh as coal IGCC

Table D-6. Fuel Gathering, Chemical Production, and Transport Data from GREET 2019, with target year 2020 [334]**. (WTP – well-to-pump, WTW – well-to-wheels, FU – functional unit, GWP – global warming potential, EU – energy use, WU – water use).**

Product		Biomass	Coal	Methyl Amine	Natural Gas	Transport
GREET Product		Switchgrass Production for Ethanol Plant	Coal for Power Plants	Production Pathway for Methyl Amine	NA NG from Shale and Regular Recovery for Electricity Generation	HD Truck: Combination Short-Haul CIDI - Low Sulfur Diesel
Type		WTP	WTP	WTP	WTP	WTW
FU		MJ	MJ	g	MJ	tonne-km
Data - Well to use						
CO_2 (g)		2.70	1.51	2.31	4.98	68.25
CO_2 Biogenic (g)		0.00	0.00	0.00	0.00	-0.01
GHG-100 (g CO_2eq)	**A**	5.13	5.74	2.66	10.68	70.84
Non-Fossil Energy	**B**	1.00	0.00	0.00	0.00	0.00
Fossil Energy	**C**	0.04	1.02	0.07	1.09	0.92
Water Total (cm^3)	**D**	11.24	13.92	2.20	11.22	64.11
Calculations - Well to use						
GWP (g CO_2eq)	**= A**	5.13	5.74	2.66	10.68	70.84
EU (MJ)	**= B+C-X**	0.04	0.02	0.07	0.09	0.92
WU (cm^3)	**= D**	11.24	13.92	2.20	11.22	64.11

***X=1 for fuels and 0 for other entries**

Environmental Impacts

Three environmental impacts, global warming potential (GWP), Energy Use (EU) and water use (WU) were calculated using Equations D- through D-9 below by replacing the quantity *I*, with the desired impact of interest. A fourth environmental impact, Energy Return on Investment (EROI) was derived based on EU using Equations D-10 and D-11.

Fuel Production and Transport

The impact of fuel production is I_{FP},

$$I_{FP}\left(\frac{unit}{kWh}\right) = \frac{1}{\eta_{PP+CC}} \cdot i_{FP}\left(\frac{unit}{MJ}\right) \cdot \frac{3.6\ MJ}{1\ kWH} \tag{D-4}$$

where i_{FP} is the environmental impact of the fuel production from GREET per MJ including transport and η_{PP+CC} is the power plant efficiency including carbon capture.

Power Generation

The environmental impact of power generation I_{PG} is calculated as,

$$I_{PG}\left(\frac{unit}{kWh}\right) = \frac{\eta_{PP,B}}{\eta_{PP+CC}} \cdot i_{PG}\left(\frac{unit}{kWh}\right) \tag{D-5}$$

where i_{PG} is the environmental impact of fuel combustion from the baseline GREET model per kWh, and $\eta_{PP,B}$ the baseline efficiency from GREET.

Carbon Capture

The environmental impact of the carbon capture process, I_{CC}, , is calculated as,

$$I_{CC}\left(\frac{unit}{kWh}\right) = \begin{cases} -\beta \cdot \frac{\eta_{PP,B}}{\eta_{PP+CC}} \cdot \dot{m}_{CO_2,B}\left(\frac{g\ CO_2}{kWh}\right),\ for\ GWP \\ 3.6 \cdot \left(\frac{\eta_{PP,B}}{\eta_{PP+CC}} - 1\right),\ for\ EU \\ \beta \cdot \frac{\eta_{PP,B}}{\eta_{PP+CC}} \cdot \dot{m}_{CO_2,B}\left(\frac{g\ CO_2}{kWh}\right) \cdot \dot{m}_w\left(\frac{cm^3\ water}{g\ CO_2}\right),\ for\ WU \end{cases} \tag{D-6}$$

where β is the capture rate, $\dot{m}_{CO_2,B}$ is the amount of CO_2 emitted by the baseline power plant, and $\dot{m}_w$ is the amount of water used by the capture system. Only several studies specify the water consumed by the capture system, summarized in Table D-7.

Table D-7. Water Use for the Carbon Capture Process of Power Plants with Carbon Capture from Literature.

Study [-]	Capture Technology [-]	Water Use Rate [m3/hr]	CO_2 Capture Rate [tonne/hr]	Water Use [cm^3/ g CO_2]
Herron et al., 2012 [285], PA1	Amine-based (Econamine)	11.4	210.9	0.054
Herron et al., 2012 [285], PA2	Oxy-fuel	0.0	194.7	0.000
Petrescu et al., 2017 [313]	Ammonia	25.5	326.7	0.078
Petrescu et al., 2017 [313]	CaL	0	485.8	0.000

Solvent

The environmental impacts of solvent processes are,

$$I_{SP}\left(\frac{unit}{kWh}\right) = \dot{m}_S\left(\frac{kg\ solvent}{tonne\ CO_2}\right) \cdot \beta \cdot \frac{\eta_{PP,B}}{\eta_{PP+CC}} \cdot \dot{m}_{CO_2,B}\left(\frac{g\ CO_2}{kWh}\right) \cdot i_{SP}\left(\frac{unit}{g\ solvent}\right) \cdot \frac{1000\ g}{1\ kg} \cdot \frac{1\ tonne}{1E6\ g} \tag{D-7}$$

$$I_{ST}\left(\frac{unit}{kWh}\right) = \dot{m}_S\left(\frac{kg\ solvent}{tonne\ CO_2}\right) \cdot \beta \cdot \frac{\eta_{PP,B}}{\eta_{PP+CC}} \cdot \dot{m}_{CO_2,B}\left(\frac{g\ CO_2}{kWh}\right) \cdot D(km) \cdot i_{ST}\left(\frac{unit}{tonne{-}km}\right) \cdot \frac{1\ tonne}{1000\ kg} \cdot \frac{1\ tonne}{1E6\ g} \tag{D-8}$$

where $\dot{m}_S$ is consumption rate of solvent, I_{SP} the calculated environmental impact of solvent production, i_{SP} the environmental impact of solvent production from GREET, I_{ST} the calculated environmental impact of solvent transport, i_{ST} the environmental impact of solvent transport from GREET, and D the distance that the solvent is transported.

Total Impact

The total environmental impact of, I_{total}, is defined as the summation of the impacts from the above processes,

$$I_{total}\left(\frac{unit}{kWh}\right) = I_{FP} + I_{PG} + I_{CC} + I_{SP} + I_{ST} \tag{D-9}$$

EROI

The energy return on investment (EROI) is calculated as,

$$EROI = \frac{1\ kWh}{E_{IN}} \tag{D-10}$$

where E_{IN} is energy in, defined as,

$$E_{IN} = EU_{total} - E_{OUT} = EU_{total} + 3.6 \tag{D-11}$$

where -3.6 MJ represents the 1 kWh of electricity generation.

Tabulated Model Results

Table D-8. Summarized performance of biomass power plants with carbon capture and compression.

Power Plant Type	Capture Type	Pre/Post	#	GWP [kg CO2/kWh]			EROI [-]			WU [l/kWh]			EU [MJ/kWh]		
				Min	Mean	Max	Min	Mean	Max	Min	Mean	Max	Min	Mean	Max
Biomass (IGCC)	Amine-based	Post	7	-0.84	-0.76	-0.73	6.9	7.7	8.0	1.65	1.72	1.90	-3.15	-3.13	-3.08
Biomass (IGCC)	Amine-based	Pre	1	-0.82	-0.82	-0.82	7.0	7.0	7.0	1.87	1.87	1.87	-3.09	-3.09	-3.09
Biomass (IGCC)	CaL	Post	1	-0.88	-0.88	-0.88	8.4	8.4	8.4	1.93	1.93	1.93	-3.17	-3.17	-3.17
Biomass (IGCC)	CaL	Pre	2	-0.84	-0.83	-0.83	8.8	9.0	9.1	1.78	1.81	1.84	-3.20	-3.20	-3.19
Biomass (IGCC)	CL	Pre	1	-0.86	-0.86	-0.86	9.6	9.6	9.6	1.69	1.69	1.69	-3.23	-3.23	-3.23
Biomass (IGCC)	Selexol	Pre	4	-0.89	-0.84	-0.78	8.3	8.8	9.4	1.72	1.84	1.96	-3.22	-3.19	-3.17
Biomass (IGCC)	SEWGS	Pre	2	-0.80	-0.77	-0.74	9.4	9.4	9.4	1.73	1.73	1.74	-3.22	-3.22	-3.22
Biomass (Steam)	Amine-based	Post	7	-3.10	-2.18	-1.79	1.9	2.8	3.3	2.55	3.11	4.42	-2.52	-2.29	-1.73
Biomass (Steam)	Ammonia	Post	1	-1.66	-1.66	-1.66	3.4	3.4	3.4	2.55	2.55	2.55	-2.55	-2.55	-2.55
Biomass (Steam)	CaL	Post	9	-1.88	-1.63	-1.34	4.0	4.6	5.3	1.93	2.24	2.55	-2.93	-2.82	-2.71
Biomass (Steam)	Membrane	Post	2	-1.58	-1.57	-1.56	4.8	4.8	4.9	2.12	2.13	2.15	-2.86	-2.85	-2.85
Biomass (Steam)	Oxy-fuel	Oxy	7	-2.05	-1.89	-1.79	3.7	4.1	4.2	2.43	2.53	2.78	-2.75	-2.71	-2.63
Blend (IGCC)	Amine-based	Post	7	-0.34	-0.30	-0.29	7.8	8.8	9.2	1.69	1.77	1.98	-3.21	-3.19	-3.14
Blend (IGCC)	Amine-based	Pre	1	-0.33	-0.33	-0.33	8.0	8.0	8.0	1.95	1.95	1.95	-3.15	-3.15	-3.15
Blend (IGCC)	CaL	Post	1	-0.36	-0.36	-0.36	10.0	10.0	10.0	2.03	2.03	2.03	-3.24	-3.24	-3.24
Blend (IGCC)	CaL	Pre	2	-0.34	-0.34	-0.34	10.5	10.7	10.9	1.85	1.88	1.92	-3.27	-3.26	-3.26
Blend (IGCC)	CL	Pre	1	-0.40	-0.40	-0.40	11.7	11.7	11.7	1.73	1.73	1.73	-3.29	-3.29	-3.29
Blend (IGCC)	Selexol	Pre	4	-0.36	-0.34	-0.31	9.8	10.5	11.4	1.77	1.92	2.06	-3.28	-3.26	-3.23
Blend (IGCC)	SEWGS	Pre	2	-0.33	-0.30	-0.27	11.3	11.3	11.4	1.78	1.79	1.79	-3.28	-3.28	-3.28
Blend (Steam)	Amine-based	Post	6	-0.92	-0.80	-0.73	4.4	5.1	5.6	2.32	2.54	2.92	-2.96	-2.89	-2.79
Blend (Steam)	Ammonia	Post	1	-0.64	-0.64	-0.64	5.7	5.7	5.7	2.32	2.32	2.32	-2.97	-2.97	-2.97
Blend (Steam)	CaL	Post	9	-0.76	-0.67	-0.48	7.3	8.1	9.1	1.86	2.09	2.31	-3.20	-3.16	-3.11
Blend (Steam)	Membrane	Post	2	-0.66	-0.66	-0.66	8.4	8.4	8.4	2.01	2.02	2.03	-3.17	-3.17	-3.17
Blend (Steam)	Oxy-fuel	Oxy	6	-0.88	-0.77	-0.73	7.2	7.5	7.6	2.23	2.27	2.37	-3.13	-3.12	-3.10

Table D-9. Summarized performance of fossil fuel power plants with carbon capture and compression.

Power Plant Type	Capture Type	Pre/Post/Oxy	#	GWP [kg CO2/kWh]			EROI [-]			WU [l/kWh]			EU [MJ/kWh]		
				Min	Mean	Max	Min	Mean	Max	Min	Mean	Max	Min	Mean	Max
Coal (IGCC)	Amine-based	Post	1	0.20	0.20	0.20	9.3	9.3	9.3	2.08	2.08	2.08	-3.21	-3.21	-3.21
Coal (IGCC)	Amine-based	Pre	1	0.19	0.19	0.19	9.5	9.5	9.5	2.04	2.04	2.04	-3.22	-3.22	-3.22
Coal (IGCC)	CaL	Post	1	0.20	0.20	0.20	13.0	13.0	13.0	2.14	2.14	2.14	-3.32	-3.32	-3.32
Coal (IGCC)	CaL	Pre	2	0.17	0.18	0.19	13.8	14.1	14.4	1.93	1.97	2.01	-3.35	-3.34	-3.34
Coal (IGCC)	CL	Pre	1	0.07	0.07	0.07	15.5	15.5	15.5	1.79	1.79	1.79	-3.37	-3.37	-3.37
Coal (IGCC)	Selexol	Pre	4	0.18	0.19	0.21	12.8	13.9	15.1	1.84	2.02	2.18	-3.36	-3.34	-3.32
Coal (Steam)	Amine-based	Post	6	0.20	0.21	0.23	7.9	8.9	9.5	2.18	2.34	2.62	-3.22	-3.19	-3.14
Coal (Steam)	Ammonia	Post	1	0.25	0.25	0.25	9.7	9.7	9.7	2.18	2.18	2.18	-3.23	-3.23	-3.23
Coal (Steam)	CaL	Post	9	0.15	0.19	0.31	13.6	14.9	16.3	1.82	2.01	2.18	-3.38	-3.36	-3.34
Coal (Steam)	Membrane	Post	2	0.17	0.17	0.18	15.2	15.3	15.3	1.94	1.95	1.96	-3.37	-3.36	-3.36
Coal (Steam)	Oxy-fuel	Oxy	6	0.10	0.17	0.19	13.4	13.9	14.1	2.12	2.15	2.22	-3.34	-3.34	-3.33
NG (NGCC)	Amine-based	Post	6	0.11	0.12	0.14	5.0	5.5	5.7	0.77	0.80	0.88	-2.97	-2.95	-2.89
NG (NGCC)	SEWGS	Pre	2	0.12	0.13	0.14	5.5	5.5	5.5	0.84	0.84	0.84	-2.95	-2.94	-2.94

Comparison of co-firing blends

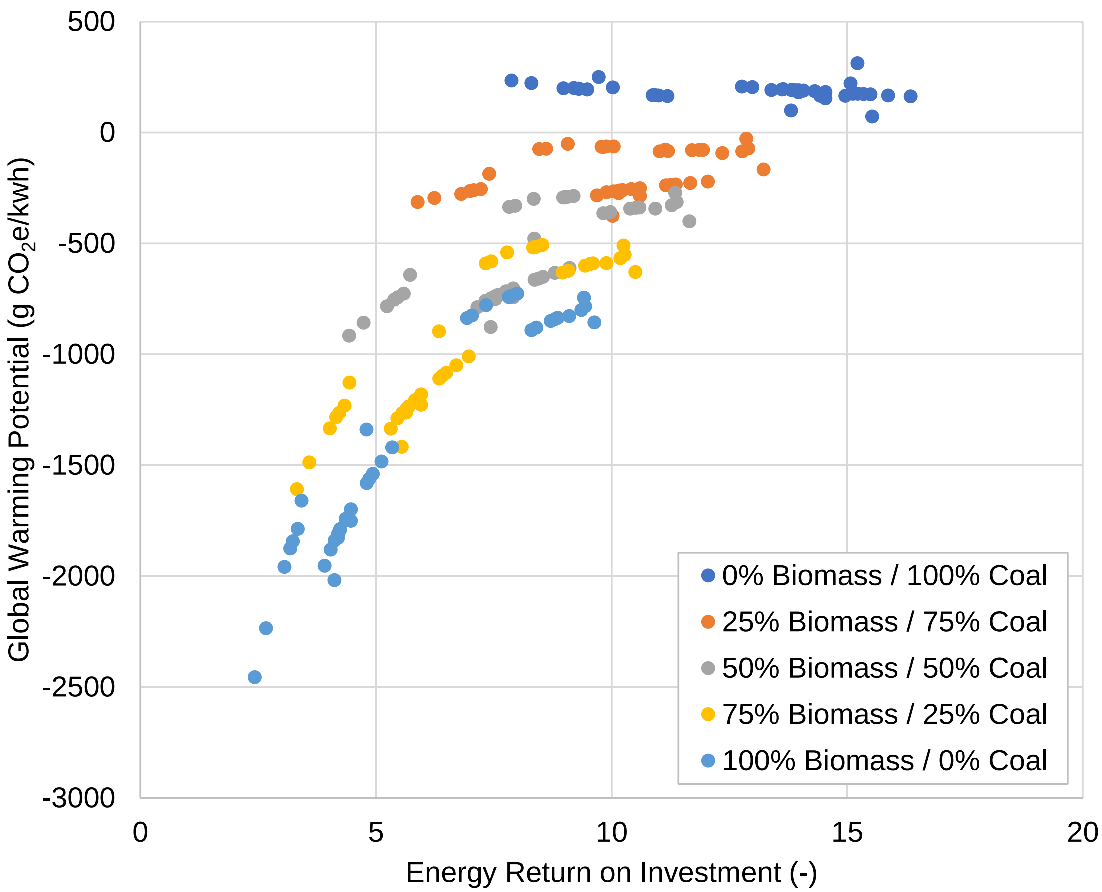

Figure D-1. Comparison of running the model with varying co-firing blends.

Appendix E – Supporting Information for Chapter 7 - The Role of Long Duration Storage and Negative Emissions in Meeting Decarbonization Goals at the Regional Scale

Model inputs

An energy system optimization model of Virginia was built by reviewing existing infrastructure, resource availability and variations in electricity demand.

Electricity demand and system parameters

System level inputs are summarized in Table E-1. The global discount rate applies to all technologies except wind and solar. The value is meant to be representative of United States inflation. Wind and solar power plants are assumed to have a higher discount rate of 8%. The basis for the reserve margin is a 36.4% difference between peak hourly demand in the model versus historical data, plus an additional 15% of planning capacity reserves based on the Dominion Integrated Resource Plan [396]. Annual electricity demand and the corresponding annual emission limit is shown in Table E-2. The annual electricity demand is calculated by applying expected transmission, substation and distribution losses to the total 2019 generation from the EIA [370]. The annual emission limit is a linear path to zero starting with current emission levels for 2025.

Table E-1. Virginia Electric System Inputs.

Parameter	Value	Ref.
Global Discount Rate	0.02	Assumption
Reserve Margin	41.86%	[373,396]

Table E-2. Yearly Demand Projection and Renewable Portfolio Standard (RPS). The 2019 value for demand is from EIA [370] **and the remaining projected demand values from a projection by Weldon Cooper Center** [369]**.**

Year	Annual Demand	Annual Emission Limit
-	PJ	Mt CO_2
2019	315	N/A
2025	461.4	23.8
2030	509.7	19.04
2035	564.8	14.28
2040	616.8	9.52
2045	668.8	4.76
2050	720.8	0.0

Transmission and Distribution

Transmission, substation, and distribution losses are based on International Energy Agency Energy Technology Systems Analysis Program (ETSAP)[109]. Transmission losses are based on 350 km of distance to represent half the length of Virginia and a loss rate of 7%/1000 km [109]. Costs of building and maintaining new transmission and distribution capacity are included in the CAPEX costs of powerplants as listed in NREL ATB 2020.

Table E-3. Transmission System Losses.

Technologies	Loss	
-	%	Ref.
Transmission Lines	2.45	[109]
Substations	0.4	[109]
Distribution Lines	7.0	[109]

Fuel

Fuel model inputs are summarized below in Table E-4. Biomass is assumed to be a carbon neutral fuel. The max activity values for biomass and natural gas were calibrated to match 2019 fuel consumption. The maximum natural gas pipeline capacity is based on the Dominion Integrated Resource Plan [396] and is equivalent to all of Dominion's currently installed 7.9 GW of natural gas generation operating simultaneously.

Table E-4. Fuel Costs and CO2 Emissions.

Fuel	Fuel Costs				Emission Activity		Max Activity	Max Capacity
	2019		Yearly Increase					
-	US M$/PJ	Ref.	%	Ref.	kt/PJ	Ref.	PJ	GW
Biomass	2.41	[397]	0	[8]	0.00	N/A	52.6	N/A
Coal	2.94	[370]	-0.31	[356]	88.43	[176]	N/A	N/A
Hydro	0.00	N/A	N/A	N/A	0.00	N/A	N/A	N/A
Natural Gas	2.99	[370]	1.57	[356]	50.30	[176]	391	19.89 [396]
Nuclear	0.63	[8]	0.15	[8]	0.0	N/A	N/A	N/A
Oil	11.27	[370]	2.41	[356]	67.58	[176]	N/A	N/A
Solar	0.00	N/A	N/A	N/A	0.00	N/A	N/A	N/A
Wind	0.00	N/A	N/A	N/A	0.00	N/A	N/A	N/A

Power Plant and Energy Storage Technologies

Power plant and energy storage technology model inputs are summarized below in Table E-5 through Table E-8. For data from the 2020 NREL ATB, Biomass was represented as “Dedicated”, Coal – Steam as “Coal-new-AvgCF” for existing and “Coal-new-HighCF” for new builds, Coal + CCS as “Coal-CCS 90%-HighCF”, Coal – IGCC as “Coal-IGCC-HighCF”, Hydro Electric as “NPD4”, Natural Gas Combined Cycle as “Gas-CC-HighCF”, Natural Gas Combustion Turbine as “Gas-CT-HighCF”, Natural Gas + CCS as “Gas-CC-CCS-HighCF”, Wind – Offshore Fixed as “Class 4 – Offshore Fixed”, Wind – Offshore Floating as “Class 12 – Offshore Floating.” The model uses solar capacity factors from the NREL ATB based on Kansas City because of its similar latitude to Virginia. The Moderate cost projections were used from the NREL ATB, and investment costs are taken as the CAPEX costs. Existing technologies use pricing from 2019 and new power plants use pricing from 2025, the first model year when power plants are built. For data from the EIA, new oil power plants are represented by “Conv gas/oil combined cycle (CC)”.

Existing coal steam power plants in Virginia operated with 16% capacity factors in 2019 [370], therefore variable costs were taken from Eshraghi et al. for legacy coal plants to represent the expected higher operational costs [364]. Power plants with carbon capture are assumed to have 90% capture rates.

Additional information about the calculation of the values for the long duration storage and negative emission technologies are presented in the following section.

In Table E-6, Oil Combined Cycle power plants are assumed to have the same capacity factor and expected lifetime as Natural Gas Combined Cycle power plants. The 100-year lifetime of Nuclear assumes re-permitting of existing power plants. Renewables use a value of 100% for efficiency because the fuel is free, and the resource is not limited.

Table E-5. Power plant and energy storage investment, fixed and variable costs. (The annual change in costs is shown in parentheses, if applicable – otherwise it remains constant).

Technologies	Investment cost		Fixed cost		Variable cost	
-	US$/kW (%/yr)	Ref.	US$/kW (%/yr)	Ref.	US M$/PJ	Ref.
Existing Technologies						
Biomass	N/A	N/A	123.0	[8]	1.31	[8]
Coal – Steam	N/A	N/A	0	[364]	2.12	[364]
Hydro Electric	N/A	N/A	43.6	[8]	0	[8]
Natural Gas Combined Cycle	N/A	N/A	12.9	[8]	0.6	[8]
Natural Gas Combustion Turbine	N/A	N/A	11.4	[8]	1.25	[8]
Nuclear	N/A	N/A	119.0	[8]	0.64	[8]
Oil Combined Cycle	N/A	N/A	12.9	[8]	0.6	[8]
12-hour Pumped Hydro Storage	N/A	N/A	3.00	[14]	1.11	[14]
Solar Photovoltaic – Utility	N/A	N/A	16.1	[8]	0	[8]
New Centralized Technologies						
2-hour Battery	592 (-1.97)	[8]	25.1 (-1.97)	[8]	0	[8]
4-hour Battery	1004 (-1.97)	[8]	25.1 (-1.97)	[8]	0	[8]
Biomass	4247 (-0.53)	[8]	123.00	[8]	1.31	[8]
Coal – Steam	4099 (-0.35)	[8]	39.7	[8]	1.22	[8]
Coal + CCS	6635 (-0.63)	[8]	58.2	[8]	2.98	[8]
Coal – IGCC	4426 (-0.46)	[8]	56.1	[8]	2.19	[8]
Natural Gas Combined Cycle	1008 (-0.40)	[8]	12.9	[8]	0.60	[8]
Natural Gas Combustion Turbine	925 (-0.41)	[8]	11.4	[8]	1.25	[8]
Natural Gas + CCS	2474 (-0.89)	[8]	27.0	[8]	1.59	[8]
Oil Combined Cycle	1008 (-0.4)	[8]	12.9	[8]	0.60	[8]
12-hour Pumped Hydro Storage	1439	[258]	3.00	[14]	1.11	[14]
Solar Photovoltaic – Utility	1095 (-1.86)	[8]	12.8 (-1.86)	[8]	0	[8]
Wind – Offshore Fixed	3245 (-1.7)	[8]	88.6 (-1.88)	[8]	0	[8]
Wind – Offshore Floating	4289 (-2.14)	[8]	78.7 (-2.05)	[8]	0	[8]
New Distributed Technologies						
Solar Photovoltaic – Commercial	1390 (-2.23)	[8]	10 (-2.23)	[8]	0	[8]
Solar Photovoltaic – Residential	1884 (-3.15)	[8]	14.1 (-3.15)	[8]	0	[8]
Emerging Technologies						
BECCS	Determined with Monte Carlo Sampling		141	Calculated	3.33	Calculated
DAC			0	[361]	4.09	[361]
24-hour OCAES			16.3	[262]	2.57	[262]
10-hour VFB			70	[14]	0	[14]

Table E-6. Power plant and energy storage capacity factors, efficiencies and expected lifetime. *Existing natural gas plants are divided into two groups based on year built (pre/post 2000), with different efficiencies.

Technologies	Capacity Factor		Efficiency		Expected Lifetime	
-	%	Ref.	%	Ref.	Years	Ref.
Existing Technologies						
Biomass	63	[370]	25.3	[8]	45	[8]
Coal – Steam	54	[8]	32.2	[396]	75	[8]
Hydro Electric	20.0	[370]	100	-	100	[8]
Natural Gas Combined Cycle*	87	[8]	43.6/54.2	[396]	55	[8]
Natural Gas Combustion Turbine*	30	[8]	28.9/34.0	[396]	55	[8]
Nuclear	94.4	[370]	32.6	[8]	100	Assumption
Oil Combined Cycle	87	[8]	53.3	[8]	55	[8]
12-hour Pumped Hydro Storage	50	Assumption	70	[14]	150	[398]
Solar Photovoltaic – Utility	26.3	[370]	100	-	30	[8]
New Centralized Technologies						
2-hour Battery	50	Assumption	85	[8]	15	[8]
4-hour Battery	50	Assumption	85	[8]	15	[8]
Biomass	61	[8]	25.3	[8]	45	[8]
Coal – Steam	85	[8]	39.5	[8]	75	[8]
Coal + CCS	85	[8]	27.3	[8]	75	[8]
Coal – IGCC	85	[8]	39.2	[8]	75	[8]
Natural Gas Combined Cycle	87	[8]	53.3	[8]	55	[8]
Natural Gas Combustion Turbine	30	[8]	35.9	[8]	55	[8]
Natural Gas + CCS	87	[8]	45.3	[8]	55	[8]
Oil Combined Cycle	87	[8]	53.3	[8]	55	[8]
12-hour Pumped Hydro Storage	50	Assumption	80	[14]	150	[398]
Solar Photovoltaic – Utility	27	[8]	100	-	30	[8]
Wind – Offshore Fixed	44	[8]	100	-	30	[8]
Wind – Offshore Floating	46	[8]	100	-	30	[8]
New Distributed Technologies						
Solar Photovoltaic – Commercial	15	[8]	100	-	30	[8]
Solar Photovoltaic – Residential	17	[8]	100	-	30	[8]
Emerging Technologies						
BECCS	61	[8]	21.5	[360]	45	[8]
DAC	90	[361]	100	-	25	[361]
24-hour OCAES	50	Assumption	70	[262]	25	[262]
10-hour VFB	50	Assumption	74	[258]	19	[258]

Capacity credits in Table E-8 are based on 2020 values from a Temoa model of the United States electric grid by Eshraghi et al. [364], with the model data available at https://raw.githubusercontent.com/TemoaProject/data/master/US_National.sql. Biomass plants are represented by E_BIOIGCC_N (new BioIGCC power plant), Coal – Steam by E_COALSTM_N (new pulverized coal steam power plant), Coal + CCS by E_COAL_IGCC_CCS (new coal IGCC with CCS power plant), Coal – IGCC by E_COAL_IGCC (new coal IGCC power plant), hydroelectric by E_HYDCONV_R (existing conventional hydroelectric power plant), combined cycle power plants by E_NGACC_R (existing natural gas combined cycle power plant), combustion turbine power plants by E_NGACT_R (existing natural gas combustion turbine power plant), natural gas with CCS by E_NGACC_CCS_N (new natural gas combined cycle with ccs power plant), solar farms are represented by E_SOLPVCEN_R (new solar photovoltaic centralized power plant), wind farms by E_WNDCL4_N (New wind class 4 power plant), and BECCS by E_BECCS_N (bio-energy with carbon capture and storage). Storage, including batteries, pumped hydro, OCAES and VFB are represented by battery storage by E_BATT (battery storage).

Table E-7. Power plant and energy storage ramp rates, capacity limits and capacity credits.

Technologies	Ramp rate		Max capacity		Capacity credits	
-	Fr/Hr	Ref.	MW	Ref.	-	%/yr
Existing Technologies						
Biomass					0.95	0.0
Coal – Steam	0.01	Baseload			0.90	0.0
Hydro Electric					0.95	0.0
Natural Gas Combined Cycle					0.95	0.0
Natural Gas Combustion Turbine					0.91	0.0
Nuclear	0.01	Baseload			0.98	0.0
Oil Combined Cycle					0.95	0.0
12-hour Pumped Hydro Storage					0.75	0.0
Solar Photovoltaic – Utility					0.29	-3.23
New Centralized Technologies						
2-hour Battery					0.75	0.0
4-hour Battery					0.75	0.0
Biomass					0.95	0.0
Coal – Steam	0.01	Baseload			0.90	0.0
Coal + CCS	0.01	Baseload			0.95	0.0
Coal – IGCC	0.01	Baseload			0.95	0.0
Natural Gas Combined Cycle					0.95	0.0
Natural Gas Combustion Turbine					0.91	0.0
Natural Gas + CCS					0.95	0.0
Oil Combined Cycle					0.95	0.0
12-hour Pumped Hydro Storage			300	[396]	0.75	0.0
Solar Photovoltaic – Utility			40000	[399]	0.23	-2.95
Wind – Offshore Fixed			5200	[396]	0.33	-2.00
Wind – Offshore Floating					0.33	-2.00
New Distributed Technologies						
Solar Photovoltaic – Commercial			10200	[400]	0.23	-2.95
Solar Photovoltaic – Residential			18300	[400]	0.23	-2.95
Emerging Technologies						
BECCS					0.95	0.0
DAC					0.0	0.0
24-hour OCAES					0.75	0.0
10-hour VFB					0.75	0.0

Table E-8 Existing power plant and energy storage installations along with estimated year built [370]**. (Year input as year built in the model).**

	Capacity installation (GW)						
Technology	**Pre-1990**	**1991-1995**	**1996-2000**	**2001-2005**	**2006-2010**	**2011-2015**	**2016-2019**
-	**(1990)**	**(1995)**	**(2000)**	**(2005)**	**(2010)**	**(2015)**	**(2018)**
Biomass	401.1	75	11	4	43.6	270.2	0
Coal – Steam	1007	1778	9	0	84.9	0	0
Hydro Electric	671.8	0	0	0	194.2	0	0
Natural Gas Combined Cycle	297.4	1069.5	363	1651	0	2033.5	3453.6
Natural Gas Combustion Turbine	330.5	1069.5	363	1651	785.7	279.1	346.2
Nuclear	3347	10	75	0	69	67	0
Oil Combined Cycle	1299.1	0	972	28	41.7	0	0
12-hour Pumped Hydro Storage	2345	0	0	572	324	0	0
Solar Photovoltaic – Utility	0	0	0	0	0	0	556.1

Model verification

To verify the model, fuel resources used in the first model year, 2019, were compared against actual usage recorded by EIA in 2019 shown in Table E-9. It was expected that all biomass available in 2019 would have been used, however only 74% was used. Based on Brown et al., the production of electricity with biomass is expensive and therefore there are expected to be other non-economic factors pushing towards the consumption of biomass [401].

Table E-9. The energy system model was verified by comparing the results of the first model year (2019) to actual fuel consumption in 2019.

	Total Electricity Production	
Energy Source	**2019 Actual** [370]	**2019 Model**
-	%	%
Biomass	3.87	2.88
Coal	3.53	5.68
Hydroelectric	1.57	1.59
Natural Gas	59.88	59.91
Nuclear	30.46	30.86
Petroleum	0.27	0.00
Pump	-1.14	-2.24
Solar PV	0.98	1.32
Others	0.58	0.00

Emerging energy technologies

This section presents the calculations behind the cost and performance parameters for the emerging technologies considered in this analysis.

Negative Emissions Technology - Bioenergy with Carbon Capture and Storage (BECCS)

BECCS – High capital cost

Fajardy et al. estimate that a BECCS plant will cost 11714 $/kW [287].

BECCS – Low capital cost

The National Energy Technology Laboratory (NETL) estimated the costs of a BECCS plant operating with 90% capture as shown in NETL Vol. 2 (Herron et al 2012) [285]. The total as spent costs includes overnight costs, owner's costs and financing costs.

Table E-10. BECCS power plant capital cost estimate from NETL (Herron et al 2012) [285]**.**

Case	**P.A.1**
Plant type	**Greenfield supercritical 100% biomass**
Capture method	Amine
Capture rate	90%
Total Overnight Cost [$/kW]	4216
Total As Spent Costs [$/kW]	4781

BECCS - O&M Estimates

Estimates of BECCS O&M costs were made by applying the relative price difference between coal power plants with and without capture to dedicated biomass plants without capture, using 2018 data from NREL ATB [8]. Calculations are shown in Table E-11 and E-12.

Table E-11. BECCS Fixed O&M Cost estimate based on NREL ATB [8]**.**

Coal plant [$/kW]	40
Coal w/ CCS [$/kW]	58
Difference	18
Bio dedicated [$/kW]	123
BECCS [$/kW]	141

Table E-12. BECCS Variable O&M Cost estimate based on NREL ATB [8]**.**

Coal plant [$/MWh]	4
Coal w/ CCS [$/MWh]	11
Difference	7
Bio dedicated [$/MWh]	5
BECCS [$/MWh]	12
BECCS [M$/PJ]	3.33

BECCS - Capture rate and negative emissions

A capture rate of 90% was assumed based on NETL [285]. Based on GREET [334], 103.91 kt CO_2 are emitted per PJ of biomass. I assume that conventional biomass power plants are carbon-neutral so that the emitted CO_2 would be reabsorbed by the biomass used to supply the power plant. For BECCS plants, I assume that 90% of those emissions are stored in the subsurface. This equates to an emission factor of –93.52 kt CO_2/PJ.

Table E-13. Bioenergy emissions and performance from GREET 2019, based on "Switchgrass (Steam Turbine) Power Plant" [334]**.**

Efficiency	25%	GREET [334]
Emissions [kt CO_2 /PJ-out]	415.63	GREET [334]
Emissions [kt CO_2 /PJ-in]	103.91	Calculated

Based on the expected range of capital costs, this capture rate equates to costs between $571 and $1400 per tonne of CO_2/year (Table E-14).

Table E-14. BECCS capital costs in terms of negative emissions.

	Low	**High**
Plant size [kW]	1	1
Capital Cost [$/kW]	4781 [285]	11714 [287]
Capacity Factor [%]	61 [8]	61 [8]
Annual power produced [kWh]	5344	5344
Efficiency [%]	21.5 [360]	21.5 [360]
Annual biomass consumed [MWh]	24.86	24.86
Annual biomass consumed [GJ]	89.5	89.5
Negative emission rate [kt CO_2 /PJ]	-93.52	-93.52
Annual negative emissions [t CO_2]	8.37	8.37
Capital cost [$/t CO_2]	571	1400

Negative Emissions Technology - Direct Air Capture (DAC)

DAC - Operation in Temoa

In order to model Direct Air Capture in Temoa, it was modeled as a power plant. The power plant is given an efficiency of 100% to simplify calculations, however the "electricity" output by DAC then goes through unique transmission lines with 99.99999% losses, effectively preventing it from being used to generate electricity.

DAC - Negative emissions

DAC is modeled as a consumer of natural gas in Temoa, therefore the negative emission potential of DAC is calculated in Table E-15 based on the consumption of natural gas.

Table E-15. DAC operation and negative emissions for a unit process based on Keith et al. [361]**.**

Quantity	**Value**	**Reference**
Atmospheric CO_2 captured [t-CO_2]	1.0	Keith et al. [361]
Natural gas consumption [GJ]	8.81	Keith et al. [361]
Natural gas emissions captured [t-CO_2/GJ]	0.0503	EIA Emission limit (50.3 kt CO_2/PJ)
Total CO_2 to storage [t-CO_2]	1.44	Calculated (For comparison, Keith et al. projects 1.3—1.5 t CO_2)
CO_2 to storage per natural gas [t-CO_2/GJ]	0.16345	Calculated
CO_2 to storage per natural gas [kt-CO_2/PJ]	163.45	Calculated

DAC - Costs

Keith et al. estimates the cost of DAC in the near-term and after further development [361]. Estimates of the capital and O&M costs for Temoa are shown in Table E-16 and Table E-17. Keith et al. assumes no fixed O&M costs, only variable. In Temoa, I use the average of the Early and Nth plant for the variable O&M cost. These calculations assume a capacity factor of 90% and 100% efficiency.

Table E-16. DAC plant capital costs based on Keith et al. [361]**.**

System cost	**Early Plant**	**Nth Plant**	**Reference**
CAPEX [M$]	1126.8	779.5	Keith et al. [361]
Capacity [atmospheric MT-CO_2/year]	0.98	0.98	Keith et al. [361]
Capacity [atmospheric t-CO_2/s]	0.0345	0.0345	Calculated
Natural gas consumption rate [GJ/t-CO_2]	8.81	8.81	Keith et al. [361]
Capacity in terms of natural gas consumption [GJ/s] [GW]	0.3042	0.3042	Calculated
CAPEX [M$/GW = $/kW]	3704	2562	Calculated
CAPEX [$/t CO_2]	1150	795	Calculated

Table E-17. DAC variable costs based on Keith et al. [361]**.**

Quantity	Early Plant	Nth Plant	Reference
Variable O&M [$/atmospheric t-$CO_2$]	42	30	Keith et al. [361]
Heat input [GJ / atmospheric t-CO_2]	8.81	8.81	Keith et al. [361]
Variable O&M [$/GJ = M$/PJ]	4.767	3.405	Calculated

Long Duration Storage - Offshore Compressed Air Energy Storage (OCAES)

OCAES - High capital cost

An OCAES capital cost of 9191 $/kW was estimated in Table E-18 based on Mouli-Castillo 2019 [46].

Table E-18. OCAES mid-range capital cost estimates from Mouli-Castillo et al. [46]**. Conversion from pounds to dollars from** [402]**.**

Component	Cost
Wells [2015 million £]	5550
Turbine [2015 million £]	93
Compressor [2015 million £]	607
Total [2015 million £]	6250
Power Output [MW]	1020
CAPEX [2015 £/kW]	6130
CAPEX [2015 $/kW]	9191

OCAES - Low capital cost

The authors estimate that the capital cost of a 200 MW OCAES system would cost $1457/kW, fixed O&M would be 16.3 $/kW and variable O&M 9.24 $/kWh (equal to 2.57 M$/PJ) [262].

Long Duration Storage - Vanadium flow batteries (VFB)

VFB - High capital cost

Beuse et al. 2020 estimates that the capital costs of VFBs can be calculated as, [258]

$$\text{Cost} = 268\ \$/\text{kWh} + 1101\ \$/\text{kW} \tag{E-1}$$

Therefore, a 10-hour system would cost 3781 $/kW.

VFB - Low capital cost

Li et al. 2020 estimates that a 10 hour system costs 182 $/kWh, equivalent to 1820 $/kW [376].

Biomass Resources

An evaluation of the available biomass energy in Virginia was made by combining EPA estimates of energy density [372] with annual harvest from the NREL Biofuel Atlas [371], summarized in Table E-19.

Table E-19. Estimate of biomass energy available in Virginia by fuel type.

Crop [-]	**Energy Density** [372] **[Btu/lb]**	**Annual Harvest** [371] **[1000 Dry t/year]**	**Harvest Energy Content [PJ]**
Primary Mill Residue	8750	1883	38.33
Corn Stover	7560	255	4.48
Wheat Straw	6840	157	2.50
Forest Residues	8570	418	8.33
Urban Wood	6150	1308	18.71
Secondary Mill Residues	8750	269	5.48
Total	-	-	77.83

References

[1] United Nations. Paris Agreement. 2015.

[2] IPCC. Summary for Policymakers. In: Masson-Delmotte V, Zhai P, Pörtner H-O, Roberts D, Skea J, Shukla PR, et al., editors. Glob. Warm. 1.5°C. An IPCC Spec. Rep. impacts Glob. Warm. 1.5°C above pre-industrial levels Relat. Glob. Greenh. gas Emiss. pathways, Context Strength. Glob. response to Threat Clim. Chang., 2018. https://doi.org/10.1016/j.oneear.2019.10.025.

[3] Regnier P, Friedlingstein P, Ciais P, Mackenzie FT, Gruber N, Janssens IA, et al. Anthropogenic perturbation of the carbon fluxes from land to ocean. Nat Geosci 2013;6:597–607. https://doi.org/10.1038/ngeo1830.

[4] Lawrence Livermore National Laboratory. Estimated U.S. Energy Consumption in 2019 2020. https://flowcharts.llnl.gov/content/assets/docs/2019_United-States_Energy.pdf (accessed February 23, 2021).

[5] DOE. Energy Resilience Solutions for the Puerto Rico Grid. 2018.

[6] Newburger E. More than 2 million people expected to lose power in PG&E blackout as California wildfires rage. CNBC 2019.

[7] Jenkins J. A Plan to Future-Proof the Texas Power Grid. New York Times 2021.

[8] NREL. 2020 Annual Technology Baseline. Golden, CO: 2020.

[9] EIA. Renewables account for most new U.S. electricity generating capacity in 2021 2021. https://www.eia.gov/todayinenergy/detail.php?id=46416 (accessed February 26, 2021).

[10] Denholm P, Hand M. Grid flexibility and storage required to achieve very high penetration of variable renewable electricity. Energy Policy 2011;39:1817–30. https://doi.org/10.1016/j.enpol.2011.01.019.

[11] Binsted M, Iyer G, Edmonds J, Vogt-Schilb A, Arguello R, Cadena A, et al. Stranded asset implications of the Paris Agreement in Latin America and the Caribbean. Environ Res Lett 2020;15. https://doi.org/10.1088/1748-9326/ab506d.

[12] EIA. Electricity Data Browser 2020. https://www.eia.gov/electricity/data/browser (accessed February 26, 2021).

[13] Gonzalez-Salazar MA, Kirsten T, Prchlik L. Review of the operational flexibility and emissions of gas- and coal-fired power plants in a future with growing renewables. Renew Sustain Energy Rev 2018;82:1497–513. https://doi.org/10.1016/j.rser.2017.05.278.

[14] Luo X, Wang J, Dooner M, Clarke J. Overview of current development in electrical energy storage technologies and the application potential in power system operation. Appl Energy 2015;137:511–36. https://doi.org/10.1016/j.apenergy.2014.09.081.

[15] Dowling JA, Rinaldi KZ, Ruggles TH, Davis SJ, Yuan M, Tong F, et al. Role of Long-Duration Energy Storage in Variable Renewable Electricity Systems. Joule 2020;4:1907–28. https://doi.org/10.1016/j.joule.2020.07.007.

[16] Rehman S, Al-Hadhrami LM, Alam MM. Pumped hydro energy storage system: A technological review. Renew Sustain Energy Rev 2015;44:586–98. https://doi.org/10.1016/j.rser.2014.12.040.

[17] Liu H, Jiang J. Flywheel energy storage—An upswing technology for energy sustainability. Energy Build 2007;39:599–604. https://doi.org/10.1016/j.enbuild.2006.10.001.

[18] Larcher D, Tarascon J-M. Towards greener and more sustainable batteries for electrical energy storage. Nat Chem 2015;7:19–29. https://doi.org/10.1038/nchem.2085.

[19] National Academies of Sciences Engineering and Medicine. Negative Emissions Technologies and Reliable Sequestration: A Research Agenda. Washington D.C.: 2019. https://doi.org/10.17226/25259.

[20] Gholami A, Aminifar F, Shahidehpour M. Front Lines Against the Darkness. IEEE Electrif Mag 2016:18–24. https://doi.org/10.1109/MELE.2015.2509879.

[21] Jufri FH, Widiputra V, Jung J. State-of-the-art review on power grid resilience to extreme weather

events: Definitions, frameworks, quantitative assessment methodologies, and enhancement strategies. Appl Energy 2019;239:1049–65. https://doi.org/10.1016/j.apenergy.2019.02.017.
[22] Viral R, Khatod DK. Optimal planning of distributed generation systems in distribution system: A review. Renew Sustain Energy Rev 2012;16:5146–65. https://doi.org/10.1016/j.rser.2012.05.020.
[23] Chicco G, Mancarella P. Distributed multi-generation: A comprehensive view. Renew Sustain Energy Rev 2009;13:535–51. https://doi.org/10.1016/j.rser.2007.11.014.
[24] Bayod-Rújula AA. Future development of the electricity systems with distributed generation. Energy 2009;34:377–83. https://doi.org/10.1016/j.energy.2008.12.008.
[25] Feng W, Jin M, Liu X, Bao Y, Marnay C, Yao C, et al. A review of microgrid development in the United States – A decade of progress on policies, demonstrations, controls, and software tools. Appl Energy 2018;228:1656–68. https://doi.org/10.1016/j.apenergy.2018.06.096.
[26] Hussain A, Bui VH, Kim HM. Microgrids as a resilience resource and strategies used by microgrids for enhancing resilience. Appl Energy 2019;240:56–72. https://doi.org/10.1016/j.apenergy.2019.02.055.
[27] Willis HL, Scott WG. Distributed power generation: planning and evaluation. New York: Marcel Dekker, Inc.; 2000.
[28] Brun K, Friedman P, Dennis R, editors. Fundamentals and Applications of Supercritical Carbon Dioxide (SCO2) Based Power Cycles. Duxford, United Kingdom: Woodhead Publishing; 2017.
[29] Lemmon EW, Huber ML, McLinden MO. miniREFPROP: An abbreviated version of NIST REFPROP 2013.
[30] Dostal V, Driscoll MJ, Hejzlar P. A Supercritical Carbon Dioxide Cycle for Next Generation Nuclear Reactors. Tech Rep MIT-ANP-TR-100 2004:1–317. https://doi.org/MIT-ANP-TR-100.
[31] Fleming D, Holschuh T, Conboy T, Rochau G, Fuller R. Scaling Considerations for a Multi-Megawatt Class Supercritical CO2 Brayton Cycle and Path Forward for Commercialization. ASME Turbo Expo 2012 Turbine Tech Conf Expo Vol 5 Manuf Mater Metall Mar Microturbines Small Turbomachinery; Supercrit CO2 Power Cycles 2012;5:953. https://doi.org/10.1115/GT2012-68484.
[32] Allam R, Martin S, Forrest B, Fetvedt J, Lu X, Freed D, et al. Demonstration of the Allam Cycle: An Update on the Development Status of a High Efficiency Supercritical Carbon Dioxide Power Process Employing Full Carbon Capture. Energy Procedia 2017;114:5948–66. https://doi.org/10.1016/j.egypro.2017.03.1731.
[33] Crespi F, Gavagnin G, Sánchez D, Martínez GS. Supercritical carbon dioxide cycles for power generation: A review. Appl Energy 2017;195:152–83. https://doi.org/10.1016/j.apenergy.2017.02.048.
[34] Clementoni EM, Cox TL, Sprague CP. Startup and Operation of a Supercritical Carbon Dioxide Brayton Cycle. J Eng Gas Turbines Power 2014;136:071701. https://doi.org/10.1115/1.4026539.
[35] Pasch JJ, Conboy TM, Fleming DD, Rochau GE. Supercritical CO2 recompression Brayton cycle : completed assembly description. 2012. https://doi.org/10.2172/1057248.
[36] Moore JJ, Cich S, Towler M, Allison T, Wade J, Hofer D. Commissioning of a 1 MWe Supercritical CO 2 Test Loop. 6th Int. Symp. - Supercrit. CO2 Power Cycles, Pittsburgh, Pennslyvania: 2018, p. 1–36.
[37] GTI. A STEP closer to transformational electric power 2021. https://www.gti.energy/step-demo/ (accessed February 26, 2021).
[38] Patel S. News & Technology for the Global Energy Industry. POWER 2019.
[39] Bennett JA, Moisseytsev A, Sienicki JJ. 5 - Modeling and cycle optimization. In: Brun K, Friedman P, Dennis R, editors. Fundam. Appl. Supercrit. Carbon Dioxide Based Power Cycles, Woodhead Publishing; 2017, p. 105–25.
[40] Moisseytsev A, Sienicki JJ. Simulation of S-Co2 Integrated System Test With Anl Plant Dynamics Code. 5th Int Symp - Supercrit CO2 Power Cycles 2016:1–19.

https://doi.org/10.1017/CBO9781107415324.004.

[41] Zitney SE, Liese EA. Dynamic modeling and simulation of a 10MWe supercritical CO2 recompression closed Brayton power cycle for off-design, part-load, and control analysis. 6th Int Symp - Supercrit CO2 Power Cycles 2018:1–26.

[42] Budt M, Wolf D, Span R, Yan J. A review on compressed air energy storage: Basic principles, past milestones and recent developments. Appl Energy 2016;170:250–68. https://doi.org/10.1016/j.apenergy.2016.02.108.

[43] Seymour RJ. Undersea pumped storage for load leveling.pdf. Calif. World Ocean '97 Tak. a look California's Ocean Resour. an agenda Futur., 1997, p. 158–63.

[44] Li B, DeCarolis JF. A techno-economic assessment of offshore wind coupled to offshore compressed air energy storage. Appl Energy 2015;155:315–22. https://doi.org/10.1016/j.apenergy.2015.05.111.

[45] Succar S, Williams RH. Compressed Air Energy Storage: Theory, Resources, and Applications for Wind Power. Princeton, NJ: 2008.

[46] Mouli-castillo J, Wilkinson M, Mignard D, Mcdermott C, Haszeldine RS, Shipton ZK. Inter-seasonal compressed-air energy storage using saline aquifers. Nat Energy 2019;4:131–9. https://doi.org/10.1038/s41560-018-0311-0.

[47] Gough C, Upham P. Biomass energy with carbon capture and storage (BECCS or Bio-CCS). Greenh Gases Sci Technol 2011;1:324–34.

[48] Stavrakas V, Spyridaki N-A, Flamos A. Striving towards the deployment of bio-energy with carbon capture and storage (BECCS): A review of research priorities and assessment needs. Sustainability 2018;10. https://doi.org/10.3390/su10072206.

[49] Mehta A. Drax targets negative emissions with world's first biomass CCS project. Reuters Events 2019. https://www.reutersevents.com/sustainability/drax-targets-negative-emissions-worlds-first-biomass-ccs-project (accessed December 12, 2020).

[50] Bioenergy International. Toshiba ESS commission Japan's first large-scale BECCS plant. Bioenergy Int 2020. https://bioenergyinternational.com/heat-power/toshiba-ess-commission-japans-first-large-scale-beccs-plant (accessed December 12, 2020).

[51] Murakami H, Levin E, Delworth TL, Gudgel R, Hsu PC. Dominant effect of relative tropical Atlantic warming on major hurricane occurrence. Science (80-) 2018;362:794–9. https://doi.org/10.1126/science.aat6711.

[52] Seidl R, Thom D, Kautz M, Martin-Benito D, Peltoniemi M, Vacchiano G, et al. Forest disturbances under climate change. Nat Clim Chang 2017;7:395–402. https://doi.org/10.1038/nclimate3303.

[53] Ji C, Wei Y, Mei H, Calzada J, Carey M, Church S, et al. Large-scale data analysis of power grid resilience across multiple US service regions. Nat Energy 2016;1:1–8. https://doi.org/10.1038/nenergy.2016.52.

[54] Gas Turbine World Handbook. vol. 33. 2018.

[55] Sovacool BK, Heffron RJ, McCauley D, Goldthau A. Energy decisions reframed as justice and ethical concerns. Nat Energy 2016;1. https://doi.org/10.1038/nenergy.2016.24.

[56] Pehl M, Arvesen A, Humpenöder F, Popp A, Hertwich EG. Understanding future emissions from low-carbon power systems by integration of life-cycle assessment and integrated energy modelling. Nat Energy 2017;2. https://doi.org/10.1038/s41560-017-0032-9.

[57] Bennett JA, Fuhrman J, Brown T, Andrews N, Fittro R, Clarens AF. Feasibility of Using sCO2 Turbines to Balance Load in Power Grids with a High Deployment of Solar Generation. Energy 2019;181:548–60. https://doi.org/10.1016/j.energy.2019.05.143.

[58] Hunter K, Sreepathi S, DeCarolis JF. Modeling for insight using Tools for Energy Model Optimization and Analysis (Temoa). Energy Econ 2013;40:339–49. https://doi.org/10.1016/j.eneco.2013.07.014.

[59] McCollum DL, Jewell J, Krey V, Bazilian M, Fay M, Riahi K. Quantifying uncertainties influencing the long-term impacts of oil prices on energy markets and carbon emissions. Nat Energy 2016;1. https://doi.org/10.1038/nenergy.2016.77.
[60] Spyrou E, Hobbs BF, Bazilian MD, Chattopadhyay D. Planning power systems in fragile and conflict-affected states. Nat Energy 2019;4:300–10. https://doi.org/10.1038/s41560-019-0346-x.
[61] Patankar N, de Queiroz AR, DeCarolis JF, Bazilian MD, Chattopadhyay D. Building conflict uncertainty into electricity planning: A South Sudan case study. Energy Sustain Dev 2019;49:53–64. https://doi.org/10.1016/j.esd.2019.01.003.
[62] Perera ATD, Nik VM, Chen D, Scartezzini JL, Hong T. Quantifying the impacts of climate change and extreme climate events on energy systems. Nat Energy 2020;5:150–9. https://doi.org/10.1038/s41560-020-0558-0.
[63] Abdin IF, Fang YP, Zio E. A modeling and optimization framework for power systems design with operational flexibility and resilience against extreme heat waves and drought events. Renew Sustain Energy Rev 2019;112:706–19. https://doi.org/10.1016/j.rser.2019.06.006.
[64] Mukhi N, Chattopadhyay D, Hobbs B, Spyrou E. Building climate resilience into power system planning : the case of Bangladesh. World Bank Rep 2017;ACS23320.
[65] Labriet M, Kanudia A, Loulou R. Climate mitigation under an uncertain technology future: A TIAM-World analysis. Energy Econ 2012;34:S366–77. https://doi.org/10.1016/j.eneco.2012.02.016.
[66] Newlun CJ, Figueroa AL, McCalley JD. Co-Optimized Expansion Planning to Enhance Resilience of the Electrical System in Puerto Rico. Fifty-Sixth Annu. Rep. Electr. Power Res. Cent., 2019.
[67] Nateghi R, Guikema SD, Quiring SM. Comparison and Validation of Statistical Methods for Predicting Power Outage Durations in the Event of Hurricanes. Risk Anal 2011;31:1897–906. https://doi.org/10.1111/j.1539-6924.2011.01618.x.
[68] Winkler J, Dueñas-Osorio L, Stein R, Subramanian D. Performance assessment of topologically diverse power systems subjected to hurricane events. Reliab Eng Syst Saf 2010;95:323–36. https://doi.org/10.1016/j.ress.2009.11.002.
[69] Panteli M, Mancarella P. Modeling and evaluating the resilience of critical electrical power infrastructure to extreme weather events. IEEE Syst J 2017;11:1733–42. https://doi.org/10.1109/JSYST.2015.2389272.
[70] Houser T, Marsters P. The World's Second Largest Blackout. Rhodium Gr 2019. https://rhg.com/research/puerto-rico-hurricane-maria-worlds-second-largest-blackout/.
[71] Lu D, Alcantara C. After Hurricane Maria , Puerto Rico was in the dark for 293 days , 7 hours and 5 minutes. Washington Post 2018.
[72] NOAA. Historical Hurricane Tracks 2019. https://www.coast.noaa.gov/hurricanes/ (accessed July 10, 2018).
[73] PREPA. Operational Profile 2013. https://www.aeepr.com/INVESTORS/OperationalProfile.aspx (accessed July 10, 2018).
[74] Campbell RJ, Clark CE, Austin DA. Repair or Rebuild: Options for Electric Power in Puerto Rico 2017.
[75] ReImagina Puerto Rico n.d.
[76] PREC. DISTRIBUCIÓN PORCENTUAL DE LA GENERACIÓN DE ENERGÍA POR TIPO. AAEPR (Autoridad Energ Electr 2016. http://energia.pr.gov/datos/distribucion-porcentual-de-la-generacion-de-energia-por-tipo/ (accessed July 28, 2018).
[77] U.S. Energy Information Administration. Puerto Rico: Territory Profile and Energy Estimates 2018. https://www.eia.gov/state/data.php?sid=RQ#Prices (accessed July 10, 2018).
[78] Hubbard S. Hazus : Estimated Damage and Economic Losses: Puerto Rico, United States. 2017.
[79] Descarga De Geodatos. Gob Puerto Rico n.d.

http://www.gis.pr.gov/descargaGeodatos/Infraestructuras/Pages/Electricidad.aspx (accessed May 15, 2018).
[80] Broxton PD, Zeng X, Sulla-Menashe D, Troch PA. A global land cover climatology using MODIS data. J Appl Meteorol Climatol 2014;53:1593–605. https://doi.org/10.1175/JAMC-D-13-0270.1.
[81] Natural Protected Areas of Puerto Rico 2015. Caribb Landsc Conserv Coop 2015. https://caribbeanlcc.databasin.org/datasets/ (accessed May 15, 2018).
[82] Global Wind Atlas 2.0, a free, web-based application developed, owned and operated by the Technical University of Denmark (DTU) in partnership with the World Bank Group, utilizing data provided by Vortex, with funding provided by the Energy Sector Managem n.d. http://globalwindatlas.com/index.html.
[83] Solargis. Solar resource map 2018. https://solargis.com (accessed July 10, 2018).
[84] Autoridad de Energia Electrica. Puerto Rico Energy Public Policy Act. n.d.
[85] IRENA. Electricity storage and renewables: Costs and markets to 2030. 2017. https://doi.org/ISBN 978-92-9260-038-9 (PDF).
[86] Loulou R, Goldstein G, Noble K. Documentation for the MARKAL Family of Models General Map of the documentation. 2004.
[87] Howells M, Rogner H, Strachan N, Heaps C, Huntington H, Kypreos S, et al. OSeMOSYS: The Open Source Energy Modeling System. An introduction to its ethos, structure and development. Energy Policy 2011;39:5850–70. https://doi.org/10.1016/j.enpol.2011.06.033.
[88] Cohen SM, Becker J, Bielen DA, Brown M, Cole WJ, Eurek KP, et al. Regional Energy Deployment System (ReEDS) Model Documentation: Version 2018. 2019. https://doi.org/doi:10.2172/1505935.
[89] Jaglom WS, McFarland JR, Colley MF, Mack CB, Venkatesh B, Miller RL, et al. Assessment of projected temperature impacts from climate change on the U.S. electric power sector using the Integrated Planning Model®. Energy Policy 2014;73:524–39. https://doi.org/10.1016/j.enpol.2014.04.032.
[90] Grinsted A, Moore JC, Jevrejeva S. Projected Atlantic hurricane surge threat from rising temperatures. Proc Natl Acad Sci U S A 2013;110:5369–73. https://doi.org/10.1073/pnas.1209980110.
[91] Staid A, Guikema SD, Nateghi R, Quiring SM, Gao MZ. Simulation of tropical cyclone impacts to the U.S. power system under climate change scenarios. Clim Change 2014;127:535–46. https://doi.org/10.1007/s10584-014-1272-3.
[92] Knutson T, Camargo SJ, Chan JCL, Emanuel K, Ho C-H, Kossin J, et al. Tropical cyclones and climate change assessment Part II: Projected Response to Anthropogenic Warming. Bull Am Meteorol Soc 2020;101:E303–22. https://doi.org/10.1175/BAMS-D-18-0189.1.
[93] Bie Z, Lin Y, Li G, Li F. Battling the Extreme: A Study on the Power System Resilience. Proc IEEE 2017;105:1253–66. https://doi.org/10.1109/JPROC.2017.2679040.
[94] Ouyang M, Dueñas-Osorio L. Multi-dimensional hurricane resilience assessment of electric power systems. Struct Saf 2014;48:15–24. https://doi.org/10.1016/j.strusafe.2014.01.001.
[95] Watson E. Modeling Electrical Grid Resilience under Hurricane Wind Conditions with Increased Solar Photovoltaic and Wind Turbine Power Generation. George Washington University, 2018.
[96] Robert T. Stafford Disaster Relief And Emergency Assistance Act, P.L. 93-288 as Amended. United ∟: 2016.
[97] Temoa Project Documentation n.d. https://temoacloud.com/temoaproject/index.html.
[98] Siemens. PREPA Renewable Generation Integration Study. vol. 1. 2014.
[99] Teichgraeber H, Lindenmeyer CP, Baumgärtner N, Kotzur L, Stolten D, Robinius M, et al. Extreme events in time series aggregation: A case study for optimal residential energy supply systems. Appl Energy 2020;275. https://doi.org/10.1016/j.apenergy.2020.115223.
[100] Mavromatidis G, Orehounig K, Carmeliet J. Design of distributed energy systems under uncertainty:

A two-stage stochastic programming approach. Appl Energy 2018;222:932–50. https://doi.org/10.1016/j.apenergy.2018.04.019.
[101] Hermann S, Miketa A, Fichaux N. Estimating the Renewable Energy Potential in Africa GIS-based approach. Abu Dhabi: 2014.
[102] Lehner B, Verdin K, Jarvis A. New global hydrography derived from spaceborne elevation data. Eos (Washington DC) 2008;89:93–4. https://doi.org/10.1029/2008EO100001.
[103] Hoogwijk M, de Vries B, Turkenburg W. Assessment of the global and regional geographical, technical and economic potential of onshore wind energy. Energy Econ 2004;26:889–919. https://doi.org/10.1016/j.eneco.2004.04.016.
[104] NREL. Energy Transition Initiative: Island Energy Snapshot - Puerto Rico (Fact Sheet). 2015. https://doi.org/DOE/GO-102015-4583.
[105] Puerto Rico Integrated Resource Plan 2018-2019. 2019.
[106] PREPA. FORTIETH ANNUAL REPORT ON THE ELECTRIC PROPERTY of the PUERTO Rico Electric Power Authority. 2013.
[107] National Renewable Energy Laboratory. NREL 2019 Annual Technology Baseline 2019. https://atb.nrel.gov/ (2019).
[108] EIA. Annual Energy Outlook 2020. 2020.
[109] IEA-ETSAP. Electricity Transmission and Distribution. 2014.
[110] Panteli M, Pickering C, Wilkinson S, Dawson R, Mancarella P. Power System Resilience to Extreme Weather: Fragility Modelling, Probabilistic Impact Assessment, and Adaptation Measures. IEEE Trans Power Syst 2017;32:1–1. https://doi.org/10.1109/TPWRS.2016.2641463.
[111] Quanta Technology. Undergrounding Assessment Phase 3 Report: Ex Ante Cost and Benefit Modeling. 2008.
[112] Schneider PJ, Schauer BA. HAZUS - Its development and Its Future. Nat Hazards Rev 2006;7:40–4. https://doi.org/10.1061/(ASCE)1527-6988(2006)7.
[113] Goodman JN. Performance Measures for Residential PV Structural Response to Wind Effects 2015.
[114] Rose S, Jaramillo P, Small MJ, Grossmann I, Apt J. Quantifying the hurricane risk to offshore wind turbines. Proc Natl Acad Sci 2012;109:3247–52. https://doi.org/10.1073/pnas.1111769109.
[115] Franklin JL, Black ML, Valde K. Eyewall Wind Profiles in Hurricanes Determined By GPS Dropwindsondes. Natl Hurric Cent Cent PACIFIC Hurric Cent 2000. https://www.nhc.noaa.gov/aboutwindprofile.shtml (accessed March 10, 2019).
[116] Hall KL. Out of Sight , Out of Mind: An Updated Study on the Undergrounding Of Overhead Power Lines 2012:1–77.
[117] EIA. Detailed State Data 2019. https://www.eia.gov/electricity/data/state/ (accessed February 26, 2019).
[118] Huber M, Dimkova D, Hamacher T. Integration of wind and solar power in Europe: Assessment of flexibility requirements. Energy 2014;69:236–46. https://doi.org/10.1016/j.energy.2014.02.109.
[119] Denholm P, Clark K, O'Connell M. On the Path to SunShot: Emerging Issues and Challenges in Integrating High Levels of Solar into the Electrical Gneration and Transmission System. Natl Renew Energy Lab 2016. https://doi.org/NREL/TP-5D00-65331; SAND2016-2524 R.
[120] Wagner FW. SB 966 Electric utility regulation; grid modernization, energy efficiency. Virginia General Assembly; 2018.
[121] Denholm P, Margolis R. Very Large-Scale Deployment of Grid-Connected Solar Photovoltaics in the United States : Challenges and Opportunities. Proc Sol 2006 Conf 2006:9–13.
[122] Bajpai P, Dash V. Hybrid renewable energy systems for power generation in stand-alone applications: A review. Renew Sustain Energy Rev 2012;16:2926–39. https://doi.org/10.1016/j.rser.2012.02.009.
[123] Kasaei MJ, Gandomkar M, Nikoukar J. Optimal management of renewable energy sources by virtual

power plant. Renew Energy 2017;114:1180–8. https://doi.org/10.1016/j.renene.2017.08.010.
[124] Nosratabadi SM, Hooshmand RA, Gholipour E. A comprehensive review on microgrid and virtual power plant concepts employed for distributed energy resources scheduling in power systems. Renew Sustain Energy Rev 2017;67:341–63. https://doi.org/10.1016/j.rser.2016.09.025.
[125] Dufo-López R, Bernal-Agustín JL, Yusta-Loyo JM, Domínguez-Navarro JA, Ramírez-Rosado IJ, Lujano J, et al. Multi-objective optimization minimizing cost and life cycle emissions of stand-alone PV-wind-diesel systems with batteries storage. Appl Energy 2011;88:4033–41. https://doi.org/10.1016/j.apenergy.2011.04.019.
[126] Das BK, Al-Abdeli YM, Kothapalli G. Optimisation of stand-alone hybrid energy systems supplemented by combustion-based prime movers. Appl Energy 2017;196:18–33. https://doi.org/10.1016/j.apenergy.2017.03.119.
[127] Kalantar M, Mousavi G. SM. Dynamic behavior of a stand-alone hybrid power generation system of wind turbine, microturbine, solar array and battery storage. Appl Energy 2010;87:3051–64. https://doi.org/10.1016/j.apenergy.2010.02.019.
[128] Zahedi A. Maximizing solar PV energy penetration using energy storage technology. Renew Sustain Energy Rev 2011;15:866–70. https://doi.org/10.1016/j.rser.2010.09.011.
[129] Ueckerdt F, Brecha R, Luderer G. Analyzing major challenges of wind and solar variability in power systems. Renew Energy 2015;81:1–10. https://doi.org/10.1016/j.renene.2015.03.002.
[130] Ahn Y, Bae SJ, Kim M, Cho SK, Baik S, Lee JI, et al. Review of supercritical CO2 power cycle technology and current status of research and development. Nucl Eng Technol 2015;47:647–61. https://doi.org/https://doi.org/10.1016/j.net.2015.06.009.
[131] Bush V. GTI STEP forward on sCO 2 Power. SCO2 Power Symp 2018.
[132] Echogen. EPS30 Heat Recovery Solution n.d.:1–2. https://www.echogen.com/_CE/pagecontent/Documents/EPS30_brochure_2017.pdf (accessed October 21, 2018).
[133] Echogen. EPS35 Heat Recovery Solution n.d.:1–2. https://www.echogen.com/_CE/pagecontent/Documents/EPS35_brochure_2017.pdf (accessed October 21, 2018).
[134] Echogen. EPS100 Heat Recovery Solution n.d.:1–2. https://www.echogen.com/our-solution/product-series/eps100/ (accessed October 21, 2018).
[135] Persichilli M, Kacludis A, Zdankiewicz E, Held T. Supercritical CO2 Power Cycle Developments and Commercialization: Why sCO2 can Displace Steam. Present. Power-Gen India Cent. Asia 2012, Pragati Maidan, New Delhi, India Supercritical: 2012, p. 1–16.
[136] Clementoni EM, Cox TL, King MA. Off-Nominal Component Performance in a Supercritical Carbon Dioxide Brayton Cycle. J Eng Gas Turbines Power 2015;138:11703–8.
[137] Moisseytsev A, Sienicki JJ. Development of a plant dynamics computer code for analysis of a supercritical carbon dioxide Brayton cycle energy converter coupled to a natural circulation lead-cooled fast reactor. 2006. https://doi.org/https://doi.org/10.2172/910536.
[138] Seong B, Ahn Y han, Kim SG, Bae SJ, Cho SK, Lee JI. Transient Analyses of S-CO2 Cooled KAIST Micro Modular Reactor with GAMMA+ Code. 5th Int Symp - Supercrit CO2 Power Cycles 2016:1–20.
[139] Holmgren WF, Hansen CW, Mikofski MA. pvlib python: a python package for modeling solar energy systems 2018. https://doi.org/10.21105/joss.00884.
[140] EIA. Frequently Asked Questions: How much electricity does an American home use ? 2018. www.eia.gov/tools/faqs/faq.cfm?id=97&t=3 (accessed February 17, 2019).
[141] EIA. Table F21: Electricity Consumption Estimates 2017. https://www.eia.gov/state/seds/sep_fuel/html/pdf/fuel_use_es.pdf (accessed February 17, 2019).
[142] WeatherUnderground. Scott Stadium WeatherSTEM Weather | Personal Weather Station:

KVACHARL80 by Wunderground.com | Weather Underground 2018. https://www.wunderground.com/personal-weather-station/dashboard?ID=KVACHARL80#history/s20170803/e20170803/mdaily (accessed October 17, 2018).
[143] Past Weather in Chalottesville, Virginia, USA n.d. https://www.timeanddate.com/weather/usa/charlottesville/historic (accessed October 24, 2018).
[144] Reda I, Andreas A. Solar Position Algorithm for Solar Radiation Applications (Revised). 2000.
[145] Maxwell EL. A Quasi-Physical Model for Converting Hourly Global Horizontal to Direct Normal lnsolation. 1987.
[146] Dobos AP. PVWatts Version 5 Manual. 2014.
[147] Marcos J, de la Parra I, Garcia M, Marroyo L. Simulating the variability of dispersed large PV plants. Prog Photovoltaics Res Appl 2016;24:326–34. https://doi.org/10.1002/pip.
[148] Edmunds T, Alzaabi O, Mills A. Flexibility Metrics to Support Grid Planning and Operations. Futur. Mark. Work., Washington, DC: 2017.
[149] DOE. Levelized Cost of Energy (LCOE) n.d. https://www.energy.gov/sites/prod/files/2015/08/f25/LCOE.pdf (accessed February 17, 2019).
[150] Travis E O. A guide to NumPy. USA: Trelgol Publishing; 2006.
[151] GE. 6B Power Plants (50/60 Hz). GEA32936 2016. https://www.ge.com/power/gas/gas-turbines/6b-03 (accessed October 12, 2018).
[152] GE. 6F Power Plants. GEA32934 2017. https://www.ge.com/power/gas/gas-turbines/6f-01 (accessed October 12, 2018).
[153] Systems PP. FT8 ® MOBILEPAC ® Gas Turbine Package. MP-FS-532017 2017. http://www.pwps.com/gas-turbine-package-ft8-mobilepac/ (accessed October 12, 2018).
[154] MHPS. H-25 Series 2018. http://www.mhps.com/products/gasturbines/lineup/h25/index.html (accessed October 12, 2018).
[155] GE. LM2500 Power Plants. GEA32937 2017. https://www.ge.com/power/gas/gas-turbines/lm2500 (accessed October 12, 2018).
[156] GE. LM6000 Power Plants. GEA32935 2017. https://www.ge.com/power/gas/gas-turbines/lm6000 (accessed October 12, 2018).
[157] Siemens. Gas turbine SGT-600. PGDG-T10012-00-7600 2016. https://www.siemens.com/global/en/home/products/energy/power-generation/gas-turbines/sgt-600.html#!/ (accessed October 12, 2018).
[158] Siemens. Gas turbine SGT-700. PGDG-T10028-00-7600 2016. https://www.siemens.com/global/en/home/products/energy/power-generation/gas-turbines/sgt-700.html#!/ (accessed October 12, 2018).
[159] Siemens. Gas Turbine SGT-750. PGDG-T10033-00-7600 2016. https://www.siemens.com/global/en/home/products/energy/power-generation/gas-turbines/sgt-750.html (accessed October 12, 2018).
[160] Siemens. Gas Turbine SGT-800. PGDG-T10040-00-7600 2017. https://www.siemens.com/global/en/home/products/energy/power-generation/gas-turbines/sgt-800.html (accessed October 12, 2018).
[161] Siemens. SGT-A35 (GT30) gas turbine. PGDG-T10036-02-7600 2018. https://www.siemens.com/global/en/home/products/energy/power-generation/gas-turbines/sgt-a30-a35-rb.html#!/ (accessed October 12, 2018).
[162] Siemens. SGT-A45 mobile unit. PGDG-T10034-02-7600 2018. https://www.siemens.com/global/en/home/products/energy/power-generation/gas-turbines/sgt-a45.html (accessed October 12, 2018).
[163] Siemens. SGT-A65 gas turbine. PGDG-T10044-00-7600 2018.

https://www.siemens.com/global/en/home/products/energy/power-generation/gas-turbines/sgt-a65-tr.html (accessed October 12, 2018).
[164] GE. TM2500 Power Plants. GEA32938 2017. https://www.ge.com/power/gas/gas-turbines/tm2500 (accessed October 12, 2018).
[165] de Groot M, Crijns-Graus W, Harmsen R. The effects of variable renewable electricity on energy efficiency and full load hours of fossil-fired power plants in the European Union. Energy 2017;138:575–89. https://doi.org/10.1016/j.energy.2017.07.085.
[166] Scaccabarozzi R, Gatti M, Martelli E. Thermodynamic Optimization and Part-load Analysis of the NET Power Cycle. Energy Procedia 2017;114:551–60. https://doi.org/10.1016/j.egypro.2017.03.1197.
[167] EIA. Cost and Performance Characteristics of New Generating Technologies. 2018.
[168] Wright S, Scammell W. Economics. In: Brun K, Friedman P, Dennis R, editors. Fundam. Appl. Supercrit. Carbon Dioxide Based Power Cycles, 2017, p. 127–45.
[169] Walnum HT, Nekså P, Nord LO, Andresen T. Modelling and simulation of CO2(carbon dioxide) bottoming cycles for offshore oil and gas installations at design and off-design conditions. Energy 2013;59:513–20. https://doi.org/10.1016/j.energy.2013.06.071.
[170] Cho SK, Kim M, Baik S, Ahn Y, Lee JI. Investigation of the bottoming cycle for high efficiency combined cycle gas turbine system with supercritical carbon dioxide power cycle. Proc ASME Turbo Expo Turbine Tech Conf Expo 2015:12. https://doi.org/10.1115/GT2015-43077.
[171] Stapp DS. A Novel SCO 2 Primary Cycle for Air-Combustible Fuels. 4th Int Symp - Supercrit CO2 Power Cycles 2014:1–10.
[172] Wright SA, Davidson CS, Scammell WO. Thermo-Economic Analysis of Four sCO2 Waste Heat Recovery Power Systems. 5th Int Symp - Supercrit CO2 Power Cycles 2016:1–16.
[173] Moroz L, Burlaka M, Rudenko O, Joly C. Evaluation of Gas Turbine Exhaust Heat Recovery Utilizing Composite Supercritical CO2 Cycle. Proc Int Gas Turbine Congr 2015 2015:7.
[174] Dyreby JJ, Klein SA, Nellis GF, Reindl DT. MODELING OFF-DESIGN AND PART-LOAD PERFORMANCE OF SUPERCRITICAL CARBON DIOXIDE POWER CYCLES. Proc. ASME Turbo Expo 2013 Turbine Tech. Conf. Expo., San Antonio, TX: 2013, p. 1–7.
[175] Cich S. Personal correspondence n.d.
[176] EIA. Carbon Dioxide Emissions Coefficients by Fuel. 2016.
[177] EIA. Henry Hub Natural Gas Spot Price 2019. https://www.eia.gov/dnav/ng/hist/rngwhhdm.htm (accessed February 24, 2019).
[178] Sandia National Laboratories. DOE/EPRI Electricity Storage Handbook 2015.
[179] EIA. Electric power monthly: Average retail price of electricity to ultimate customers by enduse sector 2014:http://www.eia.gov/electricity/monthly/epm_table_g.
[180] BloombergNEF. New Energy Outlook 2019. Bloom Financ LP 2019. https://about.bnef.com/new-energy-outlook/ (accessed October 26, 2020).
[181] Arbabzadeh M, Sioshansi R, Johnson JX, Keoleian GA. The role of energy storage in deep decarbonization of electricity production. Nat Commun 2019;10. https://doi.org/10.1038/s41467-019-11161-5.
[182] Braff WA, Mueller JM, Trancik JE. Value of storage technologies for wind and solar energy. Nat Clim Chang 2016;6:964–9. https://doi.org/10.1038/nclimate3045.
[183] Mongird K, Fotedar V, Viswanathan V, Koritarov V, Balducci P, Hadjerioua B, et al. Energy Storage Technology and Cost Characterization Report. 2019.
[184] Harper G, Sommerville R, Kendrick E, Driscoll L, Slater P, Stolkin R, et al. Recycling lithium-ion batteries from electric vehicles. Nature 2019;575:75–86. https://doi.org/10.1038/s41586-019-1682-5.
[185] Qi Z, Koenig GM. Review Article: Flow battery systems with solid electroactive materials. J Vac

Sci Technol B, Nanotechnol Microelectron Mater Process Meas Phenom 2017;35:040801. https://doi.org/10.1116/1.4983210.
[186] Jafari M, Botterud A, Sakti A. Evaluation of Energy- and Capacity-Market Revenues from Lithium-ion Battery Systems for Offshore Wind Using Advanced Battery Models. Appl Energy 2020. https://doi.org/https://doi.org/10.1016/j.apenergy.2020.115417.
[187] Electric utility regulation; environmental goals. United States: 2020.
[188] Senate Bill S6599. 2019.
[189] Mason JE, Archer CL. Baseload electricity from wind via compressed air energy storage (CAES). Renew Sustain Energy Rev 2012;16:1099–109. https://doi.org/10.1016/j.rser.2011.11.009.
[190] Cheung BC, Carriveau R, Ting DSK. Parameters affecting scalable underwater compressed air energy storage. Appl Energy 2014;134:239–47. https://doi.org/10.1016/j.apenergy.2014.08.028.
[191] Wang Z, Xiong W, Ting DSK, Carriveau R, Wang Z. Conventional and advanced exergy analyses of an underwater compressed air energy storage system. Appl Energy 2016;180:810–22. https://doi.org/10.1016/j.apenergy.2016.08.014.
[192] Pimm AJ, Garvey SD, de Jong M. Design and testing of Energy Bags for underwater compressed air energy storage. Energy 2014;66:496–508. https://doi.org/10.1016/j.energy.2013.12.010.
[193] Boehme T, Cammaert G, McCurry J, Judt M, Deckers M. WindStore - Large-scale energy storage offshore. Offshore Eur Conf - Proc 2007:242–7. https://doi.org/10.2523/108578-ms.
[194] Fukai I, Keister L, Ganesh PR, Cumming L, Fortin W, Gupta N. Carbon dioxide storage resource assessment of Cretaceous- and Jurassic-age sandstones in the Atlantic offshore region of the northeastern United States. Environ Geosci 2020;27:25–47. https://doi.org/10.1306/eg.09261919016.
[195] Li Y, Li Y, Liu Y, Cao X. Compressed air energy storage in aquifers: Basic principles, considerable factors, and improvement approaches. Rev Chem Eng 2019. https://doi.org/10.1515/revce-2019-0015.
[196] Oldenburg CM, Pan L. Porous Media Compressed-Air Energy Storage (PM-CAES): Theory and Simulation of the Coupled Wellbore-Reservoir System. Transp Porous Media 2013;97:201–21. https://doi.org/10.1007/s11242-012-0118-6.
[197] Guo C, Pan L, Zhang K, Oldenburg CM, Li C, Li Y. Comparison of compressed air energy storage process in aquifers and caverns based on the Huntorf CAES plant. Appl Energy 2016;181:342–56. https://doi.org/10.1016/j.apenergy.2016.08.105.
[198] Guo C, Zhang K, Li C, Wang X. Modelling studies for influence factors of gas bubble in compressed air energy storage in aquifers. Energy 2016;107:48–59. https://doi.org/10.1016/j.energy.2016.04.003.
[199] Guo C, Zhang K, Pan L, Cai Z, Li C, Li Y. Numerical investigation of a joint approach to thermal energy storage and compressed air energy storage in aquifers. Appl Energy 2017;203:948–58. https://doi.org/10.1016/j.apenergy.2017.06.030.
[200] Sopher D, Juhlin C, Levendal T, Erlström M, Nilsson K, Da Silva Soares JP. Evaluation of the subsurface compressed air energy storage (CAES) potential on Gotland, Sweden. Environ Earth Sci 2019;78:1–17. https://doi.org/10.1007/s12665-019-8196-1.
[201] Yang L, Cai Z, Li C, He Q, Ma Y, Guo C. Numerical investigation of cycle performance in compressed air energy storage in aquifers. Appl Energy 2020;269:115044. https://doi.org/10.1016/j.apenergy.2020.115044.
[202] Schulte RH, Critelli N, Holst K, Huff G. Lessons from Iowa : Development of a 270 Megawatt Compressed Air Energy Storage Project in Midwest Independent System Operator A Study for the DOE Energy Storage Systems Program. Sandia Rep 2012:97.
[203] Ellsworth WL. Injection-Induced Earthquakes 2013;341:1–8.
[204] Hincks T, Aspinall W, Cooke R, Gernon T. Oklahoma's induced seismicity strongly linked to

wasteater injection depth. Science (80-) 2018;1255:1251–5.
[205] De Risi R, Bhattacharya S, Goda K. Seismic performance assessment of monopile-supported offshore wind turbines using unscaled natural earthquake records. Soil Dyn Earthq Eng 2018;109:154–72. https://doi.org/10.1016/j.soildyn.2018.03.015.
[206] Bureau of Ocean Energy Management. Renewable Energy GIS Data 2020. https://www.boem.gov/renewable-energy/mapping-and-data/renewable-energy-gis-data (accessed April 29, 2020).
[207] Patil VC, Ro PI. Energy and Exergy Analysis of Ocean Compressed Air Energy Storage Concepts. J Eng (United Kingdom) 2018;2018. https://doi.org/10.1155/2018/5254102.
[208] Yan B, Wieberdink J, Shirazi F, Li PY, Simon TW, Van de Ven JD. Experimental study of heat transfer enhancement in a liquid piston compressor/expander using porous media inserts. Appl Energy 2015;154:40–50. https://doi.org/10.1016/j.apenergy.2015.04.106.
[209] Van de Ven JD, Li PY. Liquid piston gas compression. Appl Energy 2009;86:2183–91. https://doi.org/10.1016/j.apenergy.2008.12.001.
[210] Qin C, Loth E. Simulation of spray direct injection for compressed air energy storage. Appl Therm Eng 2016;95:24–34. https://doi.org/10.1016/j.applthermaleng.2015.11.008.
[211] Bollinger B. Technology Performance Report, SustainX Smart Grid Program, Demonstration of Isothermal Compressed Air Energy Storage to Support Renewable Energy Production. 2015.
[212] Qin C, Loth E. Liquid piston compression efficiency with droplet heat transfer. Appl Energy 2014;114:539–50. https://doi.org/10.1016/j.apenergy.2013.10.005.
[213] Zhang X, Xu Y, Zhou X, Zhang Y, Li W, Zuo Z, et al. A near-isothermal expander for isothermal compressed air energy storage system. Appl Energy 2018;225:955–64. https://doi.org/10.1016/j.apenergy.2018.04.055.
[214] White AJ, Meacock AJ. An evaluation of the effects of water injection on compressor performance. J Eng Gas Turbines Power 2004;126:748–54. https://doi.org/10.1115/1.1765125.
[215] Novelo DAB, Igie U. Aero engine compressor cooling by water injection - Part 1: Evaporative compressor model. Energy 2018;160:1224–35. https://doi.org/10.1016/j.energy.2018.05.170.
[216] Salles MBC, Huang J, Aziz MJ, Hogan WW. Potential arbitrage revenue of energy storage systems in PJM. Energies 2017;10. https://doi.org/10.3390/en10081100.
[217] Byers C, Levin T, Botterud A. Capacity market design and renewable energy: Performance incentives, qualifying capacity, and demand curves. Electr J 2018;31:65–74. https://doi.org/10.1016/j.tej.2018.01.006.
[218] PJM Interconnection Inc. 2021/2022 RPM Base Residual Auction Results. 2018.
[219] Simpson J, Loth E, Dykes K. Cost of Valued Energy for design of renewable energy systems. Renew Energy 2020;153:290–300. https://doi.org/10.1016/j.renene.2020.01.131.
[220] Allen RD, Doherty TJ, Erikson RL, Wiles LE. Factors Affecting Storage of Compressed Air in Porous Rock Reservoirs 1983:157.
[221] Dixon SL, Hall CA. Introduction. Fluid Mech. Thermodyn. Turbomach., vol. 1, Butterworth-Heinemann; 2010, p. 1–27. https://doi.org/10.1016/b978-1-85617-793-1.00001-8.
[222] Siemens. Siemens Air-Cooled Generators SGen-100A-2P Series. Artic No PGGT-B10013-00-7600 n.d. https://www.siemens-energy.com/global/en/offerings/power-generation/generators/sgen-100a.html (accessed October 21, 2020).
[223] Adams BM, Kuehn TH, Bielicki JM, Randolph JB, Saar MO. A comparison of electric power output of CO2 Plume Geothermal (CPG) and brine geothermal systems for varying reservoir conditions. Appl Energy 2015;140:365–77. https://doi.org/10.1016/j.apenergy.2014.11.043.
[224] White FM. Fluid Mechanics. 8th ed. McGraw Hill Education; 2016.
[225] National Oceanic and Atmospheric Administration. National Data Buoy Center, Station 44014 n.d. https://www.ndbc.noaa.gov/station_page.php?station=44014.

[226] Solar Turbines. Industrial Power Generation Titan 250 n.d. https://www.solarturbines.com/en_US/products/power-generation-packages/titan-250.html (accessed June 18, 2020).
[227] Lee TW, Park JE, Kurose R. Determination of the drop size during atomization of liquid jets in cross flows. At Sprays 2018;28:241–54. https://doi.org/10.1615/AtomizSpr.2018022768.
[228] Moran MJ, Shapiro, Howard N. Fundamentals of Engineering Thermodynamics. 5th ed. John Wiley & Sons; 2004.
[229] Bergman TL, Lavine AS, Incropera FP, Dewitt DP. Fundamentals of Heat and Mass Transfer. 7th ed. Wiley; 2011.
[230] Katz DL, Tek MR. Storage of Natural Gas in Saline Aquifers. Water Resour Res 1970;6:1515–21. https://doi.org/10.1029/WR006i005p01515.
[231] Stehly T, Beiter P. 2018 Cost of Wind Energy Review. 2019.
[232] U.S Energy Information Administration, Sargent & Lundy (S&L). Capital Cost and Performance Characteristic Estimates for Utility Scale Electric Power Generating Technologies. 2020.
[233] Aminyavari M, Mamaghani AH, Shirazi A, Najafi B, Rinaldi F. Exergetic, economic, and environmental evaluations and multi-objective optimization of an internal-reforming SOFC-gas turbine cycle coupled with a Rankine cycle. Appl Therm Eng 2016;108:833–46. https://doi.org/10.1016/j.applthermaleng.2016.07.180.
[234] Progressing Development of the UK's Strategic Carbon Dioxide Storage Resource: A summary of results from the strategic UK CO2 storage appraisal project. 2016.
[235] Kaiser MJ, Snyder BF. The Offshore Drilling Industry and Rig Construction in the Gulf of Mexico. London: Springer-Verlag; 2013. https://doi.org/10.1007/978-1-4471-5152-4.
[236] Osmundsen P, Roll KH, Tveteras R. Drilling speed-the relevance of experience. Energy Econ 2012;34:786–94. https://doi.org/10.1016/j.eneco.2011.11.016.
[237] Lukawski MZ, Anderson BJ, Augustine C, Capuano LE, Beckers KF, Livesay B, et al. Cost analysis of oil, gas, and geothermal well drilling. J Pet Sci Eng 2014;118:1–14. https://doi.org/10.1016/j.petrol.2014.03.012.
[238] Maness M, Maples B, Smith A. NREL Offshore Balance-of- System Model. 2017.
[239] Froese M. Making of the modern offshore substation. Wind Eng Dev 2016.
[240] BVG Associates. A Guide to an Offshore Wind Farm Updated and extended. 2019. https://doi.org/10.1016/S0029-5493(00)00422-2.
[241] Gu Y, Mccalley J, Ni M, Bo R. Economic Modeling of Compressed Air Energy Storage. Energies 2013;6:2221–41. https://doi.org/10.3390/en6042221.
[242] Qin C, Saunders G, Loth E. Offshore wind energy storage concept for cost-of-rated-power savings. Appl Energy 2017;201:148–57. https://doi.org/10.1016/j.apenergy.2017.04.077.
[243] US Energy Information Administration. U.S. Battery Storage Market Trends. 2018.
[244] Kiehne HA. Battery Technology Handbook. vol. 134. 2nd ed. Marcel Dekker, Inc.; 2003.
[245] Hart WE, Watson JP, Woodruff DL. Pyomo: Modeling and solving mathematical programs in Python. Math Program Comput 2011;3:219–60. https://doi.org/10.1007/s12532-011-0026-8.
[246] Shaw WJ, Pekour MS, Newsom RK. Lidar Buoy Data Analysis Basic Assessment of Observed Conditions and Instrument Performance Off Virginia and New Jersey. 2018.
[247] PJM. Data Miner 2 n.d. https://dataminer2.pjm.com/list (accessed August 26, 2020).
[248] Jonkman J, Butterfield S, Musial W, Scott G. Definition of a 5-MW reference wind turbine for offshore system development 2009:1–75.
[249] NREL. Simple Levelized Cost of Energy (LCOE) Calculator Documentation n.d. https://www.nrel.gov/analysis/tech-lcoe-documentation.html (accessed October 16, 2018).
[250] Walter L. PJM Status Quo for Capacity Storage. 2020.
[251] Albertus P, Manser JS, Litzelman S. Long-Duration Electricity Storage Applications, Economics,

and Technologies. Joule 2020;4:21–32. https://doi.org/10.1016/j.joule.2019.11.009.
[252] APPLICATION OF VIRGINIA ELECTRIC AND POWER COMPANY For approval to establish an experimental residential rate schedule, designated Time-Of-Use Rate Scheule 1G (Experimental). Richmond, VA: 2020.
[253] EIA. Table 5.6.A Average Price of Electricity to Ultimate Customers by End-Use Sector 2020.
[254] Ziegler MS, Mueller JM, Pereira GD, Song J, Ferrara M, Chiang YM, et al. Storage Requirements and Costs of Shaping Renewable Energy Toward Grid Decarbonization. Joule 2019;3:2134–53. https://doi.org/10.1016/j.joule.2019.06.012.
[255] Rutgers. New Jersey Energy Storage Analysis (ESA) Final Report. 2019.
[256] Denholm P, Mai T. Timescales of energy storage needed for reducing renewable energy curtailment. Renew Energy 2019;130:388–99. https://doi.org/10.1016/j.renene.2018.06.079.
[257] Schmidt O, Melchior S, Hawkes A, Staffell I. Projecting the Future Levelized Cost of Electricity Storage Technologies. Joule 2019;3:81–100. https://doi.org/10.1016/j.joule.2018.12.008.
[258] Beuse M, Steffen B, Schmidt TS. Projecting the Competition between Energy-Storage Technologies in the Electricity Sector. Joule 2020;4:2162–84. https://doi.org/10.1016/j.joule.2020.07.017.
[259] Patil VC, Acharya P, Ro PI. Experimental investigation of water spray injection in liquid piston for near-isothermal compression. Appl Energy 2020;259:114182. https://doi.org/10.1016/j.apenergy.2019.114182.
[260] Patil VC, Liu J, Ro PI. Efficiency improvement of liquid piston compressor using metal wire mesh for near-isothermal compressed air energy storage application. J Energy Storage 2020;28:101226. https://doi.org/10.1016/j.est.2020.101226.
[261] Patil VC, Ro PI. Experimental study of heat transfer enhancement in liquid piston compressor using aqueous foam. Appl Therm Eng 2020;164:114441. https://doi.org/10.1016/j.applthermaleng.2019.114441.
[262] Bennett JA, Simpson JG, Qin C, Fittro R, Koenig GM, Clarens AF, et al. Techno-economic analysis of offshore isothermal compressed air energy storage in saline aquifers co-located with wind power. Submitted 2020.
[263] Pollack A, Mukerji T. Accounting for subsurface uncertainty in enhanced geothermal systems to make more robust techno-economic decisions. Appl Energy 2019;254:113666. https://doi.org/10.1016/j.apenergy.2019.113666.
[264] Tacher L, Pomian-Srzednicki I, Parriaux A. Geological uncertainties associated with 3-D subsurface models. Comput Geosci 2006;32:212–21. https://doi.org/10.1016/j.cageo.2005.06.010.
[265] Bowen BB, Ochoa RI, Wilkens ND, Brophy J, Lovell TR, Fishietto N, et al. Depositional and diagenetic variability within the Cambrian Mount Simon Sandstone: Implications for carbon dioxide sequestration. Environ Geosci 2011;18:69–89.
[266] Medina CR, Rupp JA, Barnes DA. Effects of reduction in porosity and permeability with depth on storage capacity and injectivity in deep saline aquifers: A case study from the Mount Simon Sandstone aquifer. Int J Greenh Gas Control 2011;5:146–56. https://doi.org/10.1016/j.ijggc.2010.03.001.
[267] Miller KG, Browning J V., Mountain GS, Sheridan RE, Sugarman PJ, Glenn S, et al. History of continental shelf and slope sedimentation on the US middle atlantic margin. Geol Soc Mem 2014;41:21–34. https://doi.org/10.1144/M41.3.
[268] Battelle, Delaware Geological Survey, Maryland Geological Survey, Pennsylvania Geological Survey, United States Geological Survey, Lamont-Doherty Earth Observatory at Columbia University, et al. Mid-Atlantic U.S. Offshore Carbon Storage Resource Assessment Project Task 6 Risk Factor Analysis Report. DOE Cooperative Agreement No. DE-FE0026087. 2019.
[269] NOAA Office for Coastal Management. Offshore Wind Technology Depth Zones 2019. https://marinecadastre.gov/nationalviewer/ (accessed October 15, 2020).

[270] US Census Bureau GD. 2019 TIGER/Line® Shapefiles: States (and equivalent) 2019. www2.census.gov/geo/tiger/TIGER2019/STATE/tl_2019_us_state.zip (accessed July 19, 2020).
[271] Larson E, Greig C, Jenkins J, Mayfield E, Pascale A, Zhang C, et al. Net-Zero America: Potential Pathways, Infrastructure, and Impacts. Princeton, NJ: 2020.
[272] Carbon Storage Atlas Fifth Edition. 2018.
[273] Bell IH, Wronski J, Quoilin S, Lemort V. Pure and pseudo-pure fluid thermophysical property evaluation and the open-source thermophysical property library coolprop. Ind Eng Chem Res 2014;53:2498–508. https://doi.org/10.1021/ie4033999.
[274] The pandas development team. pandas-dev/pandas: Pandas 2020. https://doi.org/10.5281/zenodo.3509134.
[275] Harris CR, Millman KJ, van der Walt SJ, Gommers R, Virtanen P, Cournapeau D, et al. Array programming with NumPy. Nature 2020:357–62. https://doi.org/10.1038/s41586-020-2649-2.
[276] Michael Waskom and the seaborn development team. mwaskom/seaborn 2020. https://doi.org/10.5281/zenodo.592845.
[277] Hunter JD. Matplotlib: A 2D graphics environment. Comput Sci Eng 2007;9:90–5. https://doi.org/10.1109/MCSE.2007.55.
[278] Joblib: running Python functions as pipeline jobs n.d. https://joblib.readthedocs.io/.
[279] Barnes DA, Bacon DH, Kelley SR. Geological sequestration of carbon dioxide in the Cambrian Mount Simon Sandstone: Regional storage capacity, site characterization, and large-scale injection feasibility, Michigan Basin. Environ Geosci 2009;16:163–83. https://doi.org/10.1306/eg.05080909009.
[280] Ramakrishnan KR, Ro PI, Patil VC. Temperature abatement using hollow spheres in liquid piston compressor for Ocean Compressed Air Energy Storage system. Ocean 2016 MTS/IEEE Monterey, OCE 2016 2016. https://doi.org/10.1109/OCEANS.2016.7761341.
[281] Liu B, Zhang Y. CO2 modeling in a deep saline aquifer: A predictive uncertainty analysis using design of experiment. Environ Sci Technol 2011;45:3504–10. https://doi.org/10.1021/es103187b.
[282] Jung Y, Zhou Q, Birkholzer JT. On the detection of leakage pathways in geological CO2 storage systems using pressure monitoring data: Impact of model parameter uncertainties. Adv Water Resour 2015;84:112–24. https://doi.org/10.1016/j.advwatres.2015.08.005.
[283] Rogelj J, den Elzen M, Höhne N, Fransen T, Fekete H, Winkler H, et al. Paris Agreement climate proposals need a boost to keep warming well below 2 °C. Nature 2016;534:631–9. https://doi.org/10.1038/nature18307.
[284] Rogelj J, Luderer G, Pietzcker RC, Kriegler E, Schaeffer M, Krey V, et al. Energy system transformations for limiting end-of-century warming to below 1.5 °C. Nat Clim Chang 2015;5:519–27. https://doi.org/10.1038/nclimate2572.
[285] Herron S, Kyle A, Lewis E, Woods M. Greenhouse Gas Reductions in the Power Industry Using Domestic Coal and Biomass Volume 2: Pulverized Coal Plants. 2012.
[286] Consoli C. Bioenergy and Carbon Capture and Storage. 2019.
[287] Fajardy M, Morris J, Gurgel A, Herzog H, Mac Dowell N, Paltsev S. The economics of bioenergy with carbon capture and storage (BECCS) deployment in a 1.5°C or 2°C world. vol. 345. Cambridge, MA: 2020.
[288] Emenike O, Michailos S, Finney KN, Hughes KJ, Ingham D, Pourkashanian M. Initial techno-economic screening of BECCS technologies in power generation for a range of biomass feedstock. Sustain Energy Technol Assessments 2020;40:100743. https://doi.org/10.1016/j.seta.2020.100743.
[289] Akbilgic O, Doluweera G, Mahmoudkhani M, Bergerson J. A meta-analysis of carbon capture and storage technology assessments: Understanding the driving factors of variability in cost estimates. Appl Energy 2015;159:11–8. https://doi.org/10.1016/j.apenergy.2015.08.056.
[290] Forster P, Ramaswamy V, Artaxo P, Berntsen T, Betts R, Fahey DW, et al. Changes in Atmospheric

Constituents and in Radiative Forcing. In: Solomon S, Qin D, Manning M, Chen Z, Marquis M, Averyt K., et al., editors. Clim. Chang. 2007 Phys. Sci. Basis. Contrib. Work. Gr. I to Fourth Assess. Rep. Intergov. Panel Clim. Chang., Cambridge University Press; 2007.

[291] Mac Dowell N, Fajardy M. Inefficient power generation as an optimal route to negative emissions via BECCS? Environ Res Lett 2017;12. https://doi.org/10.1088/1748-9326/aa67a5.

[292] Cumicheo C, Mac Dowell N, Shah N. Natural gas and BECCS: A comparative analysis of alternative configurations for negative emissions power generation. Int J Greenh Gas Control 2019;90. https://doi.org/10.1016/j.ijggc.2019.102798.

[293] Gosling SN, Arnell NW. A global assessment of the impact of climate change on water scarcity. Clim Change 2016;134:371–85. https://doi.org/10.1007/s10584-013-0853-x.

[294] Hetland J, Yowargana P, Leduc S, Kraxner F. Carbon-negative emissions: Systemic impacts of biomass conversion - A case study on CO2 capture and storage options. Int J Greenh Gas Control 2016;49:330–42. https://doi.org/10.1016/j.ijggc.2016.03.017.

[295] Sgouridis S, Carbajales-dale M, Csala D, Chiesa M, Bardi U. Comparative net energy analysis of renewable electricity and carbon capture and storage. Nat Energy 2019;4. https://doi.org/10.1038/s41560-019-0365-7.

[296] King LC, Bergh JCJM Van Den. Implications of net energy-return-on-investment for a low-carbon energy transition. Nat Energy 2018;3:334–41. https://doi.org/10.1038/s41560-018-0116-1.

[297] Moeller D, Murphy D. Net Energy Analysis of Gas Production from the Marcellus Shale. Biophys Econ Resour Qual 2016;1:1–13. https://doi.org/10.1007/s41247-016-0006-8.

[298] Fajardy M, Mac Dowell N. The energy return on investment of BECCS: is BECCS a threat to energy security? Energy Environ Sci 2018;11:1581–94. https://doi.org/10.1039/c7ee03610h.

[299] Heun MK, de Wit M. Energy return on (energy) invested (EROI), oil prices, and energy transitions. Energy Policy 2012;40:147–58. https://doi.org/10.1016/j.enpol.2011.09.008.

[300] Spath PL, Mann MK. Biomass Power and Coventional Fossil Systems with and without CO2 Sequestration - Comparing the Energy Balance, Greenhouse Gas Emissions and Economics. 2004. https://doi.org/10.1074/jbc.M405933200.

[301] Corti A, Lombardi L. Biomass integrated gasification combined cycle with reduced CO2 emissions: Performance analysis and life cycle assessment (LCA). Energy 2004;29:2109–24. https://doi.org/10.1016/j.energy.2004.03.015.

[302] Carpentieri M, Corti A, Lombardi L. Life cycle assessment (LCA) of an integrated biomass gasification combined cycle (IBGCC) with CO2 removal. Energy Convers Manag 2005;46:1790–808. https://doi.org/10.1016/j.enconman.2004.08.010.

[303] Cuellar A. Plant Power: The Cost of using Biomass for Power Generation and Potential for Decreased Greenhouse Gas Emissions. Massachusetts Institute of Technology, 2012.

[304] Schakel W, Meerman H, Talaei A, Ramírez A, Faaij A. Comparative life cycle assessment of biomass co-firing plants with carbon capture and storage. Appl Energy 2014;131:441–67. https://doi.org/10.1016/j.apenergy.2014.06.045.

[305] Falano T, Thornley P, Roeder M. AIR/OXY BIOMASS COMBUSTION WITH CARBON CAPTURE AND STORAGE. 23rd Eur. Biomass Conf. Exhib., Vienna, Austria: 2015.

[306] Black JB, Haslbeck JK, Lewis E, Woods MC. Greenhouse Gas Reductions in the Power Industry Using Domestic Coal and Biomass Volume 1 : IGCC. vol. 1. 2012.

[307] Gough C, Thornley P, Mander S, Vaughan N, Lea-Langton A, editors. Biomass Energy with Carbon Capture and Storage (BECCS or Bio-CCS). John Wiley & Sons; 2018.

[308] Bennett JA, Jasmin Melara A, Colosi LM, Clarens AF. Life cycle analysis of power cycle configurations in bioenergy with carbon capture and storage. Procedia CIRP 2019;80:340–5. https://doi.org/10.1016/j.procir.2018.12.014.

[309] Rackley SA. Carbon Capture and Storage. 2nd ed. Elsevier; 2017.

[310] Cuéllar-Franca RM, Azapagic A. Carbon capture, storage and utilisation technologies: A critical analysis and comparison of their life cycle environmental impacts. J CO2 Util 2015;9:82–102. https://doi.org/10.1016/j.jcou.2014.12.001.
[311] Gazzani M, Macchi E, Manzolini G. CO2 capture in natural gas combined cycle with SEWGS. Part A: Thermodynamic performances. Int J Greenh Gas Control 2013;12:493–501. https://doi.org/10.1016/j.ijggc.2012.06.010.
[312] Rubin ES, Davison JE, Herzog HJ. The cost of CO2 capture and storage. Int J Greenh Gas Control 2015;40:378–400. https://doi.org/10.1016/j.ijggc.2015.05.018.
[313] Petrescu L, Bonalumi D, Valenti G, Cormos AM, Cormos CC. Life Cycle Assessment for supercritical pulverized coal power plants with post-combustion carbon capture and storage. J Clean Prod 2017;157:10–21. https://doi.org/10.1016/j.jclepro.2017.03.225.
[314] Petrescu L, Cormos CC. Environmental assessment of IGCC power plants with pre-combustion CO2 capture by chemical & calcium looping methods. J Clean Prod 2017;158:233–44. https://doi.org/10.1016/j.jclepro.2017.05.011.
[315] Ozcan DC, Macchi A, Lu DY, Kierzkowska AM, Ahn H, Müller CR, et al. Ca-Cu looping process for CO2 capture from a power plant and its comparison with Ca-looping, oxy-combustion and amine-based CO2 capture processes. Int J Greenh Gas Control 2015;43:198–212. https://doi.org/10.1016/j.ijggc.2015.10.021.
[316] Ortiz C, Chacartegui R, Valverde JM, Becerra JA. A new integration model of the calcium looping technology into coal fired power plants for CO2 capture. Appl Energy 2016;169:408–20. https://doi.org/10.1016/j.apenergy.2016.02.050.
[317] Kotowicz J, Bartela Ł. Optimisation of the connection of membrane CCS installation with a supercritical coal-fired power plant. Energy 2012;38:118–27. https://doi.org/10.1016/j.energy.2011.12.028.
[318] Damen K, Troost M Van, Faaij A, Turkenburg W. A comparison of electricity and hydrogen production systems with CO 2 capture and storage. Part A: Review and selection of promising conversion and capture technologies. Prog Energy Combust Sci 2006;32:215–46. https://doi.org/10.1016/j.pecs.2005.11.005.
[319] Blamey J, Anthony EJ, Wang J, Fennell PS. The calcium looping cycle for large-scale CO2 capture. Prog Energy Combust Sci 2010;36:260–79. https://doi.org/10.1016/j.pecs.2009.10.001.
[320] Schreiber A, Zapp P, Marx J. Meta-Analysis of Life Cycle Assessment Studies on Electricity Generation with Carbon Capture and Storage. J Ind Ecol 2012;16:155–68. https://doi.org/10.1111/j.1530-9290.2011.00435.x.
[321] Corsten M, Ramírez A, Shen L, Koornneef J, Faaij A. Environmental impact assessment of CCS chains - Lessons learned and limitations from LCA literature. Int J Greenh Gas Control 2013;13:59–71. https://doi.org/10.1016/j.ijggc.2012.12.003.
[322] Heath GA, Mann MK. Background and Reflections on the Life Cycle Assessment Harmonization Project. J Ind Ecol 2012;16:8–11. https://doi.org/10.1111/j.1530-9290.2012.00478.x.
[323] Vasudevan S, Farooq S, Karimi IA, Saeys M, Quah MCG, Agrawal R. Energy penalty estimates for CO2 capture: Comparison between fuel types and capture-combustion modes. Energy 2016;103:709–14. https://doi.org/10.1016/j.energy.2016.02.154.
[324] Baik E, Sanchez DL, Turner PA, Mach KJ, Field CB, Benson SM. Geospatial analysis of near-term potential for carbon-negative bioenergy in the United States. Proc Natl Acad Sci U S A 2018;115:3290–5. https://doi.org/10.1073/pnas.1720338115.
[325] EIA. Power Plants 2020. https://www.eia.gov/maps/layer_info-m.php (accessed December 7, 2020).
[326] Leboreiro J, Hilaly AK. Biomass transportation model and optimum plant size for the production of ethanol. Bioresour Technol 2011;102:2712–23. https://doi.org/10.1016/j.biortech.2010.10.144.

[327] Huang HJ, Ramaswamy S, Al-Dajani W, Tschirner U, Cairncross RA. Effect of biomass species and plant size on cellulosic ethanol: A comparative process and economic analysis. Biomass and Bioenergy 2009;33:234–46. https://doi.org/10.1016/j.biombioe.2008.05.007.
[328] Fernando R. Cofiring high ratios of biomass with coal. 2012.
[329] Rozenberg J, Vogt-Schilb A, Hallegatte S. Instrument choice and stranded assets in the transition to clean capital. J Environ Econ Manage 2020;100:102183. https://doi.org/10.1016/j.jeem.2018.10.005.
[330] Drax Group. Drax closer to coal-free future with fourth biomass unit conversion. Press Release 2018. https://www.drax.com/press_release/drax-closer-coal-free-future-fourth-biomass-unit-conversion/ (accessed December 12, 2020).
[331] Murray G. Drax moves to biomass. Can Biomass 2014. https://www.canadianbiomassmagazine.ca/drax-moves-to-biomass-4503/ (accessed December 12, 2020).
[332] Dooley B, Mason PE. Supply Chain Costs of Biomass Cofiring. London: 2018.
[333] NREL. U.S. Solid Biomass Resources by County 2014. https://www.nrel.gov/gis/biomass.html (accessed December 7, 2020).
[334] Wang M, Elgowainy A, Lee U, Benavides P, Burnham A, Cai H, et al. Summary of Expansions and Updates in GREET 2019. 2019.
[335] Koornneef J, van Keulen T, Faaij A, Turkenburg W. Life cycle assessment of a pulverized coal power plant with post-combustion capture, transport and storage of CO2. Int J Greenh Gas Control 2008;2:448–67. https://doi.org/10.1016/j.ijggc.2008.06.008.
[336] Pehnt M, Henkel J. Life cycle assessment of carbon dioxide capture and storage from lignite power plants. Int J Greenh Gas Control 2009;3:49–66. https://doi.org/10.1016/j.ijggc.2008.07.001.
[337] Giordano L, Roizard D, Favre E. Life cycle assessment of post-combustion CO2 capture: A comparison between membrane separation and chemical absorption processes. Int J Greenh Gas Control 2018;68:146–63. https://doi.org/10.1016/j.ijggc.2017.11.008.
[338] Mitsubishi Heavy Industries. CO2 Capture Plant 2020. https://www.mhi.com/products/engineering/co2plants.html (accessed December 14, 2020).
[339] Lemmon EW, Bell IH, Huber ML, McLinden MO. NIST Standard Reference Database 23: Reference Fluid Thermodynamic and Transport Properties-REFPROP, Version 10.0. Gaithersburg: 2018.
[340] Span R, Wagner W. A New Equation of State for Carbon Dioxide Covering the Fluid Region from the Triple-Point Temperature to 1100 K at Pressures up to 800 MPa. J Phys Chem Ref Data 1996;25:1509–96.
[341] Cheng F, Porter MD, Colosi LM. Is hydrothermal treatment coupled with carbon capture and storage an energy-producing negative emissions technology? Energy Convers Manag 2020;203:112252. https://doi.org/10.1016/j.enconman.2019.112252.
[342] Baker SE, Stolaroff JK, Peridas G, Pang SH, Goldstein HM, Lucci FR, et al. Getting to Neutral - Options for Negative Carbon Emissions in California. 2020.
[343] EIA. Table 6.1 Electric Generating Summary Capacity Changes (MW), October 2019 to November 2019. Electr Power Mon 2020. https://www.eia.gov/electricity/monthly/epm_table_grapher.php?t=epmt_6_01.
[344] Patel S. Billions Over Budget, Kemper Facility Gasification Portion Is Suspended. POWER 2017. https://www.powermag.com/billions-over-budget-kemper-facility-gasification-portion-is-suspended/ (accessed February 20, 2020).
[345] Patrizio P, Leduc S, Kraxner F, Fuss S, Kindermann G, Mesfun S, et al. Reducing US Coal Emissions Can Boost Employment. Joule 2018;2:2633–48. https://doi.org/10.1016/j.joule.2018.10.004.

[346] Belmont E. Combustion-based BECCS Combustion-based BECCS. Work Fed BECCS Priorities 2020.
[347] R Core Team. R: A language and environment for statistical computing. Vienna, Austria: R Foundation for Statistical Computing; 2020.
[348] Wickham H, Francois R, Henry L, Mueller K. dplyr: A Grammar of Data Manipulation 2020. https://cran.r-project.org/web/packages/dplyr/index.html.
[349] Wickham H, Bryan J, RStudio, Kalicinski M, Valery K, Leitienne C, et al. readxl: Read Excel Files 2019. https://cran.r-project.org/web/packages/readxl/.
[350] Python 3.7.6 documentation. 2019.
[351] Reback J, McKinney W, Jbrockmendel, Bossche J Van den, Augspurger T, Cloud P, et al. pandas-dev/pandas: Pandas 1.0.1 2020. https://doi.org/10.5281/zenodo.3509134.
[352] Waskom M, Botvinnik O, Ostblom J, Lukauskas S, Hobson P, MaozGelbart, et al. mwaskom/seaborn 2020. https://doi.org/10.5281/zenodo.592845.
[353] Machin SJ, Withers C. xlrd 2020. https://xlrd.readthedocs.io/en/latest/index.html.
[354] Finnish Government. Finland has an excellent opportunity to rebuild itself in line with the principles of sustainable development n.d. https://valtioneuvosto.fi/en/marin/government-programme/carbon-neutral-finland-that-protects-biodiversity (accessed February 19, 2021).
[355] University of Virginia. University of Virginia Sustainability 2020-2030 Plan. 2020.
[356] EIA. Annual Energy Outlook 2021 2021. https://www.eia.gov/outlooks/aeo/ (accessed February 19, 2021).
[357] Fuhrman J, McJeon H, Doney SC, Shobe W, Clarens AF. From Zero to Hero?: Why Integrated Assessment Modeling of Negative Emissions Technologies Is Hard and How We Can Do Better. Front Clim 2019;1. https://doi.org/10.3389/fclim.2019.00011.
[358] Zhang X, Myhrvold NP, Hausfather Z, Caldeira K. Climate benefits of natural gas as a bridge fuel and potential delay of near-zero energy systems. Appl Energy 2016;167:317–22. https://doi.org/10.1016/j.apenergy.2015.10.016.
[359] Shigematsu T. The development and demonstration status of practical flow battery systems. Curr Opin Electrochem 2019;18:55–60. https://doi.org/10.1016/j.coelec.2019.10.001.
[360] Bennett JA, Abotalib M, Zhao F, Clarens AF. Life Cycle Meta-Analysis of Carbon Capture Pathways in Power Plants: Implications for Bioenergy with Carbon Capture and Storage. Submitted 2020.
[361] Keith DW, Holmes G, St. Angelo D, Heidel K. A Process for Capturing CO2 from the Atmosphere. Joule 2018;2:1573–94. https://doi.org/10.1016/j.joule.2018.05.006.
[362] Wang Q, Chen X, Jha AN, Rogers H. Natural gas from shale formation - The evolution, evidences and challenges of shale gas revolution in United States. Renew Sustain Energy Rev 2014;30:1–28. https://doi.org/10.1016/j.rser.2013.08.065.
[363] Osborn SG, Vengosh A, Warner NR, Jackson RB. Methane contamination of drinking water accompanying gas-well drilling and hydraulic fracturing. Proc Natl Acad Sci U S A 2011;108:8172–6. https://doi.org/10.1073/pnas.1100682108.
[364] Eshraghi H, De Queiroz AR, DeCarolis JF. US Energy-Related Greenhouse Gas Emissions in the Absence of Federal Climate Policy. Environ Sci Technol 2018;52:9595–604. https://doi.org/10.1021/acs.est.8b01586.
[365] Bennett JA, Trevisan CN, DeCarolis JF, Ortiz-García C, Pérez-Lugo M, Etienne BT, et al. Extending energy system modelling to include extreme weather risks and application to hurricane events in Puerto Rico. Nat Energy 2021;6:240–9. https://doi.org/10.1038/s41560-020-00758-6.
[366] Sengupta M, Xie Y, Lopez A, Habte A, Maclaurin G, Shelby. J. The National Solar Radiation Data Base (NSRDB). Renew Sustain Energy Rev 2018;89:51–60.
[367] EIA. Existing Nameplate and Net Summer Capacity by Energy Source, Producer Type and State

(EIA-860) 2019. https://www.eia.gov/electricity/data/state/ (accessed February 20, 2021).
[368] Lewis P. 2020 Has Been a Big Year for US Offshore Wind 2020.
[369] Shobe W, Small A, Artuso A, Haley B, Kwok G. Decarbonizing Virginia's Economy: Pathways to 2050. 2021.
[370] EIA. Virginia Electricity Profile 2019 2020. https://www.eia.gov/electricity/state/virginia/ (accessed March 2, 2021).
[371] NREL. The Biofuels Atlas 2016. https://maps.nrel.gov/biomass (accessed March 4, 2021).
[372] EPA. Biomass Combined Heat and Power Catalog of Technologies. 2007. https://doi.org/10.1201/b14513-2.
[373] PJM. Data Miner 2: Hourly Load: Metered 2019. https://dataminer2.pjm.com/feed/hrl_load_metered (accessed February 25, 2021).
[374] PJM. Data Miner 2. Solar Generation 2019. https://dataminer2.pjm.com/feed/solar_gen (accessed February 25, 2021).
[375] DOE. A2e: BUOY n.d. https://a2e.energy.gov/projects/buoy (accessed February 25, 2021).
[376] Li T, Xing F, Liu T, Sun J, Shi D, Zhang H, et al. Cost, performance prediction and optimization of a vanadium flow battery by machine-learning. Energy Environ Sci 2020;13:4353–61. https://doi.org/10.1039/d0ee02543g.
[377] 26 U.S. Code § 45Q. Credit for carbon oxide sequestration. n.d.
[378] EIA. Puerto Rico's LNG imports returned to pre-Hurricane Maria levels in late 2018 2019.
[379] PREPA. Aguirre Site Economic Analysis. San Juan, PR: 2017.
[380] Aguirre Offshore Gasport n.d. https://www.offshore-technology.com/projects/aguirre-offshore-gasport/ (accessed December 18, 2019).
[381] IEA-ETSAP. Technology Brief P09 : Biomass Production and Logistics 2013:1–15.
[382] PREPA. PREPA-Ex.-1.02-Part-2-Economic-Analysis-Report-Appendices. 2017.
[383] EIA. Cost and Performance Characteristics of New Generating Technologies. Annu Energy Outlook 2019 2019:1–3.
[384] PREPA. INFORME DE LA GENERACION DIARIA DEL SISTEMA ELECTRICO Viernes 1 de enero de 2016 CAPACIDAD. 2016.
[385] PREPA. Proposed Annual Budget Current Expenses and Capital Expenditures: Fiscal Year 2014-2015. n.d.
[386] PREPA. INFORME DE LA GENERACION DIARIA DEL SISTEMA ELECTRICO Martes 1 de marzo de 2016. 2016.
[387] PREPA. INFORME DE LA GENERACION DIARIA DEL SISTEMA ELECTRICO Lunes 1 de febrero de 2016. 2016.
[388] PREPA. Estadisticas - Ley 57. n.d.
[389] EIA. Most new utility-scale solar in the United States is being built in the South Atlantic. Today In Energy 2020.
[390] Nordbotten JM, Celia MA. Similarity solutions for fluid injection into confined aquifers. J Fluid Mech 2006;561:307–27. https://doi.org/10.1017/S0022112006000802.
[391] Li Y, Zhang K, Hu L, Wang J. Numerical Investigation of the Influences of Wellbore Flow on Compressed Air Energy Storage in Aquifers. Geofluids 2017;2017. https://doi.org/10.1155/2017/9316506.
[392] Katz DL, Coats MR, Coats KH, Katz ML, Jones SC, Miller MC. Movement of underground water in contact with natural gas. New York, NY: American Gas Association; 1963.
[393] Park JK, Ro PI, He X, Mazzoleni AP. Analysis, Fabrication, and Testing of a Liquid Piston Compressor Prototype for an Ocean Compressed Air Energy Storage (OCAES) System. Mar Technol Soc J 2014;48:86–97. https://doi.org/10.4031/MTSJ.48.6.3.
[394] Dolatabadi A, Fabris D, Samara-Rubio D. Isothermal Efficiency of Liquid Piston Compressors

Employed in Compressed Air Energy Storage Systems. Proc. ASME 2013 Fluids Eng. Div. Summer Meet. FEDSM2013, Incline Villaga, Nevada, USA: 2013, p. 1–8.
[395] Cormos AM, Dinca C, Petrescu L, Andreea Chisalita D, Szima S, Cormos C-C. Carbon capture and utilisation technologies applied to energy conversion systems and other energy-intensive industrial applications. Fuel 2018;211:883–90. https://doi.org/10.1016/j.fuel.2017.09.104.
[396] Dominion Energy. 2020 Virginia Integrated Resource Plan. 2020.
[397] EIA. Table F28: Wood and Biomass Waste Price and Expenditure Estimates, 2018 2018. https://www.eia.gov/state/seds/sep_fuel/html/pdf/fuel_pr_ww.pdf (accessed January 21, 2021).
[398] Immendoerfer A, Tietze I, Hottenroth H, Viere T. Life-cycle impacts of pumped hydropower storage and battery storage. Int J Energy Environ Eng 2017;8:231–45. https://doi.org/10.1007/s40095-017-0237-5.
[399] Siting, Permitting & Land Use for Utility-Scale Solar | SEIA n.d. https://www.seia.org/initiatives/siting-permitting-land-use-utility-scale-solar (accessed February 25, 2021).
[400] Gagnon P, Margolis R, Melius J, Phillips C, Elmore R. Rooftop Solar Photovoltaic Technical Potential in the United States: A Detailed Assessment. 2016.
[401] Brown MA, Favero A, Thomas VM, Banboukian A. The economic and environmental performance of biomass as an “intermediate” resource for power production. Util Policy 2019;58:52–62. https://doi.org/10.1016/j.jup.2019.04.002.
[402] British Pound to US Dollar Spot Exchange Rates for 2015 from the Bank of England n.d. https://www.poundsterlinglive.com/bank-of-england-spot/historical-spot-exchange-rates/gbp/GBP-to-USD-2015 (accessed March 3, 2021).